ZINC OXIDE:

NEW INSIGHTS INTO A MATERIAL FOR ALL AGES

BY

AMIR MOEZZI

BSc. Chemical Engineering

A Dissertation Submitted for the

Degree of Doctor of Philosophy

University of Technology Sydney

2012

Certificate of authorship/originality

I certify that the work in this thesis has not previously been submitted for a degree nor has it been submitted as part of requirements for a degree except as fully acknowledged within the text.

I also certify that the thesis has been written by me. Any help that I have received in my research work and the preparation of the thesis itself has been acknowledged. In addition, I certify that all information sources and literature used are indicated in the thesis.

Production Note:
Signature removed prior to publication.

Amir Moezzi

11/10/2012

Printed and bound in Australia

Acknowledgements

I would like to express my special appreciation to the company PT. Indo Lysaght, of Indonesia, for financial support for my project and very kind hospitality during the visits from their chemical plants.

My greatest debts are to my principal supervisor, Prof. Michael Cortie, and my co-supervisors Dr Andrew McDonagh, who gave me the opportunity to undertake this project and for their support and encouragement throughout the project. I learned so much working with you and I am really grateful for your time and effort teaching me how to do high quality research and produce interesting and important results. I also thank you for editorial help in my thesis.

Thanks to my family for their encouragement despite a long distance between us.

Very special thank to Dr Ronald Shimmon for his extensive care and support. Also I would like to express my appreciation to Drs R. Wuhrer, M. Berkahn, A. Dowd, M. Philips, C. Ton-That, P. Thomas and L. Xiao. I also thank Mr J-P. Guerbois for his help in performing TGA and MS, Mrs S. Fenech and Mrs G. Armstrong for their help in using nitrogen measurement instrument and also Mr D. Bishop for performing the ICP-MS test. Thanks to Miss V. Schrameyer for her help in translation of German papers into English.

Sincere thanks to my fellow friends specially Mr M. Coutts for their patience and listening to long and sometimes boring discussions that we had during this period.

Thanks to Drs P. Robinson (Canada), S. Mahmud (Malaysia) and P. Stamford (Australia) for their helpful responses to our questions. Thanks to Dr H. Nguyen, from School of Chemical Engineering at UNSW for some of the BET surface area measurements and Dr K. Kannangara from School of Science and Health, UWS for solid-NMR. Support from companies for providing photographs for my publication is highly appreciated. Thanks to the Microstructural Analysis Unit (MAU) at UTS for providing me with the state-of-the-art equipment and facilities to analyse the materials. Thanks to Australian Synchrotron in Melbourne for the time they provided for the synchrotron radiation studies in this work.

Last but not least, I thank all of my friends who supported me with patience in my project.

Antoine Laurent Lavoisier (1743-1794), “father of modern chemistry”, in 1789 for the first time suggested that “Flowers of zinc” be named “zinc oxide” reflecting the elements in the nomenclature of compound.

"We think only through the medium of words. Languages are true analytical methods. Algebra, which is adapted to its purpose in every species of expression, in the most simple, most exact, and best manner possible, is at the same time a language and an analytical method. The art of reasoning is nothing more than a language well arranged."

Antoine Laurent Lavoisier, *Traité Élémentaire de Chimie*, 1789

Adopted from translation by Robert Kerr, 1790

Table of Contents

List of Figures

Page

List of Tables

Page

List of Schemes

Page

Abbreviations

α_L = coefficient of expansion

λ = thermal conductivity value

Ac = acetate ($CH_3CO_2^-$)

ASTM = American Society for Testing and Materials

a.m.u = atomic mass unit

BAW = bulk acoustic wave

BET = Brunauer, Emmett and Teller

BZA = basic zinc acetate

BZC = basic zinc carbonate

BZCl = basic zinc chloride

BZN = basic zinc nitrate

BZS = basic zinc sulphate

CHM = composite hydroxide mediated

C_p° = specific heat capacity

CP-MAS = cross polarisation magic angle spinning

cr = crystalline

CRT = cathode ray tube

CVD = chemical vapor deposition

D2EHPA = di-2-ethyl hexyl phosphoric acid

DMS = dilute magnetic semiconductors

DSC = dust settling chamber

DTA = Differential thermal analysis

E_a = apparent activation energy

EAFD = electric arc furnace dust

EG = ethylene glycol

ENR = epoxidised natural rubber

EPDM = ethylene propylene diene monomer

FID = Free induction decay

FTIR = Fourier transform infrared

FWHM = Full width at half maximum

G = Gibbs free energy

GTL = gas-to-liquid

H = Enthalpy

H_2O_2 = hydrogen peroxide

HCE = hexachloroethane

HDPE = high density polyethylene

HDS = hydroxy double salts

HVPE = hydride vapor phase deposition

ICP-MS = Inductively coupled plasma mass spectrometry

ISP = imperial smelting process/irregularly-shaped particle

ITO = indium tin oxide

K_{atm} = equilibrium constant

LDH = layered double hydroxide

LED = light emitting diodes

MBE = molecular beam epitaxy

MBT = mercaptobenzothiazole

MCP = mechano-chemical process

MOCVD = metal organic chemical vapor deposition

MS = mass spectrometry

M.W = molecular weight

$Na_2S_2O_4$ = sodium dithionite

$NaHSO_2 \cdot CH_2O \cdot 2H_2O$ = sodium formaldehyde sulfoxylate

NMR = Nuclear magnetic resonance

OECD = Organisation for Economic Cooperation and Development

PFD = process flow diagram

phr = parts per hundred

PMA = polymer-modified asphalts

PP = polypropylene

ppb = parts per billion

ppm = parts per million

PVC = poly vinyl chloride

PVDF = polyvinylidene fluoride

rpm = revolutions per minute

RT = room temperature

SAW = surface acoustic wave

SRB = sulphate-reducing bacteria

SEM = scanning electron microscopy

SHG = special high grade

s-SBR = solution styrene-butadiene rubber

SVP = seeded vapor phase

T = temperature

TCO = transparent conductive oxides

TE = thermoelectric

TEM = transmission electron microscopy

TG = thermogravimetric

TGA = thermogravimetric analysis

TMTD = tetra-methyl-thiuramdisulphide

UV = ultra violet

VLS = vapor-liquid-solid

VPT = vapor phase transport

VS = vapor-solid

w/v = weight to volume

w/w = weight to weight

XNBR = carboxylated nitrile rubber

XRD = X-ray diffraction

Zn**Ac**$_2$ = zinc acetate

$Zn(CH_3COO)_2 \cdot 2H_2O$ = zinc acetate dihydrate

ZDDP = Zinc dialkyldithiophosphate

$ZnSO_4 \cdot 7H_2O$ = zinc sulphate heptahydrate

ZT = figures-of-merit

Publications and conference presentations associated with this work

1. Moezzi, A., "Nano *vs*. Active Zinc Oxide". Presentation at the International Conference on Nanosciences and Nanotechnology (ICONN), Sydney, Australia, February 2010.
2. Moezzi, A., Cortie, M and McDonagh, A. "Aqueous pathways for the formation of zinc oxide nanoparticles". Dalton Transactions **40**(18) (2011) 4871-4878.
3. Moezzi, A., Cortie, M and McDonagh, A. "Zinc Oxide Particles: Synthesis, Properties and Applications". Chemical Engineering Journal **185-186** (2012) 1-22.

Abstract

Zinc oxide is an important material industrially and scientifically. It has a long history dating back to more than four thousand years ago. It has applications in rubber production, cosmetics, pigments and ceramics. The properties of zinc oxide such as porosity, specific surface area and optical properties change as a result of changing the synthetic method and process conditions. The suitability of ZnO for different applications depends on the properties of the material, which in turn are influenced by synthetic routes.

Knowledge of the processes underpinning the various synthetic techniques is key to understanding the properties of the ZnO end-product. In this work, various synthetic techniques have been investigated that may be amenable to large-scale production. The resultant materials were studied and important insights were obtained. For example, it was found that the precursor materials and method of processing for the production of zinc oxide have important roles in controlling the properties of the product such as specific surface area, crystal morphology, particle size and amount of surface hydroxyl groups embedded in the product.

In single-stage production methods, zinc oxide is precipitated directly from a zinc solution. Influences of reaction temperature, concentration of the reactants and feeding techniques on the properties of the products were determined.

In multi-stage routes, intermediate zinc-bearing materials including zinc peroxide and zinc hydroxy carbonate, sulphate, chloride, nitrate and acetate were synthesised. These intermediate materials were then used as precursors for the formation of zinc oxide particles. Relationships between the properties of the precursor zinc-containing compound and the end-product zinc oxide were studied and unexpected results were obtained. For example, it was shown that specific surface area of the zinc oxide product depends significantly on the precursor material from which it is produced. Techniques were investigated that can produce multiple important zinc-bearing compounds and it was found that it could be engineered by selection of the appropriate precursors and process conditions.

Chapter 1

Zinc Oxide: Synthesis, Properties and Applications

Chapter 1: Zinc Oxide: Synthesis, Properties and Applications*

1.1. Introduction and overview of the dissertation

Zinc oxide is a mature material both scientifically and industrially. It has been used for thousands of years by the humans in diverse applications [1]. Similar to any other material, its applications have seen ups and downs over time. It has many interesting physical and chemical properties, which have caused scientific and industrial attention. Although numerous scientific publications are being produced every year on this material with a steep rise more recently (**Figure 1.1**), most of them are focused low-volume, niche applications, such as the potential for the application of this material in opto-electronics. Comprehensive reviews have been prepared on different aspects of the condensed matter physics, surface chemistry, synthesis techniques and semiconducting applications of ZnO [2-10] but, to my knowledge, there has been no recent review addressing industrial aspects of ZnO until my own in 2012 [11].

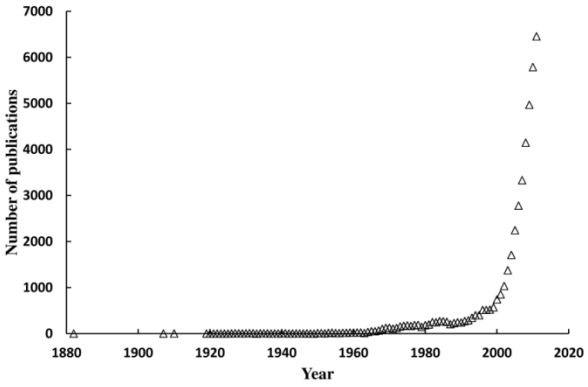

Figure 1.1. Number of scientific publications on zinc oxide since 1882 until 2011. Data available from literature database Scopus (keyword: "zinc oxide").

The goal of this work is to examine large-scale production processes for this material and to investigate novel routes to produce this chemical focusing on flexible methods to process a diverse range of raw materials.

* A significant part of the work presented in this chapter has been published (see Moezzi, McDonagh and Cortie, Chemical Engineering Journal, 185-186 (2012) 1-22).

A great deal of effort is concentrated on sourcing cheaper raw materials and finding simpler and novel techniques to produce useful products. Waste management and processing are also important. Most products end up as waste in either a waste-processing unit or in dumping sites, for example glass, plastic bottles, tires and cars. This is inevitable as everything has a life-span and eventually enters this phase. Further to this, most production processes also generate waste.

Zinc-containing materials are among such products. For example, galvanised products are well-known and useful zinc-materials that are seen everywhere around us. They are found on the roofs of houses, the body of the cars, in the kitchen and on the side of the roads. Although galvanised materials are quite useful in the battle against natural corrosion, these have the same fate as other materials and sooner or later must be replaced with freshly-made products. For example when a wrecked car is dismantled, its body would be a feed for the steel manufacturing plants and the zinc in the galvanised material is collected in the waste dust from the electric arc furnaces. Another source of zinc-bearing waste is from galvanisation process itself. Ashes and drosses containing large amount of zinc are produced, which should be processed independently. Obviously production processes and waste-processing units are parts of the same picture and these must be considered and designed together.

In the zinc oxide field, most of the material is produced from metallic zinc by a well-adapted technique known as the French process. In this method, zinc metal is melted and vaporised in a crucible and then oxidised to zinc oxide by oxygen that is free of charge and is originating from air. The market value of zinc oxide depends on the zinc metal price. Fluctuations in the price of zinc have a direct effect on the profitability of the French process zinc oxide plant.

In the current work, novel techniques are sought to provide processing flexibility for the production of zinc oxide from precursors other than zinc metal, which may be obtained from either new or, importantly, recycled zinc-containing materials. Engineering the properties of the zinc oxide made from various methods is also considered.

In Chapter 1, I look more thoroughly into the subject from a scientific and industrial perspective. A review of the extensive patent literature on ZnO is included for consideration of the industrial production methods and commercial applications of ZnO.

Patents contain important information but are generally neglected in the scientific litrature on ZnO. A comprehensive review on the history of the material is included, and the properties and relevant applications are investigated.

In Chapter 2, I study various single-stage production techniques using zinc sulphate and sodium hydroxide solutions. The effects of reaction temperature, reactant concentrations and feeding techniques are explained and the mechanism of formation of zinc oxide in the aqueous system is discussed.

In Chapter 3, I examine the single-stage process using zinc sulphate and ammonia solutions, and include a comparison between the reactions that use sodium hydroxide and ammonia.

Chapter 4 describes multi-stage routes to produce zinc oxide using zinc peroxide. Zinc peroxide is produced, then utilised as a precursor for zinc oxide manufacturing by heating.

In Chapter 5, the production of zinc oxide by multi-stage techniques using five zinc hydroxy salts is explored. Zinc hydroxy carbonate, sulphate, chloride, nitrate and acetate are synthesised, then used as precursors for the formation of various types of zinc oxide by heating.

Chapter 6 investigates the formation of zinc hydroxy nitrate via solid/liquid reactions between zinc oxide and zinc nitrate solution. Kinetics and mechanism of the reaction is explored and the solubility of the salt in water is determined.

Finally, Chapter 7 summarises the work presented in the dissertation. Some ideas for future research are also presented.

1.2. Historical aspects

The first recorded application of ZnO appears to be its use, *circa* 2000 B.C., in Egyptian medicinal ointments for the treatment of boils and carbuncles mentioned in the Edwin Smith Papyrus [1, 12]. Somewhat later, ZnO ore was exploited as a source of zinc for brass, a discovery usually attributed to the Romans [13] but which may have come from India a century or so earlier [14]. Brass could be produced by smelting a mixture of the powdered zinc ore, charcoal and granules of copper, but a by-product was the ZnO that was collected on the walls and flues of the brass smelting furnaces. The latter was known to the Romans as *cadmia fornacis* (furnace accretions) and was purified for use in ointments. Use of ZnO in skin lotions has continued up to the present day in the form of a slurry of zinc and iron oxide known in many English-speaking countries as "*calamine lotion*" [1]. Almost in the beginning of the Christian era, the Greek writer Dioscorides describes a furnace equipped with a dust-chamber to collect impure zinc oxide called *Pompholyx* that is used for skin sores [15].

Al-Muqaddasi (مقدسي) author of "*Ahsan at-Taqasim fi Ma`rifat il-Aqhalim*"[1] who travelled to Kerman, Iran in the 10th century describes that *tutia* (*tutiya*, *tutty* or *توتيا*- an impure zinc oxide, from the Persian term *dudha* - soot) is prepared from ore from mountains and is purified with a method similar to iron purification process [16]. Abu-Dulaf (ابو دلف) who also travelled to Iran in the 10th century describes the production of a variety of *tutia*. He also mentions that the Indian *tutia* is preferred in Iran [17]. The 11th century Iranian scientist, Abu Rayhan Biruni also describes the process of making *tutia* [18]. It seems that tutia was mainly in use in brass making at this time and to a lower extent for medicinal purposes [18]. These reports suggest that the art was known in the area a few centuries before the western writers reported it and a cross-border commodity trade was popular.

The German monk Theophilus (12th century) describes a cementation process for brass making in a closed vessel used in Medieval Islamic and Christian countries. In this process copper is packed in the crucible together with charcoal and zinc oxide. Zinc

1 - Translated by the author from the Arabic text of "*Ahsan at-Taqasim fi Ma`rifat il-Aqhalim"* by Al-Muqaddasi-مقدسي, أحسن التقاسيم في معرفة الأقاليم. Comment: The Arab geographer mentions that this *tutia* was named "gargoyle-like *tutia* - التوتياء المرازبي" due to the reason that after collecting the ore, it was spread over long finger-shaped ceramic pots. *Tutia* sticks to them and forms a gargoyle-like shape which is then purified. The finger-shaped pots might probably be similar to what is described by Biswas as tubular retorts which was in use in India.

oxide is previously produced by calcination of a zinc ore, probably in the form of zinc carbonate [19].

Later on in the 13th century, Marco Polo's book "The Travels of Marco Polo" also describes the production process of *tutia* in Iran from a certain ore placed in a flaming furnace covered with an iron grating. The smoke released from the ore is collected on the iron grating and forms *tutia*, which was used as a medicinal eye-ointment [13, 20, 21].

From the 12th to the 16th century, at Zawar in Rajasthan, zinc metal (to make brass) and zinc oxide (for medical purposes) were produced in tubular retorts of about 25 cm long and 15 cm in diameter with the wall thickness of about 1 cm thick installed in a furnace [20]. For example in the Hindu book Rasarnava (~1200 A.D) production of zinc metal is explained [13]. Recognition of zinc as a new metal - the 8th metal known to man - as early as 1374 is assigned to the Hindu king Madanapala [13, 22]. In the Indian text "*Rasaratnakara*", it was shown how *Rasaka* (zinc ore) upon reduction in the absence of copper forms a new "tin-like" metal. The 13th century Sanskrit alchemical treatise, *Rasa-Ratna-Samuccaya* also contains detailed information on zinc mineralogy and metallurgy [14].

The method of zinc manufacturing method apparently entered China from India in the 17th century for use in the brass industry [13]. The metallurgy and applications of this metal can be seen in the Chinese book "*Tien-kong-kai-ou*" published in 1637 [23]. Reduction of calamine ore by charcoal in clay jars under heating was apparently the method used to collect zinc [13].

In Europe, Agricola (1494-1555) and Paracelsus (1493-1541) in the 16th century mentioned the name of *zincum,* which was most likely zinc ore, not zinc metal. In the 17th century, Europeans were aware of the existence of zinc metal imported from the Orient by Portuguese, Dutch and Arab traders. Robert Boyle in 1690 suggested the commercial term *Zinc* in lieu of zincum. Although the production of metallic zinc in Europe is attributed to Marggraf who successfully reduced calamine in the presence of charcoal in 1746, commercial production of zinc in Europe was already started independently in 1743 when William Champion (1709-1789) established a zinc smelter using a vertical retort technique in England. William's brother, John, patented the

calcination process of zinc sulphide to oxide in 1758. This became the basis of zinc production from sulfidic ores that is still applied commercially today [13].

The deliberate manufacture of ZnO powder by oxidation of Zn metal was discovered by a German chemist, Cramer, in the mid-1700s and a white pigment was produced in France by these means from 1781 onwards by Courtois de Dijon [24]. However the pigment lacked opacity until 1834 when a British company called Winsor & Newton (founded in 1832 and still running) developed a method to increase the opacity of zinc oxide by calcination [25]. This pigment was then named "zinc white" or "Chinese white" indicative of the source of zinc. In England the first patent on zinc oxide pigment was registered in 1840 to Henry Philip Rouquette followed by other patents in 1846 and 1849. Leclaire and Barruel of France registered the first US patent of its kind in 1850 for a process that is still known as "French Process". The use of this white pigment then spread rapidly [26]. The new pigment competed with "white lead" (basic lead carbonate) because it did not darken in the presence of sulfurous gases and had better hiding power [24, 27], **Figure 1.2**. In the US at the same time (after 1850), Americans were improving their processes and this can be noticed from the number of registered patents. Among those, in 1855, Samuel Wetherill of the New Jersey Zinc Company was granted patents for the improvement of processes for the production of zinc white by reducing zinc ores. This process became known later as the 'American process'. He developed a roasting furnace in which a grate was charged with coal and then covered with a mixture of zinc ore and anthracite coal known as pea-coal. Zinc was reduced by the partial combustion of the coal and re-oxidised at the furnace exit [28, 29]. The French and American processes will be explained in detail later. A major development during the second half of the nineteenth century was the use of ZnO in rubber to reduce vulcanisation process times. Zinc oxide had been used as a reinforcing agent in rubber until 1912, when it was replaced by carbon black. With the discovery of the first organic accelerator for vulcanisation by Oenslager in 1906, zinc white found a new application as an activator in these materials [24, 30]. Today, the rubber industry consumes a significant proportion of the ZnO produced. This is explained in detail below.

Figure 1.2. Advertisement label for zinc oxide, 1868. (USA Library of Congress. http://www.loc.gov/pictures/item/2006679062/ Reproduction Number: LC-USZ62-51233).

1.3. Synthesis

1.3.1. Background

Zinc oxide is produced mainly by three distinct processes: directly oxidising zinc metal, or reduction of an ore to zinc metal followed by controlled re-oxidation or, to a far lesser extent, precipitation of the oxide or a carbonate from an aqueous solution followed by calcination. Not surprisingly, there is a close industrial and commercial relationship between zinc metal and ZnO. Zinc is the fourth most widely used metal in the world after iron, aluminum and copper [31]. It's the 27th most abundant element in the Earth's crust and is 100% recyclable. Approximately 70% of the world zinc production originates from zinc ores and 30% from recycled or secondary zinc sources such as zinc ash [32].

The most common zinc production process is from sulfidic ores using the hydrometallurgical roast-leach-electrowinning method [31], which accounts for around 80% of primary zinc production in the world [33]. This is quite energy-intensive with an energy consumption of ~15 GJ per ton of zinc, 80% of which is used during electrolysis

[31]. Obviously, these costs carry over to any ZnO that is produced from metallic zinc. Therefore, the price of the oxide is sometimes reckoned as the LME (London Metal Exchange) price of the metal plus some additional sum to account for the cost of manufacturing the oxide. Global annual zinc production in 2009 was more than 11 million metric tons [34].

Of the order of one million tons of ZnO is produced annually at present [35], **Figure 1.3**. Between 50% to 60% of the ZnO is used in the rubber industry [24, 35, 36] where it is normally added at between 3 to 5 parts per hundred (phr) rubber [37, 38]. Global annual rubber output was ~25 million tons in 2010 [39], about half of which is consumed by the tire industry [35]. A typical passenger tire contains of the order of 100 g of ZnO.

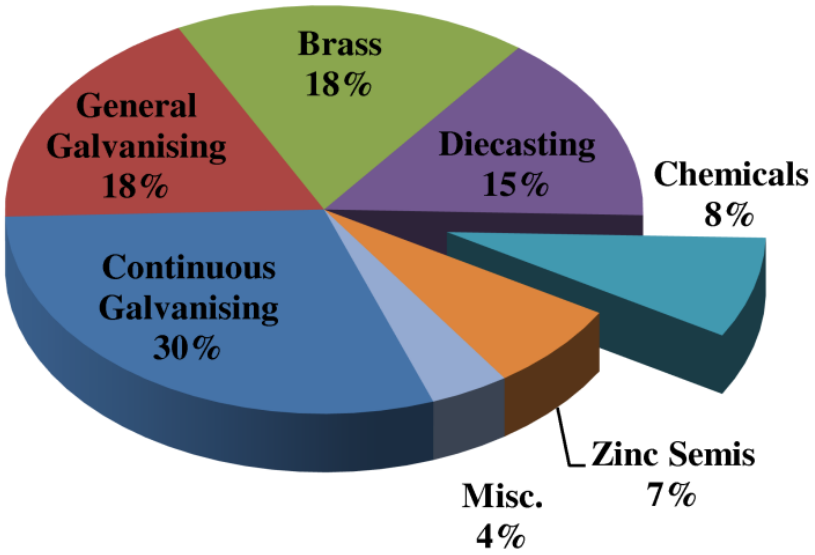

Figure 1.3. Chart showing the various uses of zinc metal. Zinc oxide is the main chemical produced from zinc metal. Compiled using data from diverse sources.

It is important to note the intertwined relationship between the ZnO and Zn industries: besides the close relationship in price, the raw materials also cross over. For example around 50% of zinc metal is consumed in hot-dip-galvanisation and between 5-15% of the of zinc metal charged to galvanising baths is collected again as zinc ash or dross, and this is an important feedstock for the production of ZnO [40]. Other industries that generate zinc-containing wastes are casting, smelting, and scrap recycling, and electric arc manufacture of steel from scrap. These wastes may contain from 10 to 96% total zinc in the form of metallic zinc, zinc hydroxy-chloride (such as

simonkolleite) and ZnO. It is estimated that more than 80% of available recyclable zinc-containing wastes are recycled, usually by hydrometallurgical or pyrometallurgical processes [32, 41-43].

There is a very large variety of zinc-containing materials available as feedstock and therefore, correspondingly, a large number of possible processing technologies. From an economic perspective, the synthetic processes for ZnO may be divided into two groups: low cost bulk industrial methods and high cost laboratory or pilot-plant scale methods. The main technological differences between the various production methods involve the zinc precursors and the process temperatures, the unit operations used and, of course, the scale at which they are carried out. In addition, an extremely wide range of laboratory or pilot-scale techniques have been reported but very few of these are of actual commercial interest.

1.3.2. Industrial production methods

Industrially, most ZnO is produced by pyrometallurgical methods (e.g. the indirect process, the direct process, or spray pyrolysis) or by hydrometallurgical methods. Zinc oxide can also be produced as a by-product of some chemical reactions such as in the production of sodium dithionite. Generally, the selection of the production process is based on the zinc-containing raw material to be consumed. Each process produces grades of ZnO with relatively different properties and hence different applications.

The largest proportion of ZnO is produced by the indirect (French) process. The direct (American) process accounts for the next greatest share followed by the hydrometallurgical processes, which generally exploit zinc-containing wastes [24]. Each of these methods is discussed below. The formal specifications of the major types of ZnO available industrially are listed in **Table 1.1**. The different grades of ZnO powder are also commonly referred to in the trade using somewhat vaguely defined terms such as “gold seal”, “white seal”, “green seal” and “red seal”, with purity decreasing in the order listed (see Section 1.4.4).

Table 1.1. Typical properties of different grades of zinc oxide according to ASTM D4295-89 [44]. Reproduced with permission, from ASTM D4295-89 (2005) Standard Classification for Rubber Compounding Materials-Zinc Oxide, copyright ASTM International, 100 Barr Harbor Drive, West Conshohocken, PA 19428.

Property	ASTM Method	American (direct) type	French (indirect) type			Secondary Types		
			Class 1	Class 2	Class 3	Chemical	Metallurgical	
							Class 1	Class 2
Zinc oxide (%)	D3280	99.0	99.5	99.5	99.5	95.0	99.0	99.0
Lead (%)	D4075	0.10	0.002	0.002	0.002	0.10	0.10	0.10
Cadmium (%)	D4075	0.05	0.005	0.005	0.005	0.05	0.05	0.05
Sulfur (%)	D3280	0.15	0.02	0.02	0.02	0.15	0.02	0.02
Heat loss at 105 °C (%)	D280	0.25	0.03	0.25	0.25	0.50	0.25	0.25
Sieve residue, 45 μm (%)	D4315	0.10	0.05	0.05	0.05	0.10	0.10	0.10
Surface area, m^2/g	D3037	3.5	9.0	5.0	3.5	40.0	5.0	3.5

Pyrometallurgical synthesis

- ***The indirect (French) process***

The indirect, so-called "French process", was developed between 1840 and 1850 to meet a demand for ZnO for use in paints. The first US patent was registered in 1850 to Leclaire and Barruel of France (**Figure 1.4**) [24, 45]. Zinc metal is the starting material in this process. A heated crucible containing zinc may be covered with a lid to pressurise the zinc vapor. In the temperature range of 1230-1270 °C, zinc vapor has a pressure of 0.2 - 1.1 MPa (zinc melts at 420 °C and boils at 907 °C). When the orifice cover is removed, zinc vapor streams into the atmosphere with a calculated nozzle speed of 8-12 m/s resulting in rapid oxidation and a greenish white flame with a length of ~30 cm and temperature of 1000-1400 °C, **Figure 1.5**. A temperature drop from the combustion temperature to about 500-800 °C within ~5 seconds between the crucible and suction hood is the main cause of non-uniform growth conditions [46]. Burner flame temperature can be controlled by the ratio of fuel to air and can be set at low oxidation state (around 1000 °C) or high oxidation state (around 1400 °C).

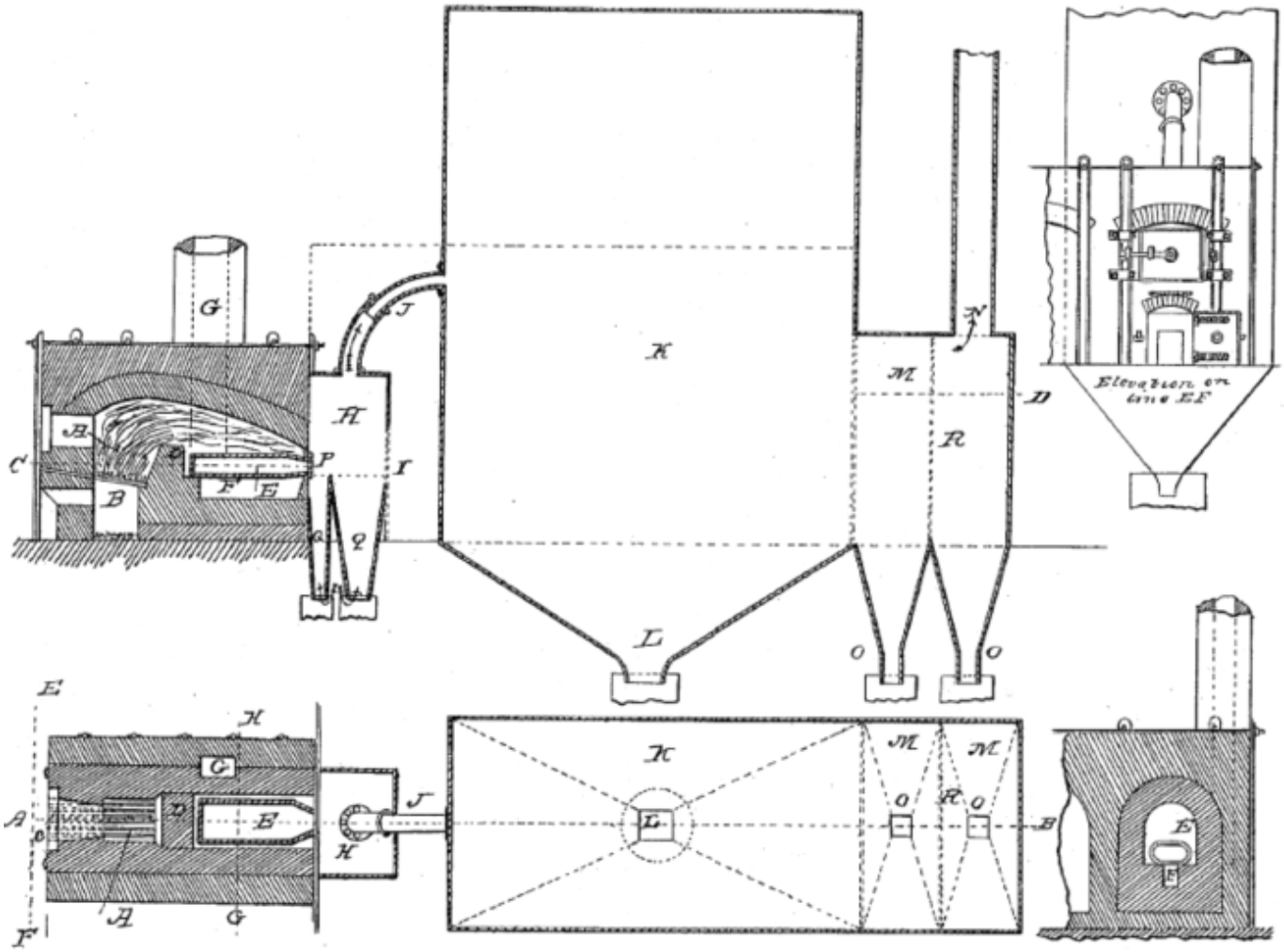

Figure 1.4. Schematic of the indirect process to produce ZnO reproduced from the 1850 US patent of Leclaire and Barruel [45].

Figure 1.5. Photograph of a French process drum in operation, by permission from PT. Indo Lysaght, Indonesia.

The ZnO powder formed by combustion then enters a 50-300 m long cooling duct (which depends on the furnace design) [47] before it is collected in the bag-house at a temperature below 100 °C by a system of vertical fabric bags and fractionated according to particle size using vibrating hopper sieves [37]. A typical bag-house dust collector is shown in **Figure 1.6** [48]. The French process is widely considered to be the fastest and most productive industrial method to mass-produce ZnO [47] but, as will be shown, the product it makes is not optimum for all applications.

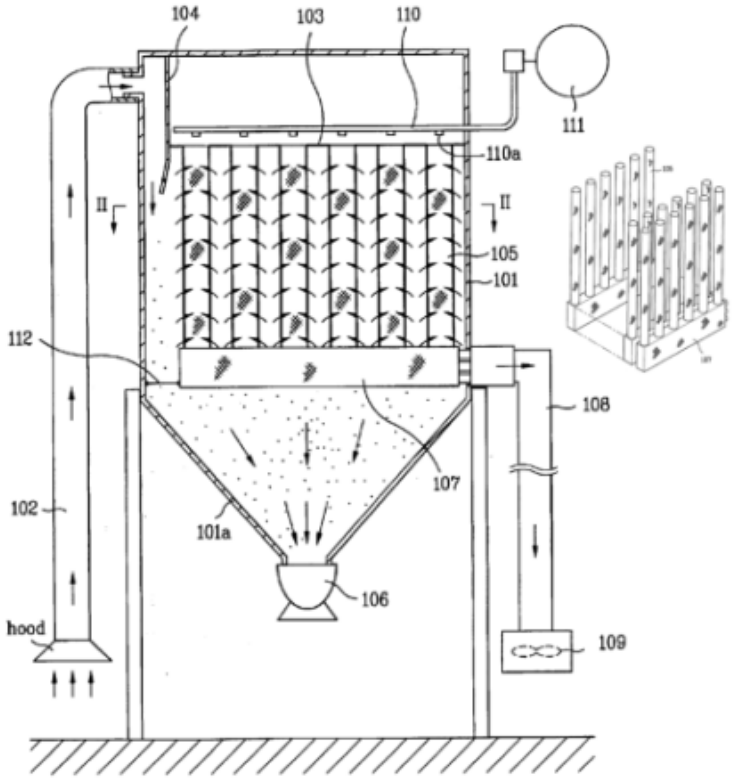

Figure 1.6. A typical bag-house design reproduced from the US patent 6786946.

The quality of the ZnO depends on the precursors used. For instance, for the production of "gold seal" or pharmaceutical grade ZnO, SHG (special high grade, 99.99% Zn) zinc metal is used whereas ordinary HG zinc (99.95%) may be adequate to produce the ZnO used in the rubber industry. Other zinc-containing feed materials such as galvaniser's dross, die-casting alloys or zinc ash may also be used for less demanding applications. However, if metal residues are to be used then various liquid or vapor-phase separation techniques may need to be applied first to eliminate Cd, Pb, Fe, and Al before the Zn is oxidised. Theoretically, the maximum yield of ZnO in the French process is 1.245 tons per ton of zinc used; but in practice ZnO recovery of around 1.2 tons is obtained when using SHG zinc as the raw material and even less if zinc dross (85-95% zinc content) is used as feedstock. Zinc ash can contain up to 30% metallic zinc with the balance composed of ZnO and zinc hydroxy-chloride, however, the metallic content must first be separated from the ash by physical separation processes such as rotary mills and sieving or thermo-mechanical devices before it can be used in the French process.

There are generally two techniques applied for the separation of metallic zinc from the ash content. In the conventional way, zinc metal is physically separated from the ash in the rotary mills. Metallic zinc in the mill acts similar to balls in the ball-mill and crushes the ash. At the outlet the metallic zinc is separated from the ash content by sieving. In a different technique, the raw material is processed in a thermo-mechanical unit. Heating the mixture above the melting point of zinc metal in a rotary drum results in recovery of molten zinc from the mixture via a tapping point. Molten zinc is then collected in a mould (see **Figure 1.7**).

Free zinc metal is separated from the ash content and is used in the pyrometallurgical processes. The remaining ash is then processed in the hydrometallurgical units as is explained in the Hydrometallurgical section later.

Zinc oxide produced by the French process can have high purity (>99%) if high purity zinc is used a feedstock. However, the product may contain traces of zinc metal, the amount of which is inversely proportional to particle size and which may render it unsuitable for some applications [44, 49, 50].

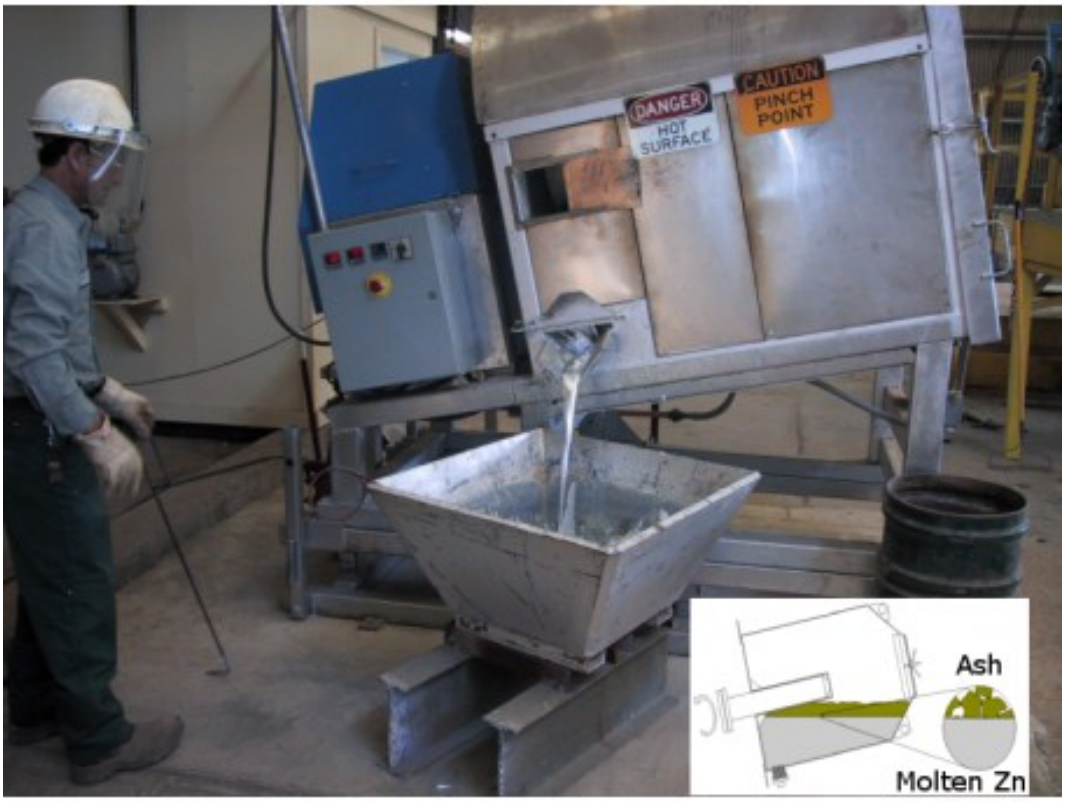

Figure 1.7. The Metaullics Zinc Recovery (MZR) system for the separation of metallic zinc from zinc ash. From Pyrotek technical documents [51, 52].

The particles are nodular in shape [44, 50] and the individual ZnO crystallites are 30-2000 nm in size. Scanning electron microscope images of typical French process ZnO are shown in **Figure 1.8**. The surface area of French process ZnO is generally 3-5 m^2/g but can reach 12 m^2/g by carefully controlling combustion conditions such as air flow and flame turbulence [24, 35] or the distance between the suction hood and nozzle (which affects the air velocity). If the flame temperature increases, the specific surface area will drop. By increasing the excess of reactant air (oxygen) by making a better circulation of air or forced flow of compressed air in the combustion zone, ZnO quenching becomes faster and finer particles can be achieved, resulting in higher specific surface area. Superheating the zinc vapor also results in finer ZnO particles. The purity of the ZnO product is solely a function of the composition of the zinc vapor.

Some relevant standards for ZnO produced by this route include ASTM D4295-89, a standard for rubber compounding [44], ISO 9298:1995(E), another rubber compounding standard [53], which also indicate the classifications of ZnO by type, and ASTM D79-86 for pigments [50].

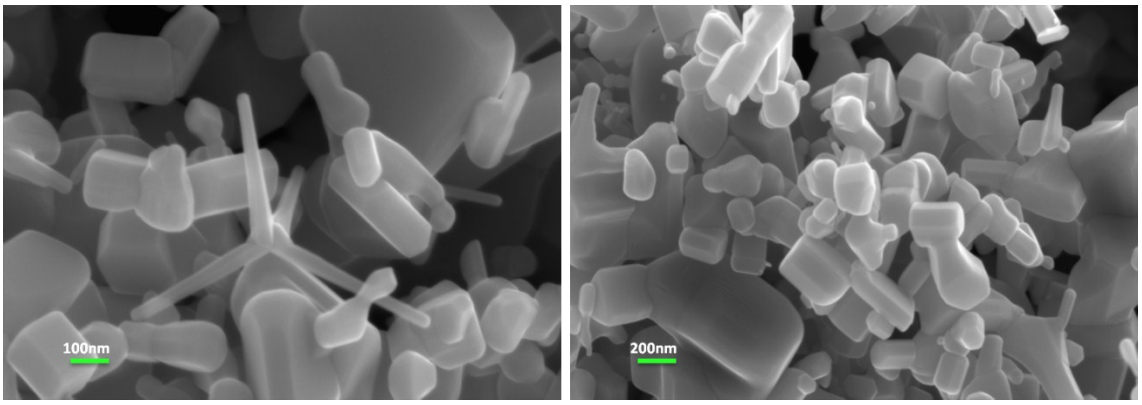

Figure 1.8. SEM images of the French process ZnO (samples from PT. Indo Lysaght, Indonesia; images by Dr R. Wuhrer, University of Technology Sydney).

There are various implementations of the French process. Older technology principally uses a batch process that takes place in a crucible with a long cooling duct, most of which is horizontal. Newer technologies use a semi-continuous process with a vertically-designed cooling duct to save space. A batch is recharged with zinc ingots at approximately four hour intervals whereas in the semi-continuous process a zinc ingot (often 25 kg) is added to the furnace every 6 minutes. The productivity of the semi-

continuous process is often higher than that of the batch process. The semi-continuous system is rarely shut down unless for an overhaul and it is generally very compact. The process flow diagram (PFD) of a basic French process furnace is depicted in **Figure 1.9**.

There are several other variations to the process, the selection of which depends on the feedstock material and local conditions. Graphite or silicon carbide muffle furnaces or retorts are utilised in the most common design, which uses Zn ingots or dross as feed material. The solid ingots may be fed into the furnace either batchwise or pre-melted and fed continuously as a liquid. The retort is generally heated from the outside using a natural gas or oil burner, although electric heating elements (silicon carbide) are in use in some plants [24]. Production capacity is generally around 70-500 kg/h per furnace per batch depending on the furnace size [54].

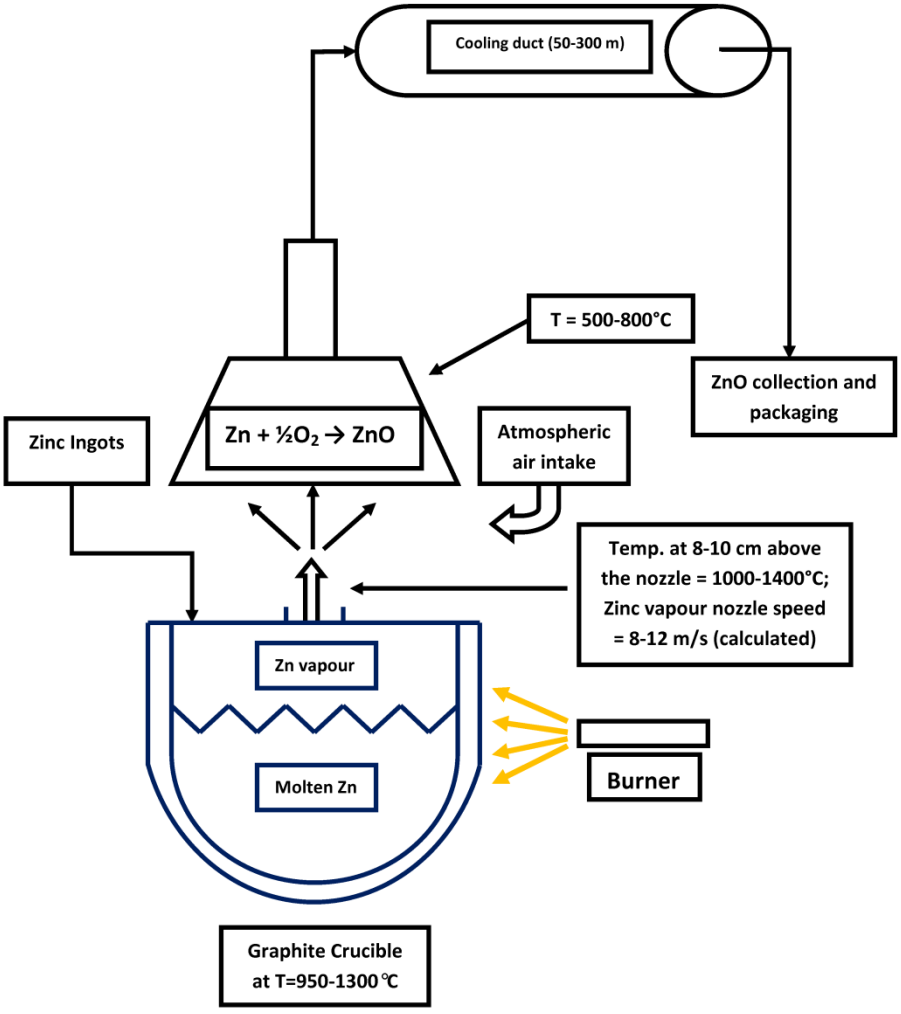

Figure 1.9. Process flow diagram (PFD) of the French process.

In another design, a fractional distillation system (invented by Lundevall from Larvik, Norway in 1960 [55]) is implemented for refining the Zn prior to its combustion to make ZnO. This technique is now referred to as the Larvik distillation technology and is in use by industrial producers of Zn/ZnO such as the multinational Umicore Group [56]. The purification process as depicted in the patent is shown in **Figure 1.10** and includes a furnace with two separate chambers and a distillation column. The raw material (mainly as large blocks of Zn dross) is fed into the melting compartment (**Figure 1.10**, 3a). This compartment is isolated with a partition wall from the second one (**Figure 1.10**, 4a) where zinc is heated by electrical heating elements and boils in the absence of air. These chambers are connected by a submerged opening under the partition wall. Zinc vapor moves towards the condensation/oxidation units. Impurities such as Fe, Pb and Cd remain behind in a set of equipment such as a lead fractional distillation column (**Figure 1.10**, 33a) and are periodically removed [55].

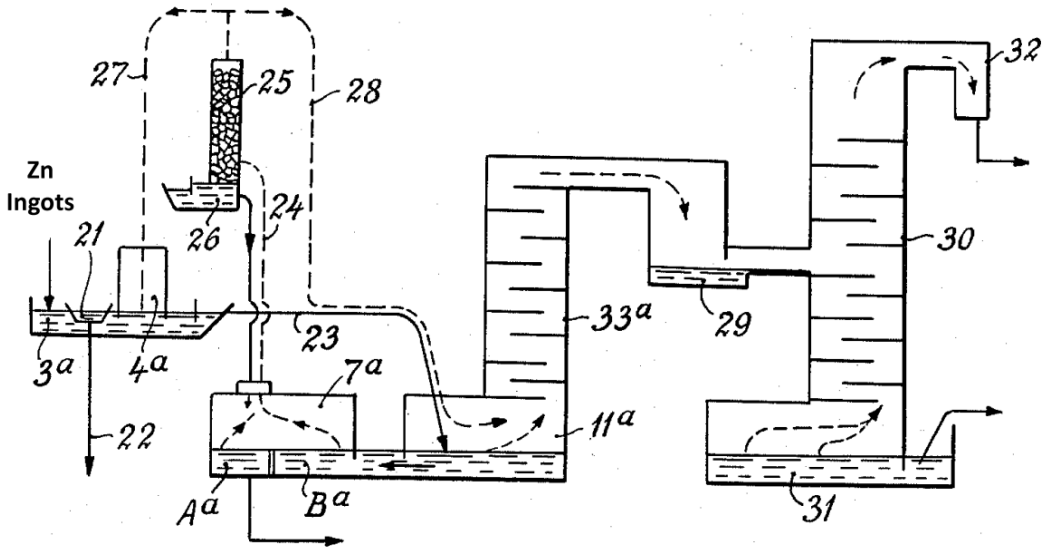

Figure 1.10. Schematic of the Larvik process designed by Lundevall [55].

The fractionation processes work because the relatively large differences in boiling point between Cd, Pb, Zn and Fe allow the Zn to be separated by fractional distillation, see **Figure 1.11**. Oxidation of the distilled zinc results in high quality ZnO [24]. Zinc has the lowest melting and boiling point among its preceding metallic elements in the first transition series; but with a boiling point (907 °C) that is higher than Cd (765 °C) but lower than Pb. Cadmium that is usually found in zinc scrap sources can be

fractionated in early stages of the run. Lead can also be a problematic element: its melting point is only 327 °C but its boiling point of 1749 °C is well above that of zinc. At temperatures above the boiling point of zinc, lead exists in the molten form. Therefore along with zinc vapor, lead mist can enter the vapor phase and must be condensed in a lead trap (e.g. splash condenser) before the zinc vapor is oxidised [55, 57].

The Larvik process is quite good for separation of lead from zinc and is therefore useful for high Pb-content raw materials. However its drawback is that high cadmium-content raw materials such as Prime Western grade recycled zinc cannot be processed in this design since all the cadmium will end up in the final product. To address this issue another design is developed in the USA, which is based on two fractionation columns (the 1st for Cd and the 2nd for Pb) in series. Zinc vapour is oxidised at the discharge from the Pb column [35].

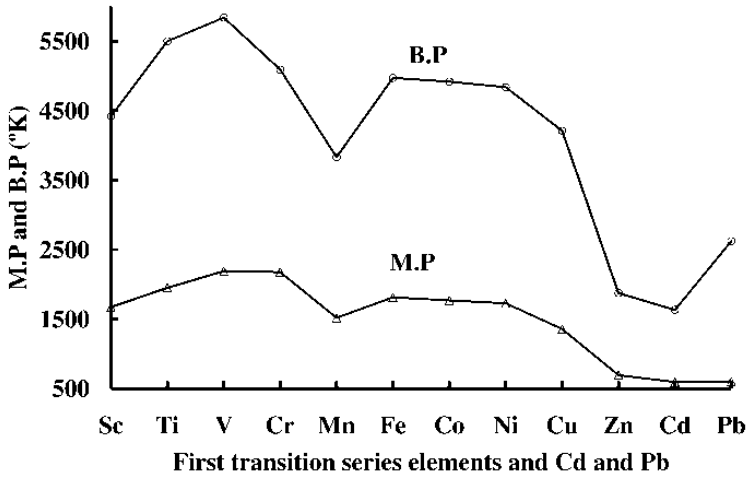

Figure 1.11. Graph of melting and boiling points of the first transition series elements, Cd and Pb.

Another technique utilises smelting in rotary kilns to minimise fuel consumption. Zinc charges (e.g. bottom dross from galvanisers) are added continuously into the rotary kiln. Energy released from combustion of Zn vapor into ZnO is used to melt and vaporise the zinc from the raw material. However the yield of this process is lower than alternative routes [24, 35, 58]. A typical zinc oxide rotary kiln is shown in **Figure 1.12**.

Figure 1.12. Zinc oxide rotary kiln. Picture by Henan Bailing Machinery Co. [58].

- ***The direct (American) process***

The direct, so-called "American" process [28, 29], makes use of a primary feedstock containing a mixture of oxidised zinc-containing raw materials (directly obtained from ore) and carbonaceous reducing agents. Zinc metal is produced from the charge by reduction at elevated temperature and is vaporised. In the case of ZnO production, the vapor moves into a combustion chamber where it is re-oxidised in a similar manner to that used in the indirect process. Finally, the oxide is collected in a bag-house [24, 37]. The distinction between the direct and the indirect processes is only the feedstock; in the indirect process zinc metal is used as the feedstock whereas in the direct process primary feedstock is applied.

Four interdependent Reactions 1.1 - 1.4 are important in the formation of the zinc vapor:

$$ZnO_{(s)} + C_{(s)} \rightleftharpoons Zn_{(g)} + CO_{(g)} \quad 1.1$$

$$ZnO_{(s)} + CO_{(g)} \rightleftharpoons Zn_{(g)} + CO_{2\,(g)} \quad 1.2$$

$$C_{(s)} + O_{2\,(g)} \rightleftharpoons CO_{2\,(g)} \quad 1.3$$

$$CO_{2\,(g)} + C_{(s)} \rightleftharpoons 2CO_{(g)} \quad 1.4$$

Zinc oxide is reduced in Reactions 1.1 and 1.2. The resultant CO_2 is reduced by carbon to form CO again according to Boudouard Reaction 1.4, providing more reductant for the reaction with ZnO [59].

Under standard state conditions, ΔG for Reaction 1.1 becomes negative for T > 940 °C (point A on **Figure 1.13**), and for T > 1317 °C for Reaction 1.2 (point B on **Figure 1.13**). It is critical to keep the temperature as high as possible to prevent the premature occurrence of the re-oxidation reaction implied by the reverse of Reaction 1.2. Another important factor along with the negative Gibbs free energy to be considered for reduction Reaction 1.2 is the equilibrium constant (K_{atm}), which increases by temperature. For instance at 850 °C its value is only 0.003. As the temperature rises to 1250 °C, its value reaches 0.54 [60].

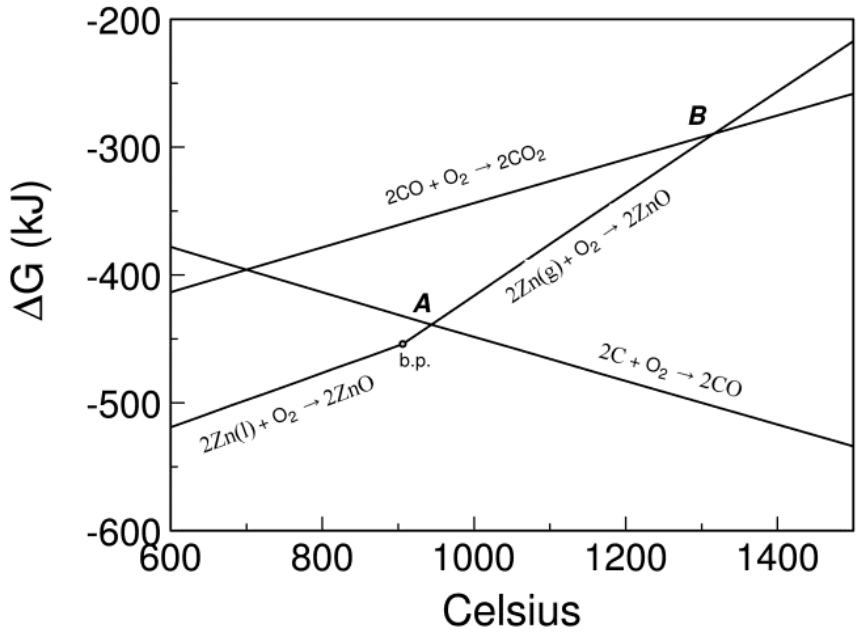

Figure 1.13. Ellingham diagram showing free energy change of indicated reactions as a function of temperature, calculated using standard state thermodynamic data for the species.

Fortunately, under conditions of increased p_{CO}, the re-oxidation temperature will be lowered, **Figure 1.14**. Reactions 1.3 and 1.4 have controlling effects on the spatial location of reduction and re-oxidation in the plant. An excess of carbon fuel controls the amount of CO necessary for reduction according to Boudouard reaction. For the carbo-reduction of metal oxides to be feasible, there should be a minimum ratio of CO to CO_2. This critical ratio shows the competition of Reactions 1.3 and 1.4. For example, at 1100

°C the ratio should be around 10 for the reduction stage (see **Figure 1.14**). Therefore Zn does not go back to ZnO in the reduction zone as long as there is an excess of carbon and/or the critical ratio of CO/CO_2 for that temperature is exceeded.

A variety of zinc-containing raw materials can be used, including zinc ores (oxidic or sulfidic), zinciferous materials and flue dusts, lead blast furnace slags, mill slimes, electrolytic-zinc leach residues, skimmings from casting furnaces, off-grade zinc oxides and zinc ash from hot dip galvanisation. Lead and chloride can be present in zinc ash and must be removed prior to the manufacture of ZnO.

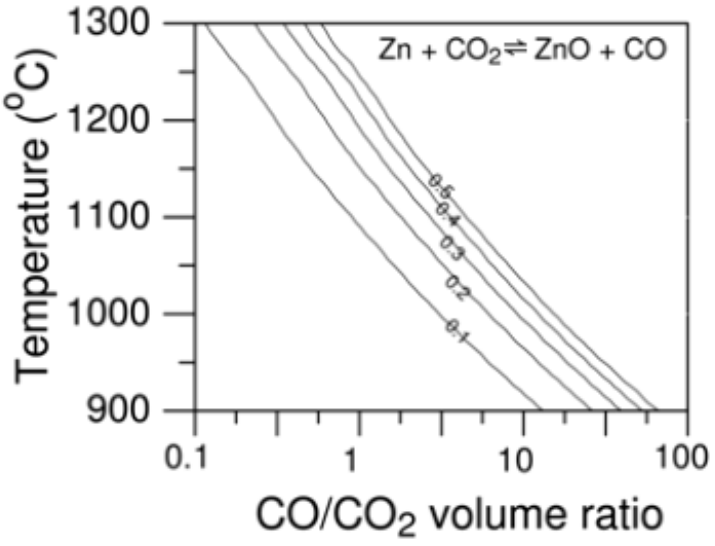

Figure 1.14. Effect of temperature and gas composition on the partial pressure of $Zn_{(g)}$ (in atm). A decrease in temperature or CO/CO_2 causes a reduction in p_{Zn} due to increased oxidation. Recalculated and redrawn after Schoukens *et al.,* [61]. Atmospheric pressure is assumed.

Because of the generally lower purity of the feed material and the carbonaceous reductant, the final product is generally of lower quality compared to that produced by the indirect method and tends to have widely varying chemical properties and physical characteristics [44, 50, 62]. It may also contain traces of lead and cadmium [63]. Traces of sulfur are often present in ZnO produced by the American process (originating from the raw material) whereas ZnO produced by the indirect process is essentially sulfur-free [44, 64]. Sulfur can be useful in some applications including rubber manufacturing but can be a harmful impurity in many other products.

The specific surface area of direct process ZnO is generally 1-3 m^2/g. Standard ASTM D79-86 defines the properties expected for use as a pigment and shows that ZnO produced from the French process has higher minimum purity (>99%) than material produced by the American process (>98.5%). A maximum moisture content of 0.5% in these grades is also of importance [50]. In general, direct process ZnO is used in the paint and ceramic industries rather than for rubber [35].

Stationary-grate furnaces, moving-chain-grate furnaces, electrothermic furnaces and rotary kilns, including Waelz kilns can be used [65]. Recovery in rotary kilns is higher than in grate furnaces [65]. In the EU, only rotary kilns, known as Waelz kilns, are now used for the direct process. These kilns can be charged by a wide variety of feed materials, generally with a zinc content of between 60 and 75%. A Waelz kiln rotates at 0.4 to 0.7 rpm and is inclined about 2%. As a result, the solid feed travels slowly in the kiln with a residence time of about 8-10 hours. By the time the charge reaches close to the discharge end, nearly all zinc is volatised leaving a slag behind. The volatilised gases, containing zinc vapor and CO, pass into a combustion zone where oxidation is completed by the suction of secondary air and, finally, ZnO is then cooled down and collected in bag filters. This system is designed to minimise fuel consumption as combustion reactions provide most of the energy needed in the reduction zone. A typical process flow diagram of this process is depicted in **Figure 1.15**.

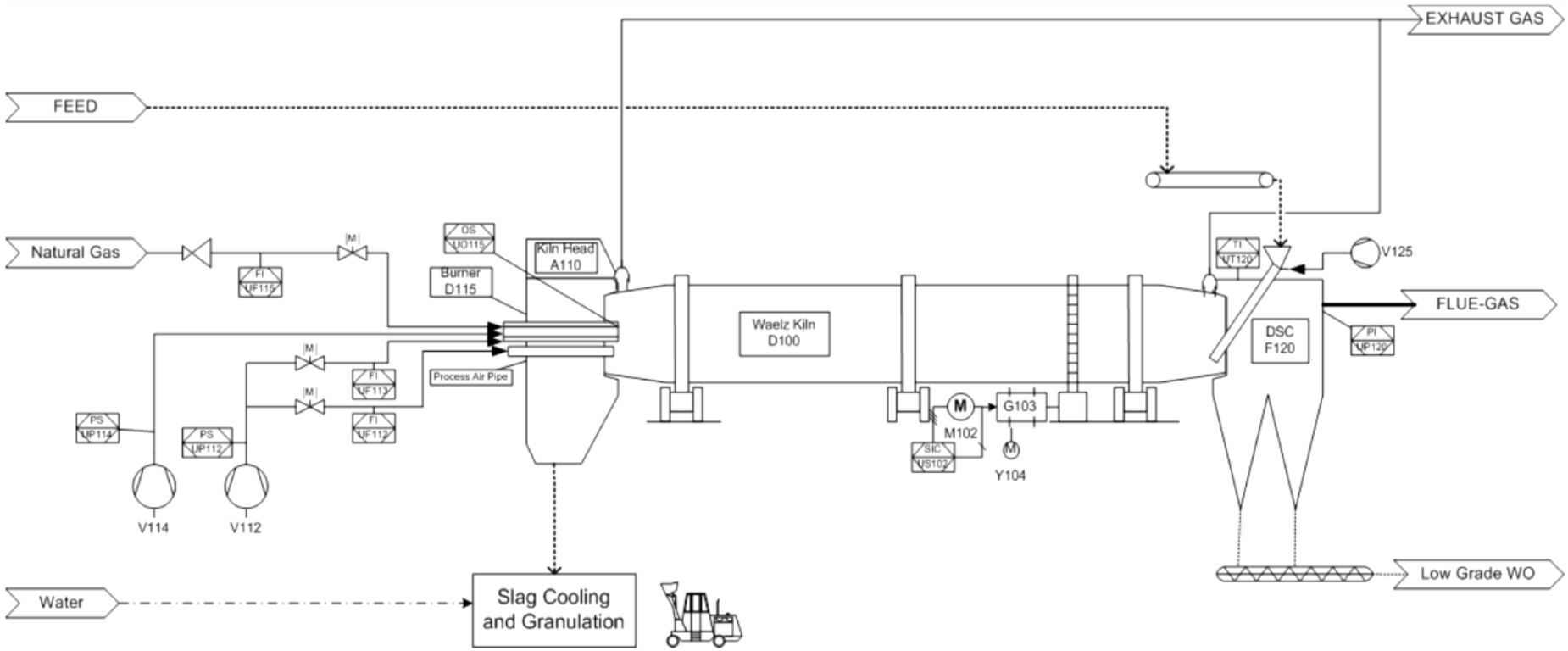

Figure 1.15. Typical process flow diagram of the Waelz process with permission from ValoRes GmbH [66]. Note: in the American process the 'process air pipe' shown in the PFD above is not normally used (private communication with Dr Juergen Ruetten, ValoRes GmbH).

The Waelz kiln shown in **Figure 1.16** can be divided into 5 Sections along its length (e.g. 55 m long). The solid feed inlet is located at 0% of the length of the kiln and the slag outlet is located at 100%. Flue gas flows counter-current to the solid charge and exits the kiln into the dust settling chamber (DSC) at the feeding side. Section 1 is the drying zone. Preheating and coke combustion zone is located at Section 2. Section 3 is the pre-reaction zone followed by section 4, which is the main reaction zone and the longest one. Finally Section 5 is the slag forming zone [66].

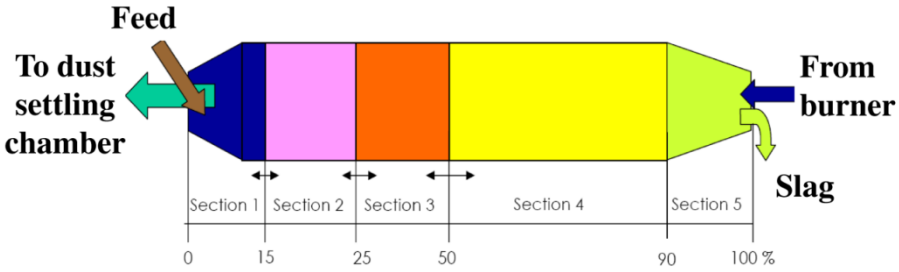

Figure 1.16. Waelz kiln Sections [66].

- ***The spray pyrolysis process***

In this process a solution of thermally-decomposable zinc-bearing salt is atomised and then thermally decomposed to ZnO in a spray pyrolysis tower, or similar apparatus. A high specific surface area is attainable, often > 12 m^2/g [49]. Material produced by this method is homogenous with uniform particle shape, narrow size distribution and controlled purity [67, 68]. Suitable precursors are aqueous solutions of a zinc salt such as zinc acetate, formate, carboxylate, nitrate or sulphate. Organic salts of zinc may be preferred to inorganic salts because of their lower decomposition temperatures. For example, the decomposition temperatures of zinc acetate, formate and sulphate are 237 °C, 553 °C [69] and 680 °C [49] respectively. However, selection of the precursor also depends on the cost, preprocessing solubility and stability, reactivity and toxicity [70]. In general, higher temperatures and more concentrated solutions result in lower specific surface area of the as-synthesised ZnO. For example at 500 °C a specific surface area of 35.6 m^2/g is reported to be obtained from a 32% w/v zinc acetate solution, but this drops to 12.5 m^2/g when the temperature is increased to 850 °C (see **Figure 1.17**). The bulk density of the as-produced ZnO powders is very low around 100 g/L [49]. A process flow diagram of the spray pyrolysis method is shown in **Figure 1.18**.

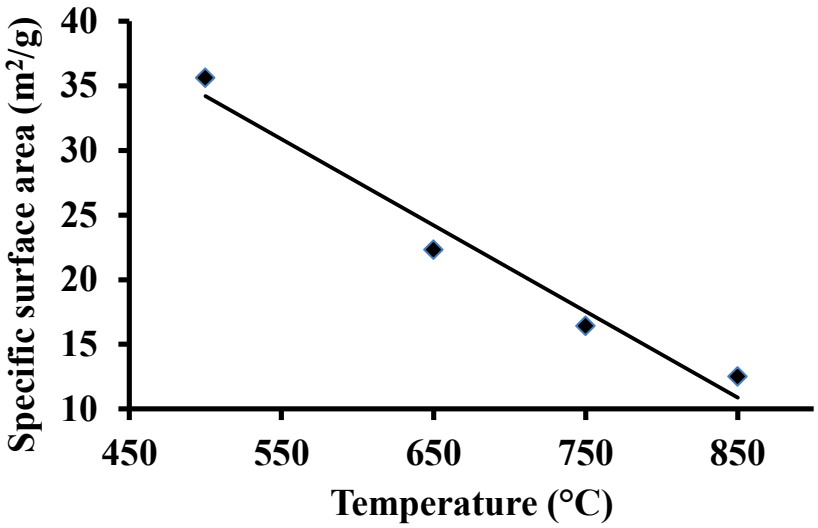

Figure 1.17. Specific surface area of ZnO *vs.* pyrolysis temperature using zinc acetate dihydrate 32.6% (w/v) aqueous solution [49].

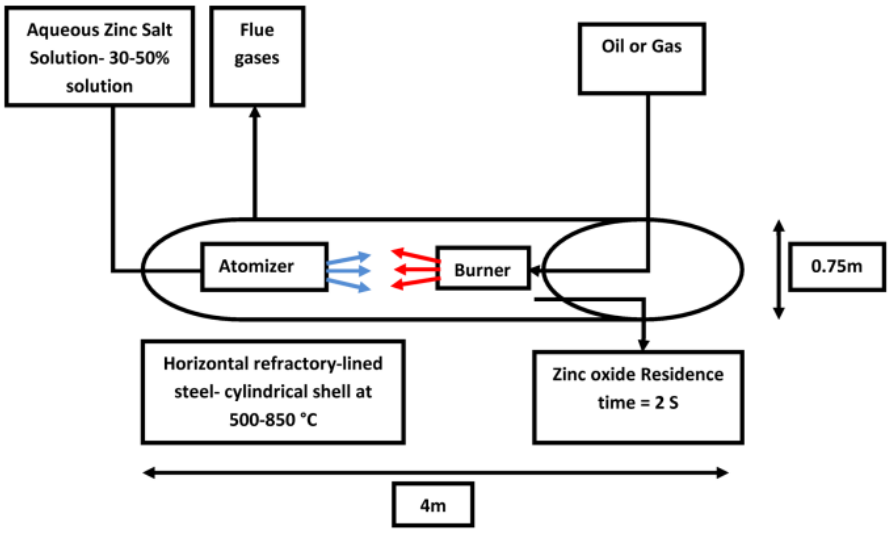

Figure 1.18. Process flow diagram (PFD) of spray pyrolysis of aqueous solution of zinc salts to ZnO.

A typical flame aerosol reactor for the production of nanoparticles consists of a droplet formation unit (atomiser), a heat-supply unit and an oxidant for the flame-assisted combustion (burner) and, finally, a filtration unit. The precursor composition, droplet size, flame temperature and also residence time in the reactor are controlling factors for the formation, growth and properties of nanoparticles of ZnO. Various designs for atomisers can be applied such as ultrasonic and gas-assisted pressurised atomisers [70].

- ***Zinc slag-fuming***

Slag processing is an important technology in the extraction of non-ferrous metals [71]. In the conventional zinc slag fuming process, metallurgical wastes such as slag from lead blast furnaces, or electric arc furnace dust (EAFD) are fed (in molten or solid form) continuously or batch-wise to a fuming furnace (generally DC arc) together with air and a reductant such as pulverised coal through tuyeres to reduce and volatilise the zinc present in the slag. The conventional slag fuming is carried out batchwise in water-jacketed furnaces [71, 72]. This process is widely used by the Cominco smelter in British Columbia, Canada for the treatment of slag produced during production of lead bullion [73]. Similar process, but in a pilot-plant scale, has been successfully applied by Mintek in South Africa to separate zinc from lead as a Prime Western grade (min. Zn content of 98.5%) in a lead splash condenser similar to that used in the conventional Imperial Smelting process (ISP) [72]. In the alternative routes, rather than condensation of zinc vapour, zinc can be oxidised and recovered as zinc oxide [74]. At the Mintek pilot-plant, before implementation of lead splash condenser unit [72], zinc vapour was combusted to zinc oxide and collected in a bag-house [61]. At Boliden in Sweden, at Rönnskär smelter, a similar fuming process is used to process slag produced from the copper production unit. From this process a range of by-products are produced including a low grade zinc oxide called “zinc clinker” [75]. ScanArc in Norway uses a submerged-plasma slag fuming technology to recover zinc oxide from steel plant dust [76, 77]. Umicore is also licensing this technology through ScanArc [77].

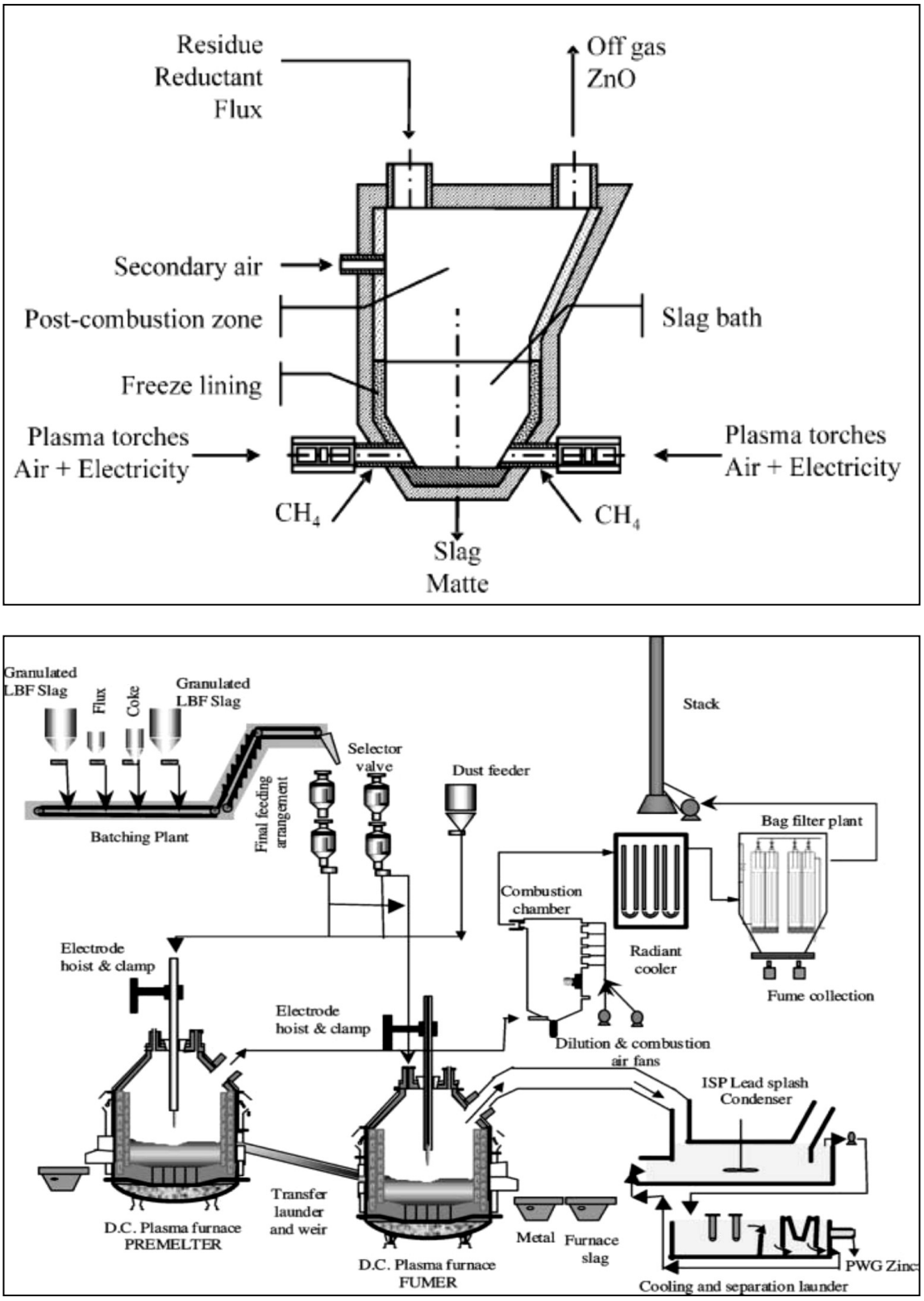

Figure 1.19. Schematics of (left) submerged plasma process [77] and (right) Mintek's Enviroplas process for zinc fuming [72].

Hydrometallurgical synthesis

Hydrometallurgical processes currently dominate the production of zinc metal [13] but are not as popular for the production of ZnO. One reason is that the ZnO they produce is often less pure and may contain a significant amount of water; another is that the particle morphology may be irregular and porous, unlike the chunky, crystalline form of the pyrometallurgical grades. On the other hand, hydrometallurgical grades of ZnO are cheaper to produce and may have a high specific surface area and chemical reactivity, which may be desirable in some applications. The term 'active zinc oxide' is widely used to denote ZnO with very high specific surface area and chemical reactivity.

Many of the industrial hydrometallurgical processes for zinc or ZnO production use a significant proportion of zinc-containing wastes such as the zinc ash from hot-dip galvanising plants (**Figure 1.20**) as input materials due to their availability and relatively lower prices.

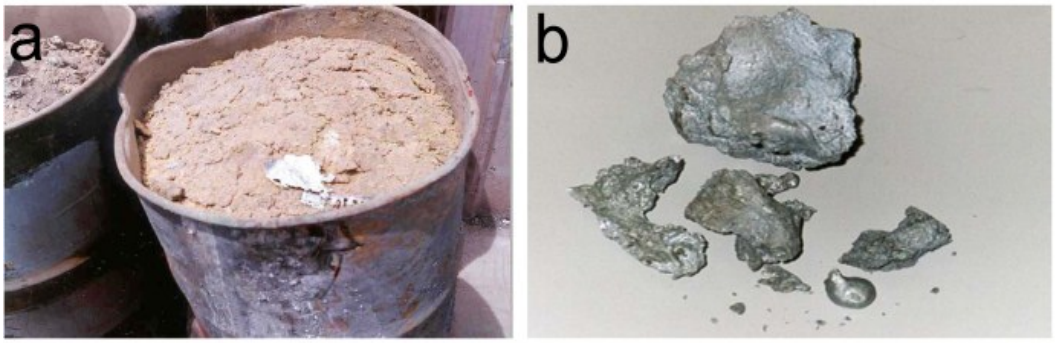

Figure 1.20. (a) Zinc ash; (b) zinc dross. © Commonwealth of Australia 2001 [78]. Photographs courtesy of Environment Australia.

In these processes, zinc-containing compounds are precipitated from aqueous solution, separated and then converted to ZnO by calcination. Direct precipitation of ZnO from aqueous solution is also possible [62, 79]. Zinc oxide produced via wet chemical processes can be categorised into three main groups: (1) ZnO produced as a by-product of the production of sodium dithionate, (2) ZnO made by the reaction of a zinc salt such as zinc sulphate and a base such as ammonium hydroxide or sodium hydroxide, followed by calcination or drying of the $Zn(OH)_2$ or ZnO produced, and (3) ZnO produced by a two-step reaction of zinc salts and carbon-containing bases such as sodium carbonate, ammonium bicarbonate or urea followed by calcination or alkaline treatment of the resultant basic zinc carbonate.

ZnO as a by-product from other processes

Zinc oxide produced as a by-product of an aqueous chemical reaction is considered to be a 'secondary type' according to the ASTM D4295 [44]. One of the main hydrometallurgical sources of ZnO is as a by-product in the synthesis of sodium dithionite ($Na_2S_2O_4$) (also known as sodium hydrosulfite) [35]. This substance is used as a reducing agent with major applications in the vat-dying of textiles and in the bleaching of wood pulp. The overall reaction for the production of ZnO from this process is given in Reaction 1.5. In this process zinc dithionite is produced first. Then addition of soda ash or sodium hydroxide to zinc dithionite results in sodium dithionite along with basic zinc carbonate or zinc oxide, respectively.

$$2NaHSO_3 + Zn \rightarrow Na_2S_2O_4 + ZnO + H_2O \qquad 1.5$$

The zinc-containing by-product is then filtered and dried and, in the case of basic zinc carbonate, is converted to ZnO either by calcination or by alkali treatment [80-82]. The specific surface area of this grade is high (>40 m^2/g) and therefore it can be considered as an "active" grade of ZnO.

A schematic of this process is shown in Figure 1.21.

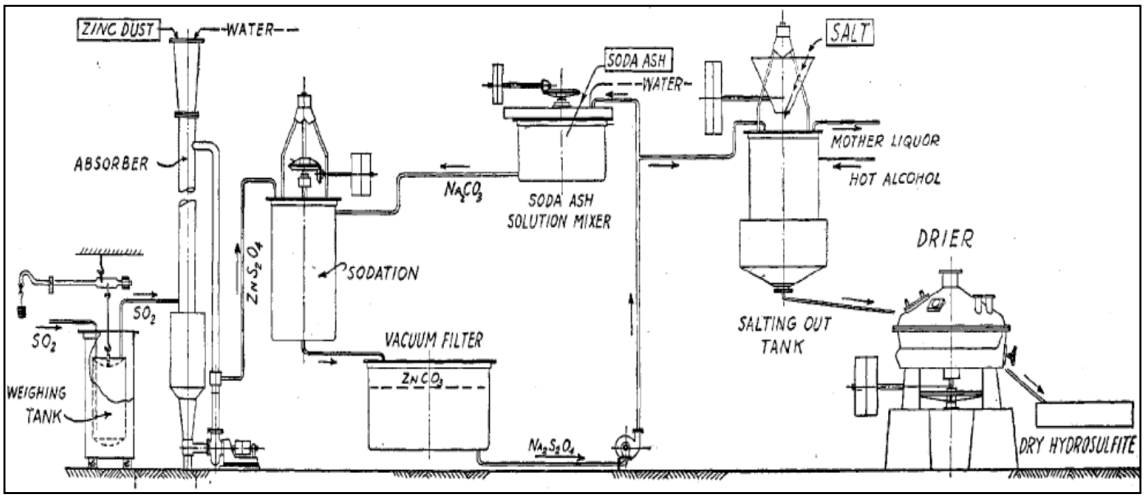

Figure 1.21. Schematic of the sodium dithionite process [83].

Zinc oxide can also be produced in a similar fashion as a by-product of the production of sodium formaldehyde sulfoxylate ($NaHSO_2 \cdot CH_2O \cdot 2H_2O$), which is produced from sodium dithionite.

Production of "active" zinc oxide by decomposition of hydrozincite

"Active" zinc oxide is an important grade of ZnO produced by wet-chemical routes. Descriptions of some variations in the process by which it can be prepared are available in the literature [84-87]. Active ZnO is considered to be superior to "white seal" ZnO (French process) in rubber compounding and rubber applications in terms of tensile strength, hardness and modulus at 300% [86]. A typical two-step process for its production is based on the formation and then decomposition of a basic zinc carbonate known as hydrozincite:

$$5ZnSO_4 \cdot 7H_2O + 5Na_2CO_3 \rightarrow Zn_5(CO_3)_2(OH)_6 + 5Na_2SO_4 + 3CO_2 + 32H_2O \quad 1.6$$

$$Zn_5(CO_3)_2(OH)_6 + \text{Heat} \rightleftharpoons 5ZnO + 2CO_2 + 3H_2O \quad 1.7$$

The decomposition reaction of hydrozincite is endothermic with standard molar enthalpy of reaction $\Delta H_r^\circ = 187\ \text{kJ mol}^{-1}$ [88, 89] and the reaction proceeds spontaneously only above about 154 °C, **Figure 1.22**. Kanari *et al.,* reported that the apparent activation energy (E_a) of basic zinc carbonate in the temperature range of 150-240 °C is in the range of 130-150 kJ/mol [90]. This was based on isothermal TG tests.

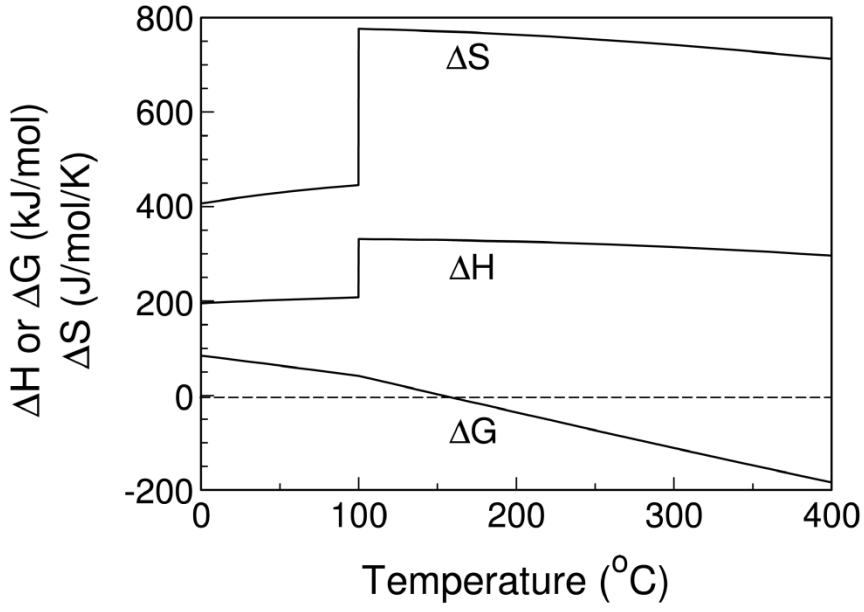

Figure 1.22. Free energy change for reaction $Zn_5(CO_3)_2(OH)_6 \rightleftharpoons 5ZnO + 2CO_2 + 3H_2O$, calculated by the authors using published thermochemical data [88, 89].

The very large specific surface area of "active" ZnO is produced when the CO_2 and H_2O are expelled from the hydrozincite lattice. Furthermore, at these low temperatures the ZnO that is formed from the hydrozincite cannot sinter, so this porosity can be retained. However, as shown in **Figure 1.22**, it is thermodynamically favorable for the ZnO to revert to hydrozincite below 154 °C in the presence of CO_2 and H_2O although the rate of this reaction will depend on the specific surface area of the ZnO. Any ZnO that has been heated to high temperatures during manufacture (such as the pyrometallurgical grades mentioned earlier) will have a relatively low specific surface area and the rate of the reverse reaction will be normally negligible, but material with higher surface area, such as that produced by decomposition of hydrozincite, is susceptible to the reverse carbonation reaction over a time period of weeks or months [91, 92].

The reverse reaction relies upon the formation of a layer of adsorbed carbonic acid ($H_2O + CO_2$), so will also depend on partial pressure of water, p_{H_2O}, and that of CO_2, p_{CO_2}. At a moisture ratio, $p_{H_2O}/(p_{CO_2} + p_{H_2O})$, below 0.1, ZnO shows no weight increase whereas the carbonation reaction occurs quickly at a ratio over 0.35, causing the properties of the ZnO to change significantly. In the intermediate range only a partial reversion occurs [91, 93].

In this author's opinion, the reverse carbonation reaction may be explained by the "shrinking core" model for gas-solid reactions [94]. H_2O is a polar molecule and since zinc oxide surfaces are also polar, the interaction between water molecules and zinc oxide surfaces is more favorable than that of a non-polar carbon dioxide and zinc oxide surface. Thus due to the effect of polarity, water molecules may interact with ZnO available surface sites more effectively than carbon dioxide molecules. In the meanwhile, CO_2 molecules may diffuse in the adsorbed water and form a layer of carbonic acid that can react with ZnO. Therefore this reaction is controlled by the mass of CO_2, which transferred into the absorbed layer of water on ZnO surfaces. Since in normal atmospheric conditions CO_2 is a trace component of the atmosphere, reverse carbonation reaction of ZnO remains partial.

Koga *et al.,* also carbonated zinc oxide under the saturated conditions with water vapor and carbon dioxide (1 atm) for 100 days and successfully converted zinc oxide to basic zinc carbonates at 8 °C and 13 °C [92].

The relevant properties of wet-chemical grades of ZnO, such as specific surface area, porosity, morphology and quality, are variable and depend on the precursors, process conditions and many other factors. An important intrinsic property of the wet-chemical ZnO grades is the presence of abundant, stable, surface hydroxyl groups. TG analysis reveals the presence of these hydroxyl groups up to ~800 °C [79]. A fully hydroxylated structure of ZnO is shown in **Figure 1.23** [8].

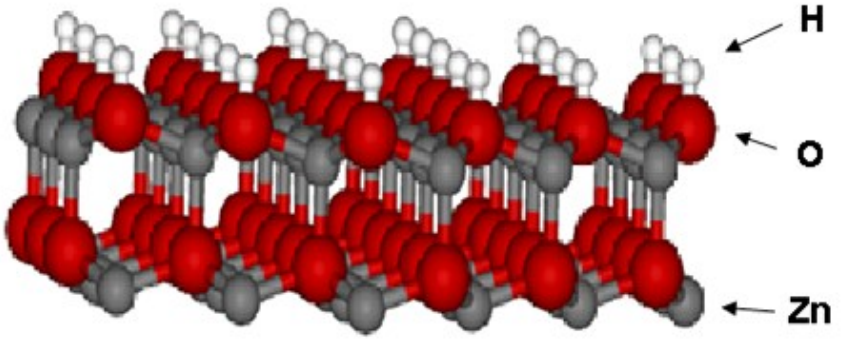

Figure 1.23. Fully hydroxylated ZnO crystal [8].

As for the pyrometallurgical routes, the purity of the starting materials used to make active ZnO is an important consideration. Zinc-bearing waste materials first undergo multi-stage physical and chemical extraction processes to yield purified zinc solutions such as zinc sulphate. The starting materials and purification process should be strictly controlled to ensure that no lead or cadmium, for example, is carried over into the final product or discharged to the environment. These processes can involve acid/base leaching, filtration, precipitation/cementation and adjustment of pH and temperature.

For the calcination stage, a gas-fired rotary kiln can be utilised where, for example, basic zinc carbonate is fed to the high end of the kiln and the ZnO is collected from the lower end of the kiln. Hot gas travels counter-current to the solid charges. A schematic of this process, as depicted in US patent 2603554, is shown in **Figure 1.24** [95]. Properties of the ZnO produced depend upon the identity of the material that is calcined, the calcination temperature profile and the residence time in the kiln. As a result, properties such as porosity, specific surface area and morphology of the particles can change dramatically. Robinson in the US patents 4071609 and 4128619 [96, 97] showed the significant effect of the calcination temperature on the specific surface area of the ZnO, which is produced from basic zinc carbonate. In a set of experiments he

concluded that the calcination temperatures between 250-350 °C are preferred. He showed that as calcination temperature increased from 300 °C to 600 °C, specific surface area decreased dramatically from 44 m^2/g to 7 m^2/g [96, 97].

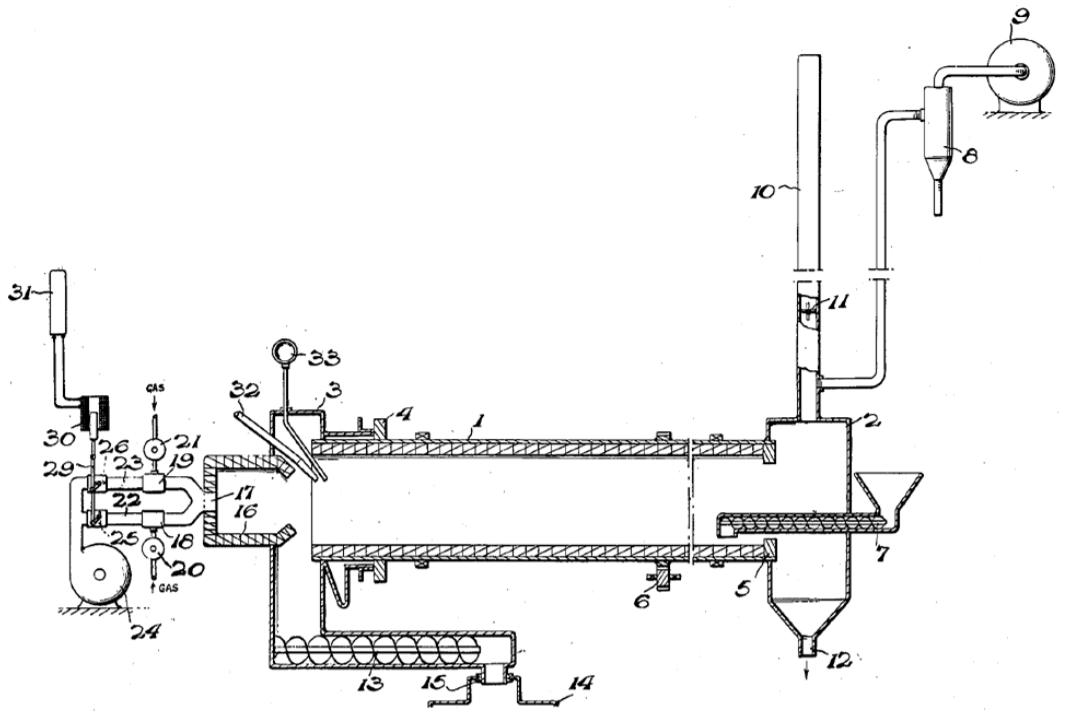

Figure 1.24. Schematic of the rotary kiln for the calcination of basic zinc carbonate as depicted in US patent 2603554 [95].

There is, of course, another method to convert basic zinc carbonate into zinc oxide in place of calcination method. Yan and Xue [98] reported a solution-based method to process as-synthesised basic zinc carbonate, which also leads to porous ZnO. In this method, they showed that by alkaline treatment of the basic zinc carbonate using aqueous KOH solution at room temperature, hollow ZnO microspheres are formed. This method does not need any thermal treatment and has advantages over the conventional method of calcination such as low-temperature conditions, better controllability of the process and morphology control [98]. However economics of the process for large scale application must be justified.

It is also possible, in principle, to convert low surface area ZnO, typically the products of the indirect or direct processes, into an active grade of ZnO with a high specific surface area using a wet carbonation reaction to form basic zinc carbonates followed by separation and calcination of the product. Conversion of ZnO to basic zinc

carbonate in the carbonation process may be as high as 76% [96]. Therefore the specific surface area of the resultant active grade totally depends on the conversion of the low surface area ZnO into basic zinc carbonate and also calcination temperature of basic zinc carbonate. An important issue to be considered in this process is the presence of water as both the reaction medium and as a reactant in liquid form. Carbon dioxide is injected into the system in the gaseous form. The conversion proceeds according to the reverse of Reaction **1.7**.

1.3.3. Small-scale production routes

There are a large number of techniques available for the production of ZnO in small quantities or in a laboratory context. Some of these are mentioned below.

Precipitation of $Zn(OH)_2$ or ZnO from aqueous solutions of zinc salts

A typical one-step process for this type of wet-chemical process is based on Reaction 1.8 [79]:

$$ZnSO_4 + 2NaOH \rightarrow ZnO_{(s)} + Na_2SO_4 + H_2O \qquad 1.8$$

However specific surface area of the grades produced by Reaction **1.8** is generally limited to <30 m^2/g which, while higher than that of ZnO produced by the pyrometallurgical processes, is still not as high as that of 'active' ZnO.

Solvent extraction and pyrolysis of zinc nitrate

A method to produce ZnO has been patented that includes an organic solvent extraction stage to extract zinc out of zinc-containing materials selectively (e.g. using a water-insoluble solvent such as di-2-ethyl hexyl phosphoric acid, D2EHPA), stripping of the organic phase with nitric acid to produce zinc nitrate and, finally, decomposition of the $Zn(NO_3)_2$ at a temperature above 200 °C to produce pure ZnO [62], **Figure 1.25**. An important aspect of this process is that the nitric acid is then regenerated by aqueous scrubbing of the gases produced by decomposition, a step which would have marked economic advantages if performed efficiently.

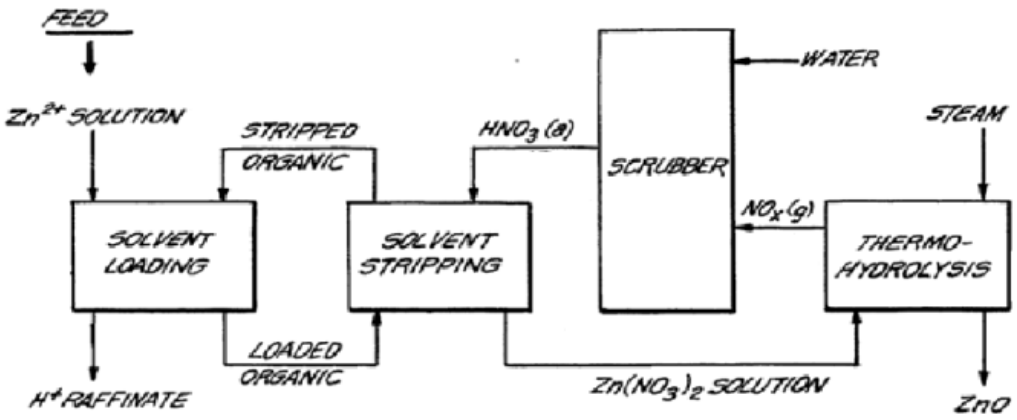

Figure 1.25. Organic solvent extraction process for the production of zinc oxide [62].

Deposition of thin films

ZnO thin films are useful materials for piezoelectric devices such as surface acoustic wave (SAW) and bulk acoustic wave (BAW) devices. Deposition of ZnO thin films may be achieved by methods such as chemical vapor deposition (CVD), metal organic chemical vapor deposition (MOCVD), pulsed laser deposition (PLD), molecular beam epitaxy (MBE) or laser MBE, reactive e-beam evaporation, rf or dc sputtering and planar magnetron sputtering [99-104].

Gas-phase synthesis

Gas phase synthesis is generally conducted in a closed chamber. The synthesis is performed within a temperature range of 500-1500 °C. Some common techniques include vapor phase transport (VPT) including vapor-solid (VS) and vapor-liquid-solid (VLS) growth, CVD, physical vapor deposition, MOCVD, thermal oxidation of pure Zn and condensation, microwave assisted thermal decomposition, seeded vapor phase (SVP) method, hydride or chloride vapor phase deposition (HVPE) [7, 103]. ZnO nanorods can also be formed by an arc-discharge technique [105]. The growth mechanism for the nanorods is assumed to be based on either VS or VLS [106]. A schematic for the arc discharge method is depicted in **Figure 1.26**.

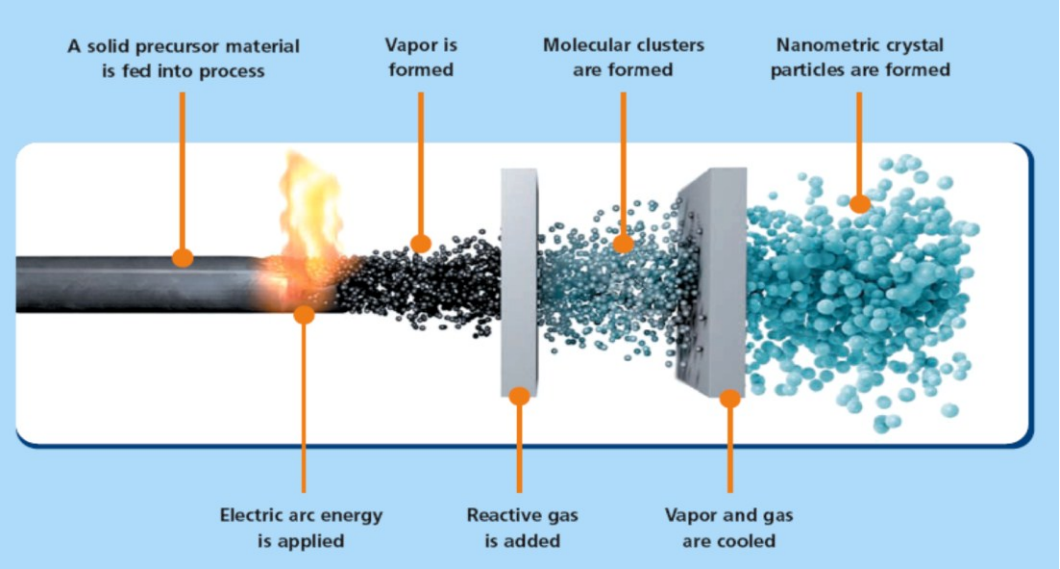

Figure 1.26. Arc discharge method schematic, reproduced from [107].

Miscellaneous other methods

Growth of ZnO from an aqueous solution is an attractive option for some morphologies because the process temperature can be below 100 °C. Large scale fabrication of nanostructure arrays can be achieved [99]. In some hydrothermal processes, the reaction takes place in a pressurised aqueous solution with a temperature that is above 100 °C. This technique is one of the main routes available for the growth of single crystals of ZnO (see Section 1.4.4). With this method, single crystals with volumes of several cubic centimeters can be formed. The production of homo- or hetero-epitaxically coated wafers of several square centimeters is also possible with hydrothermal processing. To do so, ZnO is dissolved in a base e.g. KOH at high temperatures and pressure, and is then precipitated at lower temperatures [3].

In solvothermal methods, which may be categorised under hydrothermal processes, the reaction takes place at moderate temperatures (generally 100 to 250 °C). In this process, an aqueous solution of an organic solvent such as ethanol, hydrazine or ethylenediamine is used instead of pure water [108-110]. The sonochemical technique invokes a hybridisation of hydrothermal synthesis with sonication, and has been implemented using an ultrasonic probe to provide mechanical energy for the system. The time necessary for crystal growth may be reduced by sonochemical treatment [111].

Mechano-chemical processes (MCP) are yet another hybrid. Of course, wet or dry milling of big clumps of material to form powder is not a new technique; however comminution to a particle size below about 1 micron is not usually feasible due to agglomeration of the particles and an increase in the viscosity of the charge. In the MCP processes milling is combined with a solid-state chemical reaction. This combination is suitable for the medium-scale production of nanoparticles because of its simplicity and relatively low cost but requires a relatively long reaction time. There is no solvent involved in this method. In the case of ZnO, there are three common reaction pathways, (1) milling of a mixture of zinc hydroxide carbonate and NaCl (as non-reacting diluent material) followed by calcination of the milled product to form ZnO and washing the mixture to remove NaCl, (2) milling a mixture of $ZnCl_2$ and Na_2CO_3 to form zinc hydroxide carbonate and NaCl and subsequent thermal decomposition of $ZnCO_3$ and (3) milling of a mixture of zinc acetate and oxalic acid, followed by a thermal decomposition of the product [112-115]. Wet-grinding to form nanoparticulate suspensions is also possible in principle, and has been reported for other metal oxides [116, 117].

The composite hydroxide mediated (CHM) process is another relatively new small-scale technique. In this case the reaction to form ZnO occurs in a eutectic mixture of molten hydroxides. Due to the higher viscosity of the molten hydroxide system, mass transfer processes are slower than those of reactions conducted in water. However, the higher viscosity of the molten hydroxide system is reported to result in less agglomeration of the particles [118].

1.4. Properties

Depending on end-use, ZnO may be considered as a bulk chemical or as a specialised semi-conductor. It has specific optical, electrical and thermal properties that are attractive for a range of very diverse applications. For example, its high refractive index (1.95 to 2.10) was useful in pigment applications, it can be an electrical conductor when suitably doped, and it is thermally stable to extremely high temperatures (at least ~1800 °C). The physical and chemical properties of ZnO powder ensure a large off-take as an additive in rubber. Alternatively, the high specific surface area of the ‘active’ grades permits them to be used in desulfurisation processes in chemical plants. As a

semiconductor, ZnO has applications in opto-electronics and in transparent conducting films. Awareness of its various properties is important, both for selection of this material for specific applications, and as input information for the producers of ZnO in its various forms.

1.4.1. Crystal structures

There are three crystal structures of ZnO: hexagonal wurtzite, cubic zinc-blende structure and a rarely-observed cubic rock-salt (NaCl-type), **Figure 1.27**. Under ambient conditions, the most thermodynamically stable structure is the wurtzite form. The zinc-blende structure is metastable and can be stabilised only by epitaxial growth on cubic substrates while the higher density cubic rock-salt structure is usually only stable under extreme pressure. The transition between wurtzite to cubic rock-salt starts at 9.1±0.2 GPa. On increasing pressure, two phases coexist in a pressure range of 9.1-9.6 GPa above which the transition is completed resulting in a 16.7% loss in the unit-cell volume. Upon decreasing the pressure, ZnO reverts to the wurtzite structure at 1.9±0.2 GPa below which only a single phase is observed. This shows a significant phase hysteresis [2].

Most of the lightly doped ZnO-based materials crystallise with the wurtzite structure under normal conditions. The rock-salt structure is also reported for example in $Mg_xZn_{1-x}O$ alloys in the range of 53% to 68% Mg content [10].

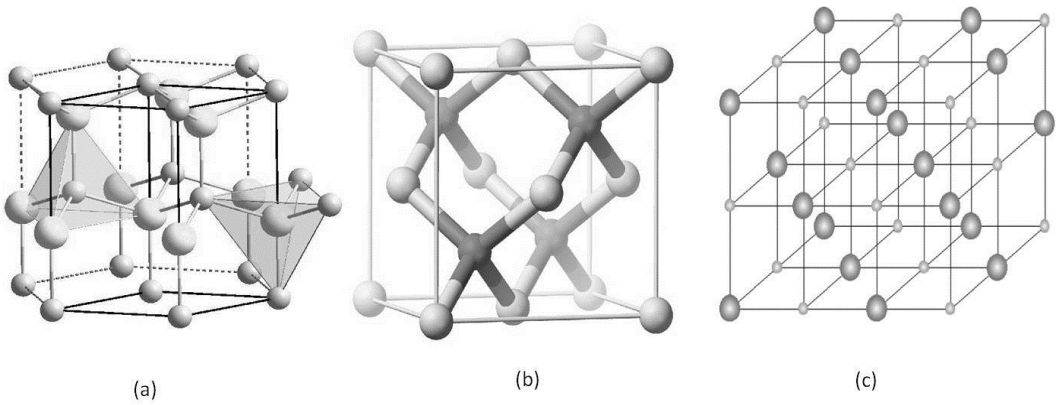

Figure 1.27. Unit cell of the crystal structure of ZnO. (a) Hexagonal wurtzite structure, (b) "zinc-blende" structure and (c) cubic rock-salt structure [2].

1.4.2. Toxicology

Zinc oxide is generally categorised as a non-toxic material. Zinc oxide does not cause skin and eye irritation and there is no evidence of carcinogenicity, genotoxicity and reproduction toxicity in humans [24, 119, 120]. However, the powder can be hazardous by inhalation or ingestion because it causes a condition known as zinc fever or zinc ague. The symptoms of this syndrome are chills, fever, cough, and tightness in the chest. Therefore appropriate safety precautions should be observed when preparing, packaging, transporting and handling ZnO. According to the recent EU hazard classifications, zinc oxide is classified as N; R50-53 (very toxic for the aquatic environment or ecotoxic). Therefore packages of ZnO in these jurisdictions must be labeled "UN3077-Class 9, Environmentally Hazardous Substance" [121].

Soluble zinc compounds are considered ecotoxic for aquatic organisms despite them being necessary for humans, animals and plants in trace amounts [24, 122]. The human body, for example, contains around 2 g of Zn and a daily intake of 10-15 mg is required for metabolism [24, 123]. It has been shown that the ecotoxicity of ZnO to the model aquatic protozoan *Tetrahymena thermophila* is caused entirely by its solubilised fraction, i.e. the Zn^{2+} ion [123]. Toxicities of bulk ZnO, nano-ZnO and soluble Zn^{2+} are similar once their different solubilities are taken into account, with 4-hr effect concentration (EC_{50}) values of about 4 or 5 mg bio-available Zn/L (5 ppm). These values are an order of magnitude lower than for soluble Cu^{2+} [123]. By comparison, the naturally occurring amount of Zn ions in seawater is three orders of magnitude smaller (5 ppb).

The International Programme on Chemical Safety (IPCS) reported a range of optimum concentrations for essential elements including zinc. "*The possibility exists both for a deficiency and for an excess of this metal. For this reason it is important that regulatory criteria for zinc, while protecting against toxicity, are not set so low as to drive zinc levels into the deficiency area*" [124].

Sources of human and environmental exposure for zinc fall into two categories: (1) natural sources and (2) anthropogenic sources. From the natural sources as a result of erosion, geological activities and forest fires, zinc can be released to water streams, oceans and to the atmosphere. Zinc can also be released to environment by human activities. During production processes and use of zinc-containing compounds such as

fertilisers and pigments, it can enter waters, soil and atmosphere that must be strictly controlled. Hence, zinc toxicity to organisms depends on local environmental conditions and habitat types and any risk assessment must consider this as well [124].

Zinc oxide has a long history of use in sunscreen compositions to block UV radiation, with the nanoparticulate form having been introduced for this application in the late 1990s. There have been occasional concerns voiced about possible adverse effects on human health or the environment. However, the current evidence shows that ZnO particles or nanoparticles do not penetrate viable skin cells and remain on the outer layer of undamaged skin (the stratum corneum) with low systemic toxicity [125-129]. Toxicity to the aquatic environment would depend on whether any ZnO washed off sunbathers was solubilised in, for example, the sea water, and whether the local environmental concentration of Zn^{2+} could thereby exceed the roughly 5 ppm threshold mentioned earlier.

1.4.3. Morphology of zinc oxide particles

The morphology of ZnO particles can be controlled by varying the synthesis technique, process conditions, precursors, pH of the system or concentration of the reactants. A wide variety of shapes are possible, **Figure 1.28**. The French and American process zinc oxides have nodular-type (0.1-5 μm) or acicular-type (needle-shape, 0.5-10 μm) particle shapes. Wet-process ZnO may have a sponge-like form with porous aggregates being up to 50 μm diameter [24, 44]. There are, however, a large number of other morphologies, each produced under some specific set of conditions. Many of these have been given whimsical names. The possibilities include nanorods [108, 130], nanoplates [109, 131], nanosheets [132], nanoboxes [131], irregularly-shaped particles (ISPs) [131], polyhedral drums [131], hexagonal prisms, nanomallets [131], nanotripods [133], tetrapods [134], nanowires [135], nanobelts [130, 135], nanocombs and nanosaws [130], nanosprings and nanospirals and nanohelixes [130, 136], nanorings [130, 136], nanocages [130, 136], nanoneedles [2, 137], nanotubes [2, 136, 138], nanodonuts [2], nanopropellers [2], and nanoflowers [79, 139].

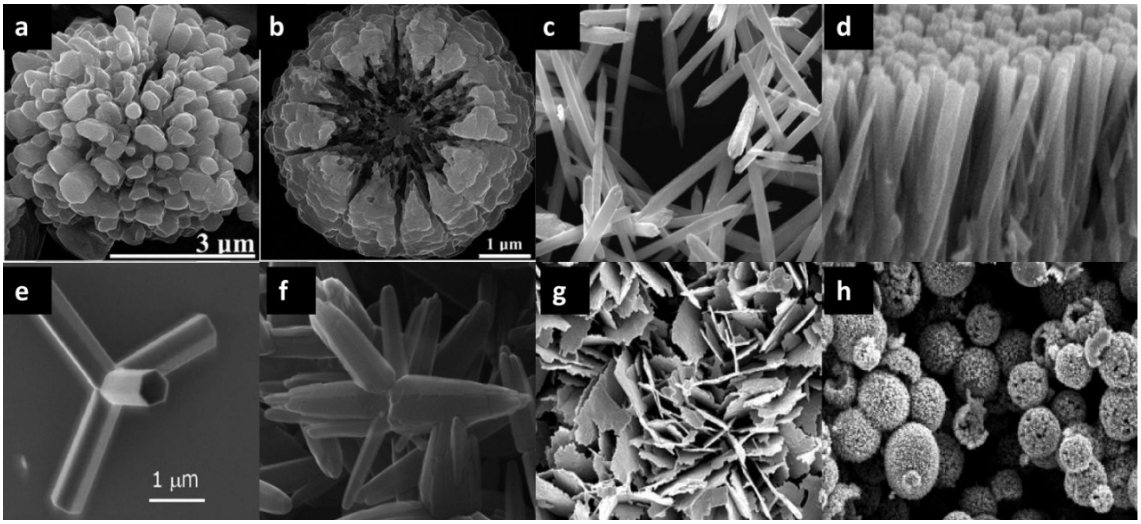

Figure 1.28. SEM images of ZnO showing various morphologies; (a) and (b) are reprinted with permission from [110], (c) from [111], (d) from [99], (e) from [140], (g) from [132], (h) from [98] and (f) is synthesised by the authors. Reproduced with permission from the various sources cited.

1.4.4. Industrial grades

There are many industrial grades of ZnO in use. Differentiation between the grades is based on the purity, composition and specific surface area of the powder, and sometimes the process through which it is made. Although some grades are covered in international standards (*e.g.* **Table 1.1**) it seems that much ZnO is still supplied to somewhat looser designations. Some of these categories are listed in **Table 1.2**. However many of the companies producing ZnO have their own nomenclature too.

Bulk zinc oxide

As mentioned earlier, most of the bulk ZnO in the world is produced by either the "French" or "American" processes. The specific surface area varies between 1 and 10 m^2/g depending on process used. Such grades of ZnO are not considered as "active" due to their low specific surface area. Highly crystalline particles are formed during the high-temperature manufacturing process.

Table 1.2. Industrial grades of zinc oxide. Data are adapted from the product datasheets from industrial producers: PT. Indo Lysaght Indonesia, US Zinc in the USA, Umicore Zinc Chemicals and Silox in Belgium, IEQSA in Peru and Grillo Zinkoxid GmbH in Germany.

ZnO Grade	Purity (%)	Specific Surface Area (m^2/g)	Production Process
Gold Seal	99.995	4-7	French Process
Pharma Grade	99.8-99.9	3-9	French Process
White Seal	99.8	3-5	French Process
Green Seal	99.6-99.7	4-10	French Process
Red Seal	99.5	3-5	French Process
American Grade	98.5-99.5	Max. 3	American Process
Active Grade	93-98	Min. 30	Wet process
Feed Grade	90-99	-	Various

Active zinc oxide by calcination of a carbonate

Low crystallinity ZnO with high specific area (generally 30-70 m^2/g or greater) is known as "active" ZnO, as mentioned in section 1.3.2. Specific surface areas as high as 200 m^2/g may be achieved by carefully controlling the temperatures of precipitation and calcination [141]. Material with such a high surface area will be very susceptible to the reverse carbonation reaction described in section 1.3.2.

Other 'wet-process' ZnO

Zinc oxide produced by other wet-chemical processes, such as precipitation, has a specific surface area that is intermediate between that of ZnO produced by the high-temperature methods and that produced by the decomposition of a carbonate. The surface area of regular (i.e., not "active") wet-process ZnO is normally in the range of 10-30 m^2/g but can attain a maximum of around 50-60 m^2/g by carefully controlling the process conditions such as concentration of the base or feeding method [79].

ZnO single crystals

Zinc oxide single crystals, **Figure 1.29**, are of interest due to potential applications in electronics. They are *n*-type irrespective of the growth method used. Synthesis of *p*-type ZnO single crystals has been proven to be quite difficult so far [6, 142], although some success has been claimed for *p*-type polycrystalline films [143-145]. Diverse methods may be used for single crystal growth, including hydrothermal growth at temperatures around 350-450 °C and pressures up to 2500 bar, vapor phase transport growth at temperatures around 1100-1400 °C, or growth from a pressurised melt of salts with low melting temperature (e.g. $ZnBr_2$) [6, 10, 146].

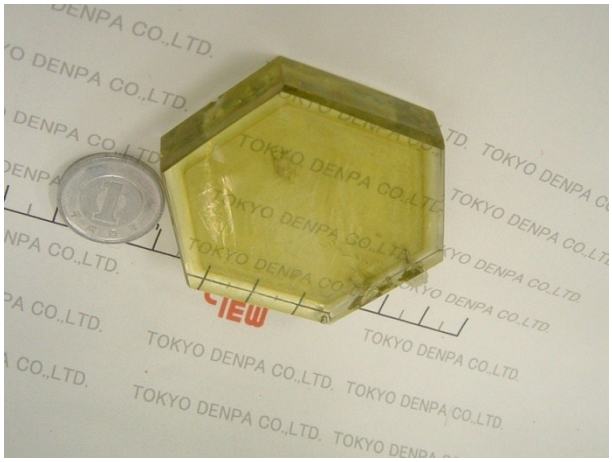

Figure 1.29. Zinc oxide single crystal, produced by the hydrothermal method. Image courtesy of Tokyo Denpa Co., Ltd. Japan.

The hydrothermal growth method yields the largest crystals but is slow, with a growth rate of 0.1-1 mm/day [146, 147]. The hydrothermal method is also associated with contamination of the crystals by ions from the mineraliser such as lithium [146, 148] and OH groups [146]. Crystal growth by the vapor phase methods is faster with a rate of around 7-8 mm/day. Crystal growth from a melt is also reported to have higher growth rate than that of hydrothermal methods and less inclusion of contamination [148-151].

1.4.5. Optical properties

Much of the recent surge in research interest in ZnO has been motivated by possible optoelectronic applications [2, 3, 5, 152]. This is because there appears to be a

possibility of replacing the GaN-based compounds currently being used in optoelectronic devices operating in the blue or UV range (for example, LEDs, laser diodes and photodetectors) with a cheaper and non-toxic alternative such as ZnO. Selection of ZnO is due to the similarity of its band gap energy (3.37 eV at RT) with that of GaN (3.39 eV at RT) and, importantly, the larger exciton binding energy of ZnO (60 meV) compared to that of GaN (18-28 meV) [153]. This would be useful in light emitting devices. Band-gap engineering of ZnO is also possible. For example, alloying with CdO decreases the band gap [6] while alloying with MgO increases the band gap [6, 152]. The compound $Mg/Cd_{1-x}Zn_xO$ has a band gap that is potentially tunable between 2.3 to 4.0 eV [6]. Emission properties of ZnO nanoparticles are influenced by many factors such as synthesis method, morphology of the nanoparticles, dopants and ligands used for surface coating [6, 152-154]. Zinc-based phosphors have been known for decades, although the precise mechanism of their operation is still said to be controversial [155, 156].

1.4.6. Electrical, thermal and magnetic properties

Zinc oxide was one of the first semiconductors to be extensively investigated. Somerville measured the resistivity of cylindrical ZnO rods up to temperatures of 1200 °C in 1912. In the early 1930s, two groups, (Jander and Stamm) and (Baumbach and Wagner), investigated the dependence of the electrical properties of oxides including ZnO on their stoichiometry, which resulted in the proof of the theory of defect equilibria by Schottky and Wagner for ionic crystals [10, 157]. However the lack of a reliable *p*-type variant has hampered efforts to use it in many types of devices.

Piezoelectricity, pyroelectricity and thermoelectricity

In 1960, it was discovered that ZnO is a piezoelectric semiconductor with a large electromechanical coupling coefficient (piezoelectric crystals can transform mechanical energy into an electric signal or vice versa). The tetrahedral coordination in ZnO crystals results in a non-centro-symmetric structure and consequently piezoelectricity and pyroelectricity. Crystals can only be piezoelectric if they are non-centro-symmetric. The piezoelectric crystals can transform mechanical energy into an electric signal or

vice versa. This led to the first electronic application of ZnO as a thin layer for SAW devices. Other applications can be in resonators, controlling tip movement in scanning probe microscopy, or as air or liquid vibration sensors [10, 130, 153].

Among the thermoelectric (TE) compounds, oxides have been researched extensively in recent years due to their interesting properties. In particular, some oxides are environmentally benign and can be used in oxidising conditions and at high temperatures. Currently, *p*-type oxide TEs are the only oxide materials, which possess reasonably high figures-of-merit (the so-called 'ZT value'). There has been less progress made in developing *n*-type oxide TEs with comparable ZTs. Doped ZnO, especially Al-doped ZnO, is an excellent *n*-type oxide TE. Other dopants, such as Ni or praseodymium (Pr) have also been considered [158-161]. Unfortunately the all-important figure-of-merit of ZnO is still inferior to many other kinds of thermoelectric substances.

Ferroelectricity, magnetism and ferromagnetism

Ferromagnetism can be induced in ZnO by doping with either ferro- or paramagnetic elements such as Fe, Co, Ni or Mn, Cr and Li, or nonmagnetic elements such as Ti, V, Cu. While semiconductor materials are used for microprocessors, magnetic materials are used for memory devices. Materials that share both of these properties, sometimes referred to as dilute magnetic semiconductors (DMS), are of potential interest for a new generation of devices. Interest in ZnO as a DMS has been intensified by theoretical calculations, which suggest that it could hold its ferromagnetism at relatively high temperatures by doping with some 3*d* transition metals. In addition, its optical transparency might provide a transparent ferromagnetic material, which would open up new device possibilities. However, synthesis, reproducibility and understanding of such materials are still a matter of much debate [10, 162-165].

Electrical conductivity

The conductivity of ZnO depends significantly on its content of charge carriers, which is in turn highly influenced by its stoichiometry. The latter can be adjusted by the oxygen or zinc partial pressure during high temperature processing. In addition,

annealing in a reducing atmosphere containing hydrogen can have a large effect on electrical conductivity. In contrast, hydrothermally grown ZnO crystals show very high resistivities due to the solvents used containing atoms such as Na, K or Li that can readily provide charge compensation in a defective lattice [10]. Electrical conductivity of ZnO, as in most other semiconductors, increases with temperature.

In piezoelectric devices, ZnO must have a very high resistivity (>10^8 Ωcm). This can be provided by doping with lithium for example, by means of which the resistivity can be increased to 10^{12} Ωcm. On the other hand, for applications, such as solar-cells, that might require a transparent conducting oxide, very high conductivity of ZnO thin-films is a prerequisite. For these purposes resistivities as low as 2 ×10^{-4} Ωcm have been achieved by high doping levels of B, Al, Ga or In. While undoped ZnO crystals show carrier concentrations as low as 10^{15} cm^{-3}, In-doped materials show carrier concentrations around 10^{20} cm^{-3} [10, 166]. However, as mentioned previously, a generally applicable process to achieve stable *p*-type ZnO with high conductivity has not been found yet. It is believed that one problem is self-compensation in the lattice of the ZnO originating from the native defects or hydrogen impurities [144, 167]. The lowest *p*-type resistivity values reported so far are around 0.5 Ωcm for example by N, Ga, As or P-doping [142]. Unrealistic hole concentrations (*p*) in the range of 10^{18}-10^{21} cm^{-3} have also been claimed by doping with e.g. P or As that is still under debate [168, 169]. Obtaining a stable high-conductivity *p*-type ZnO would provide a breakthrough in the fabrication of homo-epitaxial LEDs, laser diodes and thin film solar cells [6, 142, 145, 169, 170].

Zinc oxide can be doped intrinsically or extrinsically. Intrinsic doping is associated with defects in the crystal lattice that are caused by deviation from a perfect stoichiometry. In particular, zinc interstitials (Zn_i) or oxygen vacancies (V_O), which are shown to have low formation energies act as intrinsic dopants and result in change in conductivity. Zn_i acts as a shallow donor and may be responsible for *n*-type conductivity. Annealing the material under vacuum, reducing conditions (H_2 atmosphere) or by annealing in zinc vapor may lead in better conductivity. In contrast, annealing ZnO under oxidising conditions can result in higher resistivity. Zinc oxide can also be extrinsically doped by addition of external elements into the crystal structure. To increase the conductivity by donors, addition of dopants such as group III (Al, B, Ga, In)-oxides and Cr_2O_3, Y_2O_3, Ce_2O_3, TiO_2, ZrO_2 or HfO_2 has been reported.

For acceptors, the group V elements (N, P and As) and Sb are reported [10, 167, 171]. Hydrogen, which is almost present at all times during growth of ZnO crystals, is also an important dopant. Hydrogen acts as a shallow donor on ZnO surfaces, which works against the achievement of *p*-type doping [10, 142].

Heat capacity, thermal conductivity, thermal expansion coefficient

Zinc oxide has relatively high heat capacity and thermal conductivity [37]. The specific heat capacity (C_p°) value for ZnO is reported to be about 40 $JK^{-1}mol^{-1}$, which increases to around 50 $JK^{-1}mol^{-1}$ at 630 °C [89]. Thermal conductivity value, λ, and coefficient of expansion, α_L, of zinc oxide are functions of porosity of the powder and temperature. These values are quite sensitive to preparation method as well [161, 172]. Thermal conductivity can also be manipulated by doping with for example Al [161]. Thermal conductivity at room temperature is about 50 $WK^{-1}m^{-1}$ for bulk ZnO but this drops to 15 $WK^{-1}m^{-1}$ as the temperature or porosity increase [161, 172]. Zinc oxide has a relatively low coefficient of expansion at room temperature ($\alpha_L = 3 \text{ to } 8 \times 10^{-6}\ K^{-1}$) that increases as the porosity or temperature increase [172].

Thermochromism

Crystalline ZnO is thermochromic, changing from white to yellow when the temperature is increased to >300 °C [24] and then from yellow to white upon cooling. This is probably because of the formation of crystal lattice defects due to a loss of oxygen and the formation of the non-stoichiometric $Zn_{1+x}O$, with x increasing with temperature.

1.4.7. Surface properties

The surface properties of ZnO particles or thin films play a significant role in diverse fields, for example in sensing, catalysis or optoelectronics. As a result, physics and chemistry of the surfaces of particles is a hot topic and many groups have tackled this [2, 8, 173]. Absorbtion of molecules onto the ZnO surface has been examined with some attention focused on the adsorbates for methanol synthesis from syn-gas (H_2, CO,

CO_2) [8, 174]. The wettability of ZnO surfaces has also been examined; flat ZnO substrates exhibit the maximum water contact angle of 109 ° [175]. Super-hydrophobic ZnO has been prepared by surface treatment with fatty acids and reversibly switchable wettability between super-hydrophilicity and super-hydrophobicity has been observed by alternation of UV irradiation or oxygen plasma treatment [175-177]. The hydrophobicity of ZnO additives is an important issue in polymer blending when seeking to obtain a homogeneous particle distribution or grafting of monomers onto the metal oxide. Since most polymers are hydrophobic and ZnO is hydrophilic, the surface of the particles surface may be modified for better compatibility with the polymer matrix [178-180].

1.5. Applications

The uses of ZnO have changed markedly over time. Some major uses in photocopy paper as a photoconductive ingredient [181] (which was the second largest volume consumed in the 1970s [37]) and in linoleum have almost disappeared [35]. Furthermore ZnO is not the principal white pigment in paint anymore. Today its major uses are in the rubber industry, followed by ceramics [35], but it has many niche applications such as, for example, in drilling fluids for the oil and gas industry [182, 183] and cigarette filters [157, 184]. Most recently, ZnO is being investigated for applications such as LEDs, transparent transistors, solar cells and memory devices [2, 3] and as the basis of a transparent conducting oxide for consumer devices [10]. The more important of these applications are discussed briefly below.

1.5.1. Rubber

The major application of ZnO (more than half of the total use) is currently in the rubber industry where it is used as a vulcanising activator (a substance applied in small doses to increase the effectiveness of the vulcanisation accelerator). Early un-accelerated vulcanisation processes used ~8 parts per hundred (phr) of rubber and required temperatures above the sulfur melting point for several hours. Organic accelerators allowed the amount of sulfur and vulcanisation times to be significantly

reduced but a significant breakthrough in the vulcanisation process involved activators such as ZnO [30, 185].

Zinc oxide as well as magnesium oxide and lead oxide are also used as a curing or cross-linking agent for halogen-containing elastomers such as neoprene or polysulfides [186]. Metallic oxides not only change the rate of cure but also the 'scorch' (i.e. premature vulcanisation caused by heat during rubber processing) in neoprene [187]. In cable insulators such as ethylene propylene diene monomer (EPDM) rubber, the incorporation of ZnO imparts low water absorption and longer lifetime. It is also used in pressure sensitive adhesives (e.g. in epoxidised natural rubber, ENR) [188, 189] and in surgical tapes and also adhesive tapes for keloid therapy [190].

The addition of ZnO also considerably improves the thermal conductivity of rubber, which is crucial to dissipate the heat produced by deformation under load or cyclic stress, for example in vibration mounts or when a tire rolls. There is also evidence that the inclusion of ZnO in rubber compounds improves the abrasion resistance. It has also been found that ZnO improves the heat resistance of the vulcanisates. ZnO additions also contribute to the processing of uncured rubber by decreasing the shrinkage of molded products and improving the cleanliness of the molds. Finally, its presence appears to increase the bonding between rubber and metallic inserts, such as steel wire [185].

During the vulcanisation process, only the small quantity of ZnO at the surface of the particles is involved. Therefore, the efficiency of ZnO use in vulcanisation can be improved by the maximisation of the interfacial area between ZnO particles and accelerator. This depends on the particle size, shape and specific surface area. However, production, de-agglomeration and dispersion of small particles of ZnO are difficult and smaller ZnO particles may unintentionally diminish some desired rubber rheology characteristics [187, 191]. Standard ASTM D4620-02 (the standard test method for evaluating the effective surface area of ZnO in rubber) mentions that the specific surface area of ZnO can significantly affect cure activation and vulcanisation properties. Longer cure times indicate lower surface area and vice versa [192]. The mechanism for reaction of ZnO with organic vulcanisation accelerator, tetra-methyl-thiuramdisulphide (TMTD), is shown in **Figure 1.30**.

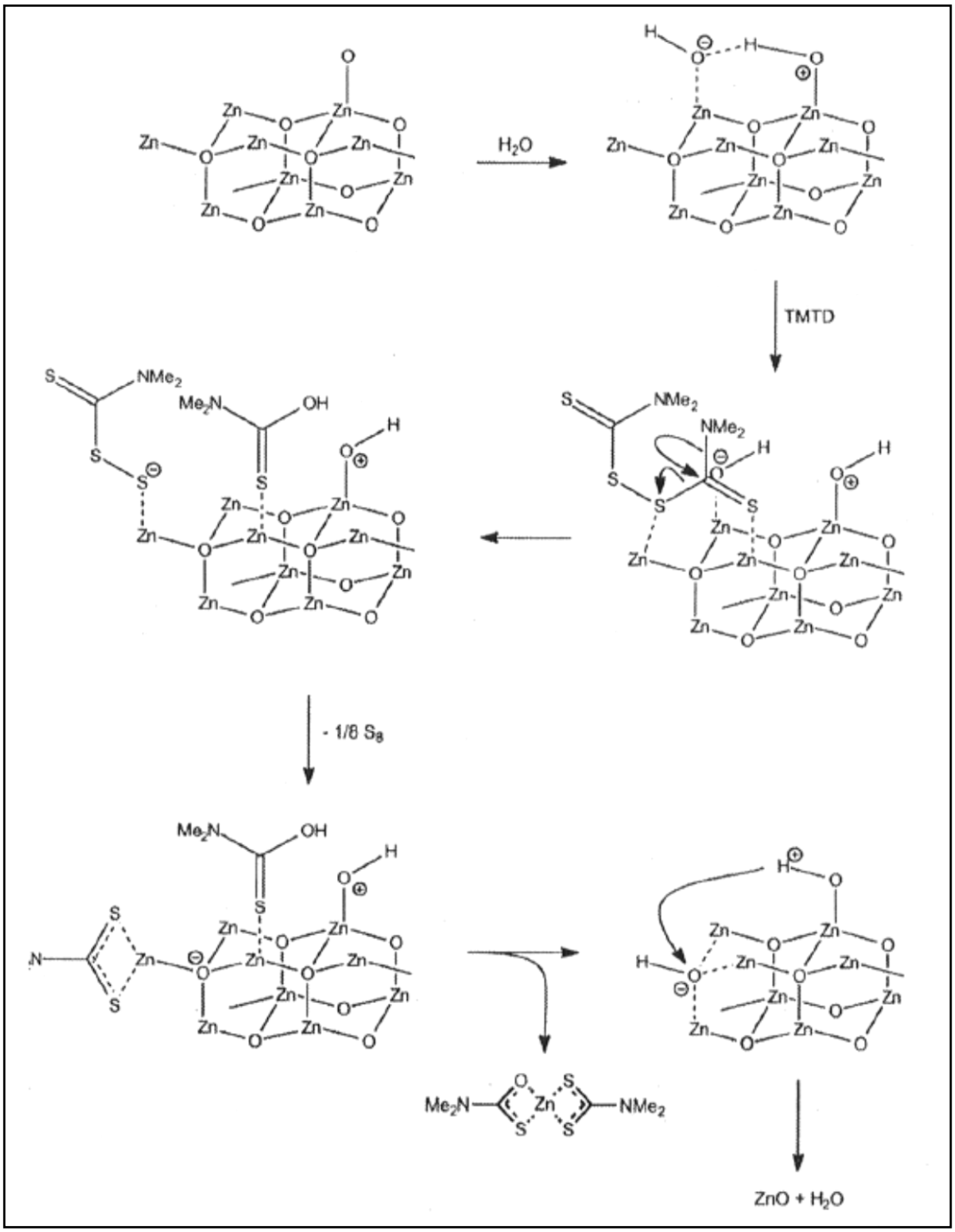

Figure 1.30. Mechanism for reaction of zinc oxide and the vulcanisation accelerator [193].

Zinc oxide must be dispersed properly in the rubber to impart the required properties. This is normally achieved by high intensity mechanical mixing, but in some cases a coating of co-activator fatty acids (particularly propionic acid or stearic acid, 0.2 to 0.4% by weight) prior to its incorporation into the rubber might be of benefit. These co-activator fatty acids make the ZnO surface hydrophobic and improve dispersion times into organic media [193, 194]. Another benefit of application of surface-treated ZnO is that such ZnO retards the initial cure, which decreases the scorching of rubber while yielding the optimum cure in approximately the same time as untreated ZnO. French or American process ZnO is suitable for the surface-treatment with fatty acids. A drawback of the surface-treated ZnO is that it is extremely dusty. Dustiness is related to the low bulk density of the particles, which causes significant disadvantages in handling, such as increased cost of transportation, process control problems and, possibly, an unpleasant working environment [194].

As explained in Section 1.3.1, more than half of the global rubber output is consumed by the tire industry. Therefore tire industry plays a decisive role in the consumption of zinc oxide in the world. Zinc oxide together with other additives for the manufacture of tire is first weighed and then vigorously mixed with rubber in Banbury mixers (**Figure 1.31**) to achieve the proper dispersion.

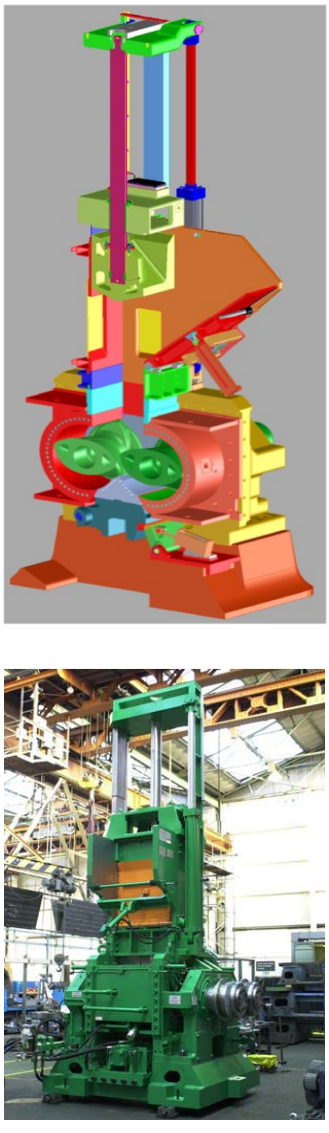

Figure 1.31. Schematic and photograph of Banbury mixer in tire manufacturing. Reproduced from technical document from Farrel corporation.

In recent years, due to the environmental and economic concerns in relation to the amount of zinc in rubber products, there is a tendency for minimisation of the zinc content. To reduce the necessary amount of ZnO, the activity of the particles should be increased. Therefore the availability of Zn^{2+} ions at the surface of the crystals should be maximised [193]. Some suggested options include the application of 'active zinc oxide', use of the so-called 'nano zinc oxide', and prior chemical reaction between the accelerators, stearic acid and the oxide before addition into the rubber matrix. Reported data indicate the possibility of reducing ZnO levels without impairing the properties of the vulcanisates [122, 186, 187, 193]. In the vulcanisation of solution styrene-butadiene rubber (s-SBR), other ways to reduce the amount of zinc in the rubber compositions include the application of CaO, MgO, zinc-m-glycerolate or zinc clay (e.g. 5 phr) as good alternatives for ZnO without damaging the cure properties. Zinc-bearing clays can be produced by modification of commonly used clays such as montmorillonite with zinc ions. By application of 2.5-5 phr of zinc clay (equivalent to 0.15-0.3 phr of pure ZnO) in s-SBR composition, physical and curing properties of the rubber remained unchanged compared to the 3 phr of pure ZnO. This change is associated with an order of magnitude reduction in the amount of zinc used [122, 193].

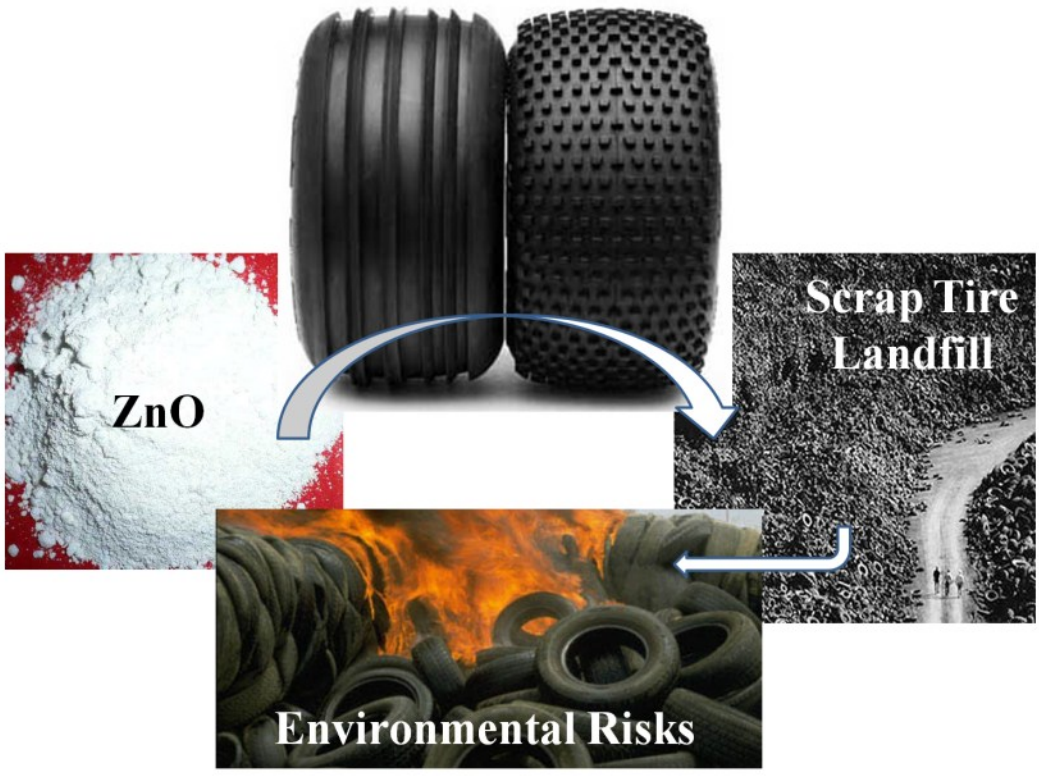

Figure 1.32. Fate of zinc oxide in tire.

1.5.2. Ceramics and concrete

The second largest application of ZnO is in ceramics [35] in particular the tile industry [36]. Both the French or American process ZnO are suitable. The relatively high heat capacity, thermal conductivity and high temperature stability of ZnO coupled with a comparatively low coefficient of expansion are desirable properties in the production of ceramics. In glazes, enamels or ceramic formulations, ZnO affects the melting point and optical properties of the glaze. Zinc oxide as a low expansion secondary flux improves the elasticity of glazes by reducing the change in viscosity as a function of temperature and helps prevent crazing and shivering. By substituting ZnO for BaO and PbO, the heat capacity is decreased and the thermal conductivity is increased. Zinc in small amounts improves the development of glossy and brilliant surfaces. However in moderate to high amounts, it produces matte and crystalline surfaces [37, 195, 196]. With regard to color, zinc has a complicated influence. It can improve or damage blues, browns, greens, pinks and is not recommended with pigments or glazes containing copper, iron, or chromium [195].

Zinc oxide acts as a metallic oxide flux in the preparation of frits and enamels for ceramic wall and floor tiles or for sanitary and tableware ceramic applications. Its fluxing action starts at around 1000 °C (e.g. in Bristol glazes). Zinc oxide may be reduced to metallic zinc under reducing conditions in the gas-fired kiln followed by volatilisation some time later. It's a late and vigorous melter. These properties are useful for low fire glazes and as a result ZnO is quite common in fast fire applications [195, 197].

Zinc oxide in concrete provides longer processing time and improves its resistance against water [3]. In the manufacture of Portland cement, ZnO can be used in the raw material mixture for the production of cement clinker [198]. Its addition in small amounts to Portland cement retards the setting and hardening effectively (at 0.25% ZnO addition: hydration is almost zero up to 12 hours; at 1% addition: hydration does not begin up to 2 days) and improves the whiteness and final strength [196, 198].

Phosphate cements generally set quickly and this property makes them useful for many civil engineering repair applications (such as highway patching or patching of preformed concrete products), as well as dental castings, phosphate-bonded refractory bricks, mortars, ramming mixes, cement pipe, sprayable foamed insulation, and flame-

resistant coatings. Different methods can be used to produce phosphate cements. For example a reaction between metal oxides such as ZnO with phosphoric acid or a reaction of metal oxides with ammonium phosphates, magnesium acid phosphates, aluminum acid phosphates, and other metal phosphates. The rate of reaction of oxides with phosphoric acid depends on the oxide alkalinity. The ZnO reaction is so rapid that the structure develops no cohesion [198].

Zinc hydroxy-chloride cements can also be produced by a reaction between ZnO and aqueous zinc chloride. The hard cement is quite stable and insoluble in water and is not attacked by acids or boiling water. However this cement hasn't found any practical applications due to the poor workability [198].

1.5.3. Plastics and linoleum

Zinc oxide may provide useful benefits when added to a plastic polymer. Once again this is commonly in the form of the French or American process material. Properties such as improved heat resistance, mechanical strength and water and fire resistance are imparted to acrylic polymers, polyvinylidene fluoride (PVDF), epoxy resins and nylon-6-6. Zinc oxide may be used as a stabiliser in polyolefin resins such as high density polyethylene (HDPE), polypropylene (PP) and unsaturated polyesters, poly-chlorofluoroethylene and poly-vinyl-halides such as PVC. In these matrices it provides UV absorption properties, thermal stability and increased tensile strength. Zinc oxide-stabilised PP and HDPE are used in safety helmets, stadium seating, insulation, pallets, bags, fibers and filaments, agricultural and recreational equipment. Zinc oxide also improves the dye-ability of polyester fibers and the antistatic, fungistatic and emulsion stability of vinyl polymers [196, 199-205].

In the production of linoleum, ZnO acts as a coloring agent that is mixed with all components such as linoleum cement, organic and inorganic fillers in a mixing unit. A typical linoleum composition may contain approximately 40% binder, 30% organic fillers, 20% inorganic mineral fillers and 10% coloring agents, including up to 5% ZnO [206, 207].

1.5.4. Pigments and coatings

Although now largely superseded by TiO_2, ZnO remains an important white inorganic pigment in niche applications. Pigments made of ZnO are known as 'zinc white' or 'Chinese white' or 'flowers of zinc', with the term 'zinc white' now reserved for ZnO pigment produced by the French process [24]. The pigment may be purchased in the dry form or as a paste in oil [24, 50]. An important property of white pigment is its low light absorbance together with high dispersion of radiation in the visible region (wavelengths of 400-800 nm). However, the scattering power depends on the particle size and also the wavelength of the incident beam [24]. Therefore by controlling the particle size, it is possible to engineer the desired scattering power to some extent.

Replacement of linseed-oil based exterior paints with latex-based ones during 1980s caused a significant decline in the demand for ZnO in the paint industry. However this trend was partially reversed during 1990s due to a ban in some countries on mercury-containing latexes (mercury has been used as a fungicide and for mold control in the latex) and introduction of ZnO into the latex due to its fungistatic properties [36]. Direct process ZnO is preferred in these applications due to its lower reactivity with resin systems.

On the other hand, ZnO as a pigment cannot compete for hiding power with TiO_2. Hiding power is the ability of a coating to mask the color of the substrate. It is related to the ability of a particle to scatter light, which in turn is directly related to refractive index. The average refractive index of rutile crystal (2.73) is considerably higher than that of ZnO (2.02) [27], a factor that in large measure explains why TiO_2 pigments now dominate the paint industry. Zinc oxide can also cause blistering when water penetrates into the coating and, as a result, its application in primers is not recommended. However, ZnO in paint contributes to mildew protection, UV absorption, hiding power and neutralisation of acids formed during paint oxidation so it still has some applications, particularly in anti-fouling paints for ships [35]. ASTM D79-86 provides information on ZnO additions to paint. An important point is that the ZnO pigment must contain less than 0.5% moisture content. Therefore the French or American process ZnO materials are used, which have very low moisture and volatile matter content. Wet-chemical ZnO, with higher moisture content and surface hydroxyl groups, cannot generally be used in such applications. There have been very significant changes to

paint formulations over the last few decades, and a very large number of standards or specifications related to the use of ZnO in paints have been cancelled or withdrawn. Therefore, care should be taken to acquire the most recent information before using ZnO in a modern paint formulation.

Zinc oxide also has a potential application as an energy-saving coating on windows [4]. As described in Section 1.4.6, ZnO becomes modestly electrically conductive when doped with elements such as Al or Ga, hence it acquires the ability to reflect infrared radiation. It can therefore be used as a component of a multilayer coating system for energy-saving or heat-rejecting windows. In these applications the visible part of the spectrum passes through the coating but the infrared radiation is either reflected back into the room (saving energy in cold weather) or it is reflected from outdoors (rejecting radiant heat in hot weather). The ZnO coating can be applied by physical vapor deposition in a vacuum chamber, using sputter targets manufactured from very pure ZnO powder. However, the market is currently dominated by pyrolytic SnO_2 coatings because these are cheaper to produce.

In space industry, to protect spacecraft components NASA scientists developed a ZnO-based coating that could tolerate the extreme conditions of space travel with a thermal cycling between 180 °C and -180 °C and the UV exposure levels equivalent to 19,000 sun hours [208].

It is also reported that the sulfide scavenging properties of ZnO can be useful for the corrosion-resistant tin coatings applied on the inside of steel cans used in the food packaging industry. Fine particles of ZnO incorporated in the coating can react with the trace amounts of H_2S given off during the cooking of foodstuffs such as corn. The reaction of ZnO with H_2S forms white ZnS. This prevents from the formation of unsightly (black) tin sulfide stains that would be caused by the reaction between H_2S and tin coatings [27].

1.5.5. Cosmetics, medical and dental

A wide range of cosmetic products e.g. moisturisers, lip products, foundations, mineral make-up bases, face powders, ointments, lotions and hand creams make use of ZnO [125]. One reason is that ZnO helps cosmetics adhere to the skin but a more

important motivation is that ZnO is a broad-spectrum UV absorber, which effectively attenuates UV radiation in both the UVA (320-400 nm) and UVB range (290-320 nm). It is photo-stable and has one of the broadest UV attenuation spectra amongst the sunblocks approved by regulatory authorities such as the USA's FDA [209, 210]. Performance of ZnO particles for UV attenuation depends on particle size with an optimal size of 20-30 nm. However it is generally used in particle size range of 30-200 nm. To facilitate its dispersion in the compositions, particles are generally surface-treated with inert coating materials, such as silicon oils, SiO_2 or Al_2O_3 [125].

Clinically, ZnO promotes wound healing [211, 212] and keeps wounds moist and clean. High surface area ZnO (active grade) can be used in lotions or creams for the treatment of acne or of fungal infections such as athlete's foot (*Tinea pedis*). Active ZnO inhibits the growth of bacteria such as *Staphylococcus Aureus* and *Propionibacterium acnes*, which results in less of the sebum (an oily substance secreted by the sebaceous glands in mammalian skin) being split into the free fatty acids that in turn act to inflame the follicle wall. ZnO may also be used in anti-dandruff shampoos and in the treatment of nappy rash, which often gets worse by the infection due to *Candida Albicans* [212]. **Table 1.3** summarises some applications of active ZnO in skincare products.

Table 1.3. Skincare products containing active ZnO *vs.* its percentage in the formulation [212].

Product	**Active ZnO %**	**Product**	**Active ZnO %**
Skin treatment gel	5	Cover-up stick	5
Non-oily moisturiser	5	Baby lotion wipes	5
Cleansing lotion	5	Nappy rash cream	5
Cleansing wash	5	Nappy cream	5
Moisture fluid	5	Shower gel	5
Anti-dandruff shampoo	2	Acne lotion	5
Men's Facial wash	5	Sensitive cleansing pads	5
Translucent complexion base	5	Overnight gel	5
Pressed powder	5	Emergency gel	5

As an ingredient in dry deodorants to reduce wetness under the arm, ZnO can be used between 0.05 to 10% by weight with average particle size in the range of 0.02 to 200 microns. Normal deodorants have an alkaline nature with a pH range of 9-10, which may cause irritation on skin. Neutral pH deodorant is more desirable for sensitive skins, which can be provided by application of small size ZnO in the formula of deodorant [213].

Zinc salts such as chloride and sulphate are useful in dental materials such as dentifrice pastes, filling material, cements and impression materials, but may cause an unpleasant lingering taste. ZnO may alleviate this problem in toothpaste, for example [214]. In dentifrice compositions, 0.1-10% ZnO is generally added as an anti-plaque, anti-gingivitis, anti-bacterial or tartar agent. Anti-plaque properties of compositions containing ZnO are improved by formation of zinc ions, which slows tartar formation. Typical compositions of toothpaste, tooth gel and tooth powder containing ZnO are disclosed in the patent literature, see for example [215]. It is recognised in the field that the useful effect of the Zn is from soluble Zn^{2+} ions rather than from ZnO itself which, as mentioned previously, is comparatively inert.

Zinc oxide can also be used as a source of zinc in mouthwash compositions. Reaction between zinc oxide and citric acid provides zinc citrate needed for the application in mouthwash liquid [216]. ZnO, NaOH, and citric acid have been claimed to alleviate bad breath by neutralising the bacterial sulfur secretions produced in the mouth [217, 218].

1.5.6. Catalysts

It was discovered by the German company, Badische Anilin und Soda Fabrik (BASF), in the 1920s that methanol was the major product of the hydrogenation of carbon monoxide over mixed zinc and chromium oxides [219]. In 1932 Henry Dreyfus patented a process for the manufacture of methyl alcohol using ZnO or a mixture of ZnO and chromium oxide [220]. Today, methanol is a very important commodity in the chemical industry, and is used as-is or as a feedstock. A methanol synthesis catalyst must be active for about four years and must also be selective to avoid formation of other unwanted species such as methane or ethanol. The catalytic process for synthesis of methanol uses synthesis gas, a mixture of H_2, CO, and CO_2. Originally a high-pressure (l00-350 bar) process over ZnO/Cr_2O_3 catalyst at 320-450 °C was applied but

this was replaced by a lower-pressure process (50-100 bar) over $Cu/ZnO/Al_2O_3$ catalyst at 200-300 °C patented in 1965 by Imperial Chemical Industries [219, 221], see **Figure 1.33**. So far the best methanol productivity reported is over catalyst $Cu/ZnO/Al_2O_3$, which is low in sodium and sulfur. This can be prepared by the co-precipitation of Cu, Zn, and Al salts such as nitrates and alkali bicarbonates or carbonates. The resulting mixed metal hydroxy-carbonates are then calcined at around 300-500 °C to form the mixed metal oxides. The ratio of the oxides is variable depending on the manufacturer, and falls in the range 40-80% CuO, 10-30% ZnO and 5-10% Al_2O_3 [219, 222, 223].

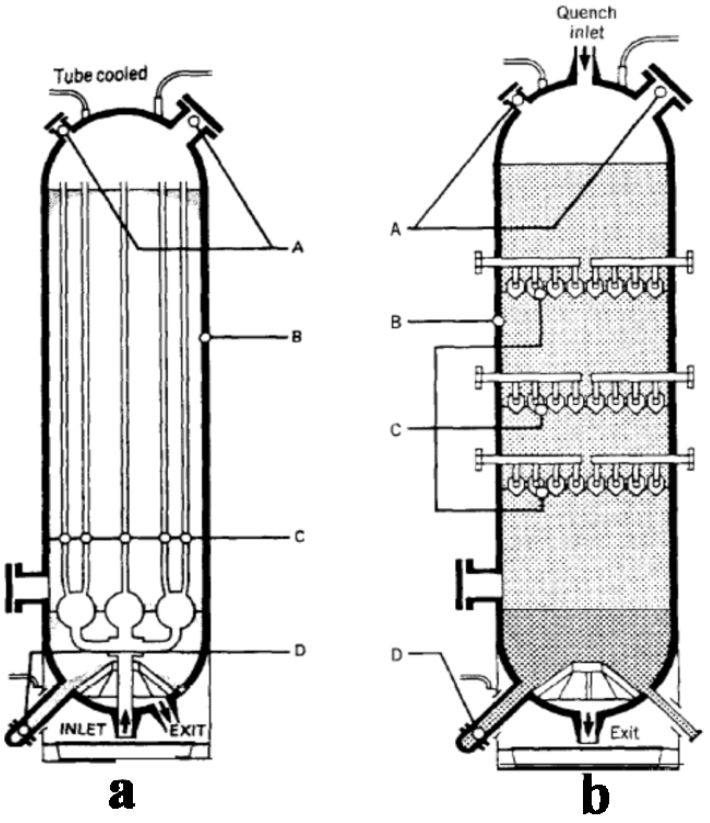

Figure 1.33. Examples of methanol synthesis converters: (a) tube-cooled, low-pressure reactor; (b) quench-cooled, low-pressure reactor [224]. Adaopted from Catalyst Handbook, ed. M.V. Twigg, Manson Publishing Company, London, 1996).

Alkali-promoted ZnO catalysts can also be used in the production of iso-butyl alcohol from synthesis gas at temperatures above 400 °C [65]. $Co/Cu/ZnO/Al_2O_3$ catalysts were also developed by Institut Français du Pétrole (IFP) to produce higher alcohols at relatively low pressures [225]. Zinc oxide has been also used as a formose catalyst. It heterogeneously catalyzes formaldehyde condensation to a complex mixture

of formose sugars at slightly acidic conditions [226]. Other uses of ZnO include as a catalyst for conversion of cyclohexanol to cyclohexanone in the course of the production of caprolactam, $(CH_2)_5C(O)NH$, which is a precursor for nylon 6 [65].

1.5.7. Desulfurisation

Application of ZnO for desulfurisation processes was suggested in 1940 by Johnstone and Singh [227, 228]. The reaction $ZnO + H_2S \rightarrow ZnS + H_2O$ has a favorable ΔG of < -75 kJ/mole between 0 and 1000 °C. Therefore, ZnO can serve as a scavenger for H_2S gas in a variety of fluids and gases, particularly hydrocarbon gases containing H_2S or other sulfur-containing compounds and industrial flue gases [228, 229]. For instance in gas-to-liquid (GTL) production plants, natural gas feedstocks may be desulfurised using ZnO fixed-bed reactors. To lower the sulfur content of process streams to an acceptable level [97, 229], the ZnO specific surface area should be above 20 m^2/g and preferably in the range 50-200 m^2/g. It is typically used in the form of granules or pellets. Operating temperatures may be between -10 °C to +200 °C with a maximum temperature below 300 °C [230]. Although ZnO can be regenerated, its recovery involves calcination at temperatures around 500 °C that releases SO_2 [231]. A schematic of a purification process using ZnO and typical desulfurisation reactors and ZnO absorbent are shown in **Figure 1.34**.

In a typical design, which is in use in the hydrogen unit in Shazand Arak Oil Refinery Company (SAORC) - the biggest single refinery in Iran - two ZnO fixed-bed reactors are used. Design length of the ZnO drum is 2.75 m and its diameter is 1.37 m. Volume of each bed is 6.13 m^3. Initial charge of ZnO to the unit is 12.26 m^3. Extruded ZnO with a bulk density of 1120 kg/m^3 is used. About 14 tonnes of ZnO is charged. The life time of the ZnO bed is around 2 years (internal communication with the refinery).

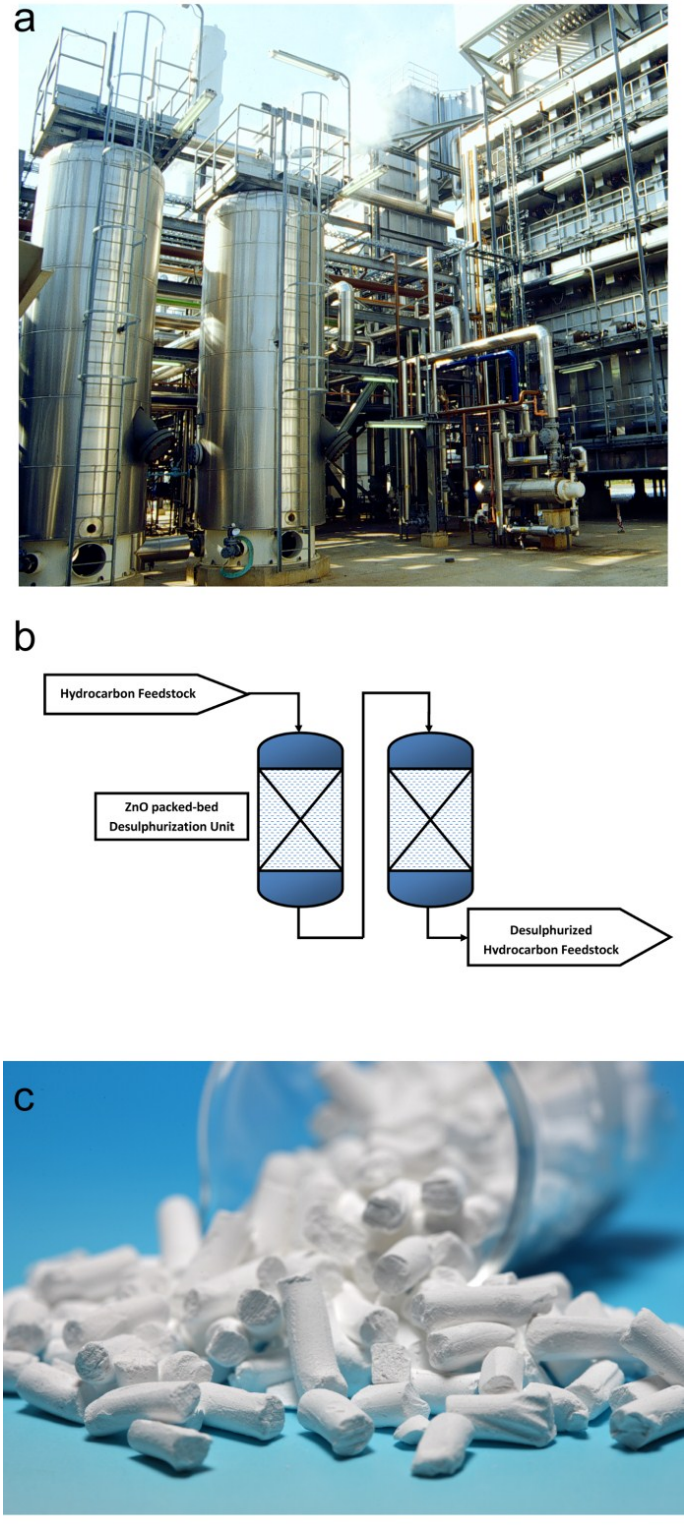

Figure 1.34. a. An industrial desulfurisation unit; b. A schematic diagram of a simplified hydrocarbon feedstock purification unit using ZnO as a desulfurisation absorbent; c. An example of a ZnO desulfurisation absorbent. By permission from Haldor Topsøe, Denmark.

1.5.8. Oil and gas well drilling fluid

Drilling fluids or "muds" in oil and gas industries are used to control formation pressure, cool the bits and carry cuttings from the drill holes to the surface. During the drilling process, H_2S can be formed by the action of sulphate-reducing bacteria (SRB) under anaerobic conditions in sea water or in formation water and can diffuse into the drilling muds. This toxic and corrosive gas should be controlled to reduce health hazards and damage to pipelines and equipment. Maximum acceptable level of this gas in the work environment is 15 ppm. The reaction kinetics and absorption capacity of ZnO make it a useful absorbent for H_2S in drilling fluids with the advantage that spent ZnO sorbent is nontoxic [182]. A very large specific surface area is helpful in this application. 'Nano-ZnO' with a crystal size of <30 nm and specific surface area of >40 m^2/g is suitable. For example, nano-ZnO samples produced by spray pyrolysis and with specific surface area over 44 m^2/g removed 100% of H_2S within 15 minutes in a simulated aqueous drilling fluid. In contrast, bulk ZnO with the specific surface area of 5 m^2/g and a crystal size of about 250 nm removed only 2.5% of the H_2S in 90 minutes [182].

Another important issue in the formulation of drilling fluids is the effect of various constituents on their density and viscosity. In geo-pressured horizontal wells, the density of the drilling fluid should be around 1400-2300 kilograms per cubic meter. Barium sulphate is used as a weighting compound in vertical wells, but is not optimum for horizontal wells, which require that such an additive be soluble in acid [183]. To address the problem, ZnO - which has a density of 5.6 g/cm^3 *vs*. 4.5 g/cm^3 for $BaSO_4$ - has been proposed for use as weighting agents in such drilling fluids [183].

1.5.9. Varistors

Varistors are protective electronic devices with an extremely nonlinear current-voltage curve, generally at low temperatures, **Figure 1.35**. As the voltage increases and reaches a certain voltage (breakdown value), a dramatic increase in current occurs [10, 232]. Zinc oxide in this ceramic form acts as a resistor below the surge voltage and a conductor above that. The I-V characteristic of a varistor is also a function of the

temperature. As the temperature increases, it loses its non-linear characteristics and leaks more readily.

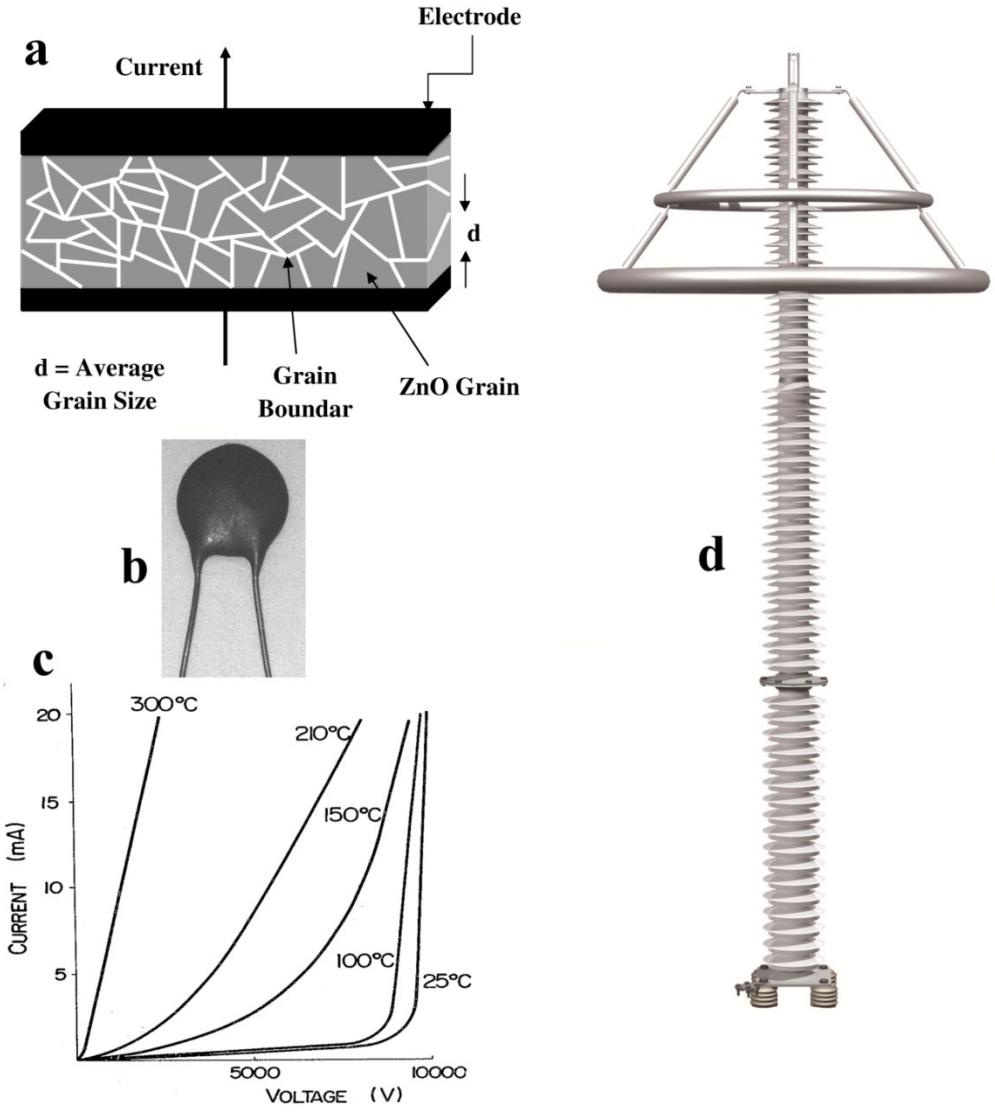

Figure 1.35. (a) Schematic of microstructure of a ZnO varistor [10]; (b) small size varistor; (c) temperature dependence of I-V curve of ZnO varistor [232] and (d) a typical silicone-rubber-housed ZnO surge arrester type PEXLIM P330-YH420 suitable for protection in 420 kV systems by permission from ABB, Sweden.

The first ZnO-Bi_2O_3-based varistor was developed by Matsuoka in Japan in 1969. Today commercially available varistors are mostly based on a polycrystalline matrix of ZnO (grain size around 10 μm) combined with other additives such as oxides of Bi, Co, Cr, Mg, Mn, Ni, Pr, Sb, Si and Ti with contents above ~0.1 mol%. ZnO-based varistors

are widely used in automotive, low-voltage electronic, high-voltage power transmission, avionic and lightning arresting applications to protect the sensitive components of electrical systems. The size of a ZnO varistor depends on the application and varies from a few millimeters for integrated circuit boards to 1 m for high voltage surge arresters. ZnO varistors are relatively cheap with a long life span and can withstand high currents and energies. Their switching response is about 500 ps [232, 233].

Large surge arrestors are made of a stack of individual ZnO varistors of up to 10 cm in diameter. Internal ZnO blocks are manufactured by premixing and pressing the ZnO (e.g. the French process grade) and other metal oxides into the mold. Then the pressed shape is sintered at temperatures above 1000 °C for several hours followed by slow cooling (~100 Kh^{-1}) to form a solid block. The solid block is next coated by a conductive layer followed by stacking the blocks together and sealing them in a vessel made of a ceramic material or molded rubber [232-234]. Detailed processes to manufacture ZnO-based varistors are disclosed in the US patents 5250281 and 4262318 [232, 233].

1.5.10. Fertilisers, food supplements and animal feed

Zinc is an essential micronutrient in all organisms including humans, which is quite important for the healthy growth and metabolism, normal functioning of immune system [235, 236]. During pregnancy the need for zinc increases [237]. It's involved in many proteins within cytoplasm and organelles of the eukaryotic cell. For the mammalian cell, zinc quota is around 10^8 atoms per cell (zinc quota is defined as the total zinc content in cell for the optimum growth) [236]. Gain and loss of the zinc in animals are regulated efficiently. In humans this is controlled by two systems: intake from the intestine and loss via pancreatic and intestine secretions [238].

Diet, therefore, is the most important factor that determines the zinc intake to the body. The efficiency of adsorption is in the range of 15-35% in adults. Zinc deficiency especially in developing countries is reported and it's estimated that around one-third of the world's population live in the zinc deficient areas and thus at risk. Zinc deficiency has a role in physical growth, morbidity and mortality from infections (such as diarrhea and pneumonia) particularly in young children and also adverse effects on the health of the mother and fetus during pregnancy and lactation [239].

Water-soluble or insoluble zinc fertilisers are used to provide traces of Zn in deficient soils. These are especially important for rice, corn, potato, beans and oil palm where relatively large amounts may be used. The zinc-containing material may be applied directly, or blended with another product such as urea [240]. Alternatively, ZnO could be added to the composition of a pesticidal-micronutrient to provide the required zinc for spray application to crops [37, 241] or suspended in water with a dispersant such as calcium lignosulphonate.

Free-flowing 'feed grade' ZnO is a special grade with Zn content between 72-79%, ZnO content of 90-99% and (usually) a high bulk density between 1600-2400 kg/m^3, which can be easily handled, stored in silo trucks and weighed automatically. Feed grade ZnO is mostly used in animal feed for piglets, cats, dogs, cattle or poultry. There is some ambiguity concerning the method by which feed grade ZnO should be manufactured. Edwards and Baker [242] examined the efficacy of four grades of 'feed grade' ZnO in the North American chicken industry and found that they varied widely. Furthermore, the materials used had been manufactured by at least three processes: the direct process (in a Waelz kiln), the sodium dithionate process and the French process. Table 3 shows the chemical composition of a typical 'feed grade' ZnO.

Table 3. Chemical purity of a typical feed grade zinc oxide [243].

Zn	Min. (%)	72.0
Pb	Max. (%)	0.04
Cu	Max. (%)	0.01
Cd	Max. (%)	0.0001
As	Max. (%)	0.005
Cl	Max. (%)	0.1

Food fortification is considered as an effective and the most economic method, which increases the dietary zinc intake and adsorption for humans [239]. Zinc oxide and to a lower extent zinc sulphate (two cheapest zinc chemicals commonly used by food industries) are generally applied to the food for example wheat, rice and maize flours [235, 239, 244, 245]. Companies such as Kellogg make use of zinc oxide in the compositions of fortified cereal and chocolate bar [246-248]. Zinc as ZnO is also seen in the compositions of multivitamin and mineral tablets as dietary supplement. A typical tablet contains 5 to 10 mg of zinc oxide. Zinc is good for skin, hair, nail and eyes. Zinc

oxide is recommended in the supplement compositions for age-related macular degeneration eye disease [249]. Zinc can be also seen in infant food formula. For example in a product by Nesle, Nan Pro Gold, average of 0.7 mg of zinc is fed to the baby per 100 ml of food in the form of zinc sulphate [250]. There is another infant food product by Locasol, which is designed for those with extreme restriction on calcium and vitamin D. This composition contains 3 mg of zinc per 100 g of powder [251]. Obviously, only the purest ZnO, *i.e.* pharmaceutical grade, should be used in these applications.

1.5.11. Zinc oxide in chemical synthesis

Zinc ferrite spinels, $ZnFe_2O_4$, are important sorbent materials for high-temperature (up to around 700 °C) desulfurisation of coal gas. Catalytic grade of zinc ferrite can be manufactured by calcination of a 1:1 mol ratio of zinc oxide and iron oxide mixture [252]. The sulfur content of the desulfurised gas is usually lower than 10 ppm, which is acceptable for use in the gas turbines in the power plants [253]. Soft Mn-Zn ferrites - $Mn_xZn_{(1-x)}Fe_2O_4$ - and Ni-Zn ferrites - $Ni_xZn_{(1-x)}Fe_2O_4$ - are also important ferromagnetic materials for electronic applications such as transformers, electromagnetic gadgets, antenna rods, magnetic recording heads, noise filters, choke coils, information storage, medical diagnostic and biomedical devices and magnetic amplifiers [254-256]. The term "*soft*" is used due to their low magnetic coercivity. Zinc ferrites containing other elements such as Mg, Cu are also used in some electronic application [257].

Zinc phosphate, $Zn_3(PO_4)_2$, is used in corrosion-resistant paints for metal structures and as a filler in the manufacture of vulcanisates to increase heat-resistance. It is also used as an anti-galling agent in the couplings of drill strings for the oil and gas industry. Zinc phosphate, which is insoluble in water, can be prepared by a reaction between ZnO and phosphoric acid in an aqueous medium [258]. See **Figure 1.36**.

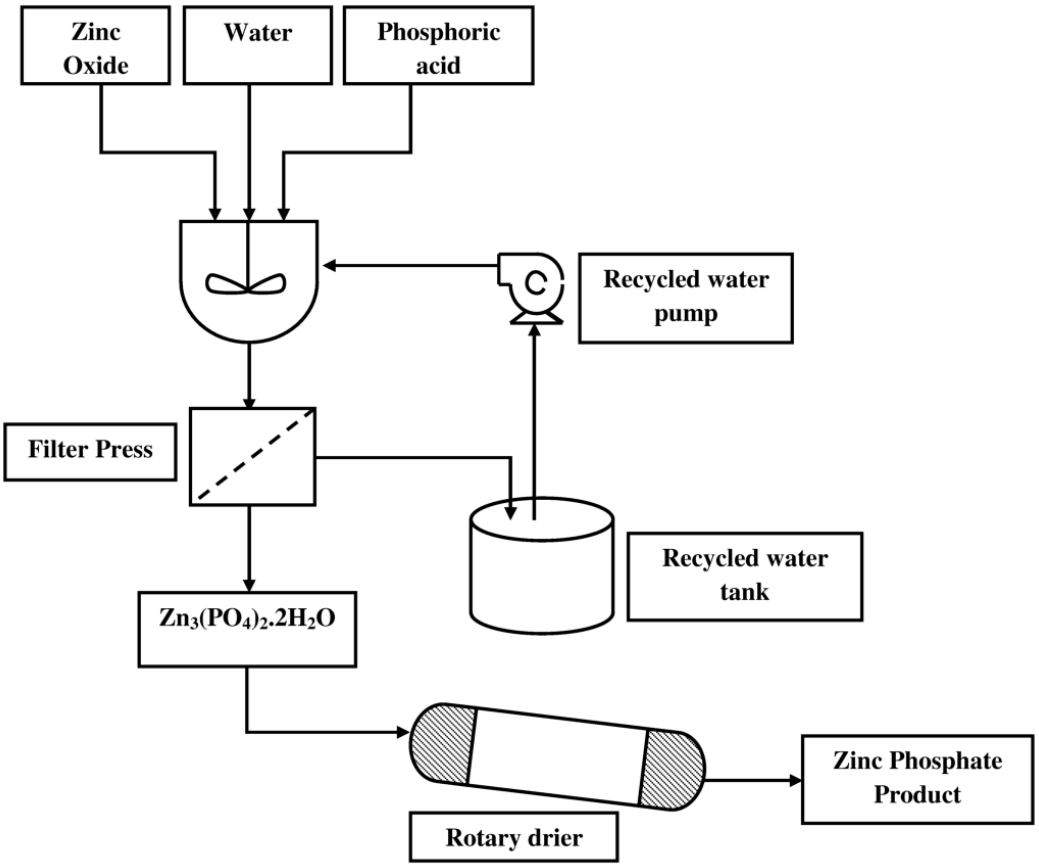

Figure 1.36. PFD of production of zinc phosphate from zinc oxide.

Zinc borate ($xZnO{\cdot}yB_2O_3{\cdot}zH_2O$) is a white powder with low water solubility and high dehydration temperature. It has applications in polymer compositions as a fire retardant and as smoke suppressant and in the wood, textile and cement industries. (ZnO is also considered a fire-retardant, for example in nylon 6,6 [201]). Zinc borate may be prepared by a reaction between ZnO and boric acid in an aqueous medium at temperatures around 90-100 °C [259, 260]. See **Figure 1.37**.

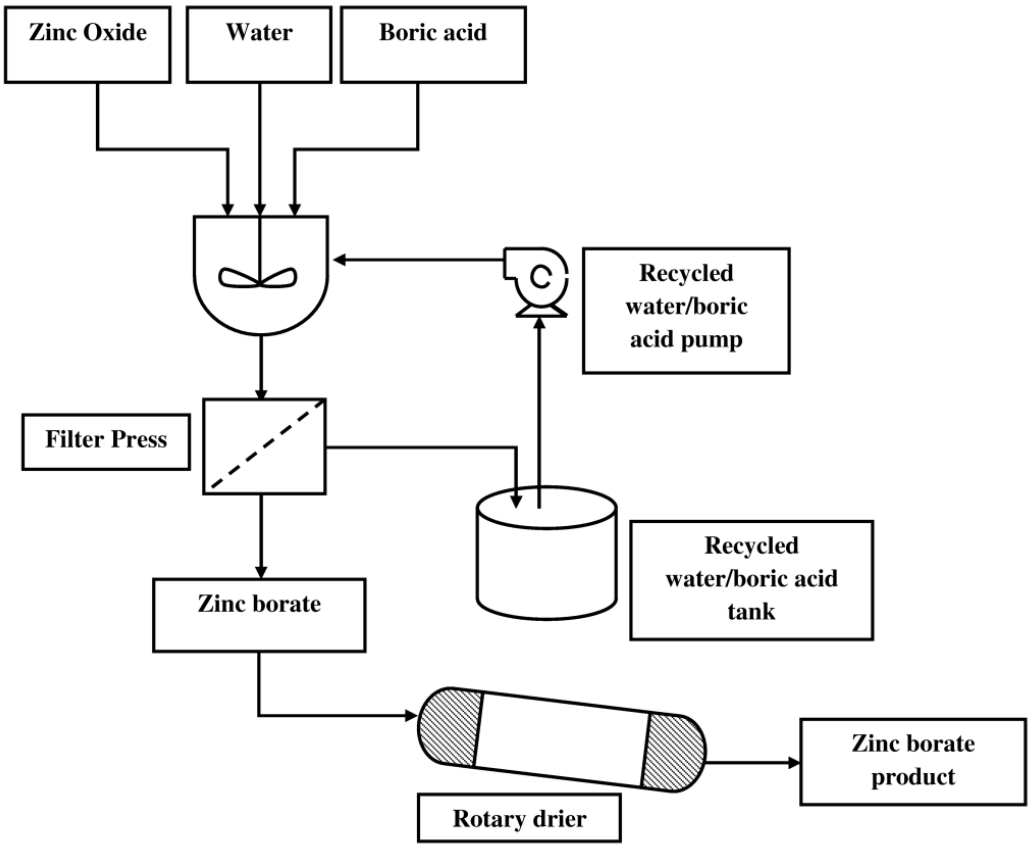

Figure 1.37. PFD of production of zinc borate from zinc oxide.

Zinc dialkyldithiophosphates (ZDDPs) are oil soluble coordination compounds used in the lubricant industry as anti-wear and anti-oxidant agents. Metal dialkyldithiophosphates were developed by Herbert Freuler and patented in 1944 [261]. Zinc oxide plays an important role in the production of ZDDPs. First, dialkyldithiophosphate is synthesised by reacting powdered phosphorous pentasulfide (P_2S_5) with alkyl alcohol, and then the dialkyldithiophosphate is neutralised by ZnO to yield the zinc dialkyldithiophosphate [262].

Zinc diacrylate used in golf balls can be prepared by reacting acrylic acid with ZnO-fatty acid mixture in a liquid medium [263].

Zinc stearate can be manufactured from zinc oxide and stearic acid. One application for it is in the tire industry, where it may be used to dress the steel molds to assist with release of the tire. It may also be added to the initial blend for the rubber, but generally in far smaller quantities than ZnO itself.

1.5.12. Miscellaneous applications

ZnO in phosphors: Phosphors are compounds (mainly of the transition metals) that luminesce with a characteristic output spectrum under certain conditions of optical excitation. A phosphor known as 'ZnO:Zn' (JEDEC No. P-15) has been used for decades in cathode ray tubes (CRTs) and other devices where an electron beam must be converted to light (green in this case). ZnO may also be used as a precursor in the manufacture of other phosphors, such as $Zn_2SiO_4:Mn^{2+}$ (JEDEC No. P-1), which is used as green phosphor in thin-film electroluminescence displays [10]. A blue-emitting phosphor, $(Li_{0.5}Ga_{0.5})_{0.5}Zn_{0.5}Ga_2O_4$, for field emission devices (FED) applications was manufactured from $ZnO\text{-}Ga_2O_3\text{-}Li_2O$ system and showed a CL efficiency up to 0.2 LmW^{-1} in the voltage range of 100–600 V [264].

Smoke-producing devices: Military smokes are used to temporarily obscure objects from visible or infrared observation. The fine airborne dispersion of liquid droplets or particulate solids causes light to be scattered. Opacity, duration of effect, cost, toxicity and dispersion properties of screening smokes are important factors in this field [201, 265]. Optimum scattering is obtained when the particle size of the aerosol is about the same as the wavelength of light to be screened. Zinc oxide-hexachloroethane (HCE) smokes are well-known in this industry. A typical composition contains aluminum powder, ZnO and HCE that is labeled HC, type C by U.S. Army in which the ratio (w/w) of ZnO to HCE is almost 1. All the constituents are in solid form and as a result can be compacted in small volumes for applications such as smoke grenades, smoke pots, and artillery shells. Reaction between HCE and ZnO forms zinc chloride-water smoke. However $ZnCl_2$ smoke produced from this reaction is relatively toxic (even more toxic than titanium-based smokes) and can cause severe respiratory symptoms [265, 266].

ZnO in paper: Another niche application for ZnO is in specialised paper coatings, high pressure laminates and wallpaper. It can improve the cohesive strength of paper coatings [267]. High purity ZnO (such as the French process ZnO) has photoconductive properties [157, 181]. It can also hold negative electrostatic charge, which can be discharged when UV or deep blue radiation is applied. These characteristics were formerly used in papers used for electrostatic photocopying. In this case, a coating of ZnO mixture with a resinous binder was applied on the paper [181].

Corrosion inhibition: A corrosion inhibitor is an additive to a fluid or gas that decreases the corrosion rate of adjacent metallic structures. Zinc oxide as a cathodic inhibitor slows the corrosion by inhibiting the reduction of water to hydrogen gas. For example, in alkaline aluminum batteries, ZnO can inhibit the corrosion of aluminum anode [268].

Polymer-modified-asphalt: Polymer-modified asphalts (PMAs) such as those modified by incorporation of elastomeric polymers (e.g. polybutadiene) are used in applications requiring improved physical and mechanical properties compared to non-modified asphalt compositions. To prepare PMAs, activators and accelerators are applied to accelerate the crosslinking reaction. Zinc oxide and mercaptobenzothiazole (MBT) are conventional activator and cross-linking agent materials, respectively. ZnO also controls the polymer tendency to gel [269].

Fungistat: Zinc oxide and its derivatives contribute effectively to the control of fungi in many different types of applications. Zinc oxide is not a fungicide per se; rather it is a fungistat; i.e. it inhibits the growth of fungi, such as mildew on the surface of exterior house paints. Its fungistat effect increases with its surface area. ZnO inhibits the growth of mycelium or the germination of spores. However it does not kill the spores or prevent their germination after exposure to a more favorable environment. It can, however, be added to fungicides for fortification to take advantage of its fungistatic property [270].

1.6. Potential and emerging applications

There are several emerging applications of ZnO in the area of electronics and optoelectronics, driven by specific optical or electrical characteristics of this semiconductor.

1.6.1. Liquid crystal displays (LCDs)

Transparent conductive oxides (TCOs) are currently used in a large variety of consumer goods, including liquid crystal displays. In general, they are based on indium tin oxide (ITO). However, there are concerns that indium resources will be insufficient to service future growth and there is an active quest for alternative or cheaper materials.

Zinc oxide films that have been doped with *n*-type dopants such as Al, Ga and In are promising candidates to fill this requirement. These materials may be deposited by magnetron sputtering, and are of special interest due to their high conductivity and optical transparency, high thermal stability and relatively lower cost [10, 166, 271, 272].

1.6.2. Light emitting diodes (LEDs)

A large exciton binding energy is an important factor in the design of LEDs. Zinc oxide, with the relatively high exciton binding energy of 60 meV, shows promise in blue/UV light emitters. The field has recently been reviewed by Choi *et al.,* [273]. A challenge for the production of ZnO-based light emitters, however, is producing reliable, low-resistivity *p*-type ZnO, a problem that is not yet resolved [9, 162, 273]. Zinc oxide is currently being explored for applications such as in UV lasers [154, 274], in blue LEDs [154], and in organic LEDs [4, 10].

1.6.3. Spintronics

Dilute magnetic semiconductors are potentially important materials for spintronics with proposed applications in, for example, integrated memory devices and microprocessors. As described in Section 1.4.6, doped materials such as ZnO:Mn are of interest because of their ability to exhibit ferromagnetism above room temperature. This field is still in its earliest phases, however, and no significant commercial application of semi-conductor spintronics has emerged yet [162].

1.6.4. Solar cells

Zinc oxide has a role in two disparate aspects of photovoltaic technology. First, use of transparent, conductive ZnO in the front electrodes of solar cells can eliminate the shadow effect related to metal-finger contacts and is also cheaper than the alternative indium oxide electrodes [4, 10]. Secondly, *n*-type ZnO films may also be used within the photovoltaic structure itself, for example as a tunnel junction in amorphous silicon cells or as part of the p/n junction in $Cu(In,Ga)(S,Se)_2$ cells [10].

1.6.5. Sensors and actuators

The sensitivity of the electrical resistivity of ZnO to gases such as ethanol, acetylene, CO, NO and NO_2 makes it potentially useful for sensing applications. A drawback, however, is its poor selectivity [5]. Selective NO_x sensing may be achieved by mixing with other selective metal oxides such as Al_2O_3 and V_2O_5 [275]. Zinc oxide nanowires may be useful in room temperature sensing applications and, for example, a glucose sensor based on ZnO nanorods has been reported [276].

The piezoelectric property of ZnO makes it suitable for applications in acoustic microscopy, BAW, acousto-optic and SAW devices [277] for use in telecommunications industries (e.g., in mobile phones and base stations), piezoelectric sensors, or torque or pressure sensors in automotive industries. A SAW ZnO sensor has been studied for its potential application in wine differentiation [278].

1.6.6. ZnO in textiles

The application of ZnO (produced by the wet chemical process) to fabrics such as cotton and polyester may impart beneficial antimicrobial characteristics, enhanced whiteness, resistance to UV radiation and anti-static properties [84, 279]. However, large-scale application of ZnO in the textile industry has not yet occurred to our knowledge. In any case, in our opinion the commercial penetration of such a product into Organisation for Economic Cooperation and Development (OECD) markets will very likely run into consumer concerns regarding the safety of nano-particles. While a clear medical case can be readily made for use of ZnO or other nano-particles in a product such as sunscreen, their use in consumer clothing might be a harder case to sell.

1.7. Conclusions

Zinc oxide has been an important industrial material for centuries and is currently the subject of considerable new interest. It has a combination of physical properties (such as relatively high electrical and thermal conductivity, optical absorption in the ultra-violet and very high temperature stability), chemical properties (such as stability at neutral pHs and mildly antimicrobial action), and techno-economic attributes (such a ready

availability and reasonable cost) that have ensured its use in an exceedingly wide range of industries.

Methods of production of ZnO have evolved continuously. The larger scale pyrometallurgical processes produce crystalline ZnO powders for the rubber and other large scale industries, but the niche applications are served by an extraordinary variety of small-scale production methods, with the choice of technique matched to the end-use properties required. There does not seem to be any feasible substitute at present for the use of ZnO in rubber, and this application is likely to remain the dominant one for decades to come. However, given the very versatile and useful nature of ZnO as a material, it is possible that new and unanticipated applications for ZnO will arise and become economically important. Current experience shows that the new applications are as likely to be supplied by one of the smaller-scale production techniques described here, as by the pyrometallurgical ones, so from a production point-of-view, the field remains lively and interesting.

Although ZnO has been used in cosmetic and medical applications for thousands of years, there has of late been a campaign in some countries within the OECD to alert the public to its potential ‘toxicity’. Certainly ZnO is not totally inert, of course, and if it was it would not be of value in many of its current applications that rely upon a small but controlled degree of chemical reactivity. Nevertheless, the issue seems to be over-rated in general. As shown here, more than half of all ZnO production goes into the rubber of motor car tires, which gradually abrade away during use anyway. The urban and roadside environment has therefore been well covered by now in particulate ZnO, but that issue hardly rates any comment in the literature.

Zinc oxide has enjoyed a variety of uses over the last century, some of which (such its use in photocopying) have appeared and then disappeared a few decades later in quite a dramatic fashion. However, in our opinion the useful set of physical and economic attributes of this material will ensure that it will continue to be considered for an impressively diverse range of existing and future applications.

Chapter 2

Single-Stage Process to Synthesise Zinc Oxide Using Sodium Hydroxide

Chapter 2: Single-Stage Process to Synthesise Zinc Oxide Using Sodium Hydroxide*

In this chapter, the effect of reactant concentrations, temperatures and feeding methods on the morphology of ZnO formed when reacting solutions of $ZnSO_4$ and NaOH are examined. The catalytic effect of hydroxide in excess relative to the stoichiometric ratio is considered. It is shown that, having fixed other reaction conditions, the end-products, particle structures and size strongly depend on the mole ratio of the precursors. The presence of zinc salt hydroxide species was confirmed at sub-stoichiometric ratios in slightly acidic conditions. At the stoichiometric ratio both zinc hydroxide and zinc oxide are formed, while only zinc oxide forms in an excess of hydroxide. The method of feeding the reactants into the reaction vessel also has a strong influence on the end-product properties, as does the reaction temperature. By control of these parameters the specific surface area could be varied from 10 to 33 m^2/g, the particle shape could be varied from equiaxed, through to star-like and needle-like, and the particle size may be varied from 50 to over 300 nm.

2.1. Introduction

As explained in Chapter 1, zinc oxide is an important material utilised in a diversity of industrial, biomedical, cosmetic and scientific applications. High volume uses include as an ingredient in rubber tires and as a pigment in corrosion-resisting paints. In addition, it has a number of small volume, high-tech applications such as in gas sensors, piezoelectric materials, transparent conducting oxide films, phosphors, UV blocking agents, anti-bacterial ointments or catalysts [2, 3, 130, 280]. High-temperature, gas-phase routes are currently the preferred method to produce ZnO particles for bulk industrial use [24, 47], while hydrothermal techniques can be used to grow single crystals suitable for some advanced applications [7]. However, a large number of low-temperature wet-chemical methods are also possible and provide access to particles with different structures and properties than those produced by gas-phase or hydrothermal

* A significant part of the work presented in this chapter has been published (see Moezzi, Cortie and McDonagh, Dalton Trans. 40(18) (2011) 4871-4878).

syntheses. In particular, precipitation reactions in unpressurised aqueous media offer relatively low cost compared to other methods of synthesis.

The shape and size of zinc oxide crystals formed from aqueous solutions is quite variable. A number of prior studies have investigated the aqueous-phase synthesis of zinc oxide and the principles are now broadly understood [7, 139, 281-286]. However, there is still considerable uncertainty regarding the possible role of zinc hydroxide in this process, the mechanism by which the zinc hydroxide (if it forms) converts to zinc oxide, and the factors effecting product morphology. There are conditions that evidently lead directly to the precipitation of ZnO [281, 282] and others in which an intermediate $Zn(OH)_2$ phase has been demonstrated [281] or claimed [283]. It is observed that this intermediate phase can convert to ZnO by the mechanism of dissolution-precipitation [139] or by solid state transformation [281, 283]. There is evidently also an interplay between kinetics and thermodynamics in these processes. For example, it is claimed [287] that zinc hydroxide can be precipitated at room temperature from a system of Zn^{2+} and OH^-. However, at higher temperatures ZnO is always the more likely end product [284, 287, 288]. Other studies have examined the very significant effects of process variables such as stirring, temperature or pH on the identity and morphology of the product [139, 281, 284].

Here a comprehensive analysis of the effect of critical reaction parameters on the morphology of the ZnO particles prepared in the $H_2O/Zn^{2+}/OH^-$ system at temperatures less than 90 °C is provided. Importantly, an understanding of the mechanisms and phenomenology of formation provide a means to control the shape and size of ZnO particles produced by this route.

In aqueous environments, the following reactions are the main contributors to the formation of zinc oxide [289-292]:

$$Zn^{2+}_{(aq)} + OH^-_{(aq)} \rightarrow Zn(OH)^+_{(aq)} \quad 2.1$$

$$Zn(OH)^+_{(aq)} + OH^-_{(aq)} \rightarrow Zn(OH)_{2\,(s)} \quad 2.2$$

$$Zn(OH)_{2\,(s)} \rightleftharpoons Zn(OH)_{2\,(aq)} \quad 2.3$$

$$Zn(OH)_{2\,(aq)} + OH^-_{(aq)} \rightarrow Zn(OH)^-_{3\,(aq)} \quad 2.4$$

$$Zn(OH)^-_{3\,(aq)} + OH^-_{(aq)} \rightarrow Zn(OH)^{2-}_{4\,(aq)} \quad 2.5$$

$$Zn(OH)_{2\,(aq)} \rightarrow ZnO_{(s)} + H_2O_{(l)} \quad 2.6$$

$$Zn(OH)_{2\,(s)} \rightarrow ZnO_{(s)} + H_2O_{(l)} \quad 2.7$$

$$Zn(OH)^-_{3\,(aq)} \rightarrow ZnO_{(s)} + H_2O_{(l)} + OH^-_{(aq)} \quad 2.8$$

$$Zn(OH)^{2-}_{4\,(aq)} \rightarrow ZnO_{(s)} + H_2O_{(l)} + 2OH^-_{(aq)} \quad 2.9$$

These reactions are primarily governed by the pH of the system. Equations **2.1** to **2.5** describe the formation of zinc hydroxide complexes. The species formed in Equation **2.1** is shown as $Zn(OH)^+$ for clarity, but a zinc hydroxide salt complex with the general formula of $Zn_a(OH)_b(X^{c-})_{(2a-b)/c} \cdot nH_2O$ (where *X* may be, for example, Cl^-, NO_3^-, CO_3^{2-}, CH_3COO^- or SO_4^{2-}) is often produced [293] when the concentration of OH^- is less than that required to produce $Zn(OH)_2$. These zinc hydroxide salt complexes vary in solubility depending on the anion, *X*. When the OH^- : Zn^{2+} molar ratio is 2 : 1 (Equation **2.2**), the reaction product is $Zn(OH)_2$ [294, 295]. $Zn(OH)_2$ has low solubility in water (K_{sp} = 3.5 ×10^{-17} at 25 °C) [284, 290] and is stable, for example it has been reported to remain unchanged after six months in water at room temperature [296]. Equations **2.4** and **2.5** indicate that if more hydroxide is added, soluble higher-order hydroxo-complexes of zinc may be formed. Importantly, these can decompose to ZnO, releasing hydroxide ions and water (equations **2.8** and **2.9**).

The solubility of the zinc-containing species is an important consideration in the pathway to the formation of ZnO. The fraction of zinc species such as $Zn^{2+}{}_{(aq)}$, $Zn(OH)^+{}_{(aq)}$, $Zn(OH)_{2(aq)}$, $Zn(OH)^-_{3\,(aq)}$ and $Zn(OH)^{2-}_{4\,(aq)}$ in solution varies over a range of pH at 25 °C [287, 289, 290]. In acidic conditions (pH<6), Zn^{2+} is the main ion present in solution, in neutral to slightly basic conditions most Zn is present as solid $Zn(OH)_2$ or ZnO, which both have very low solubility products in this range of pH, while at pH=12 or above, the main zinc species is $Zn(OH)^{2-}_4$ [297]. In such alkaline conditions precipitation of ZnO does not occur due to the stability of $Zn(OH)^{2-}_{4\,(aq)}$ ions [139, 298] according to Equations **2.4** and **2.5**. The relatively low solubility of $Zn(OH)_2$ and ZnO over the range of intermediate pHs is an important aspect of the present work.

Seven crystal forms of $Zn(OH)_2$ have been reported with ε-$Zn(OH)_2$ the most stable [288, 289, 292]. Because of the relative stability of solid $Zn(OH)_2$, it is important that this species is either avoided or re-solubilised if timely formation of the even more stable solid ZnO is to be achieved. Polynuclear zinc complexes such as $Zn_2(OH)^{3+}{}_{(aq)}$, $Zn_2(OH)_6^{2-}{}_{(aq)}$ and $Zn_4(OH)_4^{4+}{}_{(aq)}$ may also be present at high total zinc concentrations [289].

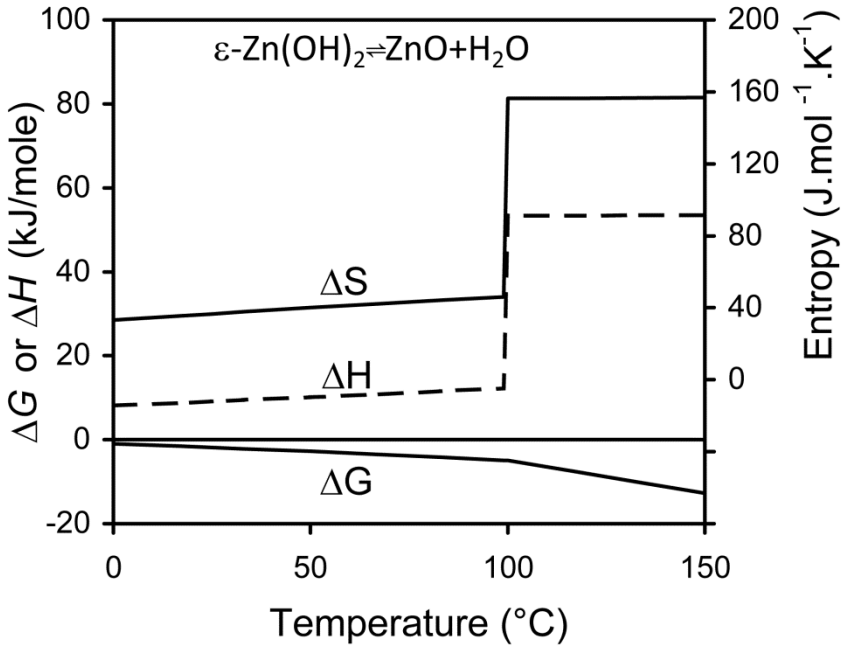

Figure 2.1. Thermodynamic parameters for the reaction of solid ε-$Zn(OH)_2$ to solid ZnO and H_2O. The values are computed from the standard states at 298 ºK at 1 atmosphere using the specific heat capacities from reference [287].

Temperature also plays an important role in the synthesis of nanoparticles by changing the kinetics of the above-mentioned precipitation reactions. The decomposition of solid zinc hydroxide to ZnO and $H_2O_{(l)}$ is endothermic at room temperature [299] (ΔH = +9.11 kJ/mol using the data of Goux *et al.,* [287]) but ΔG is slightly negative (ΔG = -1.7 kJ/mol). Values of the thermodynamic parameters can be calculated at other temperatures from knowledge of the specific heat capacities and are plotted in **Figure 2.1**. Clearly, the conversion of $Zn(OH)_2$ to ZnO will be increasingly favored at higher temperatures, both from a free energy and a kinetic perspective [288]. In this chapter, the interplay of these reaction parameters is reported and their effect on the properties of zinc-containing products using aqueous reaction conditions at temperatures less than 90 °C and at atmospheric pressure are examined.

2.2. Experimental

2.2.1. General

Zinc sulphate heptahydrate (AR grade) and sodium hydroxide pellets (AR grade) were purchased from Ajax Chemicals and used as-received. French process zinc oxide was provided by PT. Indo Lysaght, Indonesia. Milli Q water (18.2 Ω cm^{-1}) was used as the solvent. Reactions were conducted under atmospheric conditions using a two-neck round bottom flask with a digitally-controlled magnetic heater / stirrer. A magnetic stirrer bar was used at a stirring rate of 820 rpm. Precipitates were isolated by centrifugation at 4400 rpm followed by drying using a rotary evaporator at 70°C, unless otherwise stated.

X-ray diffraction data of powder samples were collected using a Siemens D5000 X-ray Diffractometer with a graphite post monochromator with the following parameters: wavelength 1.5406 Å (Cu K*a*), tube power 1.6 kW (40 kV at 40 mA), step size = 0.02 °, time per step = 2 s, divergent slit = 1 °, receiving slit = 0.02 mm, scan angle range = 3–80 °. Scanning electron microscopy images were obtained using a Zeiss Supra 55VP SEM operating in high vacuum mode. An accelerating voltage of 5-20 kV was used with 10-30 μm aperture and images were obtained using an in-lens secondary detector.

Thermogravimetric analysis (TGA) experiments were performed using a TA Instruments SDT 2960 with simultaneous DTA-TGA. A heating rate of 5 °C min^{-1} was used in a nitrogen atmosphere.

BET specific surface area measurements were performed using an Autosorb-1 from Quantachrome Instruments by a precise vacuum volumetric method for nitrogen chemisorption. Multi-point (5 points) measurement was conducted on each sample.

Fluorescence spectrometry experiments were performed at room temperature to record the fluorescence emission spectra of powder samples using a Varian Cary Eclipse with an excitation slit width of 5 nm and emission slit width of 5 nm. Both excitation and emission filters were used to screen higher order wavelengths.

Thermodynamic data for the formation of ZnO from Zn^{2+} and OH^- were calculated for reactions at 298 K and 1 atm. Standard enthalpies and Gibbs free energies of the reactions were calculated using the available thermodynamic data [89, 289]. The

solubility product for ZnO was obtained from reference [291] and that of $Zn(OH)_2$ from reference [290].

2.2.2. Reactant stoichiometry

Aqueous solutions of $ZnSO_4 \cdot 7H_2O$ (30ml, 0.05M) and NaOH (30 mL) with concentrations from 0.1 M to 0.3 M were prepared.

Table 2.1. Zinc sulphate to sodium hydroxide mole ratio. The pH of the resultant mixtures after reaction was in the range of 11 to 12.

Reaction	A	B	C	D	E	F	G	H
Zn^{2+} : OH^- mole ratio	1 : 2	1 : 2.3	1 : 2.5	1 : 3	1 : 3.5	1 : 4	1 : 5	1 : 6

Table 2.1 shows the concentration of NaOH for each of the reactions A to H. For each of these experiments, the NaOH solution was added dropwise to the zinc sulphate solution over 3 minutes. The total volume of the reaction solution for each experiment was identical. After two hours of reaction at room temperature, the various precipitates were collected and washed with water and dried at 70 °C under reduced pressure.

A separate reaction using zinc sulphate and sodium hydroxide was conducted where the OH^- : Zn^{2+} mole ratio was only 1.1 : 1. An aqueous solution of zinc sulphate heptahydrate (30 mL, 0.1 M) was added to a sodium hydroxide solution (33.5 mL, 0.1M) in a single step and the reaction maintained at room temperature for 15 minutes. The resultant white precipitate was separated, washed and dried at 60 °C under reduced pressure.

2.2.3. Method of combining the reactants

Aqueous solutions of $ZnSO_4 \cdot 7H_2O$ (30 mL, 0.05M) and NaOH (30 mL, 0.2M) were prepared. The reaction temperature was maintained at 70 °C for 2 hours. The reactants were combined using each of the following four procedures: (1) the sodium hydroxide solution was added to the zinc sulphate solution in a single step; (2) The sodium hydroxide solution was added to the zinc sulphate solution in a drop-wise manner over

3 minutes; (3) The zinc sulphate solution was added to the sodium hydroxide solution in a single step; (4) The zinc sulphate solution was added to the sodium hydroxide solution in a drop-wise manner over 3 minutes.

2.2.4. Reaction temperature

Experiments were performed with the reaction temperature maintained at 25 °C, 30 °C, 40 °C, 45 °C, 50 °C, 55 °C, 60 °C, 65 °C, 70 °C, 75 °C, 80 °C, 85 °C and 90 °C. In each case, an aqueous $ZnSO_4 \cdot 7H_2O$ solution (30 mL, 0.05 M) was added to an aqueous NaOH solution (30 mL, 0.2 M) in a single step. The reaction mixtures were stirred for two hours after which the precipitate was separated and washed.

2.3. Results and Discussion

In the current work, the variation of several reaction parameters on the resultant zinc-containing particles was investigated. The reaction parameters varied were: (i) the stoichiometry of the reactants, (ii) the method of combining the reactants, and (iii) the effect of reaction temperature.

2.3.1. The effect of reactant stoichiometry

To examine the effect of the stoichiometry, the mole ratio of $ZnSO_4$: NaOH was varied from 1:2 to 1:6, and the NaOH added drop-wise as described in the Experimental section. This range covers mole ratios from the stoichiometric ratio (1:2, Reaction A) required to convert Zn^{2+} to ZnO (Equation. **2**.**10**) to an excess of NaOH of three times the stoichiometric ratio (1:6, Reaction H).

$$Zn^{2+}_{(aq)} + 2OH^{-}_{(aq)} \rightarrow ZnO_{(s)} + H_2O_{(l)} \qquad 2.10$$

The XRD patterns revealed that the products of Reactions A and B contained a mixture of ε-$Zn(OH)_2$ and ZnO (see **Figure 2.2**). This indicates that at the stoichiometric ratio, or very close to it, significant amounts of $Zn(OH)_2$ remain after 2 hours reaction time. However, increasing the mole ratio of OH^- : Zn^{2+} from 2 : 1 (Reaction A) to 2.3 : 1 (Reaction B) leads to a significant decrease in the XRD signal

intensity for ε-$Zn(OH)_2$ compared to ZnO. The products of the reactions with even larger mole ratios of OH^- : Zn^{2+} (2.5 : 1 and above) contained ZnO only (see **Figure 2.2** and **Figure 2.3**).

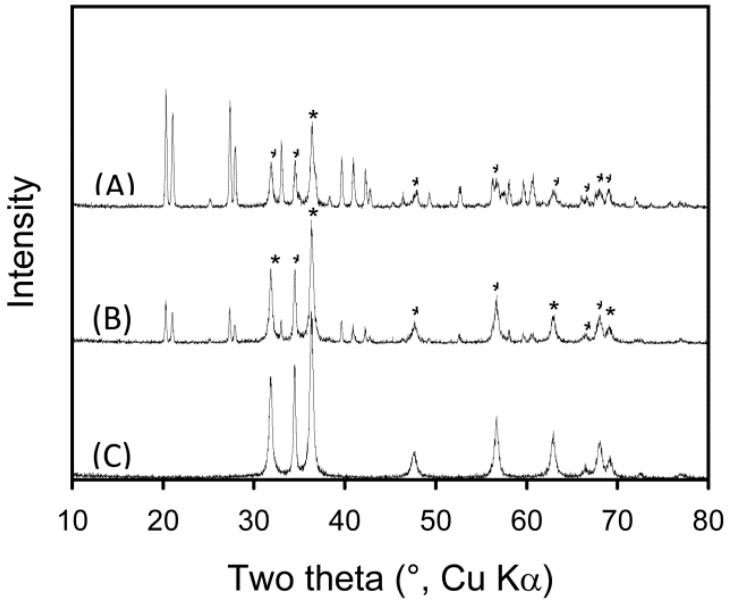

Figure 2.2. X-ray diffraction data obtained from the products of reactions A, B and C. The diffraction pattern for product C corresponds to pure ZnO (wurtzite). The peaks assigned to ZnO are indicated by * in the data for A and B. Other peaks in A and B correspond to ε-$Zn(OH)_2$.

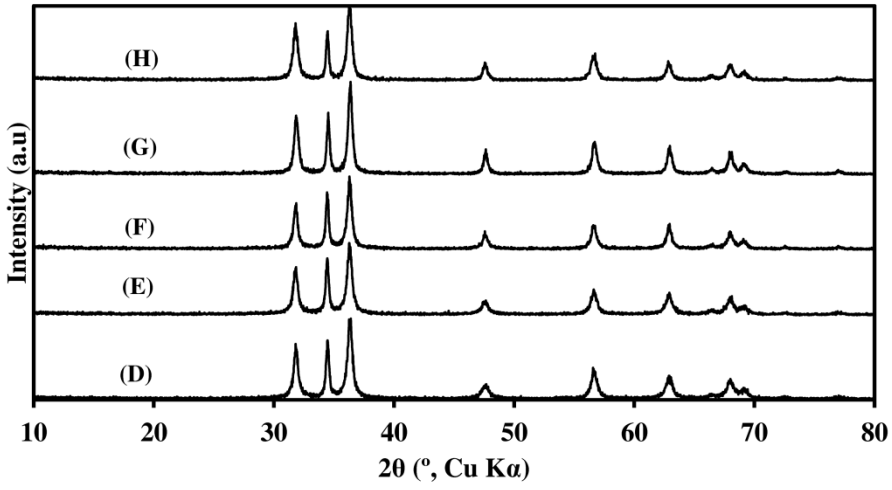

Figure 2.3. XRD on the products of reactions (D) to (H) shows patterns, which conform with zinc oxide.

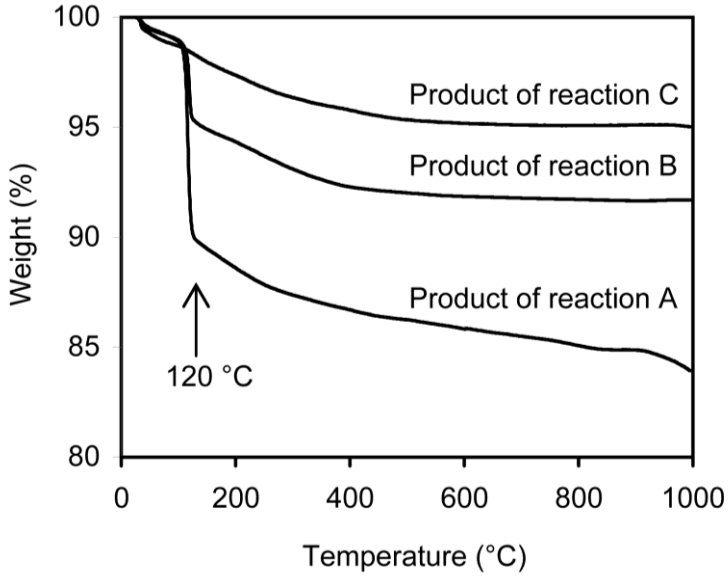

Figure 2.4. Thermogravimetric analysis data for the products of Reactions A, B and C. Heating rate was 5 °C min^{-1} in an N_2 atmosphere.

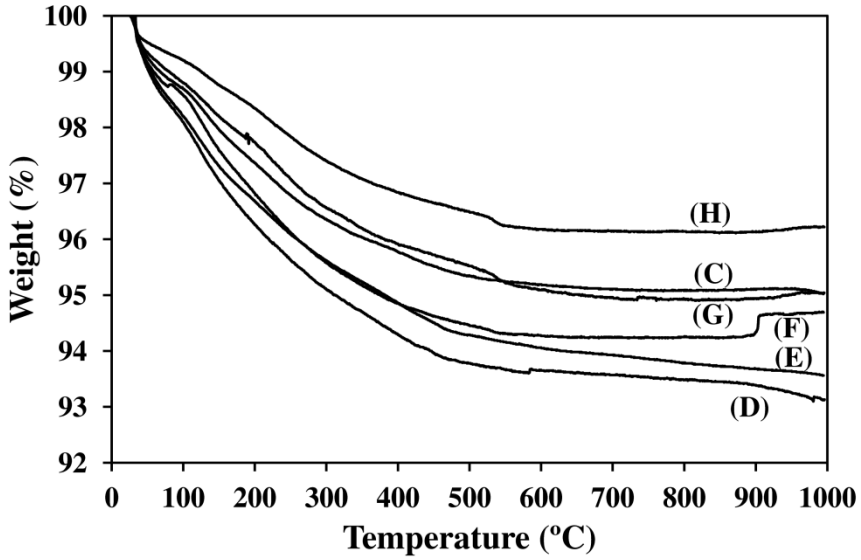

Figure 2.5. TGA comparison charts on the products of reactions (C) to (H) shows no decomposition at 120 °C. Mass loss up to the temperature of 120 °C is attributed to moisture removal and the mass loss over 120 °C is attributed to surface hydroxyl groups removal.

TGA data (see **Figure 2.4** and **Figure 2.5**) obtained for the reaction products are consistent with the XRD data. For each of the reaction products, gradual mass loss up to a temperature of 120 °C is attributed to the loss of unbound H_2O [115]. The data for the products A and B then show a rapid mass loss occurring at 120 °C due to the loss of

H_2O associated with the decomposition of $Zn(OH)_2$ to ZnO and H_2O [300]. The amount of $Zn(OH)_2$ present in the product of Reaction B was estimated from the mass loss to be 20% of the total, which is significantly less than that from Reaction A, which was estimated to be 48%. No similar rapid mass loss at 120 °C was observed for the products of reactions C to H, which is consistent with the XRD data that show zinc oxide is the only species present in those samples.

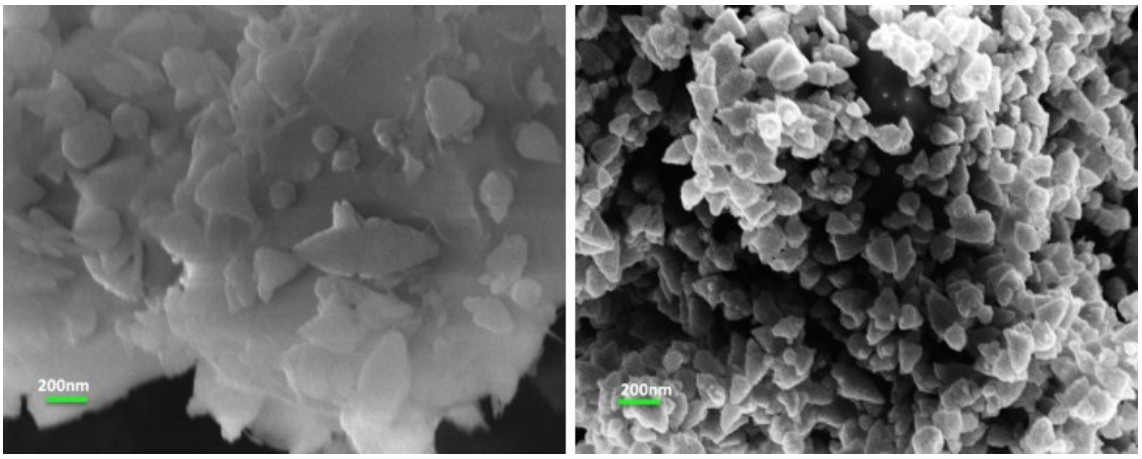

Figure 2.6. SEM images of the products of reactions A (left) and B (right). From reaction (A) smaller ellipsoidal particles are formed on top of the big plate-like structures. In (B), plate-like structures cannot be detected and smaller star-like particles are dominant.

As well as affecting composition, the stoichiometry of the reactants also had a significant effect on the structures of the resultant particles. Scanning electron microscopy (see **Figure 2.6**) revealed that the product of Reaction A is composed of plate-like structures mixed with ellipsoidal particles. The product of Reaction B is composed mainly of smaller well-separated particles with the particles size in the range of 100 - 200 nm.

Figure 2.7 shows the effect of increasing the OH^- : Zn^{2+} mole ratio from 2.5 : 1 to 6 : 1. Smaller, rounder particles are produced by reactions C and D while reactions G and H produce sheet-like particles. Reactions E and F yield a mixture of the small, round particles and the sheet-like particles. XRD data show that in each case the particles have the wurtzite structure.

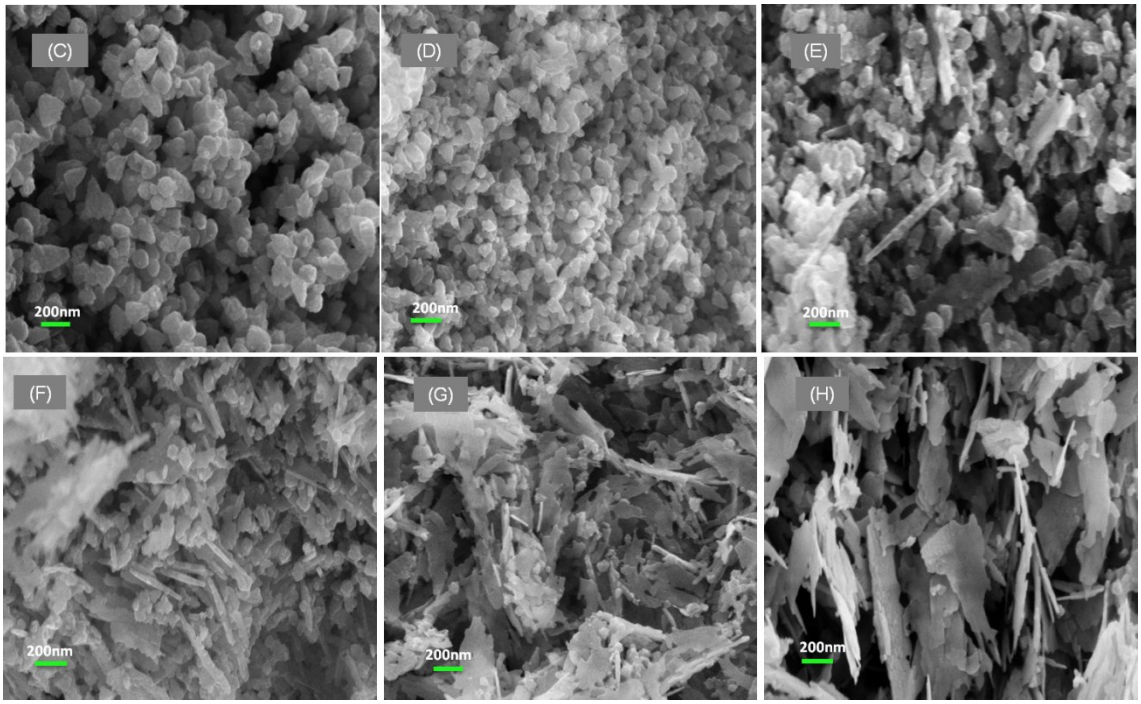

Figure 2.7. SEM images of ZnO particles produced by the reactions C to H.

In Reactions C to H, the XRD data show diffraction patterns arising from ZnO only. This indicates that the larger excess of hydroxide ions (relative to Reaction B) drives the reaction to completion within 2 hours. The higher the OH^- : Zn^{2+} mole ratio, the sooner the conversion of any $Zn(OH)_2$ present to ZnO is complete and, therefore, the more time available in the reactor for coarsening of the ZnO crystals by the equilibrium dissolution/re-crystallisation processes in the solid-liquid system [282]. The particle-shape transformation from small and round particles to sheet-like structures was attributed to this mechanism.

To examine the effect of sub-stoichiometric mixtures, the OH^- : Zn^{2+} mole ratio was fixed at 1.1 : 1 (pH = 6) and the reaction conducted as described in the Experimental section. Interestingly, in this case the precipitate was shown by XRD to be zinc hydroxide sulphate tetrahydrate ($Zn_4SO_4(OH)_6 \cdot 4H_2O$), see **Figure 2.8**. TGA revealed a mass loss of 37.5% up to 1000 °C, which is consistent with the decomposition of $Zn_4SO_4(OH)_6 \cdot 4H_2O$ to ZnO, with the complete transformation to ZnO requiring a temperature of 900 °C (see **Figure 2.9**).

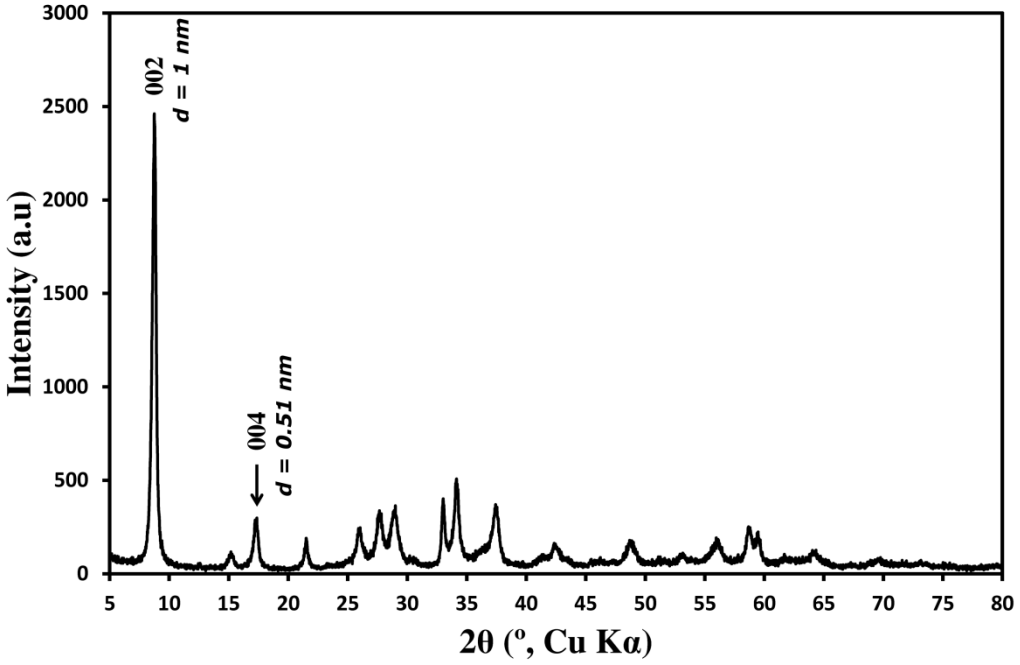

Figure 2.8. XRD associated with zinc hydroxide sulphate tetrahydrate, $Zn_4SO_4(OH)_6 \cdot 4H_2O$ (JCPDF card 00-044-0673).

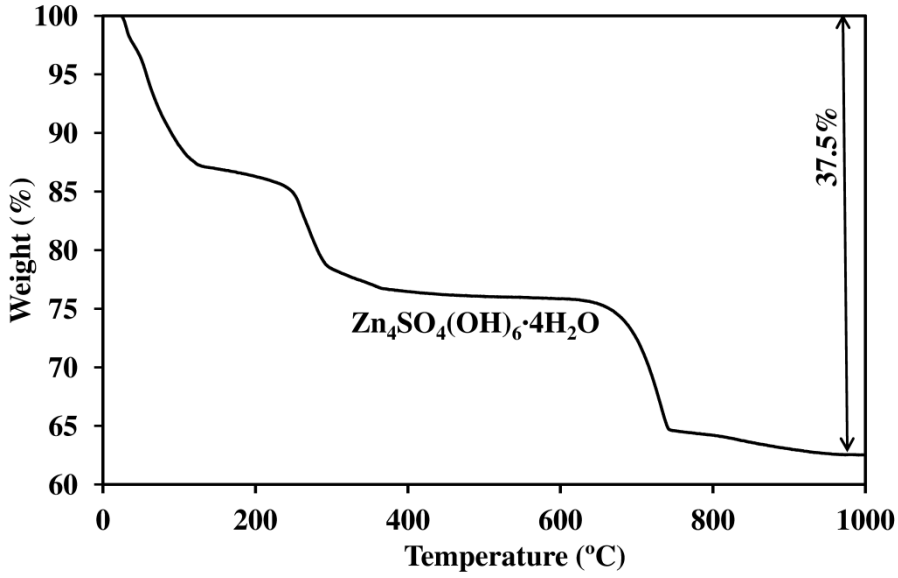

Figure 2.9. TGA on the as-produced $Zn_4SO_4(OH)_6 \cdot 4H_2O$.

2.3.2. Method of combining reactants

The effect of the method of combining the reactants was investigated by altering the order and rate of addition of the zinc sulphate and sodium hydroxide solutions. This

seemingly straightforward procedure has significant implications for laboratory and industrial applications of these reactions. With each experiment, XRD measurements revealed diffraction patterns consistent with ZnO with a hexagonal wurtzite structure for each of the four routes tested and no diffraction peaks for any other materials were detected, see **Figure 2.10**.

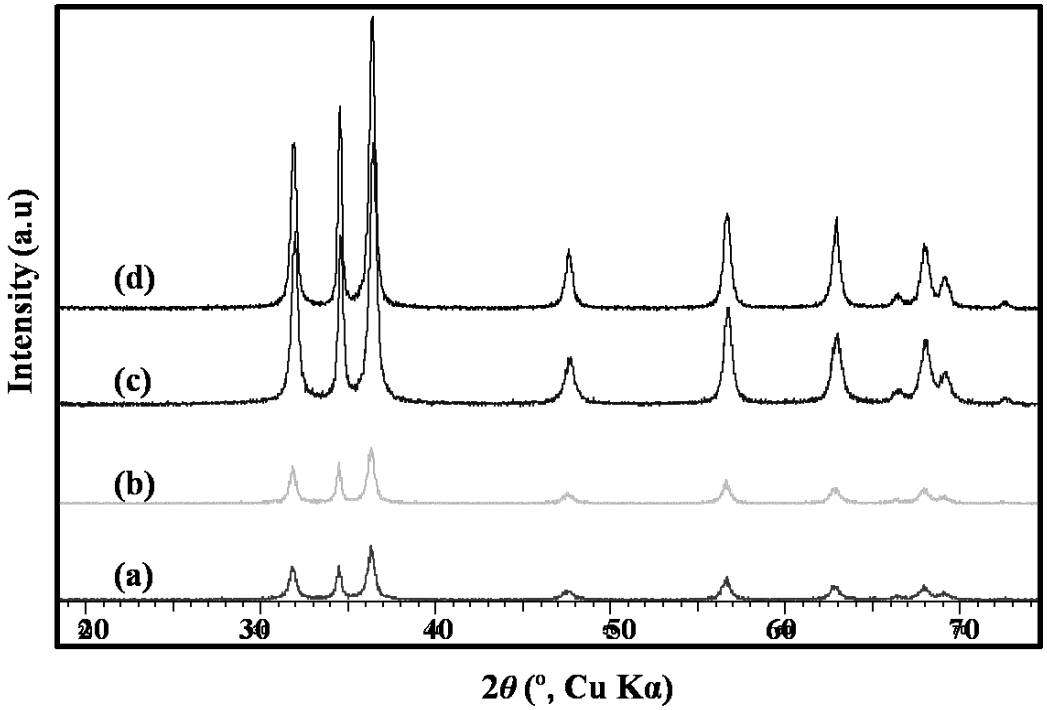

Figure 2.10. XRD data of the reaction products prepared at 70 °C using different feeding methods: (a) NaOH solution added to $ZnSO_4$ solution in a single addition; (b) NaOH solution added to $ZnSO_4$ solution in a dropwise manner; (c) $ZnSO_4$ solution added to NaOH solution in a single shot; (d) $ZnSO_4$ solution added to NaOH solution in a dropwise manner.

SEM images obtained for the reaction products are shown in **Figure 2.11**. Interestingly, the morphology of the ZnO particles differs significantly depending on the process used. When the NaOH solutions were added to the $ZnSO_4$ solutions, either in a single addition or in a dropwise manner, the resultant particles are quite spherical and small, **Figure 2.11** (a) and (b), with an average primary particle size of ~50 nm. Quite different particle morphologies were obtained when the addition method was reversed. With a single addition of $ZnSO_4$ solution to NaOH solution, irregular, conical

particles with an average particle size over 200 nm are formed (**Figure 2.11** (c)). Upon dropwise addition of $ZnSO_4$ solution to NaOH solution, clusters of star-shaped ZnO 'flowers' were generated (**Figure 2.11** (d)).

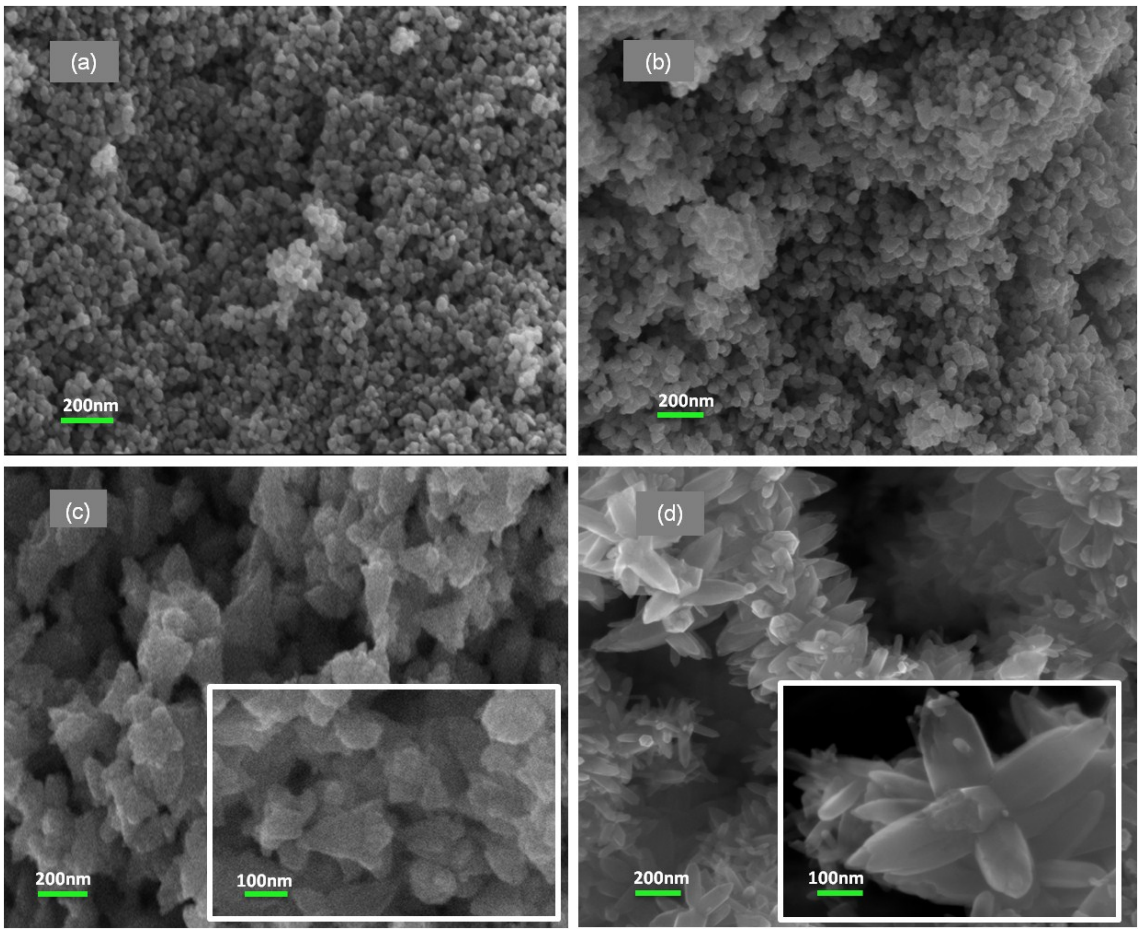

Figure 2.11. SEM images of ZnO particles produced at 70 °C with different feeding methods. (a) NaOH solution added to $ZnSO_4$ solution in a single addition; (b) NaOH solution added to $ZnSO_4$ solution in a drop-wise manner; (c) $ZnSO_4$ solution added to NaOH solution in a single addition; (d) $ZnSO_4$ solution added to NaOH solution in a drop-wise manner.

BET specific surface area measurements showed that in the case of the single addition of NaOH solution to $ZnSO_4$ solution, the surface area of the ZnO precipitate was 32.1 m^2/g. By drop-wise addition of NaOH solution to $ZnSO_4$ solution, the precipitate surface area drops to 25.9 m^2/g. The star-shaped crystals formed by adding $ZnSO_4$ solution to NaOH solution in a drop-wise manner had a specific surface area of only 9 m^2/g. However, the irregular conical crystals formed by adding $ZnSO_4$ solution to NaOH solution in a single shot had a specific surface area of 22.6 m^2/g. Clearly these have a greater degree of porosity than their conical shape would imply.

These experiments show that the method of combining the reactants can have a significant effect on the particle structure. In the case where a NaOH solution is added to the $ZnSO_4$ solution in a single addition, the amount of hydroxide passes the stoichiometric ratio very rapidly and zinc hydroxide species are formed followed by decomplexation to give ZnO in a short time. The number of nucleation sites for particle growth would therefore be large and this case results in ~50 nm round particles. When the NaOH solution is added to a $ZnSO_4$ solution in a drop-wise manner, the reaction passes slowly through the sub-stoichiometric conditions, which can result in the formation of $Zn_4SO_4(OH)_6 \cdot 4H_2O$ until the mole ratio of $ZnSO_4$: NaOH reaches at least 1:2. At this mole ratio, substitution of sulphate ions with hydroxide ions will occur. Upon further addition of hydroxide, the reaction continues to completion.

On the other hand, significant changes in the particles are observed by reversing the order of addition. In these cases, the formation of zinc hydroxide sulphate complexes do not occur as OH^- is in considerable excess at all times during the reaction. In the single-step addition of a $ZnSO_4$ solution to a NaOH solution, the reaction appears to proceed rapidly from soluble zinc complex to formation of ZnO nuclei. Fewer nuclei are formed, and these lead to the growth of the ~200 nm big conical particles. Interestingly, by drop-wise addition of the $ZnSO_4$ solution to a NaOH solution, clusters of ZnO star-like particles dominate and the surface area drops dramatically in comparison. In the early stages of addition, the mole ratio of $ZnSO_4$: NaOH is very small and therefore the higher-order hydroxy-complexes of zinc form rapidly followed by decomplexation to form ZnO nuclei. Since in all stages of addition OH^- was in excess, the excess of hydroxide catalyses the formation of ZnO (see below). At the same time, ZnO formed tends to grow on the limited number of ZnO nuclei formed in the early stages of the reaction. Thus, highly crystalline clusters of ZnO flowers with a relatively low specific surface area are formed.

2.3.3. The effect of temperature

In these experiments, the mole ratio of $ZnSO_4$: NaOH was fixed at 1 : 4 and the $ZnSO_4$ solution was added to the NaOH solution in a single step as described in the Experimental section. XRD patterns of the products showed only ZnO with the hexagonal wurtzite structure (**Figure 2.12**).

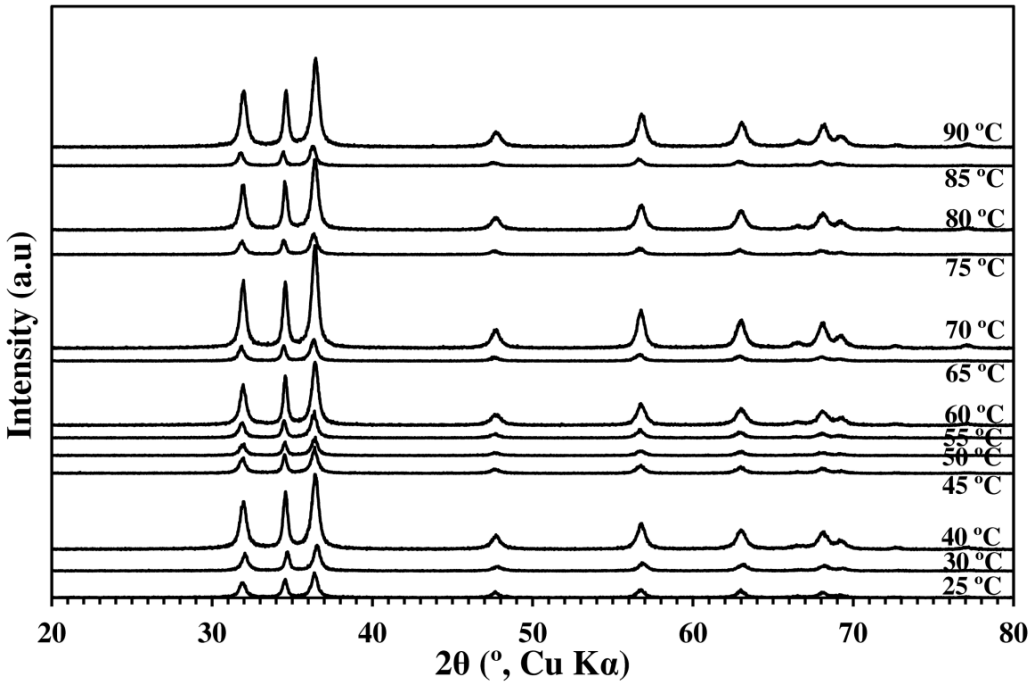

Figure 2.12. XRD shows ZnO hexagonal wurtzite structure for all the samples made at different temperatures from 25 °C to 90 °C.

Figure 2.13 shows that the morphology of ZnO synthesised is sensitive to the reaction temperature. At room temperature, irregular and sharp particles including needle-like particles in the agglomerated form are dominant. Increasing the temperature to 40 °C causes the sharpness of the aggregates to decrease and both plate-like and star-like particles can be observed. By 45 °C, star-like particles are dominant. Average particle size has decreased relative to that of reaction at 40 °C. Further increase in the temperature to 90 °C results in the particles systematically becoming more equiaxed (sphere-like), less star-like, and smaller. By 90 °C the particles are about 100 nm in diameter, which is about a third or so of the diameter of particles produced at 45 °C. Increasing the reaction temperature has two effects: an increase in the formation of nuclei - which would promote smaller particles in the end-product [287], and a faster rate of decomposition of zinc-hydroxo-complexes to ZnO, which results in the growth and coarsening of end-products. In this case, however, the increased rate of nucleation seems to dominate as the temperature of the reaction is increased in this series of reactions. The overall trend in BET specific surface area with temperature (**Figure 2.14**) is upwards, in support of the observation that particle sizes decrease as the temperature of reaction is increased.

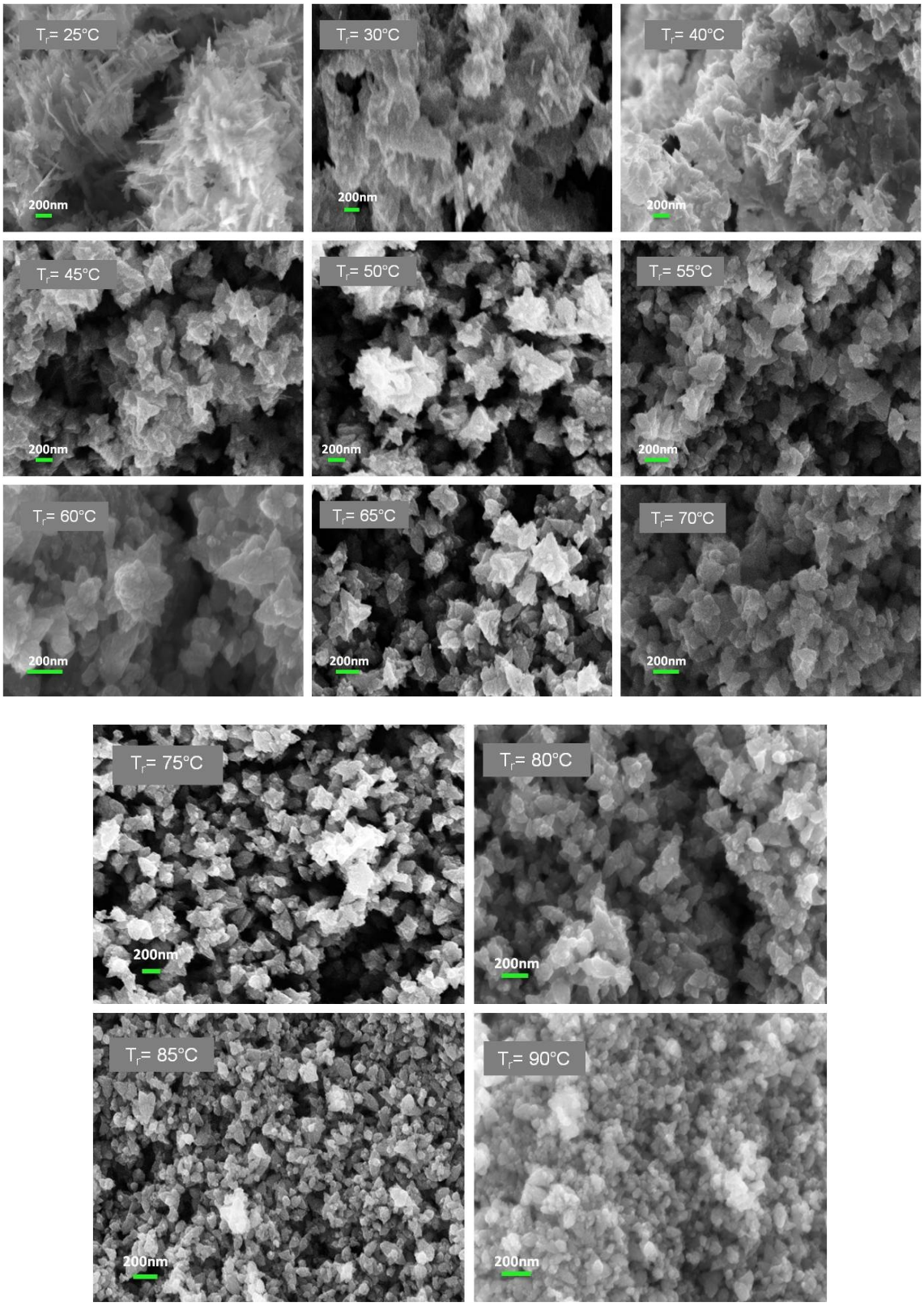

Figure 2.13. SEM images of ZnO particles synthesised at different temperatures.

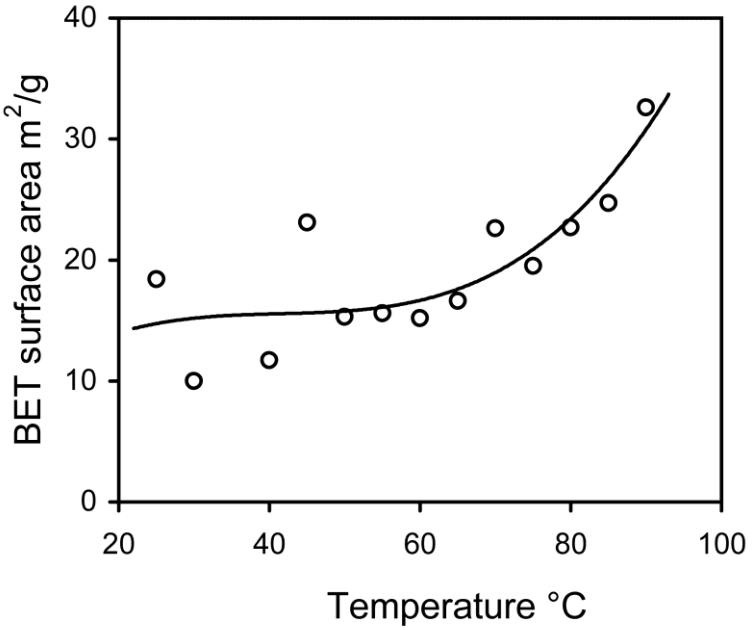

Figure 2.14. BET specific surface area (m^2/g) *vs*. reaction temperature in the range of 25 to 90 °C. The trend line shown was obtained by polynomial regression and is provided as a guide to the eye.

Factors other than an increased rate of nucleation may also contribute to the change in morphology with temperature. In particular, the stability of the soluble zinc hydroxy-complexes decreases as the temperature increases, which leads to more ZnO precipitating from the solution phase. Increasing the temperature from 25 °C to 90 °C decreases the amount of soluble zinc species almost by one order of magnitude, which results in more precipitation by almost one order of magnitude accordingly [284]. Another consideration is that decomplexation reactions of soluble $Zn(OH)_3^-$ and $Zn(OH)_4^{2-}$ to ZnO are slightly endothermic, so that increasing the solution temperature favors the precipitation of ZnO.

2.3.4. Fluorescence spectroscopy

RT fluorescence emission spectra on the commercial ZnO sample produced by the French process and the three powder samples produced from the wet-chemical reaction (where the zinc sulphate solution was added to the sodium hydroxide solution in a drop-wise manner over 3 minutes according to Section 2.3.2 and two samples produced at 60 °C and 80 °C from the reactions explained in the Section 2.3.3) were recorded. The fluorescence spectra of the powder samples are shown in **Figure 2.15**.

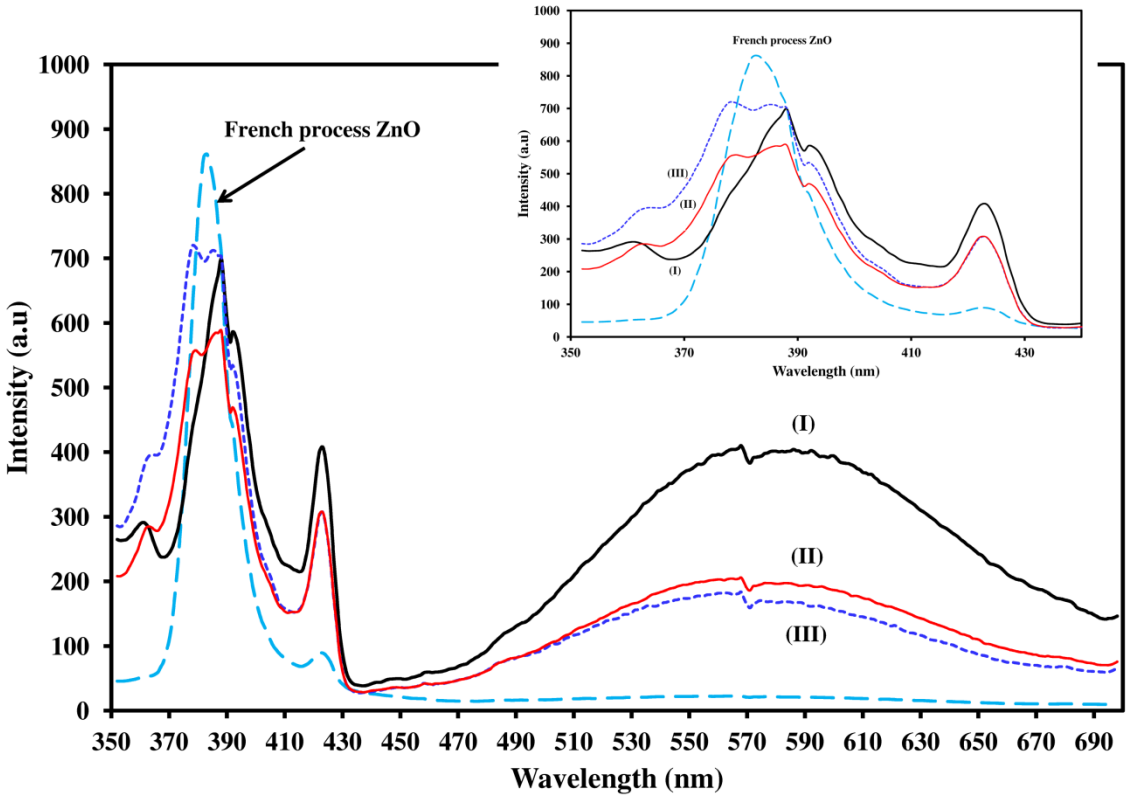

Figure 2.15. RT fluorescence emission spectra of ZnO powder samples: French process ZnO; (I) ZnO product where the zinc sulphate solution was added to the sodium hydroxide solution in a drop-wise manner over 3 minutes according to Section 2.3.2; (II) and (III) ZnO products from reactions at 80 °C and 60 °C according to Section 2.3.3, respectively. Excitation wavelength = 310 nm, excitation slit width = 5 nm (little steps at 460 and 570 nm are artefacts due to filter changes).

Relatively intense emission at around 388 nm and a broad emission with a maximum centred at around 587 nm has been reported previously. The green emission band centred at around 587 nm is thought to be related to the defects in the ZnO crystal such as oxygen vacancies [301]. Additional emissions such as the one at 420 nm are also seen in some cases. Nature of these emissions is still under debate. These might be attributed to particle size and/or zinc interstitial defects [302]. Nevertheless emission at 420 nm may also be related to presence of zinc sulfide surface particles that may form by the reaction of sulphurous gases in the atmosphere with ZnO. The emission peak at 420 nm is a characteristic of ZnS [303].

Here wet-chemically made ZnO powders were compared with the French process ZnO powder in terms of emissions after being excited at 310 nm. It was demonstrated that the method of production of zinc oxide makes significant changes in room temperature fluorescence emission spectra of the products. The powder made by the French process shows an intense emission at around 383 nm (near-UV band) when excited at 310 nm. Corresponding emission of the wet-chemically made powders is composed of more than a single peak. The most intense peaks are centred at near-UV band. A decrease in intensity of these emissions is observed for the powders made from the wet-process reaction relative to that of the French process powder. The green emission band can be observed only in the wet-chemically made powders. It can also be noticed that the ratio of the band-gap to green emission band decreases from the French process ZnO to the wet-process powders. Apart from the band-gap and green emissions, emissions located at ~420 nm in the violet region can be observed for all samples. This emission for the wet-process zinc oxide samples is relatively more intense than that of the French process powder.

2.3.5. The catalytic effect of OH^-

The dramatic change in the ratio of zinc hydroxide to zinc oxide upon proceeding from Reaction A to Reaction C was attributed to the presence of hydroxide ions in excess of the stoichiometric ratio. It appears that hydroxide ions may have a catalytic effect on the transformation of zinc hydroxide to zinc oxide. To examine the pathways that result in the formation of zinc oxide in aqueous systems, standard enthalpies and Gibbs free energies were calculated for a number of reactions (see **Scheme 2.1**). Thermodynamic calculations show that the Gibbs free energy for all the reactions leading to zinc oxide is negative.

Starting with aqueous Zn^{2+} ions (or more formally $Zn(H_2O)_6^{2+}$, which are slightly acidic in nature [284, 289]), addition of a sub-stoichiometric amount of OH^- initially gives the $Zn(OH)^+$ species. Formation of cationic species such as $Zn(OH)^+$, $Zn_2(OH)^{3+}$, $Zn_4(OH)_4^{4+}$ in acidic or near-neutral solutions has been reported [289] although a zinc sulphate hydroxide species also forms in the present case, as discussed separately below. Addition of a second hydroxide ion results in the formation of $Zn(OH)_2$, which has low solubility in water (K_{sp} = 3.5 ×10^{-17} at 25 °C) [284, 290]. Crystalline ε-$Zn(OH)_2$

is thermodynamically metastable with respect to crystalline ZnO at 25 °C with $\Delta G_r^\circ = -4.07\ \mathrm{kJ.mol^{-1}}$ (see dotted line in **Scheme 2.1**) but the rate of transition of solid ε-$Zn(OH)_2$ to ZnO is negligible at ambient temperature [289, 296] as the solid state reaction is endothermic ($\Delta H_r^\circ = +5.62\ \mathrm{kJ.mol^{-1}}$ if the data of Zhang and Muhammed are used [289]). ΔG_r° for the transformation of aqueous zinc hydroxide to zinc oxide and water is negative but the rate of this reaction in these experiments is small due to the low solubility of zinc hydroxide. Solid zinc hydroxide has been reported to remain unchanged after six months in water at room temperature; at 65 °C no significant change was observed up to three weeks, at 75 °C conversion was less than 10% in three weeks but at 100 °C the zinc hydroxide formed ZnO in less than one hour [296].

The addition of hydroxide in excess relative to the stoichiometric ratio contributes to the solubilisation of crystalline zinc hydroxide by formation of soluble hydroxo-complexes of zinc (Equations (**2.4**) and (**2.5**)). These complexation reactions followed by decomplexation (Equations (**2.8**) and (**2.9**)) are the main contributors to the room temperature formation of ZnO in the current work. The driving force for the precipitation of ZnO from higher-order hydroxo-complexes of zinc is the thermodynamic instability of such complexes with respect to ZnO. Importantly, hydroxide ions are returned to the reaction mixture upon formation of ZnO, thus producing a catalytic effect. After completion of the reaction, the system is basic and the only product is stable crystalline ZnO (in equilibrium with soluble ZnO) as well as water from the reaction. Increasing the hydroxide concentration over the stoichiometric ratio also considerably accelerates the rate of reaction.

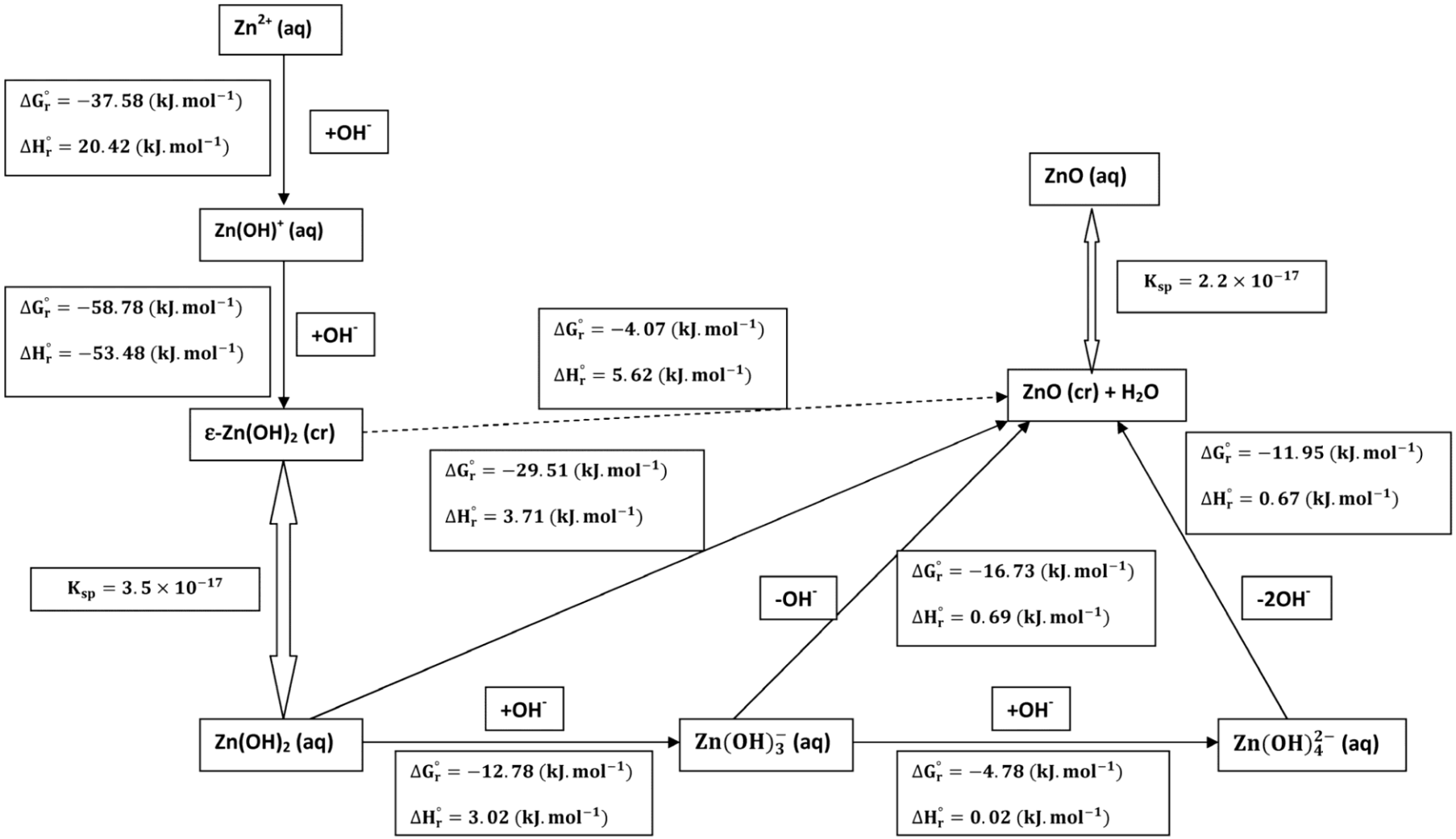

Scheme 2.1. Thermodynamic data for the formation of ZnO from Zn^{2+} and OH^- at 298 ºK and 1 atm. Standard states have been assumed. For consistency, data from Zhang and Muhammed were used [289].

2.4. Conclusions

The morphology of ZnO and $Zn(OH)_2$ precipitates formed from $ZnSO_4$ solutions is acutely sensitive to the pH, temperature and method by which the reactants are mixed. For molar ratios of $ZnSO_4$ to NaOH between 1 : 1 and 1 : 2.5 the precipitate that forms first is $Zn(OH)_2$. In aqueous conditions $Zn(OH)_2$ is converted to ZnO by a hydroxide-catalyzed process, with the process accelerating as pH is increased. A basic zinc sulphate is precipitated when the ratio is below 1 : 1 while no precipitate is formed if sufficient base is present to raise the pH above 12 and solubilise the Zn as $Zn(OH)_4^{2-}$. The order of additions is also an important parameter. If small nanoparticles are desired then it is essential to add the NaOH *into* the $ZnSO_4$ precursor. This ensures that prolific nucleation of $Zn(OH)_2$ particles occurs because conditions become favorable for precipitation almost immediately. When the addition is done in the opposite sense (*i.e.* $ZnSO_4$ *into* NaOH) fewer nuclei are formed and the final particles are larger and more crystalline because the initial conditions favor formation of soluble complexes rather than precipitates. In general, it appears that the $Zn(OH)_2$ converts to ZnO, with the rate of the process increased by both temperature and pH. A comparison between the RT fluorescence emission spectra of some of the wet-process ZnO powders and the French process ZnO powder demonstrates significant effects of change of the method of production on the emission pattern of zinc oxide powders. The green emission band, which is correlated with structural defects of various kinds, can only be observed in the wet-chemical grades while their band-gap emission is relatively smaller than that of the French process one.

Chapter 3

A Single-Stage Process to Synthesise Zinc Oxide Using Ammonia

Chapter 3: A Single-Stage Process to Synthesise Zinc Oxide Using Ammonia

3.1. Introduction

In the previous chapter, production of ZnO by a single stage wet-chemical method using zinc sulphate and sodium hydroxide has been discussed and role of hydroxide ions on precipitation of zinc oxide in the $H_2O/Zn^{2+}/OH^-$ system at temperatures less than 90 °C has been revealed. The work presented in this chapter was performed to investigate the effect of change of the alkaline reagent to ammonia on the properties of the product.

Here the $NH_3/H_2O/Zn^{2+}/OH^-$ system was considered and it was shown that the mechanism of the reaction and morphology of the particles changes by involvement of the ammonia in the system.

Here, zinc- ammine[§] complexes are also generated in aqueous solution that coexist with the zinc hydroxy-complexes described in the previous chapter. The system is thermodynamically more complex as a result of presence of new complexes. Some of the reported zinc-ammine complexes in the aqueous system are $Zn(NH_3)^{2+}_{(aq)}$, $Zn(NH_3)^{2+}_{2\,(aq)}$, $Zn(NH_3)^{2+}_{3\,(aq)}$ and $Zn(NH_3)^{2+}_{4\,(aq)}$ [285]. Presence of these zinc-ammine complexes has been reported to have influence on the morphology of the ZnO products [304]. Temperature also plays an important role for the solubility of ZnO in ammoniacal solutions. Increasing the temperature unexpectedly decreases the solubility of ZnO in such solutions. This means that for the precipitation of ZnO, higher temperatures are more favourable [285]. Transition between zinc-ammine complexes to zinc-hydroxy complexes seems to have a role in the precipitation of zinc oxide from ammoniacal solutions [285].

In aqueous ammoniacal environments, apart from the Reactions **2.1** to **2.9** described in the previous chapter, the following reactions can also be involved in the formation of zinc oxide [99].

§ "ammines" are aqueous complexes of metals that contain NH_3. They are different to "amines", which are organic molecules.

$$NH_3 \cdot H_2O_{(aq)} \rightleftharpoons NH_{4\,(aq)}^{+} + OH_{(aq)}^{-} \quad 3.1$$

$$Zn_{(aq)}^{2+} + nNH_3 \rightleftharpoons [Zn(NH_3)_n]_{(aq)}^{2+} \text{ (where } n = 1 \text{ to } 4) \quad 3.2$$

$$[Zn(NH_3)_4]_{(aq)}^{2+} + 4OH_{(aq)}^{-} \rightleftharpoons Zn(OH)_{4\,(aq)}^{2-} + 4NH_{3\,(aq)} \quad 3.3$$

$$[Zn(NH_3)_4]_{(aq)}^{2+} + 3OH_{(aq)}^{-} \rightleftharpoons Zn(OH)_{3\,(aq)}^{-} + 4NH_{3\,(aq)} \quad 3.4$$

$$[Zn(NH_3)_4]_{(aq)}^{2+} + 2OH_{(aq)}^{-} \rightleftharpoons Zn(OH)_{2\,(aq)} + 4NH_{3\,(aq)} \quad 3.5$$

$$[Zn(NH_3)_4]_{(aq)}^{2+} + 2OH_{(aq)}^{-} \rightleftharpoons Zn(OH)_{2\,(cr)} + 4NH_{3\,(aq)} \quad 3.6$$

Equation **3.1** shows the hydrolysis equilibrium of ammonia. The concentration of ammonia controls the amount of the hydroxide in the system and subsequently the pH of the environment, and also influences the formation of zinc-ammine complexes according to Equation **3.2**. The fraction of each zinc species in solution is pH and temperature dependent [285]. In ammoniacal solutions, at room temperature and at the pH range of 8 to 11, $Zn(NH_3)_4^{2+}$ is the dominant species in solution. As the temperature increases, the pH range associated with the presence of $Zn(NH_3)_4^{2+}$ fraction shrinks and shifts towards lower pH [285]. Zinc-ammine cations in the presence of hydroxide anions in the system (due to Equation **3**.**1**) can then undergo transformation to the zinc-hydroxy species by releasing ammonia in solution according to equations **3**.**3** to **3**.**6** [99, 285]. In this chapter, the role of ammonia in the formation of zinc-containing materials has been examined. The properties of the zinc oxide made from this method have been investigated and the mechanism by which the precipitation reactions occur was investigated.

3.2. Experimental

Zinc sulphate heptahydrate (AR grade) and ammonia solution 28% (AR grade) were purchased from Ajax Chemicals and used as-received. Milli-Q (18.2 Ω cm^{-1}) water was used as the solvent. The reaction was conducted under atmospheric conditions using a two-neck round bottom flask equipped with a condenser with a digitally-controlled

magnetic heater/stirrer. A magnetic stirrer bar was used at a stirring rate of 700 rpm. Aqueous solutions of $ZnSO_4 \cdot 7H_2O$ (31 mL, 0.05M) and ammonia (30 mL, 0.2M) were prepared. The reaction temperature was maintained at 65 °C. Ammonia solution was added to the flask and allowed to reach thermal equilibrium. The zinc sulphate solution was added to the ammonia solution in a drop-wise manner over 3 minutes. The reaction continued for 2 hours under stirring. Then the system was allowed to cool down and kept still overnight to settle. The precipitates were isolated by vacuum filtration followed by vacuum drying at room temperature.

X-ray diffraction, thermogravimetric analysis (TGA), scanning electron microscopy, fluorescence spectrometry experiments and BET specific surface area measurement experiments have been done as in the previous chapter.

3.3. Results and Discussion

In this chapter, the reaction between zinc sulphate and ammonia was investigated to indicate the role of ammonia in place of sodium hydroxide as the alkaline reactant to precipitate ZnO. A comparison has been done between the materials formed using similar methods of synthesis via the NaOH route and ammonia route.

3.3.1. Characterisation and thermogravimetric analysis

The product of the reaction was identified by XRD to be ZnO, **Figure 3.1**. TGA data (**Figure 3.2**) on the ZnO made from the wet-chemical reaction between zinc sulphate and ammonia shows a mass loss around 4.5% when heated to 1000 °C. Similar to what was shown in the previous chapter (**Figure 2.4** and **Figure 2.5**), a gradual mass loss up to a temperature around 120 °C is attributed to unbound water and, over this temperature, further mass loss is attributed to the liberation of surface hydroxyl groups. It can be seen that wet-chemically made zinc oxides contain significant amount of embedded contamination, which can be released by heating. The surface hydroxyl groups are quite stable up to temperatures around 800 °C.

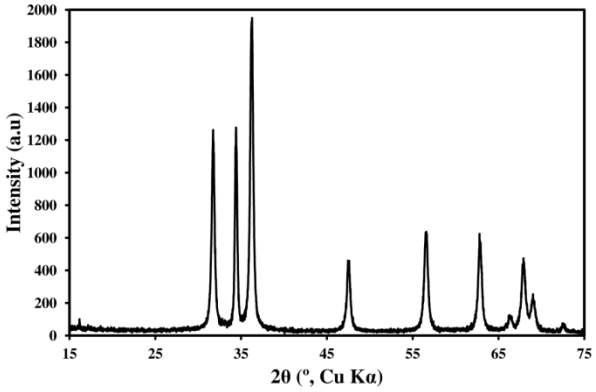

Figure 3.1. X-ray diffraction data obtained from the product of reaction between zinc sulphate and ammonia correspond to pure ZnO (wurtzite), JCPDF card 01-089-7102.

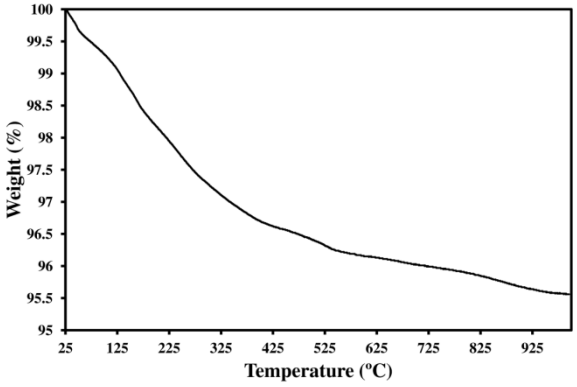

Figure 3.2. TGA on the ZnO product. Mass loss up to the temperature of 120 °C is attributed to moisture removal and the mass loss over 120 °C is attributed to removal of surface hydroxyl groups.

3.3.2. Microscopy and BET surface area measurement

SEM images of the ZnO particles, which have a prism-like structure, are shown in **Figure 3.3**. Since the zinc sulphate solution is added to the ammonia solution in a drop-wise manner, it is believed that the number of nuclei in the early stages of the addition is small. Few ZnO seeds are formed by ammonia-disengagement/dehydroxylation process. Then, upon addition of more zinc sulphate into the solution, more ZnO is formed and grows on the nuclei available in solution. This results in the formation of highly crystalline prism-like clusters. The mechanism is similar to the one explained in Section 2.3.2. However by comparing (**Figure 2.11**, d) and (**Figure 3.3**), it is obvious

that the change of the reactant from NaOH to ammonia significantly affects the morphology of the zinc oxide clusters.

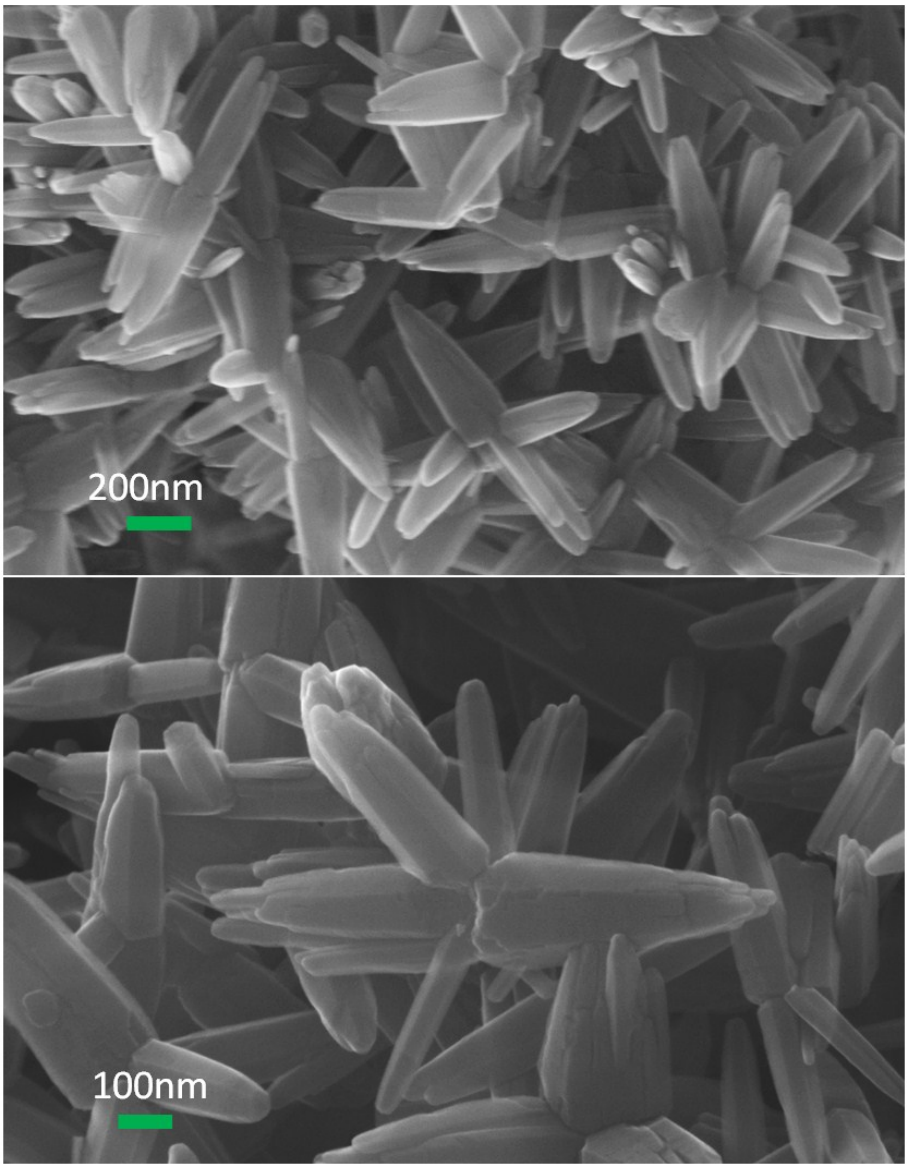

Figure 3.3. SEM images of zinc oxide crystals produced at 65 °C by feeding the zinc sulphate in a drop-wise manner to the ammonia solution.

BET specific surface area measurement showed that ZnO made by this method has a specific surface area of only 7.3 m^2/g, which is very similar to that of the product made by adding $ZnSO_4$ solution to NaOH solution in a drop-wise manner described in section 2.3.2. This indicates that the specific surface area of the ZnO crystalline clusters that are grown with the prism or star-shape using a drop-wise feeding technique via either NaOH or ammonia routes tends to be relatively low.

3.3.3. Fluorescence spectroscopy

A RT fluorescence emission spectrum on the ZnO sample produced by this method was recorded after being excited at 310 nm, see **Figure 3.4**. It is similar to the spectrum obtained from the zinc oxide product where the zinc sulphate solution was added to the sodium hydroxide solution in a drop-wise manner over 3 minutes (**Figure 2.15**, I). The most intense peak is located at 388 nm (near-UV band) followed by a violet band peak centred at 423 nm. A wide green emission band centred at 567 nm also is observed. The result shows that ZnO formed by the effect of ammonia rather than NaOH but with the similar feeding method has basically very similar defect structure.

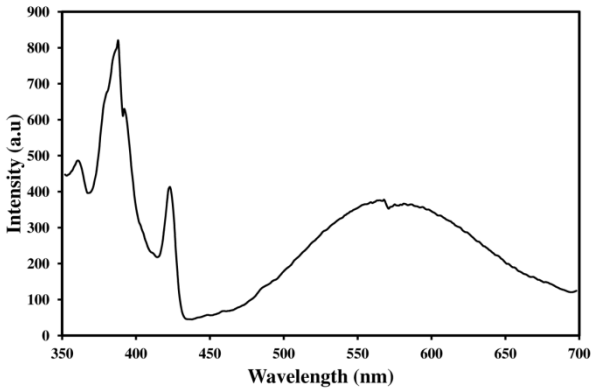

Figure 3.4. RT fluorescence emission spectra of ZnO powder sample made by drop-wise addition of zinc sulphate solution to ammonia over 3 minutes according to section 3.2. Excitation wavelength = 310 nm, excitation slit width = 5 nm (little steps at 460 and 570 nm are artefacts due to filter changes).

3.3.4. The catalytic role of NH_3 and OH^-

In the previous chapter, the catalytic role of hydroxide anions in solution was explained. Hydroxide anions that are once added into the system as an alkaline reagent and become engaged in the anionic zinc-hydroxy complexes in solution are later released from the soluble zinc species. This results in precipitation of ZnO and regeneration of hydroxide anions.

In the ammonia-water-zinc system, hydroxide is not directly added into the system; rather ammonia hydrolysis is responsible for the formation of some hydroxide in solution according to Equation **3**.**1**. The amount of ammonia in the system controls the

amount of hydroxide ions available for the formation of zinc-hydroxy complexes. Presence of ammonia in the system also plays an important role for the formation of cationic zinc-ammine complexes according to Equation **3**.**2**. Thermodynamic calculations at the standard state conditions for Equation **3**.**2** revealed that the Gibbs free energies of reactions and also the enthalpy of reactions when n = 1, 2 and 3 are positive whereas those of the reaction when n = 4 are negative. This indicates that at the standard state conditions only zinc-tetra-ammine complex can be formed in an exothermic reaction. As a result, an interplay between anionic zinc-hydroxy complexes and cationic zinc-tetra-ammine complex exist, which depends on the pH and temperature of the system [285].

Zinc-hydroxy complexes are thermodynamically more stable than the zinc-ammine species (Equations **3**.**3** to **3**.**6**). For instance thermodynamic calculations at the standard conditions for the transformation of zinc-tetra-ammine cation to zinc-tetra-hydroxy anion according to Equation **3**.**3** show that ΔG_r° is -35.1 kJ/mol, thermodynamic data adapted from [89, 285, 289].

As described in Chapter 2, Section 2.3.5, transformation of zinc-hydroxy complexes to zinc oxide is also thermodynamically favourable with the negative Gibbs free energy for all decomplexation reactions.

Therefore, in the ammonia-water-zinc system, formation of zinc-ammine complex is suggested to happen first followed by decomplexation to form zinc-hydroxy complexes and release of ammonia in water. Disengaged-ammonia from the complexes enters the solution again. This shifts the hydrolysis Reaction **3**.**1** towards right according the Le Chatelier's Principle, which provides more hydroxides for the hydroxylation Reactions **3**.**3**-**3**.**6**.

Zinc-hydroxy complexes are thermodynamically instable with respect to ZnO, which results in precipitation of insoluble ZnO. This stage follows the same mechanism described in Chapter 2. Importantly, regeneration of ammonia and hydroxide anions in the system suggests the catalytic role of these two species. It should be mentioned that only the hydroxide in excess of the stoichiometric ratio has the catalytic role, see Section 2.3.5.

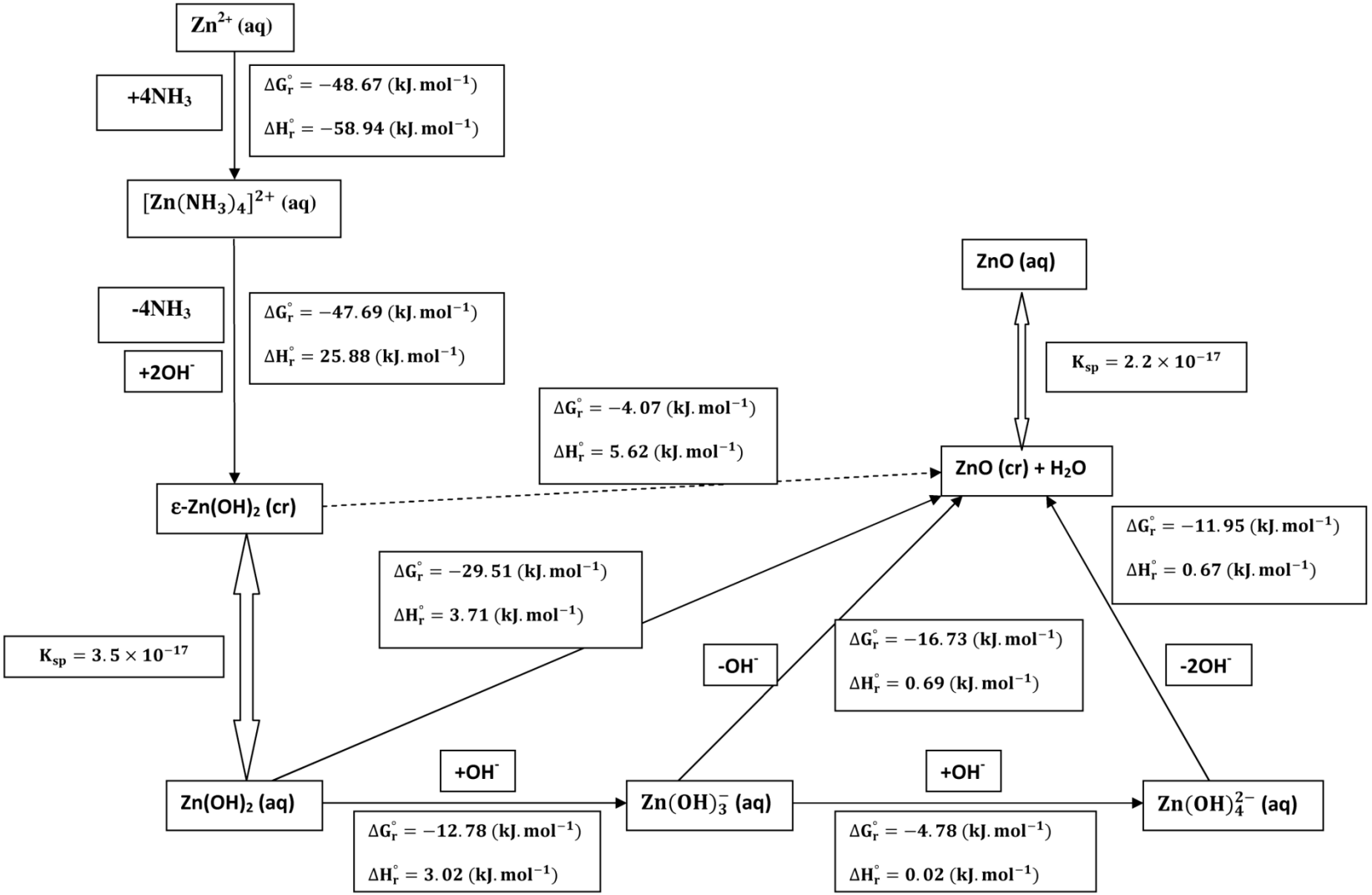

Scheme 3.1. Thermodynamic data for the formation of ZnO from Zn^{2+}-water-ammonia system at 298 ºK and 1 atm. Standard states have been assumed. Data adopted from [89, 285, 289].

3.4. Conclusions

A comparative study was performed between the reaction of zinc sulphate and NaOH solutions (explained in the previous chapter) and the reaction between $ZnSO_4$ and ammonia solutions with a molar ratio of 1 : 4 where the method of feeding was drop-wise addition of zinc sulphate solution *into* the alkaline solution. It was shown that the end-product is well-crystallised ZnO with a cluster morphology. Provided that at all times of the addition alkaline solution is more than the stoichiometric amount, formation of soluble zinc-hydroxy and/or zinc-ammine complexes is feasible. This method of addition allows the fast nucleation of small number of zinc oxide particles in the beginning of addition from the soluble zinc-complexes through a decomplexation-precipitation route and further growth of zinc oxide on the available nuclei sites upon addition of more zinc salt solution. This results in larger crystals with lower specific surface area. Zinc-amine complexes are believed to be involved in the system in the presence of ammonia before their transformation into zinc-hydroxy complexes. Thermodynamic instability of the soluble zinc-amine and zinc hydroxy complexes with respect to zinc oxide is the driving force for the decomplexation and precipitation reactions. Ammonia and excess of hydroxide anions catalyse the precipitation reaction. The RT fluorescence emission spectrum obtained from ZnO made by the ammonia route shows very similar behaviour to that of the similarly-made oxide from the NaOH route.

Chapter 4

Multi-Stage Routes to Synthesise Zinc Oxide Using Zinc Peroxide

Chapter 4: Multi-Stage Routes to Synthesise Zinc Oxide Using Zinc Peroxide

4.1. Introduction

In the previous two chapters, single-stage wet-processes to synthesise ZnO in alkaline solutions have been discussed. In this chapter two-stage production processes will be discussed. Stage one is wet-chemical reaction to form zinc peroxide using zinc salts and hydrogen peroxide. Stage-two is conversion of zinc peroxide into ZnO by heating. Morphology, thermal behaviour and composition of the end-product materials and mechanism of the reactions are determined.

The importance of zinc oxide has been discussed previously. Zinc peroxide is also an important material. It is mainly used in the rubber industry e.g. for vulcanisation of carboxylated nitrile rubber (XNBR) [305-307], in the plastic industry [305, 307], in explosive and pyrotechnic compositions [307, 308] and in cosmetic and medical applications [305, 308]. Furthermore, it can be used as a precursor for zinc oxide particles [305, 307]. The latter is the reason why it is investigated here.

Various techniques to produce zinc peroxide are reported for example by reactions between zinc oxide, zinc hydroxide or zinc salts and a solution of hydrogen peroxide [305, 309]. Its chemical formula is generally reported as $ZnO_2 \cdot 0.5O_2$ [310]. Zinc peroxide is stable up to temperatures of around 200 °C. It decomposes at moderate temperatures (200-250 °C) to ZnO by releasing oxygen according to exothermic Reaction **4.1** [305, 307]. The resultant ZnO is reported to be oxygen deficient. For example calcination of ZnO_2 at 200 °C results in $ZnO_{0.9905}$. Oxygen deficiency decreases as the calcination temperature increases. The defects have influence on the colour of the resultant ZnO. The stoichiometric ZnO is white while non-stoichiometric material made from the calcination of ZnO_2 is yellowish [311].

$$2ZnO_{2\,(cr)} \rightleftharpoons 2ZnO_{(cr)} + O_{2\,(g)} + Heat \qquad 4.1$$

4.2. Experimental

4.2.1. General

Zinc acetate dihydrate, sodium hydroxide pellets and hydrogen peroxide 35% were purchased from Ajax Chemicals and used as-received. Milli-Q water (18.2 Ω cm^{-1}) was used as the solvent. Reaction was conducted under atmospheric conditions using a round bottom flask with a digitally-controlled magnetic heater/stirrer. A magnetic stirrer bar was used at a stirring rate of 820 rpm. Precipitates were isolated by centrifugation at 4400 rpm followed by drying using a rotary evaporator at 60 °C, unless otherwise stated.

X-ray diffraction, thermogravimetric analysis and scanning electron microscopy experiments have been done according to what was explained in Chapter 2.

4.2.2. Synthesis

ZnO_2 via zinc acetate and H_2O_2 reaction

Aqueous solutions of $Zn(CH_3COO)_2 \cdot 2H_2O$ (30 mL, 0.02M) and H_2O_2 (40 mL, 0.6M) were prepared. Hydrogen peroxide solution was added to the zinc acetate solution in a single step. The reaction continued for 2 hours and at room temperature. After 1 hour, 10 mL of H_2O_2 35% (11.7M) was injected into the reaction vessel and the reaction continued for another 1 hour. The pH of the system after 2 hours of reaction was measured at 6 and the system was transparent. To form a precipitate the system was made alkaline using sodium hydroxide solution (pH=13) in a dropwise manner. A white precipitate was formed at pH=7. Addition of NaOH solution was continued until the pH=9 was achieved. The white precipitate was separated and washed and dried and characterised.

ZnO from as-synthesised ZnO_2

Some of the abovementioned precipitate was calcined at 250 °C for 1 hour in a box furnace. The remaining solid was weighed and characterised.

ZnO_2 via $Zn_4SO_4(OH)_6 \cdot 4H_2O$ and H_2O_2 reaction

2.4×10^{-4} moles of zinc hydroxide sulphate ($Zn_4SO_4(OH)_6 \cdot 4H_2O$) solid produced according to the method described in Section 2.2.2 by a sub-stoichiometric reaction between zinc sulphate and sodium hydroxide (OH^- : Zn^{2+} mole ratio was only 1.1 : 1) was transferred to the reaction vessel (see also Section 2.3.1) at 70 °C. Then hydrogen peroxide solution (60 mL, 1M) was added to the solid in a single step and the reaction continued for 2 hours. The pH of the system was 5 after the reaction. The solid was then separated, washed and dried at 75 °C and characterised.

ZnO from as-synthesised ZnO_2

Some of the abovementioned solid was calcined at 250 °C for 1 hour in a box furnace. The remaining solid was weighed and characterised.

4.3. Results and Discussion

In this chapter, two techniques to produce zinc peroxide and zinc oxide are investigated. It is shown that ZnO_2 can be formed by the effect of hydrogen peroxide on a zinc salt solution. Alternatively, ZnO_2 can be formed by the reaction of H_2O_2 and $Zn_4SO_4(OH)_6 \cdot 4H_2O$. The latter is reported here for the first time as a synthetic technique for ZnO_2. It was shown that ZnO with small particle size and low-crystallinity can be produced by calcination of zinc peroxide at intermediate temperatures.

4.3.1. Characterisation

Products from reaction of zinc acetate and H_2O_2

The product of the reaction between zinc acetate and hydrogen peroxide, and the material formed by calcination of this product, were characterised by XRD to be zinc peroxide and zinc oxide, respectively (see **Figure 4.1**). XRD on ZnO shows broad peaks, which suggests small crystallite size.

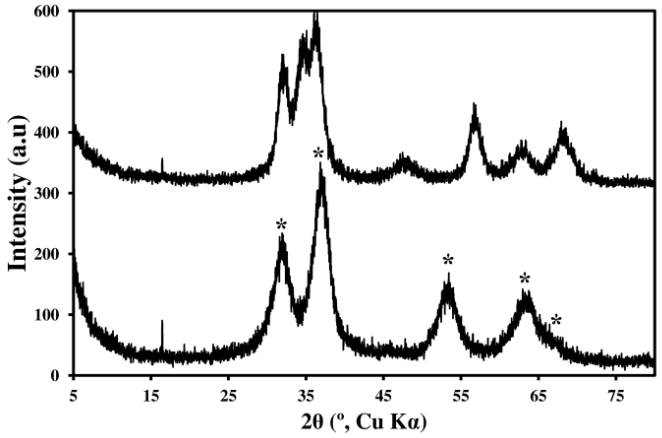

Figure 4.1. XRD on (bottom) product of the reaction between zinc acetate and hydrogen peroxide corresponds to zinc peroxide (JCPDF card 01-077-2414) and (top) product of calcination of as-produced zinc peroxide corresponds to zinc oxide (JCPDF card 01-075-0576). Peaks marked with "*" are associated with zinc peroxide.

Products from reaction of $Zn_4SO_4(OH)_6 \cdot 4H_2O$ and H_2O_2

The product of the reaction between solid zinc hydroxy sulphate and hydrogen peroxide was characterised by XRD to be ZnO_2. The material formed by calcination of as-made zinc peroxide was shown to be a mixture of ZnO and ZnO_2 (see **Figure 4.2**).

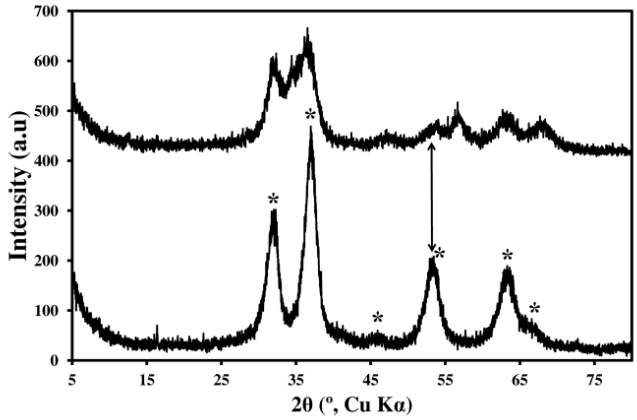

Figure 4.2. XRD on (bottom) product of the reaction between $Zn_4SO_4(OH)_6 \cdot 4H_2O$ and H_2O_2 corresponds to ZnO_2 (JC-PDF 01-077-2414) and (top) product of calcination of as-produced ZnO_2 corresponds to mainly to ZnO (JC-PDF 00-001-1136) and some remaining ZnO_2. Peaks marked with "*" are associated with zinc peroxide.

4.3.2. Thermogravimetric analysis

TGA-DTA analysis on ZnO_2 formed via the zinc acetate-H_2O_2 route showed a total mass loss of ~25% up to the temperature of 1000 °C. This includes a mass loss of ~8% up to the temperature of ~120 °C due to expulsion of moisture. In the temperature range of 120-250 °C, ~14% mass loss can be detected that is attributed to decomposition of ZnO_2 to ZnO by releasing O_2. Above 250 °C, ~3% mass loss is attributed to the release of surface hydroxyl groups from ZnO particles. Release of surface hydroxyl groups has been also shown in Chapter 2. An exothermic peak in the DTA is centred at ~210 °C, which corresponds to the decomposition temperature of ZnO_2.

TGA on the ZnO_2 formed by the $Zn_4SO_4(OH)_6{\cdot}4H_2O$-$H_2O_2$ route showed a total mass loss of ~24% up to the temperature of 1000 °C with a similar pattern to that described above (**Figure 4.3**).

DTA on the ZnO_2 formed by the $Zn_4SO_4(OH)_6{\cdot}4H_2O$-$H_2O_2$ route, however, shows an exothermic peak centred at ~230 °C (**Figure 4.4**). DTA peaks located at around 230 °C have been shown in previous works [305, 312]. However the reason for the lower decomposition temperature for ZnO_2 made via zinc acetate/H_2O_2 route could not be determined.

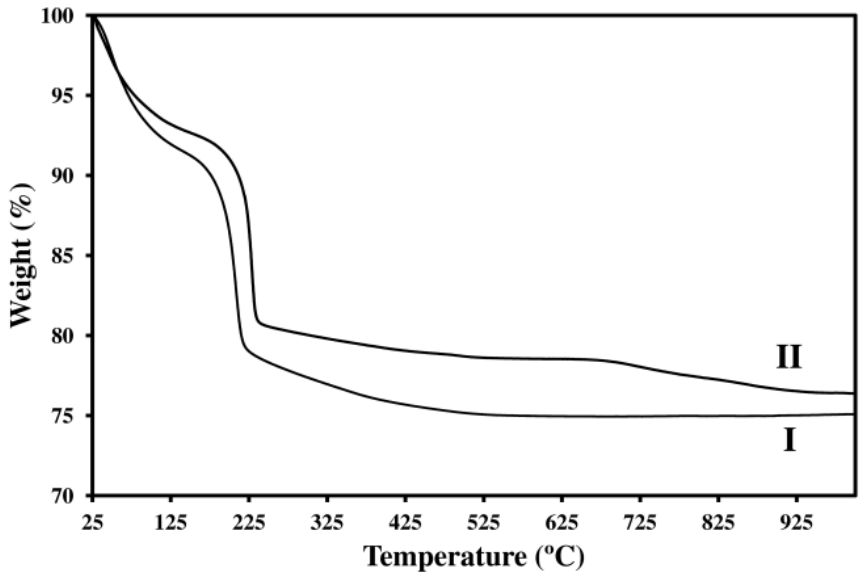

Figure 4.3. TGA on zinc peroxide made from (I) zinc acetate-H_2O_2 route and (II) $Zn_4SO_4(OH)_6{\cdot}4H_2O$-$H_2O_2$ route.

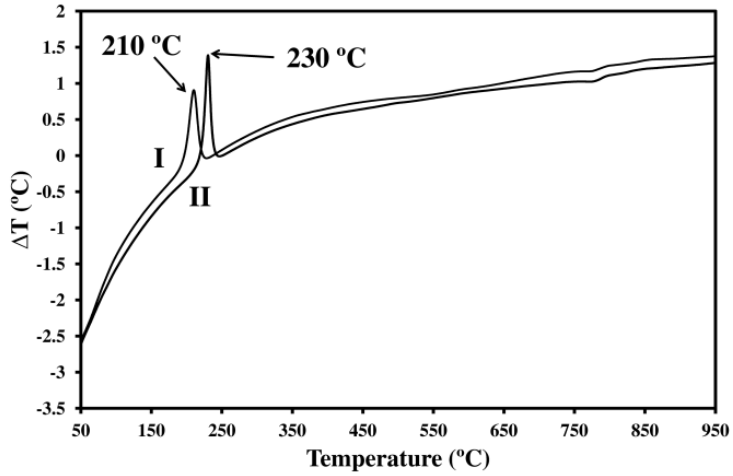

Figure 4.4. DTA on zinc peroxide made from (I) zinc acetate-H_2O_2 route and (II) $Zn_4SO_4(OH)_6 \cdot 4H_2O$-$H_2O_2$ route.

4.3.3. Mechanisms of formation of zinc peroxide

Zinc acetate-H_2O_2 route

Formation of zinc peroxide by the reaction between zinc acetate and H_2O_2 in the hydrothermal system was proposed in [313] to be according Equations **4.2** to **4.6**.

$$Zn(CH_3COO)_2 \cdot 2H_2O \rightarrow Zn^{2+}{}_{(aq)} + 2(CH_3COO)^-_{(aq)} + H_2O_{(l)} \quad 4.2$$

$$(CH_3COO)^-_{(aq)} + H_2O_{(l)} \rightarrow OH^-{}_{(aq)} + CH_3COOH_{(aq)} \quad 4.3$$

$$Zn^{2+}{}_{(aq)} + 2OH^-{}_{(aq)} \rightarrow Zn(OH)_2 \quad 4.4$$

$$Zn(OH)_2 + H_2O_{2(l)} \rightarrow ZnO_{2(cr)} + 2H_2O_{(l)} \quad 4.5$$

$$2H_2O_{2(l)} \rightarrow O_{2(g)} + 2H_2O_{(l)} \quad 4.6$$

The system was at room temperature, transparent and at pH=6 after the reaction. Acidic condition is due to the acidic nature of both reactants. The pH is adjusted to the neutral and then alkaline conditions by using NaOH solution to precipitate ZnO_2. Interestingly ZnO did not precipitate by addition of NaOH. A SEM image of the ZnO_2 formed by this method is shown in **Figure 4.5**. Small-size ZnO particles were formed

by calcination of as-made ZnO_2. The structure is porous and non-uniform (see **Figure 4.6**).

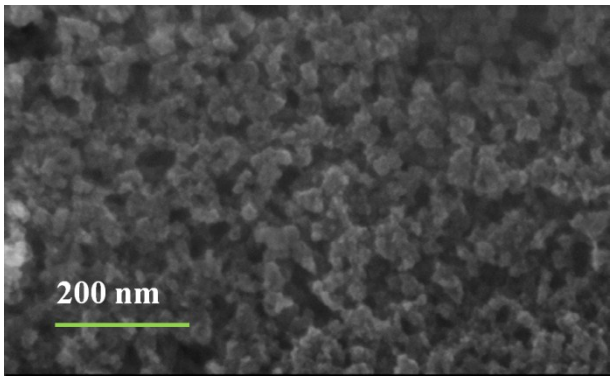

Figure 4.5. SEM image on nano-particles of ZnO_2 made via zinc acetate-H_2O_2 route.

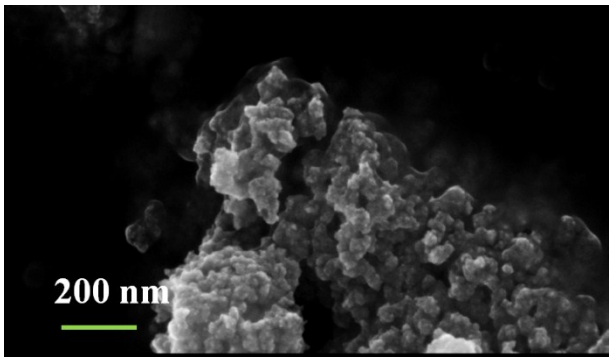

Figure 4.6. SEM image on ZnO particles made via zinc acetate-H_2O_2 route.

$Zn_4SO_4(OH)_6{\cdot}4H_2O$-$H_2O_2$ route

As far as I could determine, this route is reported for the first time. Here a solid/liquid reaction between zinc hydroxide sulphate and hydrogen peroxide results in ZnO_2. The mechanism is different from what was described above for a liquid-liquid reaction. Here $Zn_4SO_4(OH)_6{\cdot}4H_2O$ is dissolved in an acidic solution of H_2O_2 (Equation **4.7**). Soluble zinc species then are hydrolysed to form zinc-hydroxy complexes (see Equation **4.4**). Reaction between zinc hydroxy species and peroxo anions then proceeds as described in Equation **4.5**. A SEM image of the ZnO_2 produced via this route is shown in **Figure 4.7**.

$$Zn_4(OH)_6SO_4 \cdot 4H_2O \rightleftharpoons 4Zn^{2+}{}_{(aq)} + 6OH^- + SO_4^{2-}{}_{(aq)} + 4H_2O_{(l)} \qquad 4.7$$

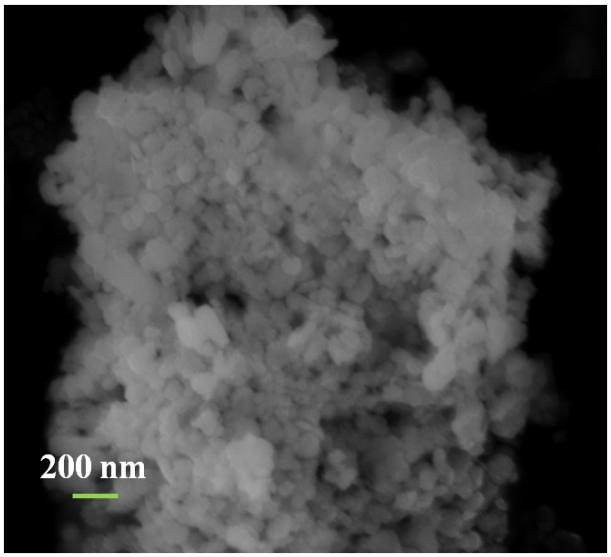

Figure 4.7. SEM image on ZnO_2 made via $Zn_4SO_4(OH)_6 \cdot 4H_2O/H_2O_2$ route.

Calcination of the ZnO_2 at 250 °C for 1 hour did not result in complete conversion of peroxide to oxide. SEM images of the product are shown in **Figure 4.8**. As shown by TGA-DTA results, the peroxide formed by the $Zn_4SO_4(OH)_6 \cdot 4H_2O$-$H_2O_2$ route is thermally more stable (DTA peak centred at 230 °C) than the one made by zinc acetate-H_2O_2 route (DTA peak centred at 210 °C).

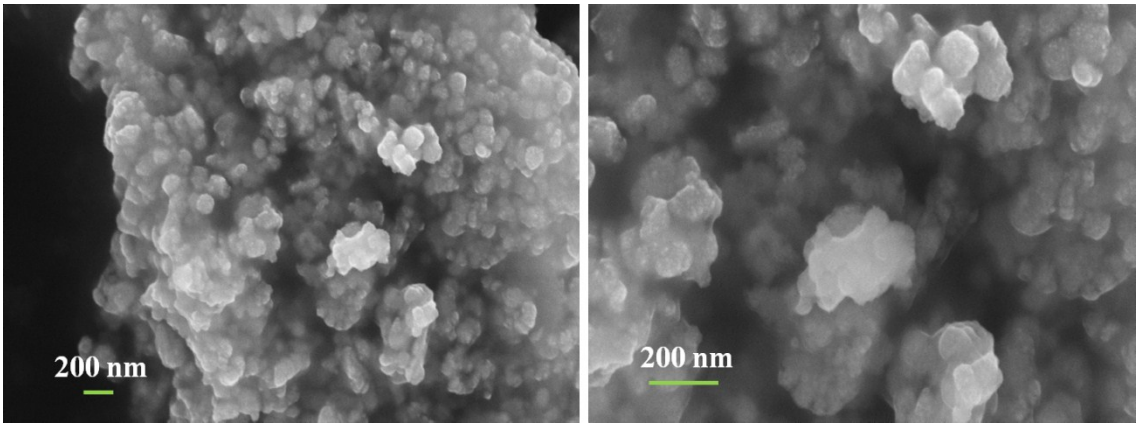

Figure 4.8. SEM images on ZnO/ZnO_2 particles made via $Zn_4SO_4(OH)_6 \cdot 4H_2O$-$H_2O_2$ route.

4.4. Conclusions

Zinc peroxide has been produced by two different methods: (1) by a liquid-liquid reaction between zinc acetate and H_2O_2 and (2) by a solid/liquid reaction between $Zn_4SO_4(OH)_6 \cdot 4H_2O$ and H_2O_2. It was shown that ZnO_2 can be formed directly from route 2 whereas in order to precipitate ZnO_2 from route 1, the system must be basified. Although both products are characterised as ZnO_2 by XRD, thermal behaviour of the products is slightly different. Decomposition temperature of the product made by route 2 was shown by TGA-DTA to be ~20 °C higher than that of the product of route 1. As a result calcination of the ZnO_2 from route 1 resulted in pure ZnO whereas a mixture of ZnO/ZnO_2 was produced by calcination of the one from route 2. Here it was shown that the method of production has direct effect on the thermal stability of ZnO_2 and consequently the composition of the calcined products. The mechanism of the route 1 follows the formation of zinc hydroxy species, which then react with peroxo anions to form ZnO_2. Route 2 follows a slightly different mechanism. Dissolution of $Zn_4SO_4(OH)_6 \cdot 4H_2O$ happens first in the acidic solution of H_2O_2. Zinc species are then hydrolysed to generate zinc-hydroxy complexes, which then follow the same mechanism as route 1 to form ZnO_2.

Chapter 5

Multi-Stage Routes to Synthesise Zinc Oxide Using Zinc Hydroxy Salts

Chapter 5: Multi-Stage Routes to Synthesise Zinc Oxide Using Zinc Hydroxy Salts*

5.1. Introduction

The industrial significance of ZnO was discussed in detail in Chapter 1. In this chapter alternative multi-stage routes for the production of ZnO will be explored. A variety of possible candidate precursors are considered and their thermal decomposition patterns are studied. Materials selected here as precursors for the production of ZnO belong to a class of layered hydroxide salts of zinc generally known as zinc hydroxy salts or basic zinc salts. Five basic zinc salts have been synthesised and used for the production of ZnO: (1) basic zinc carbonate (BZC), (2) basic zinc sulphate (BZS), (3) basic zinc chloride (BZCl), (4) basic zinc nitrate (BZN) and (5) basic zinc acetate (BZA).

Layered hydroxide salts are important materials per se. These salts with interlayer anions are candidates for anion exchange, catalysis and sensing applications. Large 2D layered compounds are useful in assembly technology. Anion-exchangeable layered compounds are rare as most of the ion-exchangeable materials are cation-exchangeable such as cationic clays, silicates, metal phosphates and phosphonates [314-319]. Some of them are being used directly in existing applications; e.g. basic zinc sulphate is utilised as a zinc fertiliser or as a white pigment [320-322]. Other ones are used as precursors for production of useful materials; e.g. basic zinc carbonate is used for the production of *active* ZnO.

As described in Chapter 1, most ZnO is produced by the high temperature 'French' or 'American' gas phase processes but these necessarily produce material of relatively large particle size and correspondingly low specific surface area. If ZnO of larger specific surface area is sought, it must be produced by other means. However crystalline ZnO grades such as the French process grade are currently more desirable for the big consumers (e.g. tire and ceramic manufacturers). Therefore alternative processes that lead to the end-products with high crystallinity and low specific surface area were also sought.

* A significant part of the work presented in this chapter has been submitted for publication.

Real-time in-situ synchrotron powder diffraction was conducted at Australian Synchrotron in Melbourne on the abovementioned basic zinc salts to study the phase transformations over a range of temperatures. Fascinating results were revealed by this study. It was shown that crystallinity of ZnO formed by thermal decomposition of basic zinc salts significantly depends on the crystallinity of the precursors, i.e. the more crystalline the salt, the more crystalline ZnO will be. This finding is important especially for an industrial grade of zinc oxide called *active* ZnO that is produced by calcination of BZC. It was revealed that since BZC has the lowest crystallinity among the precursors studied, the resultant ZnO is of the lowest crystallinity as well as having the highest specific surface area.

5.2. Experimental

5.2.1. General

Sodium carbonate and lab-grade ethanol (95%) were purchased from Chem-Supply Pty. Ltd. AR grade zinc sulphate heptahydrate, zinc nitrate hexahydrate, zinc acetate dihydrate, zinc chloride, zinc oxide powder and sodium hydroxide pellets were purchased from Ajax Chemicals and used as-received. Milli-Q water (18.2 Ω cm^{-1}) was used as the solvent. Reactions were conducted under atmospheric conditions using a two-neck round bottom flask with a digitally-controlled magnetic heater/stirrer. A magnetic stirrer bar was used at a stirring rate of 820 rpm and isolation of the precipitates was performed by vacuum filtration followed by drying using a rotary evaporator at 70 °C, unless otherwise stated.

X-ray diffraction, thermogravimetric analysis (TGA), scanning electron microscopy and fluorescence spectrometry experiments have been done according to the methods explained in Chapter 2 unless otherwise stated. Multi-point (5 points) BET specific surface area measurements were performed using Autosorb-1 from Quantachrome Instrument or using Micromeritics Gemini VII 2390 by precise vacuum volumetric method for nitrogen chemisorption. All the samples were out-gassed at 100 °C for 1 hour before actual measurements. Freeze drying was conducted using Christ-Alpha 2-4-LD Plus at -87 °C and 0.009×10^{-3} mbar.

For transmission electron microscopy (TEM) images, small amount of the powder samples was suspended in Milli-Q water and sonicated. Then a drop of the dispersed solution was put in a carbon-coated copper grid and dried. The TEM images of samples were taken using a JEOL JEM-2200FS microscope at the accelerating voltage of 200 kV equipped with EDS or JEOL 1400 microscope at the accelerating voltage of 120 kV.

Simultaneous thermogravimetric analysis-mass spectrometry (TGA-MS) experiments were conducted using Quadrupole mass spectrometer (model: Thermostar QMS 200 M3) from Balzers Instruments in a platinum crucible. Raman spectroscopy was performed using a Renishaw inVia Raman Microscope System. A 633 nm laser with the laser power of 100% was used. The scan range was 100-3200 cm^{-1}. Fourier transform infrared (FTIR) spectroscopy was performed using a Thermoscientific, Nicolet 6700 instrument with 64 scans at a resolution of 4 cm^{-1} in transmission mode using KBr. The scan range was 400-4000 cm^{-1}.

^{13}C Cross Polarisation Magic Angle Spinning (CP-MAS) NMR measurements were performed using a Bruker 200 MHz NMR Spectrometer operating at 50 MHz. Samples were loaded into 4 mm zirconium oxide rotors with Kel-F caps, and spun at 5000 Hz. A pulse width of 4.5 μs was used with a contact time of 2 ms. In total 485 scans were collected per sample. Free induction decay (FID) signals were obtained during a 0.05 sec acquisition time, followed by a 5 s delay. Chemical shifts were measured with respect to adamantane as an external standard at 38.48 ppm.

In-situ synchrotron phase studies were performed to identify the phases and to investigate phase transformation of the materials by continuous X-ray powder diffraction with high resolution and accuracy at the Australian Synchrotron in Melbourne over a range of temperatures with a heating rate of 5 °C min^{-1}. The synchrotron wavelength was set at 0.696603 Å. LaB_6 was used as a standard reference. Data collection was performed in two-minute intervals.

To generate the colour-coded 3D and contour graphs and for numerical analysis, MATLAB version 7.10.0.499 (R2010a) was used. Synchrotron raw data were imported into MATLAB. Intensity data for all samples were corrected by division of the intensity figure by the integrated ion chamber count figure multiplied by 10^5 to generate an arbitrary unit. To resolve low-angle XRD peaks, Topas software supplied by Bruker was used and a number of Split Pearson VII distribution functions fitted.

5.2.2. Synthesis of zinc hydroxy salts

Zinc hydroxy carbonate

Aqueous solutions of $ZnSO_4 \cdot 7H_2O$ (30 ml, 1M, pH=6) and Na_2CO_3 (30 ml, 1M, pH=12) were prepared. Zinc sulphate solution was added to the sodium carbonate solution at 70 °C in a single shot. Immediately after the addition, the solution became white and cloudy. The reaction continued for 1 hour (where the pH was 7). The white precipitate was then filtered, washed and dried at 60 °C in an oven overnight.

Zinc hydroxy sulphate

Zinc hydroxy sulphate tetrahydrate: Aqueous solutions of NaOH (33.5 ml, 0.1M) and zinc sulphate heptahydrate (30 ml, 0.1M) were prepared. Zinc sulphate solution was added to NaOH solution at 25 °C. Immediately after addition, the solution became milky white. Reaction continued for 15 mins (where the pH was 6). Then the white gelatinous suspension was centrifuged for 10 mins at 4400 rpm. The resultant white precipitate was separated, washed and dried at 60 °C under reduced pressure.

Zinc hydroxy sulphate monohydrate: Aqueous solutions of zinc sulphate (60 ml, 1.5M, pH=6) and NaOH (60 ml, 1.5M, pH=14) were prepared. NaOH solution was added to the zinc sulphate solution in a single step at 25 °C and at the stirring rate of 500 rpm (pH=7 after addition). Reaction continued for 2 hours (where the pH was still 7). Then the white and sticky precipitate was filtered, washed and dried at 60 °C in an oven overnight.

Zinc hydroxy chloride

An aqueous solution of $ZnCl_2$ (30 ml, 6M, pH=3) was prepared. An equimolar amount of ZnO powder was suspended in 70 ml water. The zinc chloride solution was added to the ZnO suspension in a single step at 90 °C and at the stirring rate of 500 rpm. The reaction continued for 2 hours (where the pH was 7). Then the white suspension was filtered, washed and dried.

Zinc hydroxy nitrate

Aqueous solution of $Zn(NO_3)_2 \cdot 6H_2O$ (30 ml, 3M, pH=3) was prepared. An equimolar amount of ZnO powder was suspended in 80 ml of water. The zinc nitrate solution was added to the ZnO suspension in a single step at 25 °C. The reaction continued for 1 hour (where the pH was 7). Then the white suspension was filtered, washed and dried at 50 °C under reduced pressure.

Zinc hydroxy acetate

BZA has been synthesised via two independent routes:

- Aqueous solutions of zinc acetate (60 ml, 1.5M, pH = 6) and NaOH (60 ml, 1.5M, pH=14) were prepared. NaOH solution was added to the zinc acetate solution in a single step at room temperature. Reaction continued for 2 hours (where the pH was 7). The white suspension was filtered, washed and dried at 60 °C in the oven;
- Aqueous solution of zinc acetate (60 ml, 1.5M, pH = 6) was prepared. 0.09 mol ZnO powder was suspended in 60 ml of water. Zinc acetate solution was added to the ZnO suspension in a single step. The mixture was stirred for 4 hours at room temperature. The white suspension was then filtered, washed and dried.

Product of reaction between zinc hydroxy acetate and ethanol

This reaction was carried out to clarify some reports in the literature [323, 324]. BZA (0.4947 g) made from the latter route was added to 50 ml of ethanol and stirred vigorously at room temperature in a closed vessel for four days. Each day the solid was isolated by centrifugation at 4400 rpm and resuspended in 50 ml of fresh ethanol. After 4 days the solid was separated by centrifuge and was divided into two parts. One part was dried at 50 °C under the reduced pressure and the other part was freeze-dried for 24 hours. The dried powders were then analysed by XRD, TGA-DTA, Raman spectroscopy, FTIR spectroscopy, and solid-NMR spectroscopy.

5.2.3. Synthesis of ZnO from zinc hydroxy salts

Process conditions to synthesise ZnO from basic zinc salts were selected based on the thermogravimetric analysis data. ZnO was formed by calcination of basic zinc salts using a preheated oven set at specific temperatures for each salt according to the Table 5.1. In the case of multiple-stage calcination, after each stage, the product was cooled down naturally to room temperature under still air.

Table 5.1. Calcination conditions to produce ZnO using basic zinc salt precursors.

Precursor	BZC	BZS	BZCl	BZN	BZA
Stage 1 calcination temp (°C)	300	900	400	250	400
Residence time (hr)	1	1	2	1	2
Stage 2 calcination temp (°C)	-	-	400	300	-
Residence time (hr)	-	-	4	1	-
Stage 3 calcination temp (°C)	-	-	600	-	-
Residence time (hr)	-	-	4	-	-

5.3. Results and Discussion

In this work, formation of some basic zinc salts i.e. basic zinc carbonate, sulphate, chloride, nitrate and acetate and their transformation into ZnO were investigated. Discrepancies in the mechanism of formation of ZnO from some of the basic zinc salt precursors in terms of the presence of some intermediate phases were observed. As a result, by using a combination of techniques such as *in situ* synchrotron radiation study and TGA-MS on the gaseous products, these issues have been clarified.

5.3.1. Zinc hydroxy carbonate

Basic zinc carbonate (BZC) - other names: hydrozincite, zinc hydroxy/hydroxide carbonate - with the chemical formula of $Zn_5(CO_3)_2(OH)_6$ or $3Zn(OH)_2{\cdot}2ZnCO_3$ (M.W=548.95) is an industrially important precursor for the production of wet-process ZnO that is generally precipitated from the secondary sources. Different compositions for BZC have also been reported such as $Zn_2CO_3(OH)_2$, $Zn_3CO_3(OH)_4$ and $Zn_4CO_3(OH)_6{\cdot}H_2O$ [92, 325, 326]. The resultant grade of ZnO, which is well-known for a long time in industry is called *active* or *activated* ZnO due to the higher specific

surface area compared to e.g. that of the French process ZnO [24, 86, 96, 97, 327-335], see also section 1.3.2.

Mechanism and kinetics of thermal decomposition of BZC have been investigated in previous works [90, 92, 325, 326, 336]. In the present work, the phase transformation of BZC to ZnO using real-time in-situ synchrotron radiation was investigated. BZC was also calcined in a separate experiment at a temperature range of 250-350 °C (with 10 °C intervals) and the specific surface area of the resultant materials was measured. It was shown that ZnO made from BZC is highly porous and has high specific surface area.

Precipitation of BZC proceeds according to equation **5.1**.

$$5ZnSO_4 \cdot 7H_2O_{(aq)} + 5Na_2CO_{3\,(aq)} \rightarrow Zn_5(CO_3)_2(OH)_{6\,(s)} + 5Na_2SO_{4\,(aq)} + 3CO_{2\,(g)} + 32H_2C \quad 5.1$$

Characterisation, TGA-DTA and microscopy

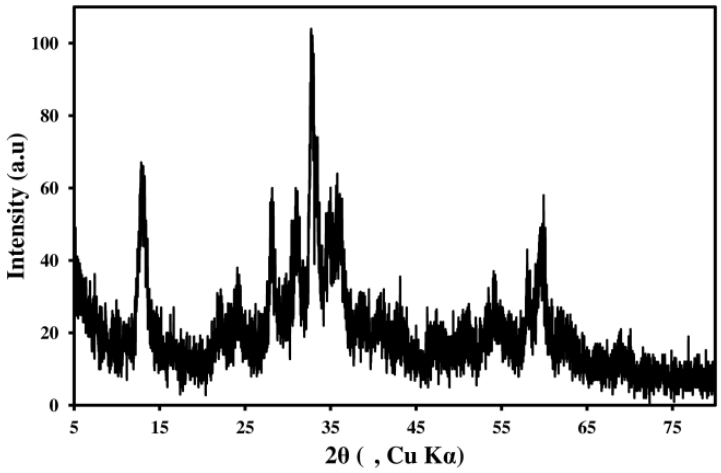

Figure 5.1. XRD (Cu Kα) on the product corresponding to hydrozincite (JC-PDF card 00-019-1458). The peaks are broad.

The precipitate formed by this reaction was separated and characterised by XRD as hydrozincite, **Figure 5.1**. Theoretical mass loss of hydrozincite when decomposed to ZnO is ~25.9%. TGA shows ~26% mass loss up to a temperature of 1000 °C, which is in accordance with the theoretical mass loss value. The sample contains a small amount of moisture. A small and gradual mass loss can be observed in the temperature range of

120-250 °C. DTA shows a sharp endothermic peak centred at ~248 °C along with a sharp mass loss seen in TGA, **Figure 5.2**. Mass loss above 250 °C is attributed to surface hydroxyl groups.

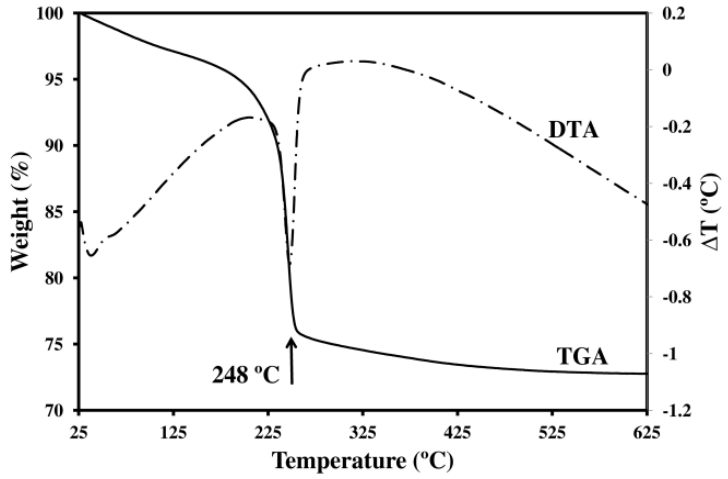

Figure 5.2. TGA-DTA on hydrozincite.

Independently some BZC was calcined at 300 °C for 1 hour. It was observed that the calcined product at 300 °C shows a yellowish-white colour, which over cooling to room temperature gains its whiteness. This is in accordance with thermochromism properties of ZnO [24, 337, 338]. XRD on the calcined product showed that the product is only ZnO (**Figure 5.3**). SEM images of the BZC and the highly porous ZnO produced from this precursor are shown in **Figure 5.4**.

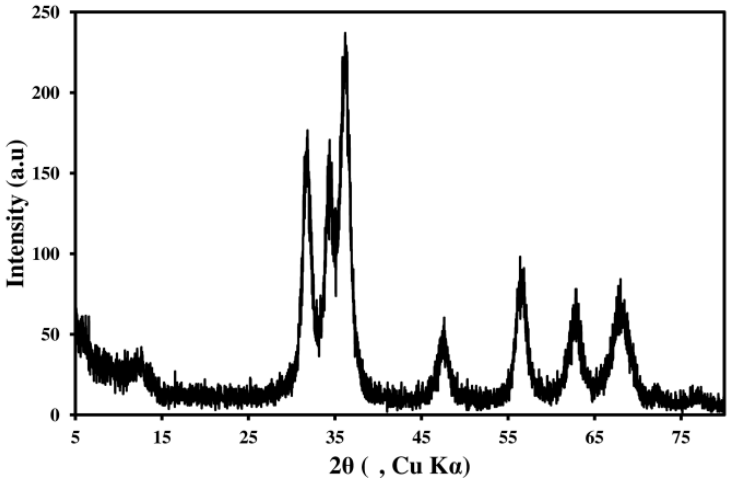

Figure 5.3. XRD (Cu Kα) on the calcined product corresponds to ZnO (JC-PDF card 00-005-0664).

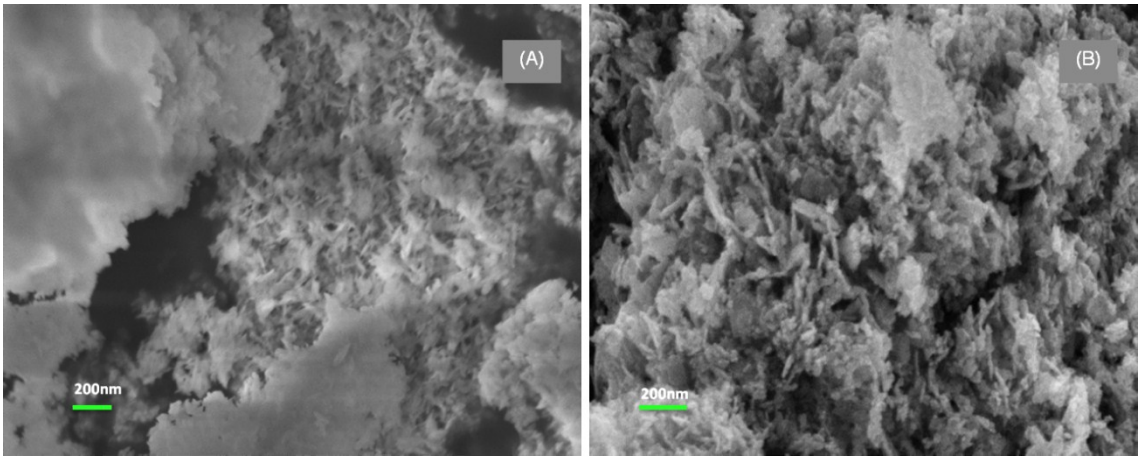

Figure 5.4. SEM images of (A) BZC; (B) highly porous ZnO produced from calcination of BZC.

TEM images, **Figure 5.5**, on the ZnO revealed that crystal particle size is in the range of 5-20 nm. Some amorphous material was also detected, which is bigger in size. This is consistent with the XRD pattern on the material that shows low intensity peaks associated with ZnO.

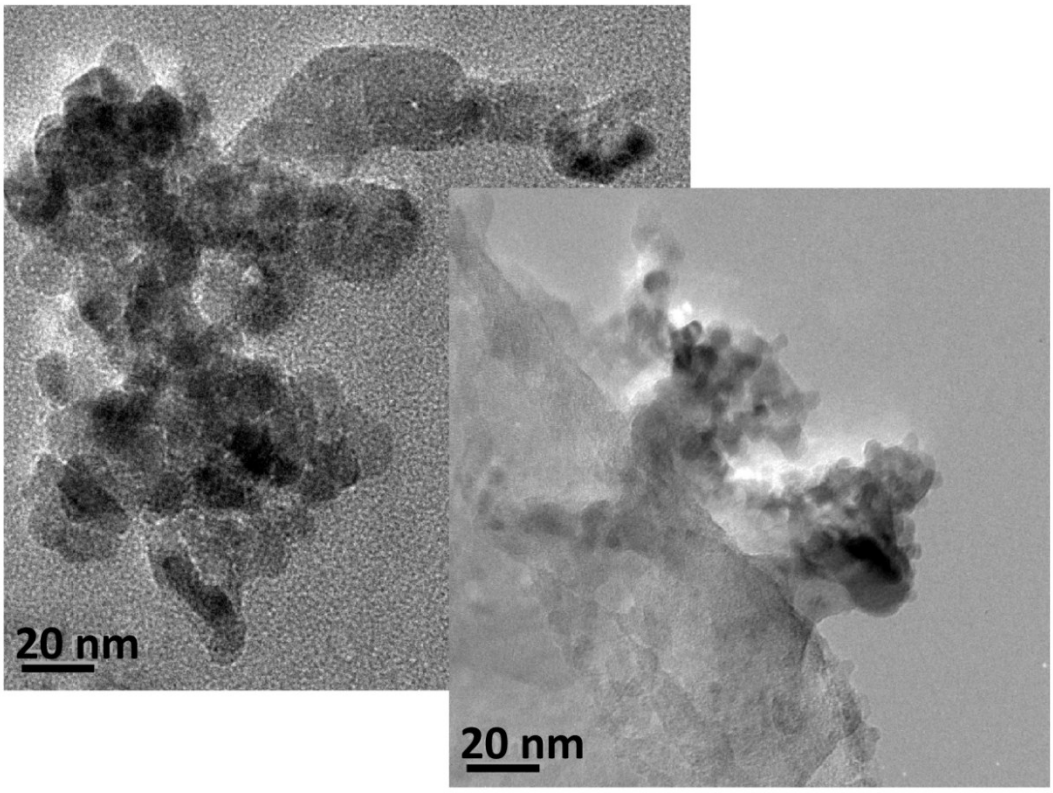

Figure 5.5. TEM images on the ZnO particles produced from calcination of BZC (courtesy of Dr A. Dowd).

Real-time synchrotron radiation study

In-situ synchrotron study on BZC in the temperature range of 25-600 °C confirmed a single stage phase transformation for this material into ZnO, see **Figure 5.6** and **Figure 5.7**. Up to temperatures around 230 °C only hydrozincite peaks can be detected with shrinkage in peak intensity as temperature increases. The only phase transformation takes place at temperatures ~230 °C over which only ZnO peaks can be observed. The minimum temperature required for the completion of decomposition of BZC to ZnO is therefore around 230 °C, which also depends on the rate of heating. This is important for industrial rotary kiln design.

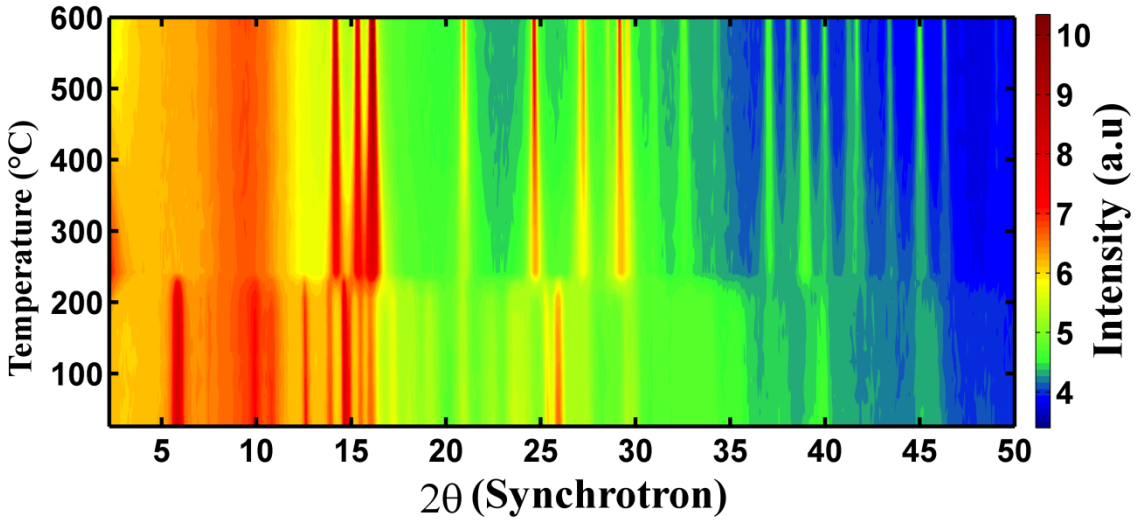

Figure 5.6. Colour-coded contour XRD (synchrotron) graph shows the real-time transformation of hydrozincite to ZnO. The intensity is colour-coded.

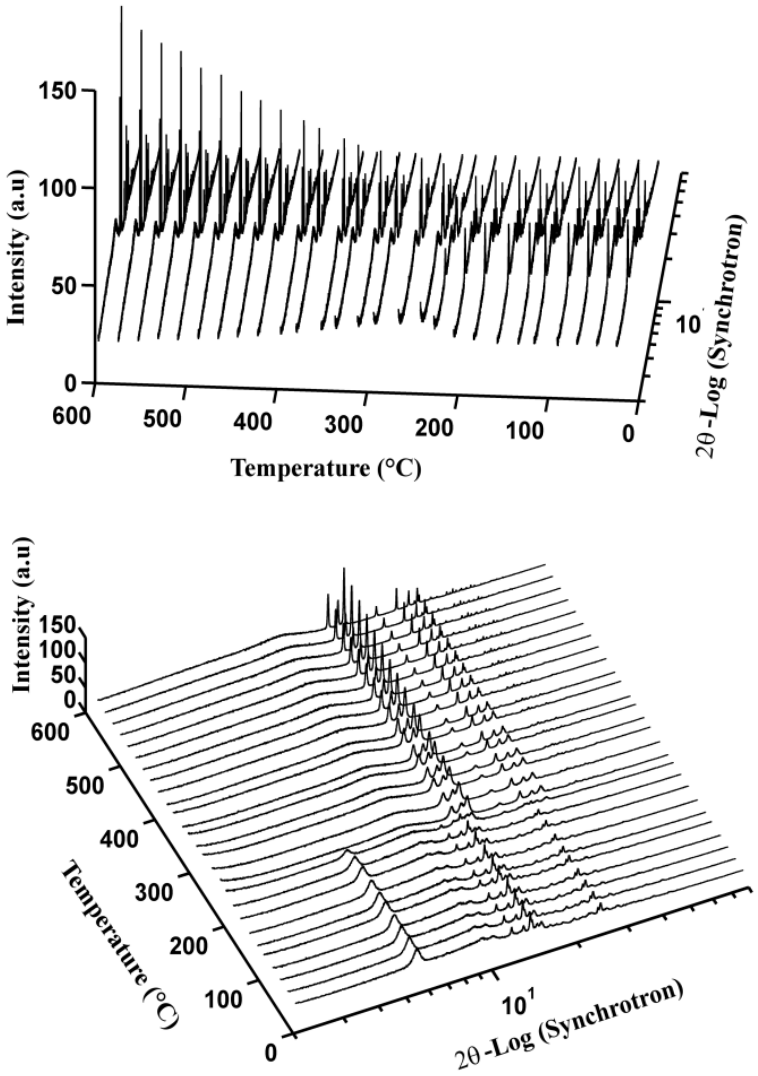

Figure 5.7. Two projections of 3D-stacked XRD (synchrotron) patterns on BZC show that intensity of BZC is lower than that of the end-product ZnO. ZnO peaks are intensified by increasing the temperature.

Based on the TGA-DTA and synchrotron radiation study, it was shown that decomposition of BZC to ZnO proceeds in a single stage according to the Reaction **5.2**.

$$Zn_5(CO_3)_2(OH)_6 \xrightarrow{T>230\ ^\circ C} 5ZnO + 3H_2O + 2CO_2 \qquad 5.2$$

BET surface area measurements

To investigate the effect of temperature of calcination on the specific surface area of ZnO product, some BZC was divided into 11 parts and the samples were calcined at 250, 260, 270, 280, 290, 300, 310, 320, 330, 340, 350 °C for 1 hour, respectively.

After calcination, all products were characterised by XRD to be ZnO, **Figure 5.8**. No specific relationship between the XRD patterns and temperature of calcination could be detected. It was expected that by increasing the temperature of calcination, BET specific surface area drops, but this was not the case, **Figure 5.9**. BET specific surface area of the ZnO samples was measured to be in the range of 47-65 m^2/g.

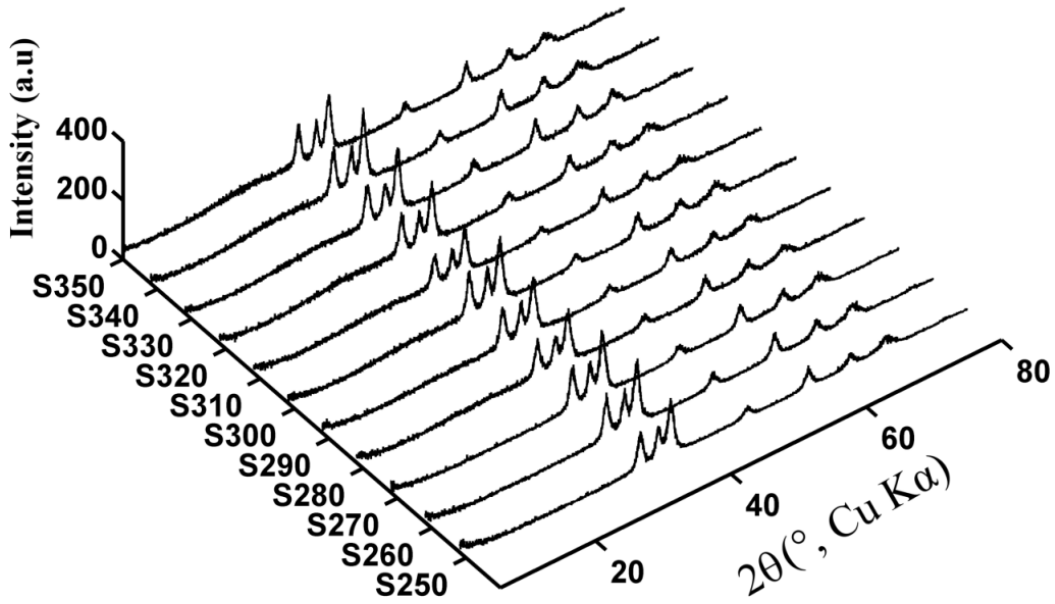

Figure 5.8. XRD (Cu Kα) on the products of calcination of BZC at a temperature range of 250-350 °C for 1 hour shows only ZnO peaks.

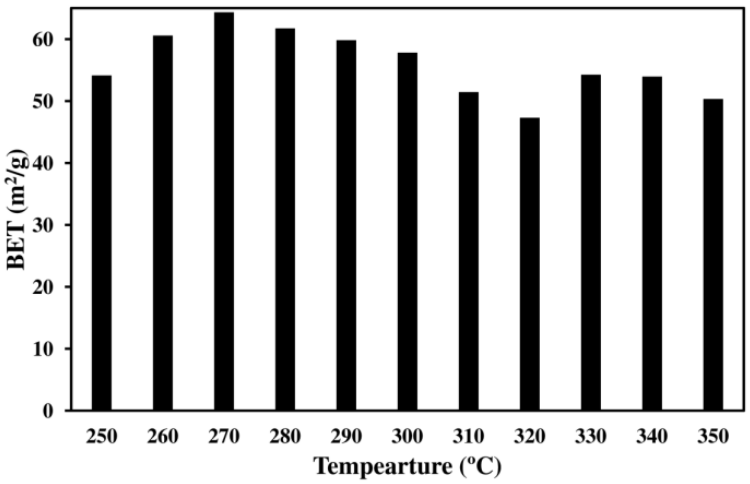

Figure 5.9. BET specific surface area of ZnO samples prepared by calcination of BZC at 250-350 °C.

5.3.2. Zinc hydroxy sulphate

Zinc hydroxide sulphates (BZS) - other name: basic zinc sulphate - with general formula of $xZnSO_4 \cdot yZn(OH)_2 \cdot zH_2O$ are Berthollide compounds with variable, non-integral ranges of *x, y* and *z*. Studies on $3Zn(OH)_2 \cdot ZnSO_4 \cdot zH_2O$ showed that it can hold different number of water of crystallisation with z = 0, 0.5, 1, 3, 4 and 5 [320, 339-343]. Disparity in the nomenclature of the similar chemicals can be observed. For example in [320] "zinc hydroxy-sulphate" is misleadingly named zinc oxy-sulphate or in [344] "basic zinc sulphate" was used instead of "zinc oxy-sulphate". Similar naming confusion can be seen in commercial application [321]. It must be noted that zinc hydroxy-sulphate and oxy-sulphate are two different groups of materials with the chemical formula of $xZnSO_4 \cdot yZn(OH)_2 \cdot zH_2O$ and $nZnSO_4 \cdot mZnO$, respectively. Basic zinc sulphate is specifically reserved for zinc hydroxy sulphate [345].

Synthesis of the basic zinc sulphate has been a matter of confusion as well. For example Yadav *et al.,* [346] tried to synthesise ZnO using a reaction between NaOH and $ZnSO_4$ with a sub-stoichiometric molar ratio of reactants (1:2.2). It was not noticed in their work that a sub-stoichiometric reaction between the reactants does not form ZnO; rather basic zinc sulphate is precipitated [79].

Precipitation of BZS tetrahydrate and monohydrate proceeds according to Reactions **5.3** and **5.4**, respectively with slightly different methods described in experimental section.

$$6NaOH_{(aq)} + 4ZnSO_4 \cdot 7H_2O_{(aq)} \rightarrow Zn_4(OH)_6SO_4 \cdot 4H_2O_{(s)} + 3Na_2SO_{4(aq)} + 24H_2O \qquad 5.3$$

$$6NaOH_{(aq)} + 4ZnSO_4 \cdot 7H_2O_{(aq)} \rightarrow Zn_4(OH)_6SO_4 \cdot H_2O_{(s)} + 3Na_2SO_{4(aq)} + 27H_2O \qquad 5.4$$

Characterisation and TGA-DTA

Using XRD, the precipitate formed by Reaction **5.3** was identified as BZS tetrahydrate (00-044-0673). However the XRD pattern obtained from the precipitate formed by Reaction **5.4** could not be identified by the available XRD data (**Figure 5.10**). Using TGA on both precipitates, a similar pattern of decomposition was detected, which was a sign that the chemicals are of similar nature with a slightly different mass loss due to the dehydration stage at temperatures up to 110 °C. Theoretical mass loss due to the complete conversion of $BZS \cdot 4H_2O$ to ZnO is 38.75% and that of $BZS \cdot H_2O$ to

ZnO is 31.82%. TGA (**Figure 5.11**) on the samples prepared by different methods shows mass loss values consistent with the theoretical figures. Therefore based on the TGA data, the unidentified phase was speculated to be BZS monohydrate. DTA on the unidentified phase shows sharp endothermic peaks while DTA peaks associated with BZS·4H_2O are broader and smaller, **Figure 5.12**. To confirm the presence of BZS monohydrate, a comparative study between the data obtained from real-time synchrotron study on the calcined BZS·4H_2O at 113 °C and the XRD (Cu Kα) data on the product, which is believed to be BZS·H_2O was performed, see synchrotron study section.

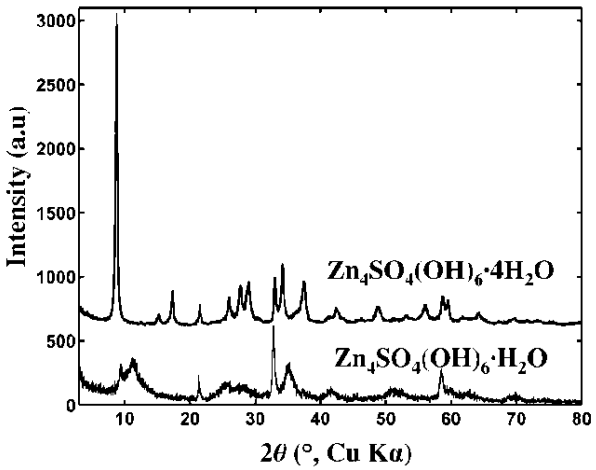

Figure 5.10. XRD (Cu Kα) on the BZS tetrahydrate and the phase, which is believed to be BZS monohydrate.

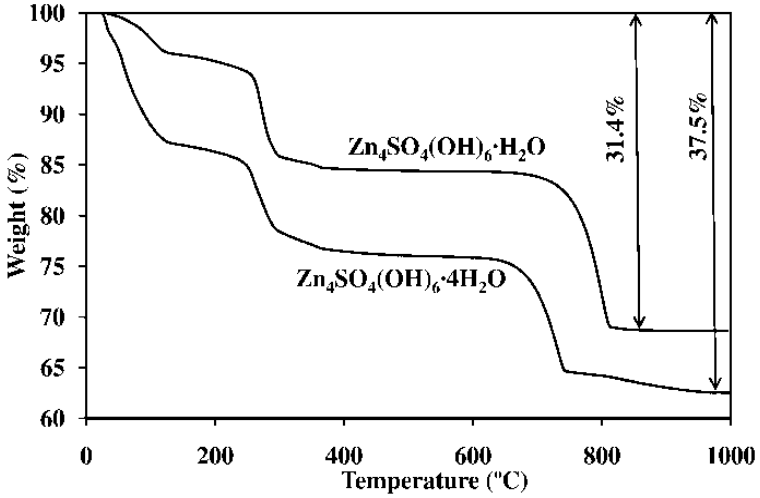

Figure 5.11. TGA on BZS tetrahydrate and monohydrate.

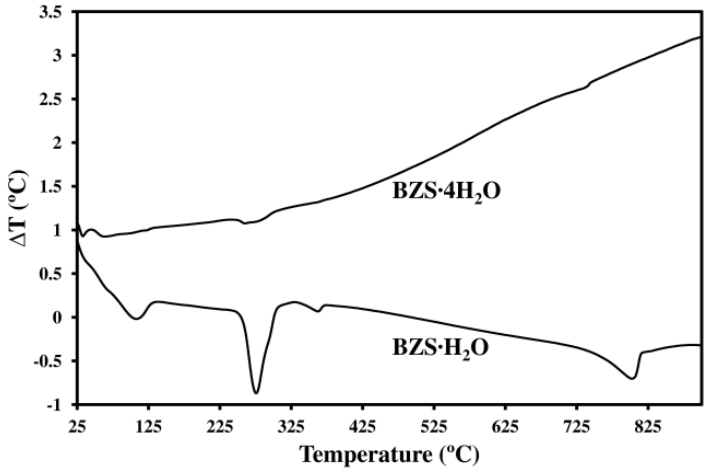

Figure 5.12. DTA on BZS tetrahydrate and monohydrate.

Synchrotron radiation study and TGA-MS

In-situ real-time synchrotron radiation study on BZS·4H_2O was performed, which revealed astonishing information on this chemical. Crystalline intermediate phases involved during thermal decomposition of this compound were identified, see **Figure 5.13** and **Figure 5.14**.

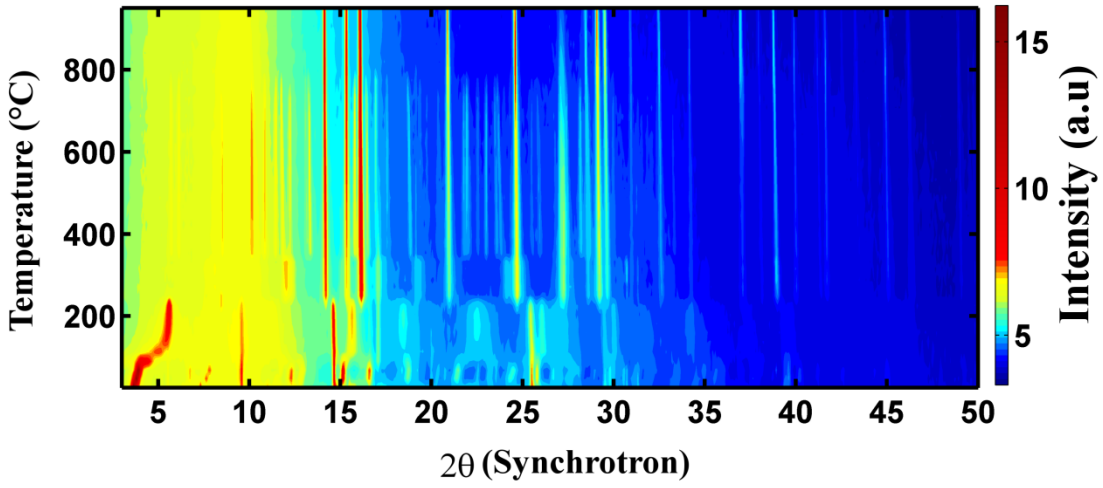

Figure 5.13. Colour-coded contour XRD (synchrotron) graph shows the real-time transformation of BZS·4H_2O to ZnO. The intensity is colour-coded.

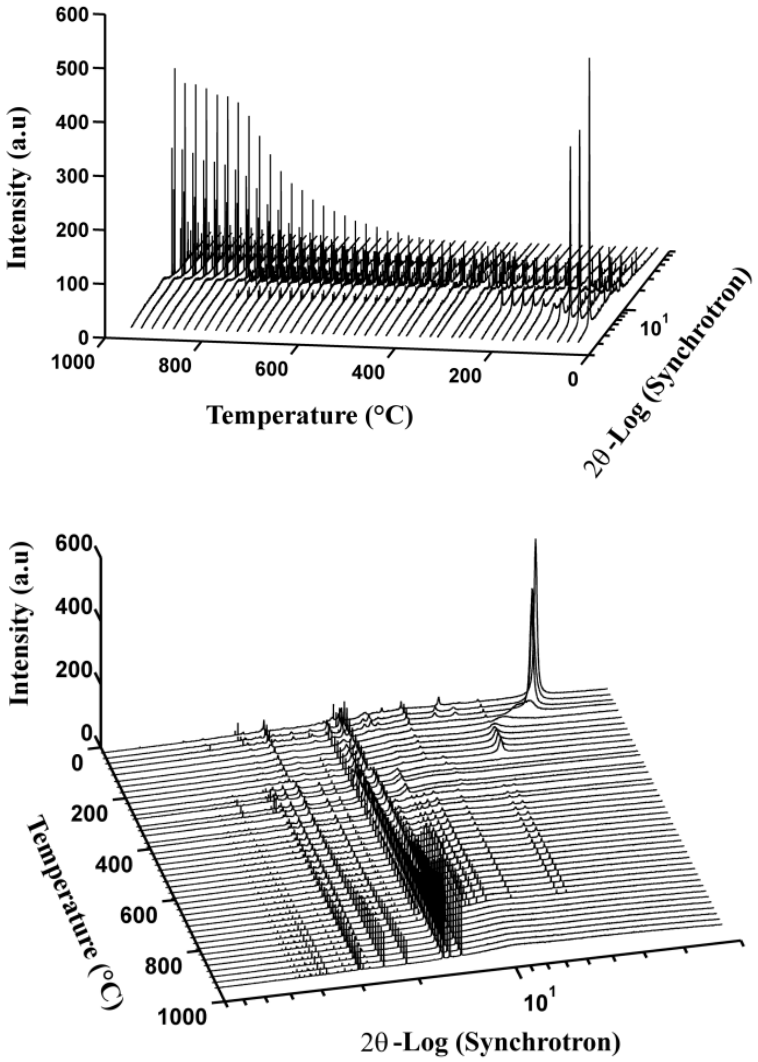

Figure 5.14. Two projections of 3D-stacked XRD (synchrotron) graphs on $BZS{\cdot}4H_2O$.

It was observed that $BZS{\cdot}4H_2O$ undergoes dehydration to form $BZS{\cdot}H_2O$ at 89-113 °C followed by complete dehydration at temperature range between 113-140 °C according to Reactions **5**.**5** and **5**.**6**, respectively.

$$Zn_4SO_4(OH)_6{\cdot}4H_2O \xrightarrow{89-113\,℃} Zn_4SO_4(OH)_6{\cdot}H_2O + 3H_2O \qquad 5.5$$

$$Zn_4SO_4(OH)_6{\cdot}H_2O \xrightarrow{113-140\,℃} Zn_4SO_4(OH)_6 + H_2O \qquad 5.6$$

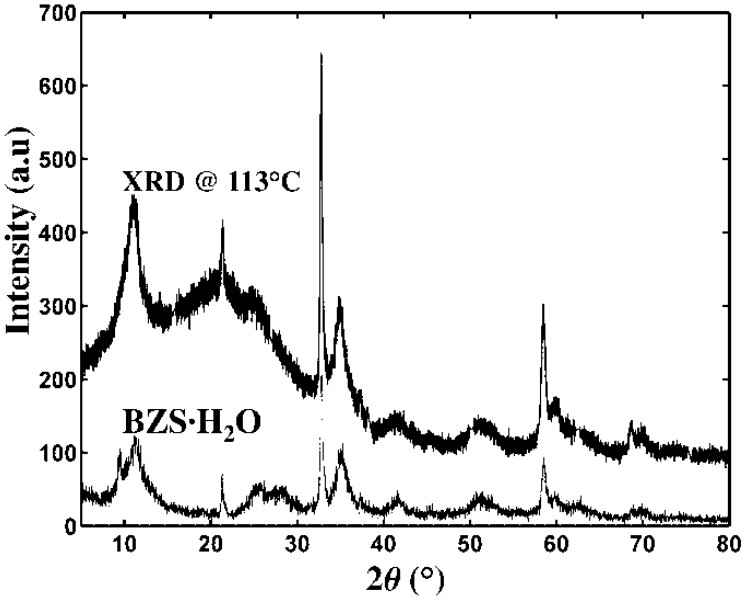

Figure 5.15. Top pattern: XRD pattern on the calcined $BZS{\cdot}4H_2O$ at 113 °C obtained by synchrotron radiation (synchrotron 2θ values are converted to the equivalent of Cu Kα). Bottom pattern: XRD (Cu Kα) pattern on unidentified BZS. The two patterns match perfectly with each other.

Synchrotron data obtained at 113 °C was compared with the unidentified phase mentioned previously, which is believed to be $BZS{\cdot}H_2O$. XRD revealed that two phases are identical, see **Figure 5.15**. Using both the TGA-DTA and the synchrotron study, it can be stated that the unidentified precipitate of Reaction **5.4** is $BZS{\cdot}H_2O$.

Dehydration of BZS is a dynamic process with other possible intermediate phases involved, see **Figure 5.13** and **Figure 5.16**.

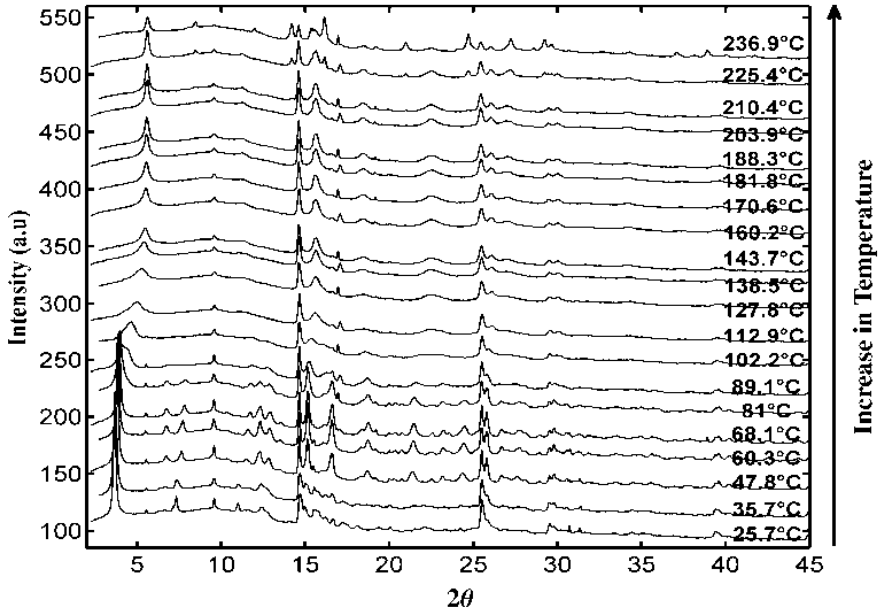

Figure 5.16. Stacked XRD (synchrotron) on the BZS·$4H_2O$ under calcination shows a dynamic phase transformation due to the dehydration by increasing the temperature.

At ~140 °C, dehydrated BZS is observed. This phase remains stable up to the temperatures ~225 °C where the first signs of the formation of ZnO can be tracked. This is consistent with TGA data. Available XRD data (JC-PDF file: 00-044-0675) for dehydrated zinc hydroxide sulphate, $ZnSO_4 \cdot 3Zn(OH)_2$, was assigned to the XRD patterns observed at 140-225 °C, see **Figure 5.17**. A detailed dehydration study on basic zinc sulphate is also available in [339].

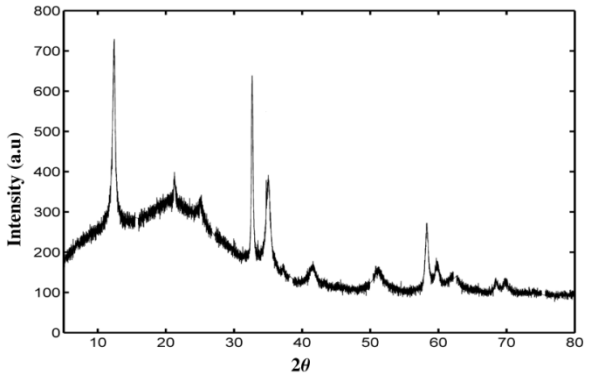

Figure 5.17. XRD pattern on the calcine at 204 °C obtained by synchrotron radiation (synchrotron 2θ value is converted to its equivalent of Cu Kα).

Next transformation in the XRD pattern is observed in the temperature range of 225-350 °C with formation of two new phases one of which was identified as ZnO and the

other is believed to be in the form of zinc oxy-sulphate ($Zn_3O(SO_4)_2$ or $ZnO{\cdot}2ZnSO_4$) according to Reaction **5.7**. This is consistent with TGA-DTA data in this temperature range.

$$2Zn_4SO_4(OH)_6 \xrightarrow{225-350℃} 5ZnO + Zn_3O(SO_4)_2 + 6H_2O \qquad 5.7$$

No available XRD data for zinc oxy-sulphate (i.e. JC-PDF files 031-1469, 071-2475, 016-0821) could be assigned to the unknown peaks. It was also attempted to match available XRD data for lower order zinc hydroxy-sulphate such as $Zn_2(OH)_2SO_4$ to the peaks with the hope that hydroxide groups were still present in the system. This also showed that lower order zinc hydroxy sulphates are not involved at this temperature range, which is in contrast with the pathway suggested by Biswick *et al.,* [347, 348].

Consequently and based on the observed mass loss by TGA and also with a support from TGA-MS on $BZS{\cdot}H_2O$ (**Figure 5.19**), it was calculated that up to the temperatures around 350 °C (where a phase transformation can be observed), equivalent to 7 moles of water are evolved from the BZS tetrahydrate. Four of these waters are the hydration water and the remainder are evolved due to the decomposition of the dehydrated BZS, which results in ZnO and zinc oxy-sulphate according to Reaction **5.7**. Formation of $Zn_3O(SO_4)_2$ has been confirmed in previous works during thermal decomposition of ordinary $ZnSO_4$. It was shown that $Zn_3O(SO_4)_2$ is stable up to ~750 °C. Also it was shown that $Zn_3O(SO_4)_2$ can be formed at 600 °C and 700 °C with a different technique i.e. a solid-solid reaction between anhydrous $ZnSO_4$ and ZnO with a correct proportion of excess $ZnSO_4$ [344, 349-353]. This compound is in fact categorised under metal oxocentred complexes [354].

Next transformation proceeds due to the presence of ZnO in excess in the system, which is enough for the formation of higher order zinc oxy-sulphate at higher temperatures via a solid-solid reaction. As the temperature reaches ~350 °C, sintering between some free ZnO and $Zn_3O(SO_4)_2$ occurs to form a higher order zinc oxy-sulphate with the chemical formula of $Zn_5O_2(SO_4)_3$ according to Reaction **5.8**.

$$ZnO + 3Zn_3O(SO_4)_2 \xrightarrow{T \cong 350\,℃} 2Zn_5O_2(SO_4)_3 \qquad 5.8$$

Interestingly, TGA does not show any mass loss at these temperatures. However, DTA shows a small endothermic peak that was assigned to the phase change between two forms of zinc oxy-sulphate, see **Figure 5.11** and **Figure 5.12**. This form of zinc

oxy-sulphate is then stable up to the temperatures around 775 °C where it starts to decompose to ZnO. This is in accordance with the published data on $Zn_5O_2(SO_4)_3$ by Hoschek [355]. XRD patterns were identified as $Zn_5O_2(SO_4)_3$ (00-016-0305) and ZnO (01-089-7102), Figure 5.18. It is interesting to mention that presence of different forms of zinc oxy-sulphate has been controversial. For instance Ibanez *et al.,* with reference to the older work by Ingraham and Kellogg, stated that two forms of oxy-sulphate [$Zn_3O(SO_4)_2$ and $Zn_5O_2(SO_4)_3$] might be one form and claimed that the presence of different forms could be due to the experimental error in previous works [351, 355, 356]. However, it has been shown in the present work that this is not necessarily true and these two phases can exist independently.

It was noticed that in all of the abovementioned works, the materials considered were the products of thermal decomposition of zinc sulphate ($ZnSO_4$) or zinc sulfide (ZnS) or a zinc oxy-sulphate (misleadingly named basic zinc sulphate in some works), which is produced by the reaction between dehydrated $ZnSO_4$ and ZnO where $ZnSO_4$ is in excess. This might be the reason why a consensus on the formation of $Zn_3O(SO_4)_2$ is reached by most of the researchers rather than formation of $Zn_5O_2(SO_4)_3$ that was reported by some other ones. Nevertheless none of the publications referred to the decomposition of zinc hydroxy sulphate, which can provide the system with the excess of ZnO and can result in the formation of $Zn_5O_2(SO_4)_3$ according to Reaction **5.8**.

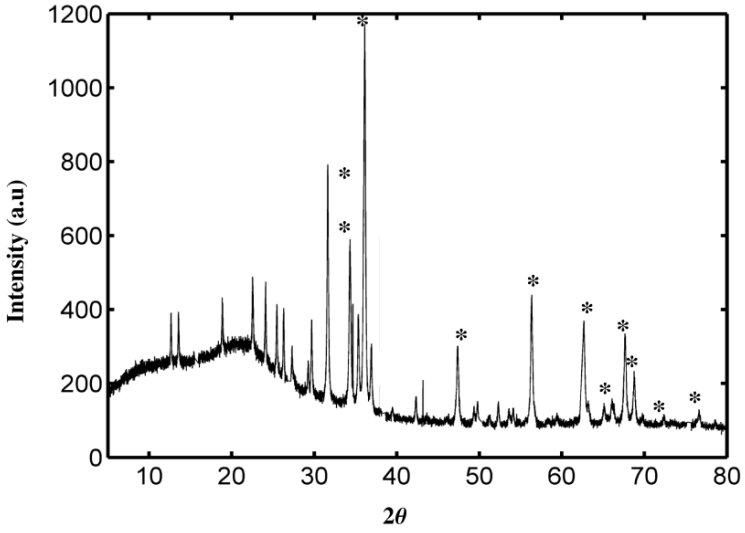

Figure 5.18. XRD pattern on the calcined sample at 555 °C obtained by synchrotron radiation (synchrotron 2θ value is converted to its equivalent of Cu Kα). ZnO peaks (JC-PDF 01-089-7102) are indicated by "*". The remaining peaks have been identified as $Zn_5O_2(SO_4)_3$ (JC-PDF 00-016-0305).

In the last step of transformation, $Zn_5O_2(SO_4)_3$ decomposes to ZnO by releasing sulfur dioxide and oxygen gases according to reaction **5.9**.

$$2Zn_5O_2(SO_4)_3 \xrightarrow{T>775\ ^\circ C} 10ZnO + 6SO_2 + 3O_2 \qquad 5.9$$

Despite the claims on the formation of sulfur trioxide as the major gas species evolved due to the decomposition of zinc oxy-sulphate [349, 351, 357], here it was demonstrated by TGA-MS on aged $BZS{\cdot}H_2O$ under argon atmosphere with a heating rate of 3 °C min^{-1} that sulfur dioxide and oxygen are the major gas species evolved. SO_3 was only detected in trace amounts and its relative peak intensity was about three orders of magnitude less than those of SO_2 and O_2. Presence of SO_3 is probably due to the partial oxidation reaction of sulfur dioxide to trioxide in the presence of ZnO according to Reaction **5.10** with $x < 1$ at the current process conditions.

$$x(2SO_2 + O_2 \xrightarrow{metal\ oxide\ catalyst} 2SO_3) \qquad 5.10$$

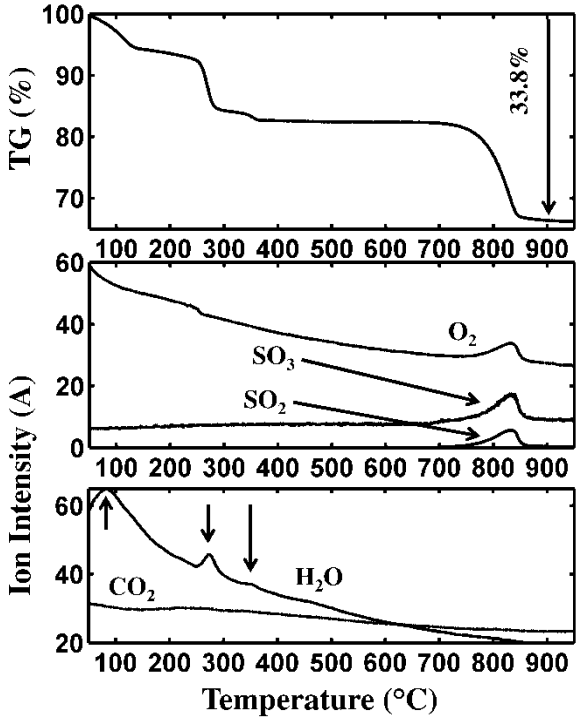

Figure 5.19. TGA-MS graphs on aged $BZS{\cdot}H_2O$. Shown ion intensities for H_2O, O_2, CO_2, SO_2 and SO_3 are $\times10^9$, $\times10^{10}$, $\times10^{11}$, $\times10^{10}$ and $\times10^{13}$, respectively.

The oxidation reaction of SO_2, that is industrially important in the contact process for production of sulphuric acid, is possible at high temperatures in the presence of metal oxide catalysts such as V_2O_5 [358-363].

By TGA-MS the presence of CO_2 was also investigated and it was shown that this gas in trace amounts is involved in this system due to its probable prior adsorption from atmosphere, **Figure 5.19**. TGA on BZS·H_2O, here, shows ~2.4% more mass loss compared to the TGA done on the same sample before aging that was assigned to the adsorption of moisture (compare **Figure 5.11** and **Figure 5.19**).

Microscopy and BET surface area measurement

In a separate experiment, some BZS·$4H_2O$ was calcined at 900 °C for 1 hour. XRD on the product showed ZnO (01-089-7102), **Figure 5.20**. BET surface area measurement on ZnO showed a surface area of 0.7 m^2/g. SEM images on the precursor (BZS·$4H_2O$) and ZnO particles made from that are shown in **Figure 5.21**. Highly crystalline ZnO particles are observed.

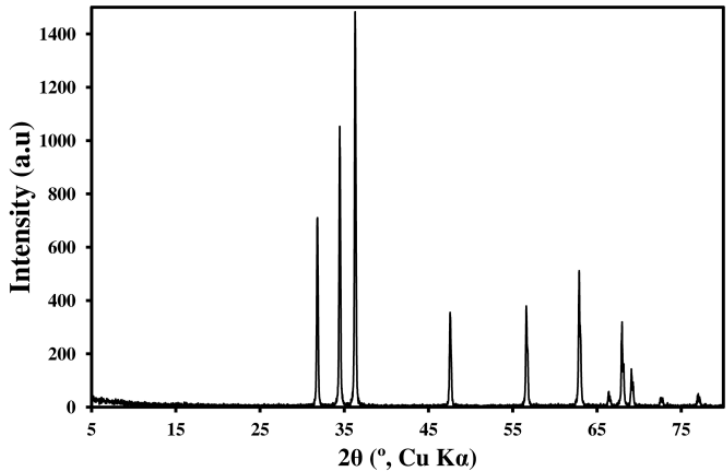

Figure 5.20. XRD on the product of calcination of BZS at 900 °C shows ZnO peaks.

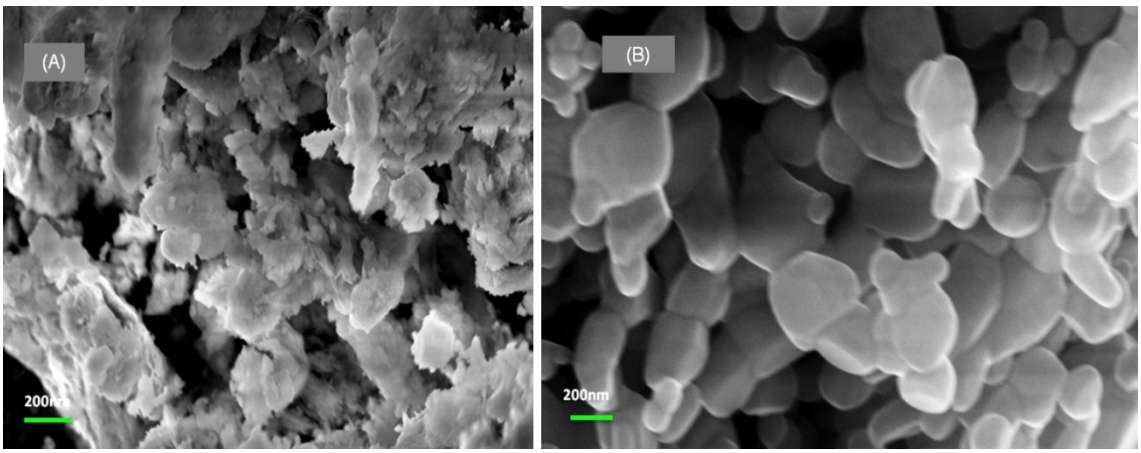

Figure 5.21. SEM images on (A) precursor and (B) ZnO particles made from that.

Mechanism

Consequently, the thermal decomposition mechanism for the transformation of BZS·4H_2O to ZnO is suggested to follow the schematic shown in **Scheme 5.1**.

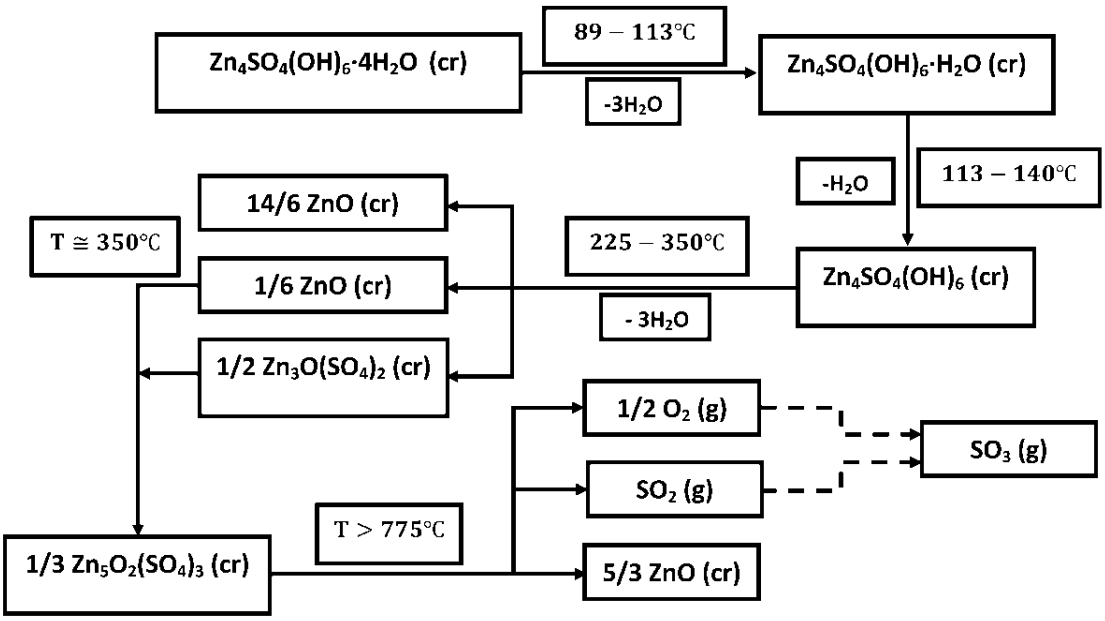

Scheme 5.1. Schematic of suggested mechanism for thermal transformation of BZS·4H_2O into ZnO. Dotted arrows show partial side reaction.

5.3.3. Zinc hydroxy chloride

First reported by Sorel in 1855 [364], composition of zinc hydroxy chloride and its decomposition mechanism have been controversial. Many compositions and phases for this compound have been proposed suggesting that this layered chemical can be categorised as a Berthollide compound with general formula of $x\mathrm{ZnCl_2}\cdot y\mathrm{Zn(OH)_2}\cdot z\mathrm{H_2O}$. Among all of the reported phases, $4\mathrm{Zn(OH)_2}\cdot\mathrm{ZnCl_2}\cdot\mathrm{H_2O}$ (alternative formula and names: $\mathrm{Zn_5(OH)_8Cl_2}\cdot\mathrm{H_2O}$, basic zinc chloride and Simonkolleite), $\mathrm{ZnO}\cdot\mathrm{ZnCl_2}\cdot 2\mathrm{H_2O}$ and β-Zn(OH)Cl are by consensus the most stable ones. Crystal structure of β-Zn(OH)Cl (single crystal made from ZnO and $\mathrm{ZnCl_2}$ by wet-chemistry) was first established by Forsberg and Nowacki in 1959, but the hydration state has never been stated to date [365, 366]. Oswald and Feitknecht reported three different phases of Zn(OH)Cl labelled as α-phase, β-phase and γ-phase. They mentioned that the γ-phase is probably the same as a mixture of α-phase and $4\mathrm{Zn(OH)_2}\cdot\mathrm{ZnCl_2}\cdot\mathrm{H_2O}$ phase and is misleadingly reported in previous works. They also observed that β-phase is the most stable phase, which transforms into $\mathrm{ZnCl_2}$ and $4\mathrm{Zn(OH)_2}\cdot\mathrm{ZnCl_2}\cdot\mathrm{H_2O}$ in the presence of air [367]. Reports on zinc oxy-chlorides such as ZnOCl and $\mathrm{Zn_2OCl_2}$ also adds to the confusion [368]. Existence of numerous forms of zinc hydroxy/oxy-chloride is one of the reasons why a lot of discrepancies can be seen in the literature on thermal behaviour of these salts.

$\mathrm{Zn_5(OH)_8Cl_2}\cdot\mathrm{H_2O}$ (abbreviated here as BZCl) is one the constituents of zinc ash skimmed from the surface of molten zinc baths used in the hot-dip galvanisation process. The high temperatures on the surface of molten zinc bath imply that this compound is quite stable [41, 369].

BZCl is in the family of layered hydroxy double salts (HDS). These compounds are also called anionic clays and are similar to hydrotalcites in structure. BZCl possesses quite similar hydration/adsorption properties to clays. Its large interlayer distance (7.87 Å) allows accommodation of some $\mathrm{H_2O}/\mathrm{CO_2}$ in the interlayer distance in the available void sites (molecular diameter of $\mathrm{H_2O}$ is 2.75 Å and that of $\mathrm{CO_2}$ is 3.3 Å) [345, 370-375]. In some clay structures, one, two, three or four layers of $\mathrm{H_2O}$ can be intercalated, which may result in the crystal swelling [376-378]. Kloprogge *et al.,* in their TGA-MS work on various hydrotalcites including chloride-bearing hydrotalcite proved that dehydration can occur at quite high temperatures ~400 °C with a loss of chloride at a

slightly above 400 °C [379]. The adsorption/desorption properties of CO_2 has been previously studied in similar layered materials and it was shown that CO_2 can be quite stable up to around 300 °C [374, 375].

Previously, thermal decomposition of BZCl has been studied by different groups and numerous and very different mechanisms have been suggested.

Sorrell, based on mass loss data, reported that BZCl phase decomposes to ZnO and $ZnO{\cdot}ZnCl_2{\cdot}2H_2O$ phase at around 160 °C and $ZnO{\cdot}ZnCl_2{\cdot}2H_2O$ loses one water of hydration at around 230 °C. Finally, $ZnO{\cdot}ZnCl_2{\cdot}H_2O$ loses its one water together with $ZnCl_2$ in the last stage [365].

Srivastava and Secco suggested two steps for the decomposition of BZCl. Their TGA-DTA was conducted with a heating rate of 20 °C min^{-1} under the air flow. They claimed that BZCl decomposes to ZnO and $ZnCl_2$. $ZnCl_2$ then melts and finally evaporates off the system at temperatures above 400 °C. Decomposition is reported to be complete at 535 °C. They assigned two observed DTA endothermic peaks at 262 °C and 708 °C to the melting and boiling points of $ZnCl_2$, respectively. They observed a big temperature difference between TGA (535 °C) and DTA (708 °C) for volatilisation of $ZnCl_2$ and assigned this to the experimental conditions. In case of β-Zn(OH)Cl, they also claimed that this compound decomposes to ZnO and $ZnCl_2$ similar to the higher order BZCl [380].

Hoffman and Lauder conducted thermal decomposition studies on $Zn_5(OH)_8Cl_2{\cdot}H_2O$ and β-Zn(OH)Cl only up to 250 °C. They produced their samples according to the method suggested by Oswald and Feitknecht - slow evaporation of a $ZnCl_2$ solution and ZnO [367, 381]. They only ran a MS analysis on β-Zn(OH)Cl and reported on the detection of $ZnCl^+$ and $ZnCl_2^+$ ions as the temperature rose to 200 °C. They observed that β-Zn(OH)Cl, which had traces of $ZnCl_2$, was converted to $Zn_5(OH)_8Cl_2{\cdot}H_2O$. Having observed zinc chloride species in the MS, which can be due to the possible reverse reaction in their β-Zn(OH)Cl sample, they surprisingly concluded that decomposition of the mentioned compounds up to 250 °C forms ZnO and $ZnCl_2$ and H_2O and extended this assumption to decomposition mechanism of $Zn_5(OH)_8Cl_2{\cdot}H_2O$ as well [382].

Rasines and Morales de Setién studied the thermal decomposition of $Zn_5(OH)_8Cl_2{\cdot}H_2O$ up to 1000 °C with a heating rate of 12 °C min^{-1} under the flow of air

and N_2. They also conducted long time isothermal heating in a temperature range of 100-1000 °C and identified the products of each stage by XRD. They reported on the formation of Zn(OH)Cl as an intermediate, which may convert to ZnO, $ZnCl_2$ and water between 210-300 °C. The $ZnCl_2$ formed is then volatilised at temperatures above 300 °C and escapes from the system. The theoretical mass loss for the suggested mechanism was calculated as 41%. However they observed 35.7% and assigned the difference to the hydrolysis of some $ZnCl_2$ to form ZnO. Clearly they had problems with assigning the DTA endothermic peaks, which correspond to the melting and boiling points of $ZnCl_2$. They observed a peak at 678 °C and reported this as the boiling point of $ZnCl_2$ [383].

Garcia-Martinez *et al.,* claimed that β-Zn(OH)Cl and $ZnCl_2$ are formed as the intermediate products of decomposition of BZCl followed by hydrolysis of $ZnCl_2$ to form ZnO and HCl. They also observed that mass loss values measured in TGA under different conditions are all above 32%, which is well above theoretical value of 26.3% for the complete conversion to only ZnO (except one experiment under stagnant atmosphere with a heating rate of 1 °C min^{-1} that resulted in around 28% mass loss). To explain the difference in observed mass losses, they postulated the presence of $ZnCl_2$ as an intermediate that they could not identify. However in the latter case where they saw 28% mass loss, they suggested the complete hydrolysis of $ZnCl_2$ to ZnO [384].

Formation of an anhydrous zinc salt as an intermediate product of decomposition of basic zinc salts has been also claimed by Biswick *et al.,* by referring to the same references above [347, 348].

Tanaka and Fujioka suggested yet another mechanism. They claimed that the formation of β-Zn(OH)Cl and $Zn(OH)_2$ was followed by complete decomposition of these two intermediates to ZnO and HCl and H_2O at 225 °C [385]. However formation of $Zn(OH)_2$ at such temperatures does not seem logical as it decomposes to ZnO at around 120 °C [79, 300].

In another case of disagreement, Krunks *et al.,* postulated that BZCl decomposes to $ZnO{\cdot}ZnCl_2{\cdot}2H_2O$ followed by decomposition to ZnO and $ZnCl_2$ [386].

Zhang and Yanagisawa suggest that BZCl decomposes only to ZnO and HCl and water with the release of HCl in the last stage of the decomposition after observing only around 27% mass loss in their TGA [293].

And recently, Kozawa *et al.,* studied BZCl having considered the effect of water vapour during the thermal decomposition pattern of this compound. They synthesised BZCl by a hydrothermal technique. Then in a few independent TGA-DTA experiments up to 520 °C they applied air and dry N_2 and humid N_2 with $P_{(H2O)}$ of 4.5 and 10 kPa. Interestingly, they observed that mass loss is a function of partial pressure of water and related the more-than-expected value for the mass loss in dry-condition experiments to the formation of the volatile $ZnCl_2$ at some stage. They also showed that under humid conditions, mass loss is quite close to the theoretical value of around 26.3% (on the basis of complete conversion to only ZnO). They also showed the reversibility of some of the reactions under cooling (reconstruction of the higher-order zinc hydroxy-chlorides) [387]. This finding is important and the role of partial pressure of water on limiting the formation of volatile zinc-containing species under equilibrium conditions will be discussed in this work.

Disparities in the suggested mechanisms might be mainly because of more-than-expected observed mass loss in TGA results and confusing DTA data. The fact that this chemical was almost free of unbound moisture led to conclusions that the excess mass loss (relative to theoretical value of 26.3% for the complete conversion to only ZnO) is related to volatile compounds other than water and HCl such as $ZnCl_2$. Nevertheless, the existence of this species was not proved in any of the mechanisms in which its role as an intermediate $ZnCl_2$ or final product was proposed.

This issue was investigated in this work with the aim to solve this puzzle. BZCl was synthesised according to the experimental section. A combination of TGA-DTA, TGA-MS and in-situ real-time synchrotron radiation studies on BZCl was performed to visualise the phase transformations, crystalline intermediate phases and gases evolved during thermal decomposition of this compound. Evolution of volatile and hydroscopic zinc-containing compounds during thermal decomposition of BZCl has been confirmed and the identity of the volatile material was clarified.

Characterisation, BET surface area measurement and microscopy

The precipitated product of this reaction was separated and characterised by XRD (Cu Kα) as $Zn_5(OH)_8Cl_2 \cdot H_2O$ (01-077-2311), see **Figure 5.22**, a.

Some BZCl was then calcined in three consecutive isothermal stages in a furnace under stagnant air: (1) at 400 °C for 2 hours; (2) at 400 °C for an extra 4 hours and (3) at 600 °C for 4 hours. After each calcination stage, the product was naturally cooled down and was characterised by XRD.

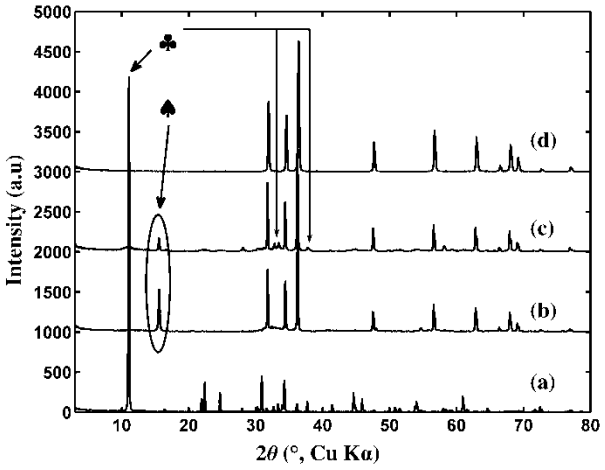

Figure 5.22. XRD results on (a) BZCl; (b) calcined BZCl for 2 hours at 400 °C; (c) calcined BZCl for 6 hours at 400 °C and (d) calcined BZCl for 6 hours at 400 °C plus 4 hours at 600 °C. Peaks marked with ♠ in (b) and (c) correspond to $ZnO{\cdot}ZnCl_2{\cdot}2H_2O$ and the peaks indicated with ♣ correspond to $Zn_5(OH)_8Cl_2{\cdot}H_2O$.

Surprisingly, it was found that after each isothermal calcination at 400 °C, ZnO is not the only product. The extra XRD peaks were assigned to $ZnO{\cdot}ZnCl_2{\cdot}2H_2O$ (00-045-0819). Intensity of the peaks associated with $ZnO{\cdot}ZnCl_2{\cdot}2H_2O$ declined after 6 hours of calcination but conversion to ZnO was not complete. Also minor peaks associated with BZCl were detected after calcination at 400 °C and cooling to room temperature (see **Figure 5.22**, b and c). This behaviour is also reported in another work. However the intermediate phase was identified as β-Zn(OH)Cl [387]. The property known as 'reconstruction' is observed in calcined layered double hydroxide (LDH) compounds under equilibrium conditions with water vapour. However if the temperature is higher than the temperature necessary for complete conversion of the salt to metal oxide, reconstruction cannot happen [388, 389]. In the next stage, the product was calcined at 600 °C for 4 hours and the product was characterised by XRD to be only ZnO, 01-075-0576 (see **Figure 5.22**). The as-made ZnO was slightly yellowish white.

BET specific surface area of the ZnO was 1.3 m^2/g. After 14 months of aging, TGA on the ZnO showed a small mass loss of ~0.4% up to 1000 °C (see Appendix, **Figure**

A. 1). SEM images on the precursor (BZCl) and the ZnO particles made from that are shown in **Figure 5.23**. BZCl morphology is plate-like with micronsized crystals.

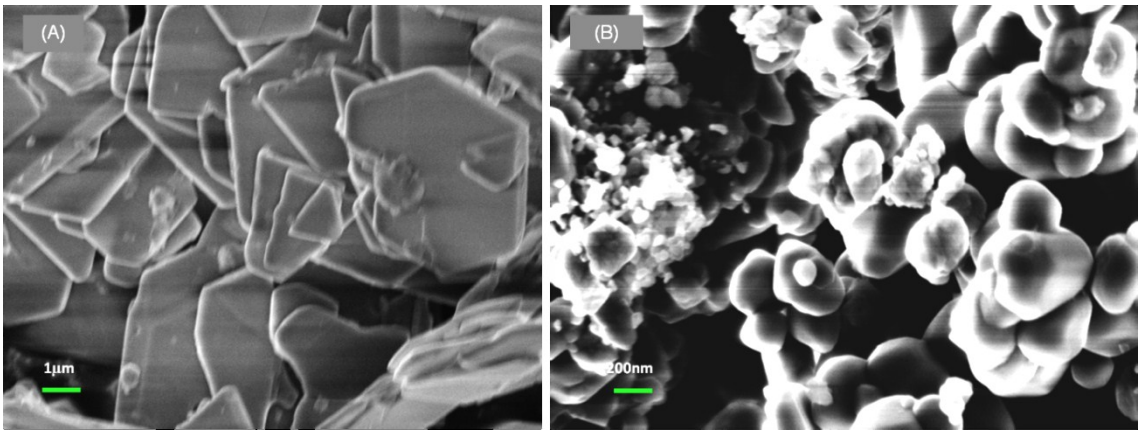

Figure 5.23. SEM images of (A) BZCl and (B) ZnO made of that.

Synchrotron radiation study, TGA-DTA and TGA-MS

In-situ real-time synchrotron radiation study on BZCl revealed surprising information on this chemical. Crystalline intermediate phases involved during thermal decomposition of this compound were visualised, see **Figure 5.24** and **Figure 5.25**. TGA-DTA was performed on both the freshly-made BZCl and the same sample aged for 13 months, **Figure 5.26**. TGA results showed that the mass loss of the former sample is around 26.5% and that of the latter is around 5% more (31.5%).

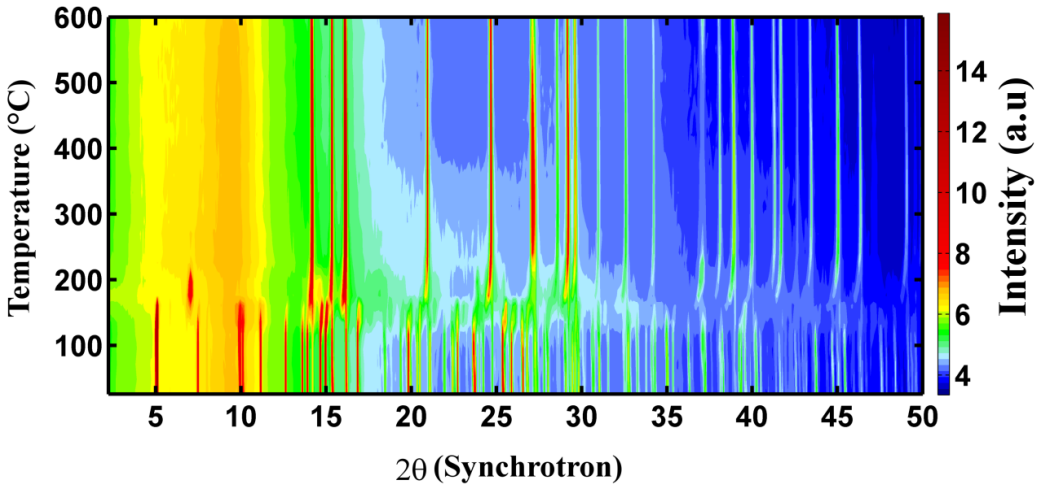

Figure 5.24. Colour-coded contour XRD (synchrotron) graph shows the real-time transformation of BZCl to ZnO. The intensity is colour-coded.

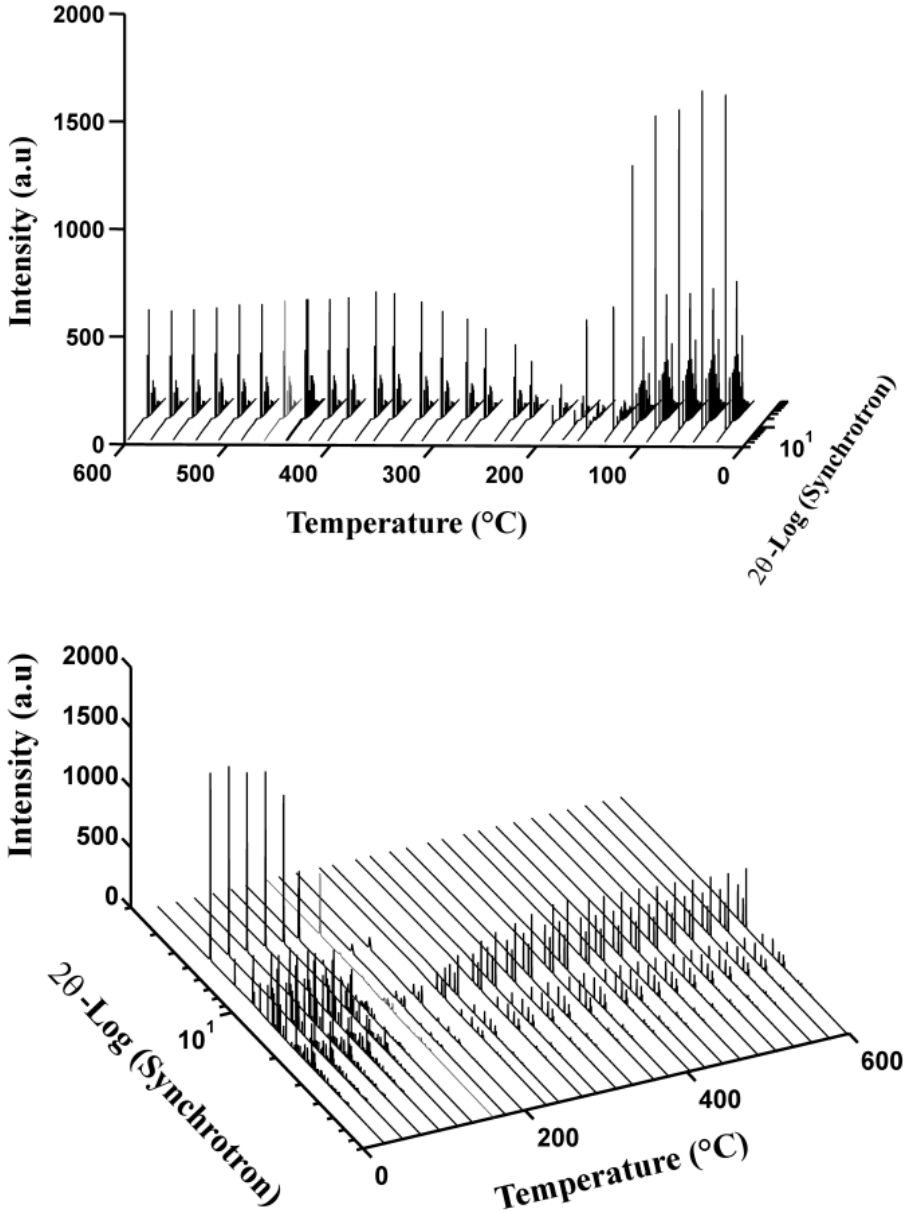

Figure 5.25. Two projections of 3D-stacked XRD (synchrotron) graphs on BZCl.

Interestingly, it was realised by using TGA that under 100 °C almost no mass loss occurs for both freshly-made and aged BZCl samples. This proves that before and after aging, both samples are free of unbound moisture. The TGA graphs are divided into 4 zones. Mass loss values in Zones A and B for both samples were almost equal. However mass loss in Zone C and particularly in Zone D has been shown to be increased in the aged sample relative to the freshly made one, **Figure 5.26**.

The first transformation at 100-161 °C can be seen as the synchrotron intensity peaks shrink. This corresponds to dehydration, which is indicated in Reaction **5**.**11**. This is consistent with Zone A in TGA graph, **Figure 5.26**.

$$Zn_5Cl_2(OH)_8 \cdot H_2O_{(cr)} \overset{100-161\,^{\circ}C}{\rightleftharpoons} Zn_5Cl_2(OH)_{8\,(cr)} + H_2O_{(g)} \qquad 5.11$$

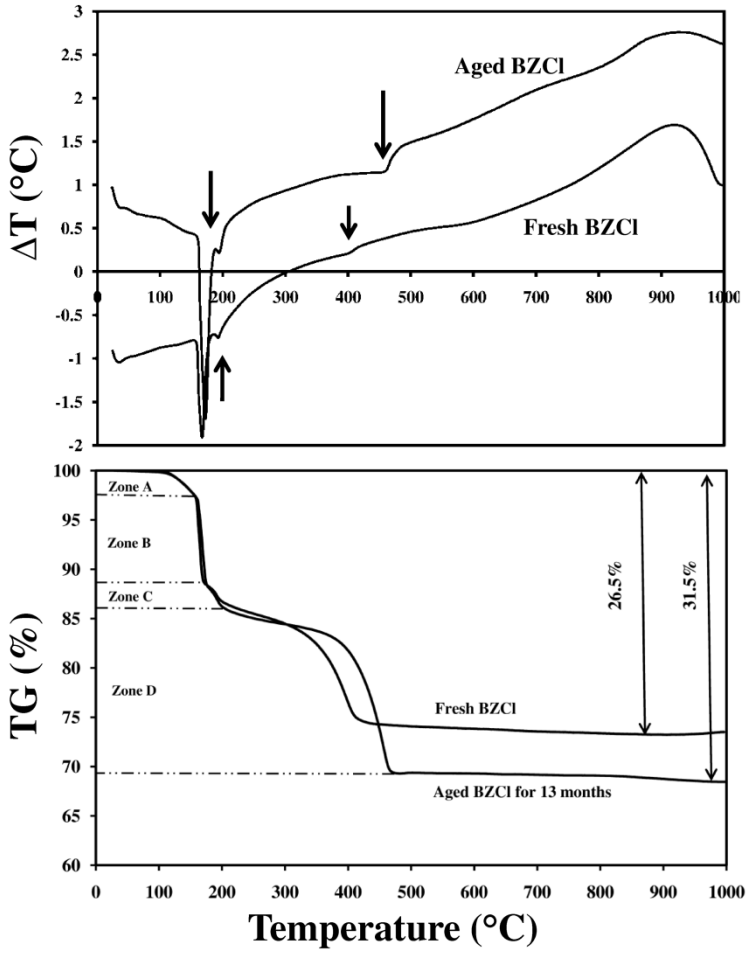

Figure 5.26. TGA-DTA on the freshly made BZCl and aged BZCl after 13 months.

Next transformation in the X-ray pattern takes place in the range of 161-197 °C where the low angle peak corresponding to the BZCl disappears and first signs of formation of ZnO appear. A new phase also takes form that matches with $ZnO \cdot ZnCl_2 \cdot 2H_2O$ (00-045-0819), a lower order zinc hydroxy chloride. This step is shown in reaction **5.12**. In spite of some claims on the probable formation of β-Zn(OH)Cl (01-072-0525) in some suggested mechanisms, the XRD pattern was matched with $ZnO \cdot ZnCl_2 \cdot 2H_2O$ rather than β-Zn(OH)Cl. Chemical formula of these two phases look quite similar to each other; however these are two different phases with a slight difference in XRD patterns. DTA shows an endothermic peak corresponding to this decomposition at ~164 °C. Equivalent of 3 moles of water is released in these two stages corresponding to Zones A and B in the TGA graph, **Figure 5.26**.

$$Zn_5Cl_2(OH)_{8\,(cr)} \overset{161-197\,^{\circ}C}{\rightleftharpoons} 3ZnO + ZnO{\cdot}ZnCl_2{\cdot}2H_2O_{(cr)} + 2H_2O_{(g)} \qquad 5.12$$

From this point forward, only one more transformation in the synchrotron data is observed: all the peaks except those for ZnO disappear, **Figure 5.25**. This strange behaviour, which happens at temperatures between 197-225 °C, matches with a small endothermic peak centred at ~190 °C in the DTA data and a mass loss corresponding to Zone C in **Figure 5.26**. Presence of only ZnO at such low temperatures was in contradiction with the TGA-DTA experiments, which show some other higher temperature events during thermal decomposition. The only change observed between 197-400 °C in the synchrotron patterns was an increase in intensity of the ZnO peaks. The intensity of the ZnO peaks then became stable, **Figure 5.25**. Despite the claims on the formation and melting of an intermediate compound ($ZnCl_2$), disappearing of X-ray peaks (except those of ZnO) above 197 °C was assigned to formation of an amorphous phase, $Zn(OH)_2{\cdot}ZnCl_2$, from rearrangement and dehydration of the crystalline intermediate in the previous thermal stage. The amorphous material is formed by dehydration of $ZnO{\cdot}ZnCl_2{\cdot}2H_2O$ between 197-225 °C according to Reaction **5**.**13**. It is important to note that some zinc complexes (e.g. zinc borate - $xZnO{\cdot}yB_2O_3{\cdot}zH_2O$) exist that can hold either crystalline or amorphous structure based on synthesis method and temperature. It is also known that such complexes do not release their hydration water up to temperatures around 400 °C [259, 390, 391]. In addition, it is reported that when layered hydroxide salts are calcined at moderate temperatures of 300-500 °C (depending on the chemical), amorphous materials may be formed [375, 388, 392].

$$ZnO{\cdot}ZnCl_2{\cdot}2H_2O \overset{197-225\,^{\circ}C}{\rightleftharpoons} Zn(OH)_2{\cdot}ZnCl_2\ (amorphous) + H_2O_{(g)} \qquad 5.13$$

The last stage of decomposition is quite confusing. It was mentioned that TGA in different times results in different mass loss values particularly in Zone D, **Figure 5.26**. The major reaction involved is believed to be the decomposition of amorphous $Zn(OH)_2{\cdot}ZnCl_2$ into ZnO by releasing HCl according to reaction **5**.**14**. DTA shows an endothermic peak corresponding to this stage at around 397 °C. It was also postulated that other side reactions might be involved in this stage that possibly result in volatile zinc-bearing materials, which increase the mass loss value as opposed to the theoretical value. Formation of zinc chloride as proposed by many other authors has been

investigated by TGA-MS and supplementary sublimation experiments as described in the following sections.

$$x[Zn(OH)_2 \cdot ZnCl_2 \text{ (amorphous)} \xrightarrow{T > 400\ ^\circ C} 2ZnO + 2HCl_{(g)}] \quad 5.14$$

TGA-MS

To investigate whether zinc chloride is involved during thermal decomposition of BZCl, four TGA-MS experiments on the aged BZCl have been conducted: (1) under argon atmosphere, heating rate of 4 °C min^{-1} and up to 600 °C; (2) under argon atmosphere, heating rate of 3 °C min^{-1} and up to 800 °C; (3 and 4) two tests under air atmosphere , heating rate of 3 °C min^{-1} and up to 900 °C. Surprisingly, fluctuation for 136 a.m.u associated with $ZnCl_2$ was not detected in MS, see **Figure 5.27**. However this could be due to the condensation of any volatile zinc-containing material evolved in the furnace in the connecting tube between the furnace and MS unit. The tube temperature is lower than 200 °C. Therefore any volatile zinc-containing species might be condensed and trapped in there. HCl, water and CO_2 were detected by MS. The mass loss values (in situ TGA) were around 32.2%, 32.6%, 32.4% and 29.5% in these experiments, respectively (see Appendix). The TGA-MS graphs of the last experiment are shown in **Figure 5.27**. It was shown by MS that in Zones C and D (**Figure 5.26**), CO_2 is also involved. Presence of CO_2 could be due to the adsorption and intercalation of this species in the interlayer space and/or formation of carbonates that are decomposed at over 200 °C. Evolution of HCl is confirmed in Zone D. Release of water has been confirmed up to temperatures around 230 °C with three MS peaks associated with the TGA Zones A, B and C.

Combining the TGA and MS results suggests that the last stage of decomposition can occur in quite a broad range of temperatures. For example TGA graphs in **Figure 5.26** (see also Appendix) show completion of the decomposition in the last stage between 400 °C to 500 °C, whereas TGA in **Figure 5.27** shows that this stage of decomposition is stretched up to 800 °C. Signal for the HCl in MS also follows the mass loss curve. Comparing the results shows various patterns of decomposition for the same precursor. The thermal decomposition behaviour of the BZCl is suggested to be related to the moisture content of atmosphere under which the material is decomposed. This is supported by the evidence provided by Kozawa *et al.,* [387] explained previously.

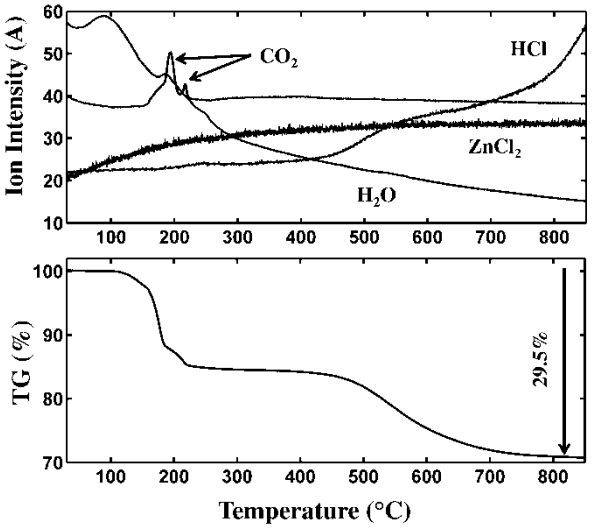

Figure 5.27. TGA-MS graph on aged BZCl under air atmosphere with a heating rate of 3 °C min^{-1}. Shown I_{18} for H_2O, I_{36} for HCl, I_{44} for CO_2 and I_{136} for $ZnCl_2$ are $\times 10^9$, $\times 10^{12}$, $\times 10^{11}$ and $\times 10^{14}$, respectively.

Sublimation test

Since existence of possible volatile zinc-containing materials during thermal decomposition of BZCl was not proved by the methods described before, a supplementary sublimation test has been conducted. A sublimation unit was set up according to **Figure 5.28**. Some BZCl was first dehydrated in a preheated oven at 300 °C for 1 hour and then the dehydrated sample was transferred to the sublimation unit and was heated to 450 °C using a heat gun. It was observed that at such temperature the solid sample turns to strong greenish-yellow colour. A condensate was formed on the water-cooled core that is likely to be HCl, which disappeared after some time. A bit higher than the heating centre on the wall of the vessel, whitish crystals started to form. By directing the heat gun to these crystals, they melted and by moving the heat gun away, the crystals were reformed. No boiling was observed from the melt at 450 °C. After cooling the sublimate was collected and it was observed that these crystals are quite hygroscopic. TGA-DTA under air flow was conducted on the sublimate, which showed a mass gain of more than 1% from room temperature up to around 50 °C followed by losing mass above this temperature. This confirms the hygroscopicity of the sublimate. Separately a TGA-DTA test was conducted on the zinc chloride dihydrate as a reference. The graphs were compared, **Figure 5.29**. The big difference in the mass

loss values for two compounds can be due to the presence of hydration water in one and absence in the other. The more dehydrated zinc chloride, the more mass loss can be observed. It is reported [384, 393] that if hydrated zinc chloride is heated, it does not form dehydrated zinc chloride; rather it forms Zn(OH)Cl that decomposes to ZnO or $ZnCl_2$. On the other hand dehydrated zinc chloride can undergo boiling rather than decomposition. See Equations **5.15** to **5.17**.

$$n[ZnCl_{2(g)} + 2H_2O \xrightarrow{over\ cooling} ZnCl_2 \cdot 2H_2O \xrightarrow{over\ heating} ZnO + 2HCl_{(g)} + H_2O_{(g)}] \quad 5.15$$

$$m[ZnCl_{2(g)} + 2H_2O \xrightarrow{over\ cooling} ZnCl_2 \cdot 2H_2O \xrightarrow{over\ heating} \beta\text{-}Zn(OH)Cl + HCl_{(g)} + H_2O_{(g)}] \quad 5.16$$

$$\text{Dehydrated } ZnCl_{2(s)} \xrightarrow{over\ heating} ZnCl_{2(l)} \xrightarrow{over\ heating} ZnCl_{2(g)} \quad 5.17$$

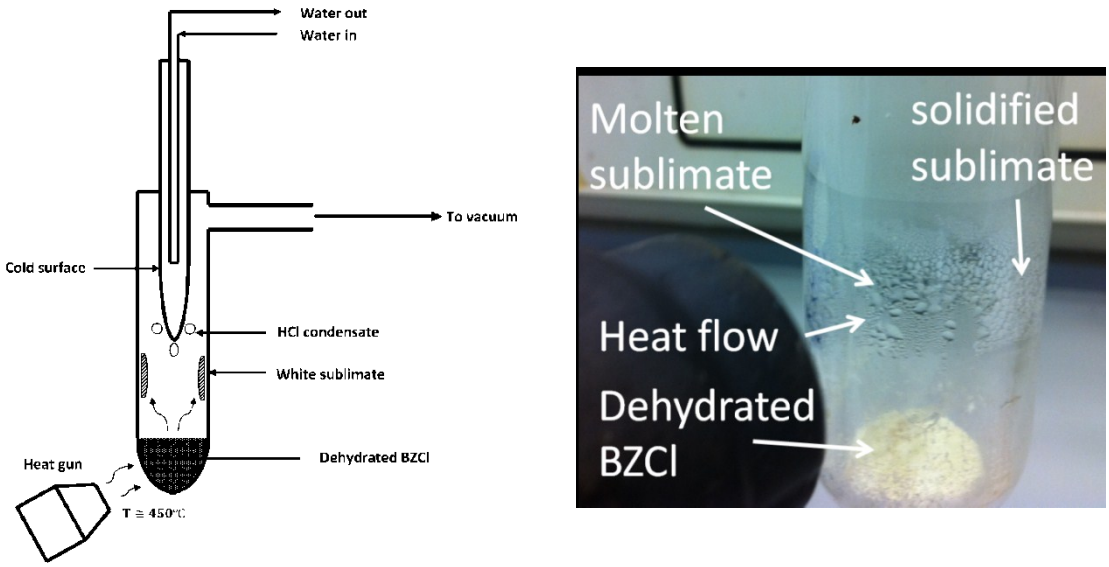

Figure 5.28. Sublimation set-up to trap the volatile zinc-containing material.

The TGA results confirmed that more than 99% mass loss occurs for the sublimate, which is almost completely dehydrated. Both materials however show endothermic peaks at around 300 °C that were assigned to melting point of them since almost no mass loss can be observed.

XRD was also conducted on the sublimate with some modifications. To avoid hydration of moisture-sensitive sublimate, a heat-stage was set up in the XRD chamber and the temperature was set at 100-120 °C. The sublimate was carefully transferred on the heated stage and XRD was performed with time per step of 5.6 s. XRD showed that

the sublimate is a mixture of α-$ZnCl_2$ (01-074-0519) and β-$ZnCl_2$ (01-072-1284), **Figure 5.30**. No peak associated with β-Zn(OH)Cl was detected.

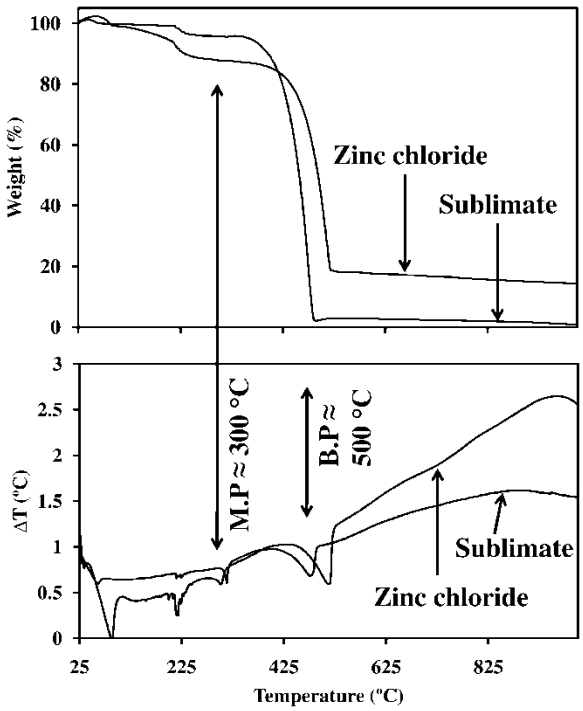

Figure 5.29. TGA-DTA on $ZnCl_2 \cdot 2H_2O$ and $ZnCl_2$ sublimate collected.

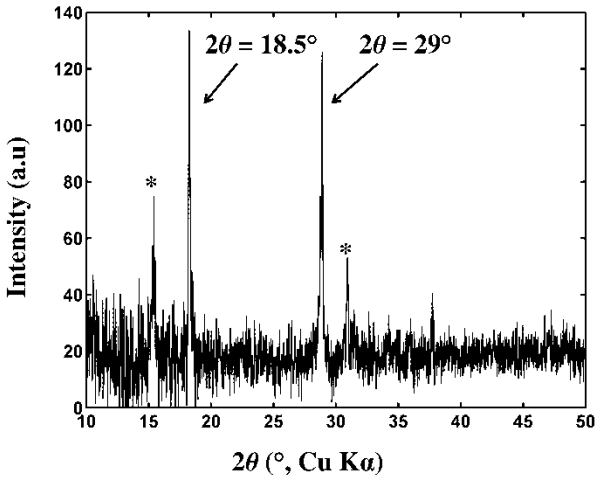

Figure 5.30. XRD conducted at 100-120 °C and time per step = 5.6 s on the zinc-containing sublimate matches with α and β-zinc chlorides. Peaks marked with * are associated with β-$ZnCl_2$ (JC-PDF 01-072-1284) and the rest are related to α-$ZnCl_2$ (JC-PDF 01-074-0519) with major peaks located at 2θ = 18.5 ° and 29 °.

Consequently, here it was proved that heating of BZCl may form $ZnCl_2$, see Equation **5.18**. Nonetheless amount of $ZnCl_2$ formed depends on the moisture content of

the atmosphere under which the precursor is thermally decomposed. This directly influences the TGA mass loss value. While the moisture of the atmosphere increases, the amount of volatile $ZnCl_2$ decreases. Presence of moisture shifts the Reaction **5.18** towards left according to the Le Chatelier's Principle. Consequently the competing reaction **5.14** dominates ($x \gg y$). Therefore for every mole of BZCl decomposed, more ZnO would be produced (closer values to the theoretical 5 moles of ZnO for every mole of BZCl decomposed). On the other hand in dry atmospheres some zinc will be volatilised that results in mass loss values higher than 26.3%.

$$y[Zn(OH)_2{\cdot}ZnCl_2\ (\text{amorphous}) \overset{T > 400\ ^\circ C}{\rightleftharpoons} ZnO + ZnCl_{2\ (g)} + H_2O] \qquad 5.18$$

It is also worth mentioning that in this work the presence or absence of zinc oxy-chloride species, Zn_2OCl_2, could not be identified. This species is reported in [368]. There might be another side reaction involved in the system according to Reaction **5.19**.

$$Zn(OH)_2{\cdot}ZnCl_2\ (\text{amorphous}) \overset{T > 400\ ^\circ C}{\rightleftharpoons} Zn_2OCl_{2(g)} + H_2O_{(g)} \qquad 5.19$$

Mechanism

The thermal decomposition mechanism for the transformation of BZCl into ZnO is suggested to follow the schematic shown in **Scheme 5.2**.

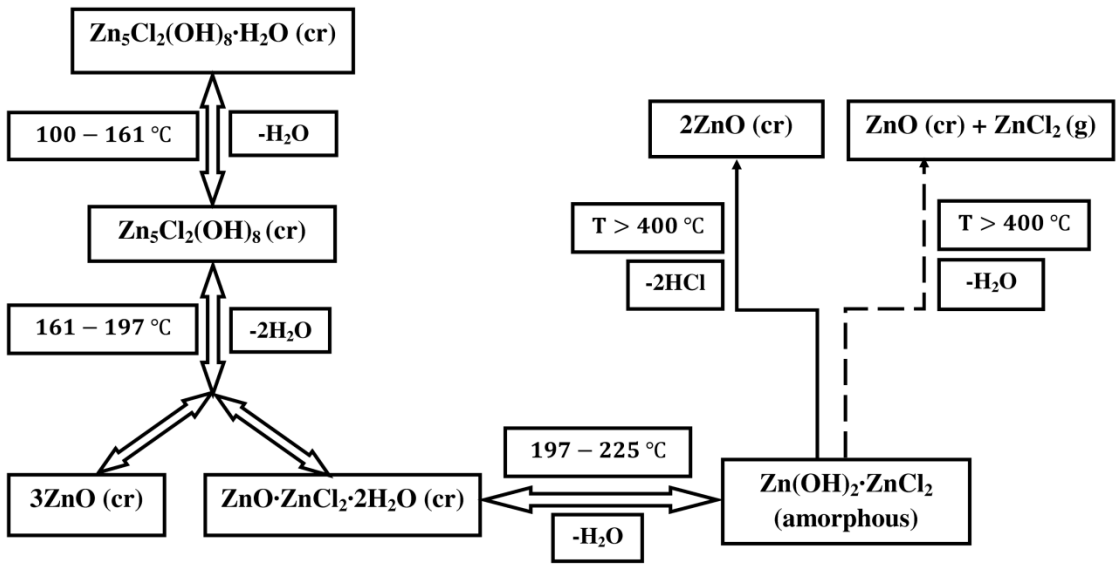

Scheme 5.2. Schematic of suggested mechanism for thermal transformation of BZCl into ZnO. Partial side reaction is indicated by dotted arrow, which is responsible for the excess of mass loss during some TGA experiments.

5.3.4. Zinc hydroxy nitrate

Zinc hydroxy nitrate in the form of $Zn_5(OH)_8(NO_3)_2$ was first reported in 1933 by Feitknecht (hydration state was not mentioned) [334]. In 1964, Weigel *et al.,* in the course of pyrolysis of zinc nitrate hexahydrate reported the presence of basic zinc nitrate [394]. Its crystal structure was first established in 1970 by a French group [395] and independently by a German group [396]. In 1970 Stählin and Oswald compared its crystal structure with those of the basic zinc chloride (reported in 1961) and the basic zinc carbonate, (reported in 1964) and concluded that they are similar in structure [396]. Interestingly they reported on the chemical bonding of nitrate anions in the structure and compared that to those of the basic zinc carbonate and chloride. Chemical bonding modes of anions to zinc atoms in these three materials are different. The carbonates in basic zinc carbonate coordinate to both octahedral and tetrahedral zinc atoms. The chlorides in basic zinc chloride only coordinate to tetrahedral zinc atoms whereas in basic zinc nitrate, nitrates are purely ionic [396].

Zinc hydroxy nitrates can be categorised as Berthollide with general formula of $xZn(NO_3)_2 \cdot yZn(OH)_2 \cdot zH_2O$. Four forms of zinc hydroxy nitrate have been reported i.e. $Zn_5(OH)_8(NO_3)_2 \cdot 2H_2O$, $Zn_5(OH)_8(NO_3)_2$, $Zn_3(OH)_4(NO_3)_2$ and $Zn(OH)NO_3 \cdot H_2O$ with the last compound not possessing a layered crystal structure [347, 397, 398]. Layered $Zn_5(OH)_8(NO_3)_2 \cdot 2H_2O$ (other name: basic zinc nitrate; here abbreviated as BZN; M.W= 622.95) has an interlayer distance of around 9.9 Å [399] and is quite similar to hydrotalcites in structure [379]. Thermal decomposition mechanism of this material was also a subject of debate [319, 347, 397, 400]. BZN was synthesised according to the method described in the experimental section.

Thermal decomposition of BZN as a precursor material for ZnO was investigated. A combination of real-time synchrotron radiation study, laboratory XRD, TGA-DTA and TGA-MS was applied to identify the crystalline intermediate phases and gaseous products.

Characterisation, BET surface area measurement and microscopy

Using laboratory XRD (Cu Kα), the product was characterised as $Zn_5(OH)_8(NO_3)_2 \cdot 2H_2O$ (01-072-0627), **Figure 5.31**, bottom graph. Some BZN was then

calcined in two consecutive isothermal stages: (1) at 250 °C for one hour and (2) at 300 °C for an extra one hour. The product of the 1st stage calcination was characterised by XRD to be a mixture of $Zn_3(NO_3)_2(OH)_4$ (00-052-0627) and ZnO (01-070-2551), **Figure 5.31**, middle graph. Mass loss of the white powder was 14.64% (theoretical mass loss is ~34.7%, on the basis of complete conversion to ZnO). XRD on the product of the 2nd stage calcination showed only ZnO, **Figure 5.31**. BET specific surface area of the as-produced ZnO was 1.6 m^2/g. SEM images on the precursor (BZN) and the ZnO particles made from that are shown in **Figure 5.32**. BZN is composed of well-defined square-shape plates with micronised crystals. The resulting ZnO is highly crystalline with a particle size of 200-500 nm.

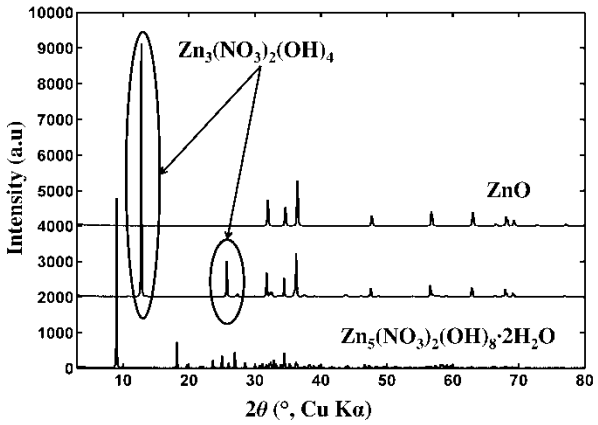

Figure 5.31. XRD results on (bottom graph) BZN; (middle graph) calcined BZN for 1 hour at 250 °C; (top graph) calcined BZN for 1 hour at 250 °C plus 1 hour at 300 °C.

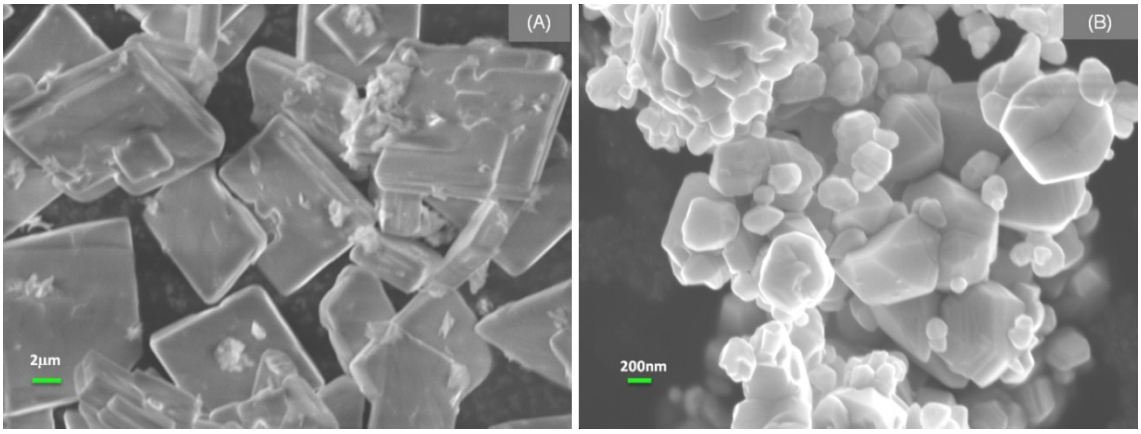

Figure 5.32. SEM images of (A) BZN and (B) ZnO made of that.

Synchrotron radiation study and TGA-DTA

TGA-DTA on BZN showed 33.8% mass loss, which is quite close to the theoretical value of ~34.7% for the complete decomposition of this material to ZnO, **Figure 5.35**. By TGA, it was demonstrated that decomposition of BZN into ZnO is complete at around 250 °C. DTA shows three endothermic peaks centred at 110 °C, 165 °C and 202 °C. In-situ real-time synchrotron radiation study on BZN has been conducted to visualise the crystalline intermediate phases evolved during thermal decomposition of this compound, see **Figure 5.33** and **Figure 5.34**. Below 94 °C, only peaks associated with BZN dihydrate can be observed. In the range of 94-134 °C, the first phase transformation occurs that corresponds to dehydration of BZN according to reaction **5.20**. In this range, new peaks associated with dehydrated BZN can be observed. This is consistent with TGA-DTA data.

$$Zn_5(NO_3)_2(OH)_8 \cdot 2H_2O \xrightarrow{94-134\,^{\circ}C} Zn_5(NO_3)_2(OH)_8 + 2H_2O \qquad 5.20$$

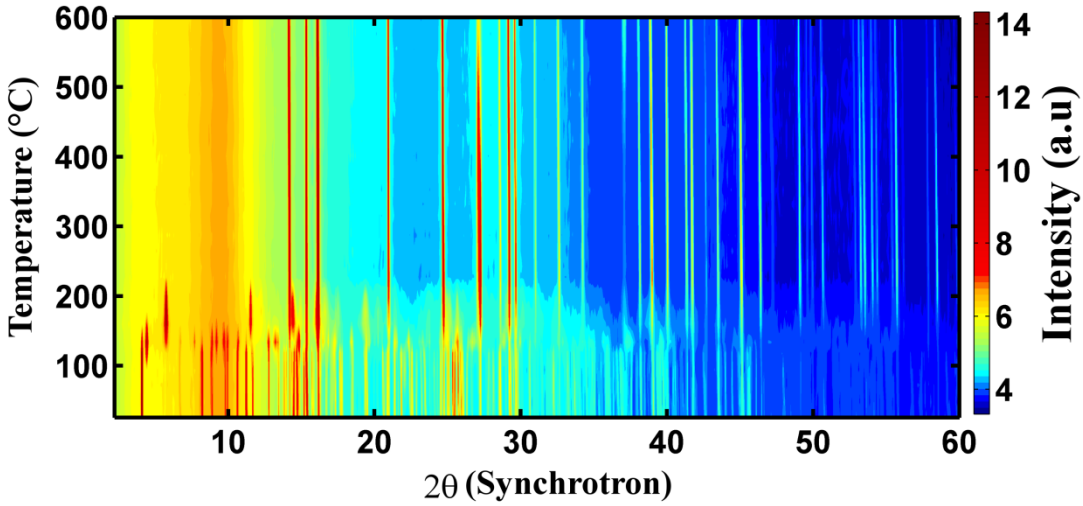

Figure 5.33. Colour-coded contour XRD (synchrotron) graph shows the real-time transformation of BZN to ZnO. The intensity is colour-coded.

Next transformation in the X-ray pattern takes place in the range of 134-199 °C where the low angle peaks corresponding to the dehydrated BZN disappear along with the formation of peaks associated with a lower-order zinc hydroxyl-nitrate, $Zn_3(NO_3)_2(OH)_4$ and the first signs of formation of ZnO. This stage is shown in reaction **5.21**. At around 220 °C, all peaks related to $Zn_3(NO_3)_2(OH)_4$ vanish and only ZnO peaks can be detected. This is again in complete accordance with the TGA-DTA data on

BZN. Importantly the peak intensity of the ZnO remains almost constant after the completion of decomposition of BZN over 220 °C, see **Figure 5.34**. This finding shows that there is no significant crystal growth for ZnO by increasing the temperature to 600 °C.

$$Zn_5(NO_3)_2(OH)_8 \xrightarrow{134-199\,^{\circ}C} 2ZnO + Zn_3(NO_3)_2(OH)_4 + 2H_2O \qquad 5.21$$

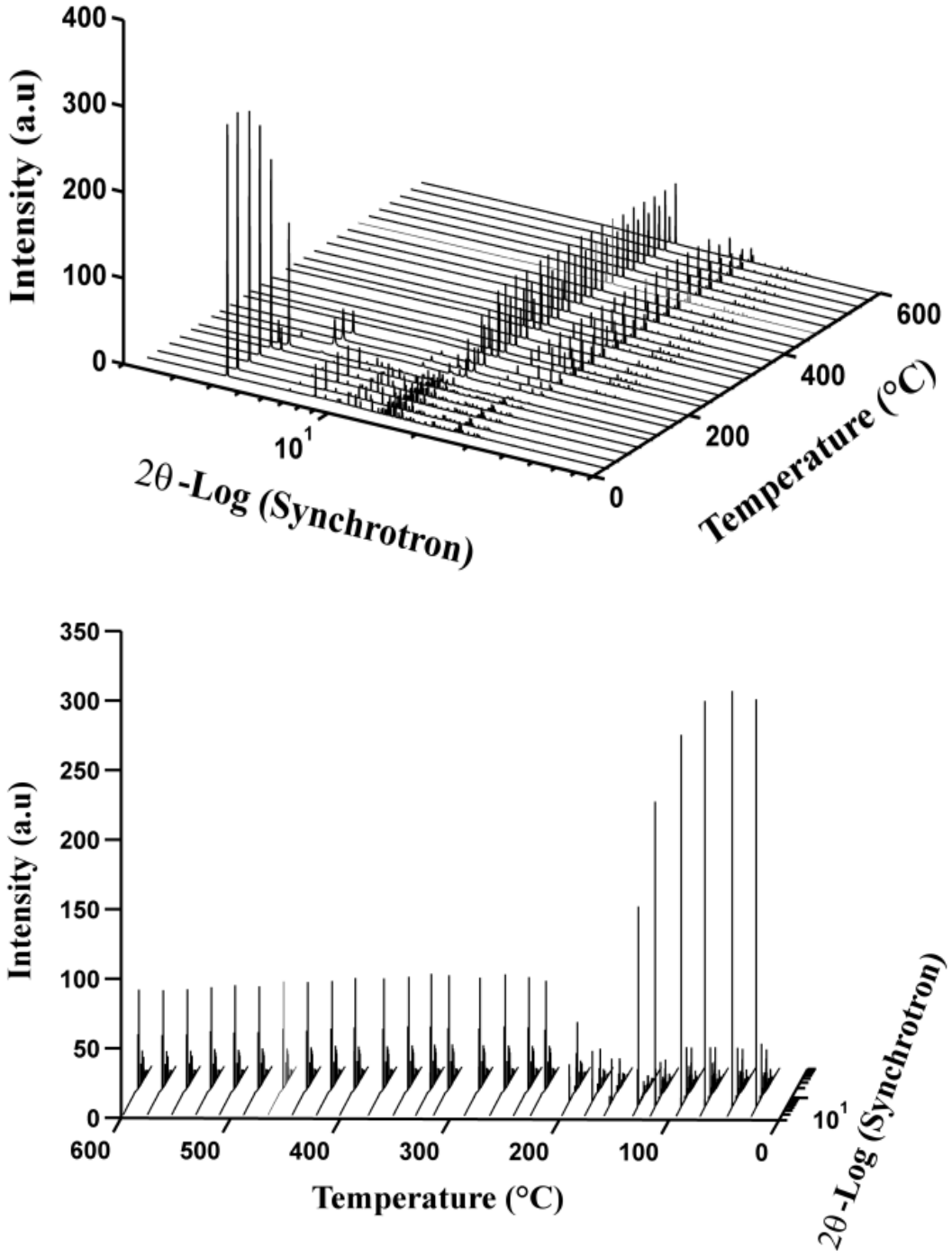

Figure 5.34. Two projections of 3D-stacked XRD (synchrotron) graphs on BZN.

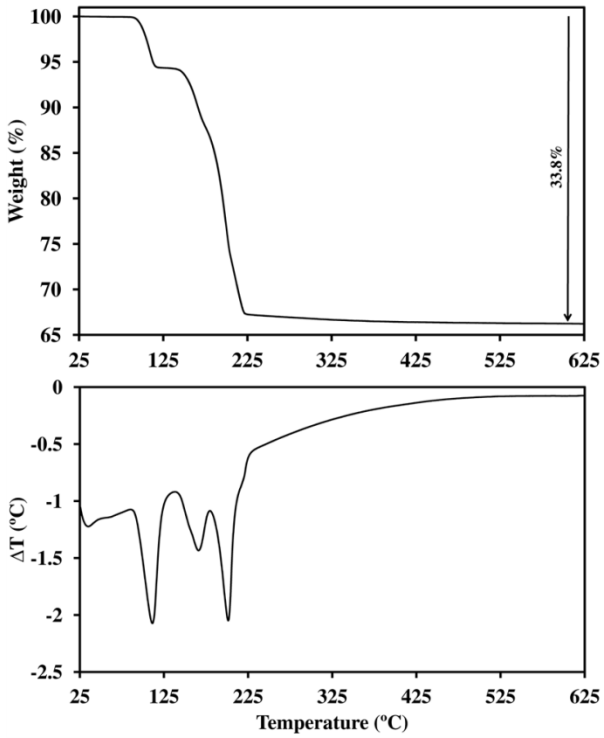

Figure 5.35. TGA-DTA on BZN.

TGA-MS

The last stage of the decomposition was a matter of discrepancy. For example, Biswick *et al.,* [347], proposed that in this stage of decomposition anhydrous zinc nitrate is produced. But they could not observe any X-ray signal associated with the proposed phase. They explained that this is because this phase is poorly crystallised. On the other hand Auffredic and Louër did not consider the formation of anhydrous zinc nitrate [397]. To clarify this issue and characterise the evolved gaseous species, simultaneous TGA-MS tests have been performed on BZN according to **Table 5.2**.

Table 5.2. TGA-MS experiments conditions and species tested.

Exp.	Heating Rate (°C·min^{-1})	Atm.	TG (%)	Ionic currents investigated
MS1	1.5	Ar	32.5	I_{12} (C^+), I_{18} (H_2O^+), I_{28} (N_2^+/CO^+), I_{30} (NO^+), I_{32} (O_2^+), I_{44}, I_{46} (NO_2^+), I_{63} (HNO_3^+)
MS2	2	Ar	32	I_{18} (H_2O^+), I_{30} (NO^+), I_{32} (O_2^+), I_{46} (NO_2^+)
MS3	3	Ar	33	I_{18} (H_2O^+), I_{28} (N_2^+/CO^+), I_{30} (NO^+), I_{32} (O_2^+), I_{44}, I_{46} (NO_2^+), I_{63} (HNO_3^+)
MS4	5	Air	31.8	I_{18} (H_2O^+), I_{30} (NO^+), I_{32} (O_2^+), I_{46} (NO_2^+)
MS5	10	Ar	35.3	I_{18} (H_2O^+), I_{28} (N_2^+/CO^+), I_{30} (NO^+), I_{32} (O_2^+), I_{44}, I_{46} (NO_2^+), I_{63} (HNO_3^+)

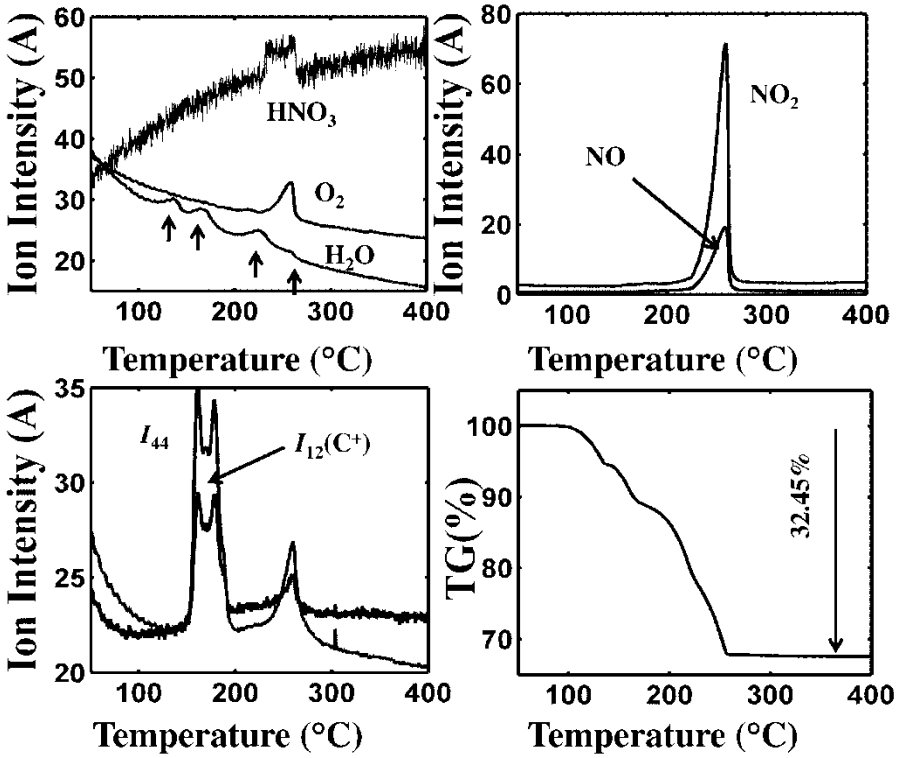

Figure 5.36. TGA-MS graphs for MS1. I_{12} for C^+ and I_{44} are shown $\times 10^{12}$ and $\times 10^{11}$, respectively. I_{18} for H_2O, I_{32} for O_2, I_{30} for NO, I_{46} for NO_2 and I_{63} for HNO_3 are shown $\times 10^{9}$, $\times 10^{10}$, $\times 10^{10}$, $\times 10^{12}$ and $\times 10^{14}$, respectively.

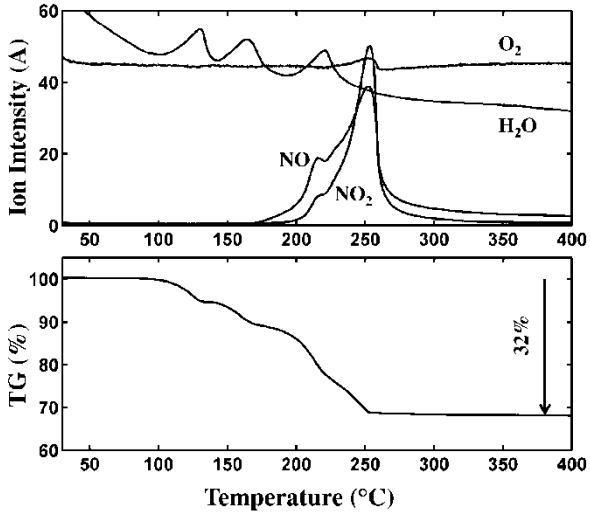

Figure 5.37. TGA-MS graphs for MS2. I_{18} for H_2O, I_{30} for NO, I_{46} for NO_2 and I_{32} for O_2 are shown $\times 10^{9}$, $\times 10^{10}$, $\times 10^{11}$ and $\times 10^{12}$, respectively.

In all experiments, release of H_2O, NO_2 and NO has been confirmed (**Figure 5.36** to **Figure 5.40**. Evolution of oxygen in all experiments was confirmed except under air atmosphere due to the dilution of system. Evolution of N_2, N_2O, HNO_3, CO_2 and CO

during decomposition of BZN was also considered. In MS1, MS3 and MS5 almost no fluctuation for I_{28} (N_2^+ or CO^+) signal has been detected. Therefore release of N_2 or CO is not probable in this system. Release of traces of nitric acid was detected in MS1, MS3 and MS5 but the amplitude of I_{63} (HNO_3^+) was significantly lower than those of the other species. But it (I_{63}) was gradually increasing with temperature, with a broad peak centred at the very last step of decomposition.

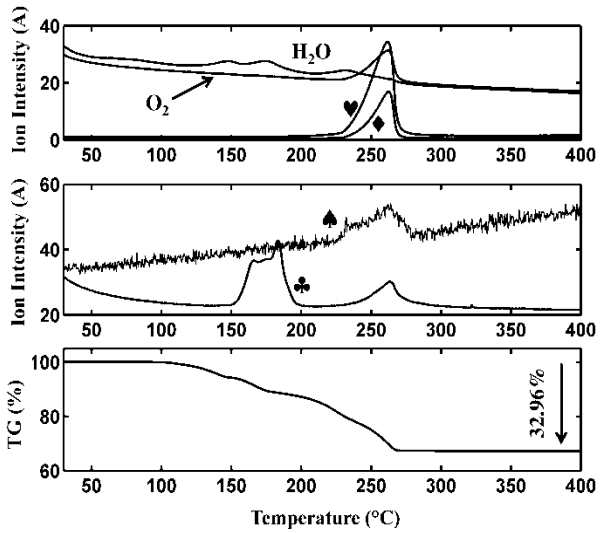

Figure 5.38. TGA-MS graphs for MS3. I_{44} ($\times 10^{11}$) for N_2O or CO_2 is indicated by ♣. I_{63} ($\times 10^{14}$) for HNO_3 by ♠ and I_{30} ($\times 10^{10}$) for NO is indicated ♥ by and I_{46} ($\times 10^{11}$) for NO_2 is indicated by ♦. I_{18} for H_2O and I_{32} for O_2 are Shown $\times 10^9$ and $\times 10^{10}$, respectively.

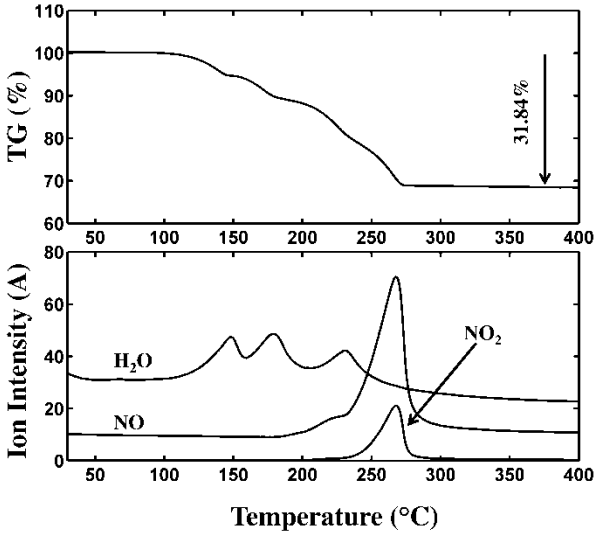

Figure 5.39. TGA-MS graphs for MS4. I_{18} for H_2O and I_{30} for NO and I_{46} for NO_2 are shown $\times 10^9$,$\times 10^{10}$ and $\times 10^{10}$, respectively.

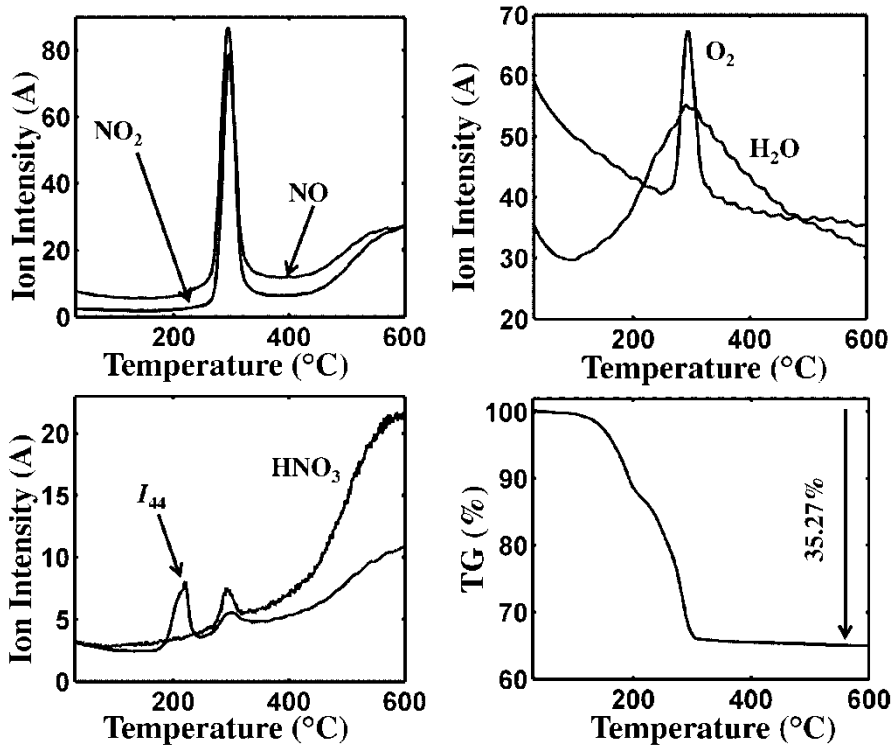

Figure 5.40. TGA-MS graphs for MS5. I_{44} and I_{18} for H_2O and I_{32} for O_2 and I_{63} for HNO_3 are shown $\times 10^{10}$, $\times 10^{9}$ and $\times 10^{13}$, respectively. Shown I_{30} for NO and I_{46} for NO_2 are $\times 10^{10}$ and $\times 10^{11}$, respectively.

In MS1, MS3 and MS5, possibility of release of N_2O and CO_2 was considered. The I_{44} signal showed an interesting pattern in all three cases with peaks in at least two regions. The first release occurs at temperatures in the range of ~150-200 °C and the 2nd one at slightly higher temperatures, in the range of ~250-300 °C (which depends on heating rate). At lower heating rates (see **Figure 5.36**), the lower temperature evolution breaks into two shoulders. By increasing the heating rate, two shoulders merge and form one peak (see **Figure 5.38** and **Figure 5.40**). Since the ionic current I_{44} corresponds to both N_2O and CO_2 ($I_{44} = I_{CO_2^+} + I_{N_2O^+}$), distinguishing between these two species just by considering this signal is not possible. As a result, the I_{12} signal as a unique indication for existence of C^+ was also considered. The I_{12} channel is a result of fractionation of CO_2 due to the electron impact. Based on the set-up of the MS instrument, the ratio of I_{12}/I_{44} would be approximately 6% in the absence of N_2O. Presence of N_2O would result in the decrease of this ratio. It was noticed that at certain cycles where the peaks appear, the ratio is approximately 8%. This is one indication that N_2O is not evolved in this system. Another important indication for the presence of only CO_2 is that I_{12} curve follows the I_{44} curve with exactly the same pattern (**Figure 5.36**).

Therefore it seems that only CO_2 evolution is responsible for such behaviour. Nevertheless the existence of nitrous oxide in this system could not be disproved by only using these techniques. It was concluded that presence of CO_2 may be due to its absorption from atmosphere and intercalation in the interlayer distance similar to the case of BZCl described before.

In this work, it was confirmed that during the 1st and 2nd stages of decomposition, only water is involved that is accepted by consensus by other authors as well. This was already shown in Reactions **5**.**20** and **5**.**21**. While I_{18} signals show a declining trend with three to four peaks involved in MS1-MS4, I_{18} signal in MS5 shows a gradual inclining trend with a broad peak occurring at the same time with nitrogen oxide and oxygen at around 300 °C (see **Figure 5.40** and **Figure 5.41**).

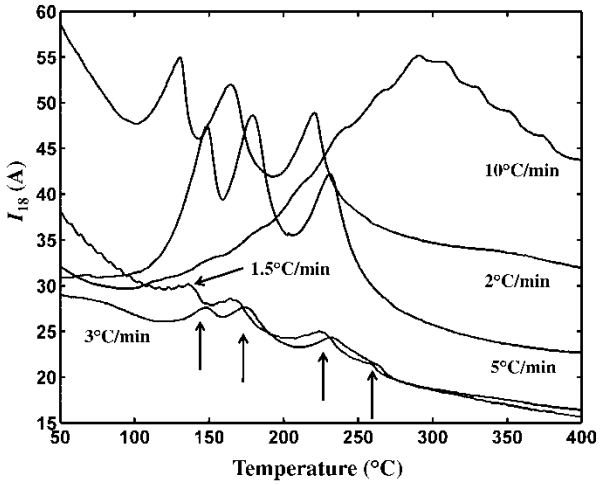

Figure 5.41. I_{18} (H_2O^+) curves for various heating rates.

Considering the TGA-MS results obtained from MS1-MS5 (see **Figure 5.36** to **Figure 5.41**), it was concluded that decomposition pattern of BZN is a complex function of rate of heating as well. It seems that water is always present up to the last stage where BZN decomposition undergoes completion. However its major evolution occurs at lower temperatures. In all MS experiments, the ion intensity associated with NO was relatively higher than that of NO_2. In MS1, it was shown that four peaks for water are involved last one of which is the smallest. The pattern of evolution of nitrogen oxides changes dramatically with rate of heating. In MS1 (**Figure 5.36**), NO and NO_2 release happens only at one stage together with oxygen. In MS2 (**Figure 5.37**), their evolution breaks into two sections with the minor peak centred at ~220 °C with no sign of oxygen followed by the major release at ~250 °C together with oxygen. In MS3

(**Figure 5.38**), evolution of nitrogen oxides and oxygen is similar to MS1 but at slightly higher temperature. In MS4 (**Figure 5.39**), NO_2 only shows only one peak, but NO shows a broad minor peak followed by the major peak together with NO_2. In MS5 (**Figure 5.40**), release of nitrogen oxides and oxygen is again similar to MS1 and MS3, but at slightly higher temperatures around 300 °C. Mass loss curves that follow the release pattern of the gaseous species change shape as well, see **Figure 5.42**.

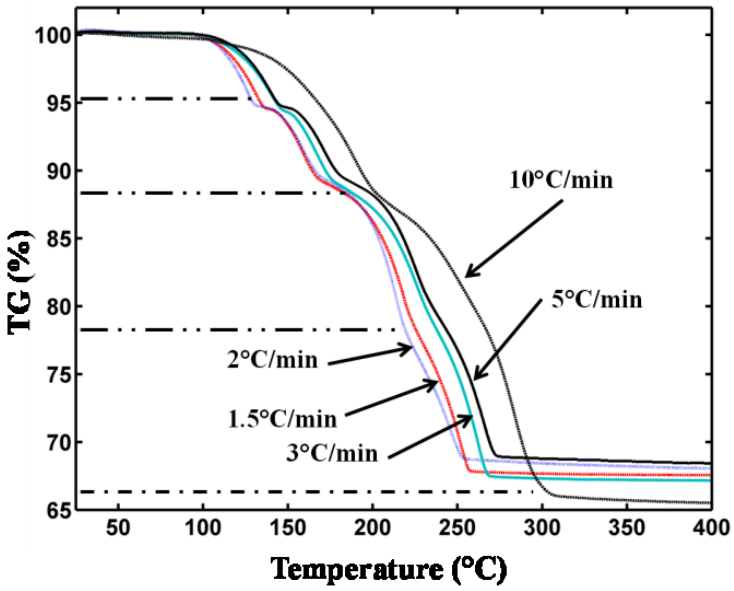

Figure 5.42. TGA comparative graphs obtained during TGA-MS tests.

Ion intensity fraction for NO, NO_2 and O_2 versus rate of heating during the TGA-MS studies is summarised in **Table 5.3**. It was observed that the composition of the gaseous materials evolved during the thermal decomposition of BZN depends on the rate of heating. This is also shown in **Figure 5.43**.

Table 5.3. Ion intensity fraction for NO (X), NO_2 (Y) and O_2 (Z) *vs.* rate of heating.

Rate of Heating (°C/min)	X= $I_{30}/(I_{30}+I_{46}+I_{32})$	Y= $I_{46}/(I_{30}+I_{46}+I_{32})$	Z= $I_{32}/(I_{30}+I_{46}+I_{32})$
1.5	0.37	0.01	0.62
2	0.88	0.11	0.01
3	0.50	0.03	0.47
10	0.54	0.05	0.41

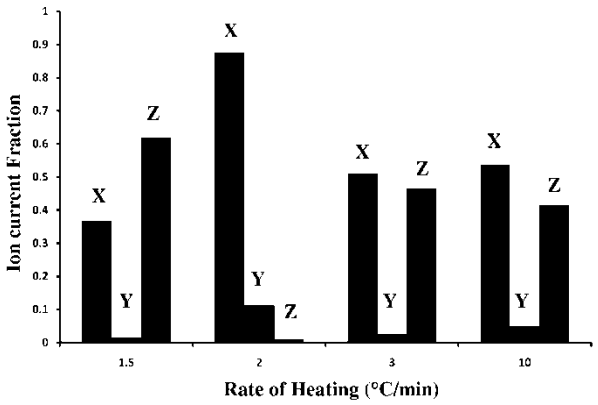

Figure 5.43. Fraction of ionic currents for NO (X), NO_2 (Y) and O_2 (Z) *vs.* rate of heating.

Despite the claim in the literature regarding the formation of amorphous anhydrous zinc nitrate as an intermediate compound to justify the strange thermal behaviour of BZN [347], it is quite unlikely that normal zinc nitrate forms and decomposes to ZnO. Some authors mentioned that anhydrous by heating the hydrated zinc nitrate, $Zn(NO_3)_2 \cdot nH_2O$, anhydrous zinc nitrate cannot be formed [401, 402] and some state the opposite [403]. What is known, however, is that during pyrolysis of hydrated zinc nitrate, zinc hydroxy nitrate species may be formed [394, 401-403]. As shown in [402] and also in this work on zinc nitrate hexahydrate, thermal decomposition of zinc nitrate needs temperatures over 300 °C the last stage of which involves the release of water and nitrogen oxides and oxygen simultaneously (see **Figure 5.44**). On the other hand decomposition of BZN to ZnO undergoes completion at fairly lower temperatures with a different pattern (compare **Figure 5.42** with **Figure 5.44**). Considering these and also based on the isothermal calcination experiment at 250 °C for 1 hour, which was explained before, presence of normal zinc nitrate as an intermediate in the last stage of decomposition is quite unlikely.

What can probably be concluded by applying a combination of techniques is that after the 2nd stage of decomposition, destruction of layered structure of $Zn_3(NO_3)_2(OH)_4$ into ZnO takes place. In $Zn_3(NO_3)_2(OH)_4$ structure, nitrates are located in the interlayer distance holding the layers together. Decomposition of this layered compound takes place continuously with dehydroxylation kinetically faster than the major release of the nitrogen oxides and oxygen (depending on the heating rate). Therefore an extended decomposition pattern can be seen, which looks like that it is in two separate stages; but

in fact it is a single-stage process, which does not necessarily form any other stable intermediate phase. This is shown in Reaction **5**.**22**.

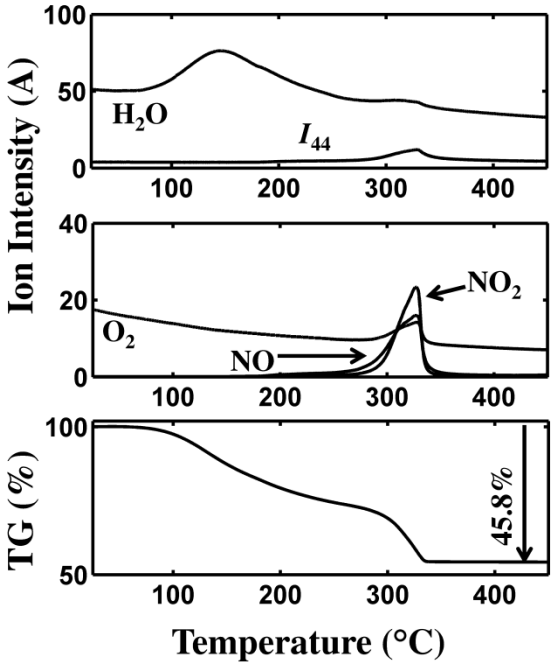

Figure 5.44. TGA-MS on $Zn(NO_3)_2{\cdot}6H_2O$ under argon with a heating rate of 4 °C min^{-1}. It can be seen that decomposition of $Zn(NO_3)_2$ undergoes completion at temperatures over 324 °C with the release of nitrogen oxide species. I_{18} for H_2O, I_{32} for O_2, I_{30} for NO, I_{46} for NO_2 and I_{44} are shown $\times10^9$, $\times10^9$ and $\times10^9$, $\times10^{10}$ and $\times10^{10}$, respectively.

$$x[Zn_3(NO_3)_2(OH)_4 \xrightarrow{T > 199\,^{\circ}C} 3ZnO + 2H_2O + (2n)NO + (2\text{-}2n)NO_2 + [(2n+1)/2]O_2] \quad 5.22$$

Besides, detection of traces of nitric acid might be due to either direct decomposition of $Zn_3(NO_3)_2(OH)_4$ according to Reaction **5**.**23** or more probably due the reverse reaction between nitrogen oxides, oxygen and water in the system according to Reactions **5**.**24** and **5**.**25** with $0 \leq z \; and \; t \leq 1$. Reactions **5**.**24** and **5**.**25** are quite temperature and pressure sensitive. Lower temperatures and higher pressures result in a shift towards right in Reaction **5**.**24**. In Reactions **5**.**22** and **5**.**23**, $x + y = 1$.

$$y[Zn_3(NO_3)_2(OH)_4 \xrightarrow{T > 199\,^{\circ}C} 3ZnO + 2HNO_3 + H_2O] \quad 5.23$$

$z(2NO + O_2 \rightleftharpoons 2NO_2 \rightleftharpoons N_2O_4)$ 5.24

$t(3NO_2 + H_2O \rightleftharpoons 2HNO_3 + NO)$ 5.25

It is also important to mention that oxygen is a result of decomposition of nitrate anions according to Reaction **5.26** [404] with $0 \leq n \leq 1$. Based on the MS experiments, it seems that n is a function of heating rate with more probably $0.5 \leq n \leq 1$ (see **Table 5.3** and **Figure 5.43**).

$$NO_3^- \rightarrow (n)NO + (1-n)NO_2 + [(2n+1)/4]O_2 + (1/2)O^{2-} \quad 5.26$$

Mechanism

The thermal decomposition mechanism for the transformation of BZN to ZnO is suggested to follow **Scheme 5.3**.

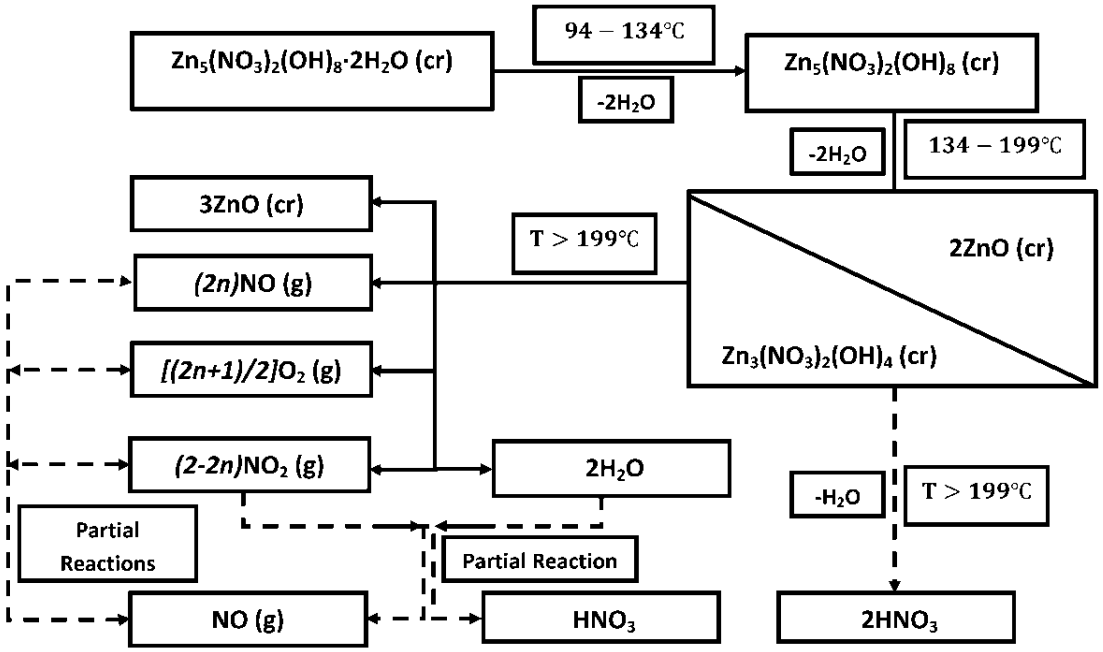

Scheme 5.3. Schematic of suggested mechanism for thermal transformation of BZN to ZnO. Dotted arrows represent probable side reactions that are not balanced.

5.3.5. Zinc hydroxy acetate

Zinc hydroxy acetate should not be confused with a zinc oxy-acetate complex with the nominal formula of $Zn_4O(CH_3CO_2)_6$ and a cubic crystal structure, which was first reported in 1924 [405, 406]. Zinc oxy-acetate in some works has been called "basic zinc acetate" [405, 407]. In others e.g. [314, 324, 330, 408] zinc hydroxy acetate was labelled as a basic salt. A *basic* salt is a "*hydroxy"* salt of a metal with a general formula $[M(OH)_{2-x}][A^{n-}]_{x/n}$ (M = metal, A = Anion) [345]. There are also a few other related compounds, including the ordinary zinc acetate salt, which can be hydrated or anhydrous, and a polymeric zinc oxydiacetate, $Zn(C_4H_4O_5)(H_2O)_2 \cdot H_2O$ [409].

Morioka *et al.,* showed that it is possible to exchange the inorganic anions such as nitrate in the zinc hydroxide salts with organic anions with various chain sizes [373]. Organic basic zinc salts can be categorised as Berthollide compounds with general formula of $xZn(CH_3(CH_2)_zCOO)_2 \cdot yZn(OH)_2 \cdot nH_2O$ similar to the inorganic anionic species with the only difference that the anions located in the interlayer distance are organic. When z = 0, zinc hydroxy acetate is formed.

In this work, synthesis of pure basic zinc acetate of type $Zn_5(OH)_8(CH_3CO_2)_2 \cdot nH_2O$ (abbreviated as BZA) and its transformation by calcination to ZnO were of interest for the purpose of producing so-called 'nano-zinc oxide'.

$Zn_5(OH)_8(CH_3CO_2)_2 \cdot nH_2O$ is a layered hydroxide, comprised of sheets of $[Zn^{octa}_3\{Zn^{tetra}(OH)_3\}_2(OH)_2]^{2+}$ with intercalated anions [324, 373], in this case $[CH_3CO_2]^-$. Nevertheless the mode of chemical bonding of acetate in the interlayer distance has been under debate as well. Although it was stated, only based on FTIR spectroscopy, that the bonding of acetates to zinc cations are purely ionic [348] or unidentate/chelating [410, 411], it is known that coordination mode of carboxylates cannot be resolved based on FTIR data only [412]. This issue will be resolved in this work using solid-state NMR.

On the other hand, the number of waters of crystallisation *n* is reported to be between 1.5 and 4 (depending on the synthesis method), with the different values for *n* solely deduced from the observed TGA mass loss values (the theoretical mass loss upon complete conversion to ZnO is 34.0% if *n* = 2 and 37.7% if *n* = 4).

Several synthesis routes are reported. For example, $Zn_5(OH)_8(CH_3CO_2)_2{\cdot}nH_2O$ can be made by titrating zinc acetate solution with an alkaline solution such as sodium hydroxide [348, 373] or by reaction of ZnO powder with zinc acetate solution [413] or by anion exchange reaction between zinc hydroxy chloride and zinc acetate dihydrate [414]. Formation of pure $Zn_5(OH)_8(CH_3CO_2)_2{\cdot}nH_2O$ by ammonium hydroxide [408] or in alcohol media [323, 324, 415] have been also claimed, which are sources of confusion.

Surprisingly, to date, the influence of the inclusion of organic or inorganic materials used during reactions to synthesise pure $Zn_5(OH)_8(CH_3CO_2)_2{\cdot}nH_2O$, which were assumed to be non-reactive have not been considered in most of the publications. In this work this puzzle is resolved and it was shown that presence of such materials in the system not only may change the chemical composition (formula) of the layered zinc complex, but also may result in the expansion of the interlayer distance.

Table 5.4 summarises some reports on $Zn_x(OH)_y\mathbf{Ac}_z.nH_2O$ type compounds (**Ac** = CH_3CO_2 here), and the associated values of the interlayer spacing(s) and the synthetic route (note that generated chemical formula in all reports only include zinc, hydroxide, acetate and water).

Table 5.4. Layered zinc hydroxy-acetates of the $Zn_x(OH)_y\mathbf{Ac}_z{\cdot}nH_2O$ family, **Ac** = acetate $[CH_3CO_2]^-$. The interlayer *d*-spacings are obtained from the text of the source or by analysing the published X-ray diffraction pattern.

As reported ($Zn_x(OH)y\mathbf{Ac}_z{\cdot}nH_2O$)	nominal y, z and *n* if *x* = 1	Interlayer *d*-spacing, nm	Synthesis route	Waters of hydration if formula is written as $Zn_5(OH)_8\mathbf{Ac}_2$	Ref.
$Zn(OH)_{1.58}\mathbf{Ac}_{0.42}{\cdot}0.31H_2O$	1.6, 0.4, 0.3	1.47 (note 1)	In ethanol/ethylene glycol/1,2-propandiol mixture	1.55	[323]
$Zn_5(OH)_8\mathbf{Ac}_2{\cdot}3H_2O$	1.6, 0.4, 0.6	1.38	Anion exchange reaction between zinc hydroxy chloride and zinc acetate dihydrate for 48hr	3.0	[414]
$Zn_5(OH)_8\mathbf{Ac}_2{\cdot}2H_2O$	1.6, 0.4, 0.4	1.34 & 1.64	ZnO-$Zn(Ac)_2$ reaction for 24 hr	2	[416]
$Zn_5(OH)_8\mathbf{Ac}_2{\cdot}2H_2O$	1.6, 0.4, 0.4	1.34	NaOH titration	2	[314]
$Zn_5(OH)_8\mathbf{Ac}_2{\cdot}2H_2O$	1.6, 0.38, 0.63 (note 2)	1.34 & 2.02	NaOH titration	2	[373]
$Zn_5(OH)_8\mathbf{Ac}_2{\cdot}4H_2O$	1.6, 0.4, 0.8	1.36 & 1.92	ZnO-$Zn(Ac)_2$ reaction for 24 hr	4	[413, 417]
$Zn_5(OH)_8\mathbf{Ac}_2{\cdot}2H_2O$	1.6, 0.4, 0.4	1.33 & 1.98 (note 3)	In ammonia	2	[408]
$Zn_5(OH)_8\mathbf{Ac}_2{\cdot}4H_2O$	1.6, 0.4, 0.8	1.34 (note 1)	NaOH titration	4	[348]
$Zn_5(OH)_8\mathbf{Ac}_2$	1.6,0.4, 0	-	NaOH titration	0	[348]
$Zn_3(OH)_4\mathbf{Ac}_2$	1.33, 0.66, 0	0.95	NaOH titration	0	[348]
$Zn_5(OH)_8\mathbf{Ac}_2{\cdot}4H_2O$	1.6, 0.4, 0.8	1.34 (note 1)	NaOH titration	4	[418]
$Zn_5(OH)_8\mathbf{Ac}_2{\cdot}2H_2O$	1.6, 0.4, 0.4	1.31 to 1.44 (note 4)	In methanol	2	[324]
$Zn_5(OH)_8\mathbf{Ac}_2{\cdot}2H_2O$	1.6, 0.4, 0.4	1.47	In methanol	2	[415]
$Zn_5(OH)_8\mathbf{Ac}_2{\cdot}2H_2O$	1.6, 0.4, 0.4	1.24 (note 1)	In water, hexamethylenetetramine and sodium citrate	2	[419]
$Zn(OH)_{1.75}(CH_3CO_2)_{0.26}{\cdot}0.57H_2O$	1.8, 0.3, 0.6	1.33 & 2.03	In ammonia	2.9	[410]
$Zn(OH)_{1.6}\mathbf{Ac}_{0.4}{\cdot}0.7H_2O$	1.6, 0.4, 0.7	1.34	Hydrolysis	3.5	[411]

As reported ($Zn_x(OH)y\mathbf{Ac}_z \cdot nH_2O$)	nominal y, z and *n* if *x* = 1	Interlayer *d*-spacing, nm	Synthesis route	Waters of hydration if formula written at $Zn_5(OH)_8\mathbf{Ac}_2$	Ref.
$Zn(OH)_{1.4}\mathbf{Ac}_{0.6} \cdot 0.8H_2O$	1.4, 0.6, 0.8	1.34 & 2.1	Hydrolysis	4.0	[411]
$[Zn(C_4H_4O_5)(H_2O)_2] \cdot H_2O$	4, 2, 0	0.76	Aging in oxydiacetic acid	-	[409]
$Zn(OH)_a\mathbf{Ac}_b \cdot c$H2O	-	1.32 & 1.91	In ammonia combined with CTAB	-	[420]
$Zn(OH)_{1.75}\mathbf{Ac}_{0.26} \cdot 0.57H_2O$	1.8, 0.3, 0.6	1.36 & 1.77 & 2.05	In ammonia	2.9	[421]
$Zn_5(OH)_8\mathbf{Ac}_2 \cdot 2H_2O$ mixed with ε-$Zn(OH)_2$	1.6, 0.4, 0.4	1.34 & 2.0	In ammonia	2	[422]

Note 1. Due to the limited range of 2θ sampled, a peak with a *d*-spacing of >1.75 nm cannot be excluded.

Note 2. Based on reported content of C and H and taking ratio of OH to Zn to be fixed at 1.6.

Note 3. Based on location of probable second order peak at *d*=0.99 nm. Due to the limited range of 2θ sampled, a first order peak with *d* = 1.98 nm would have been missed.

Note 4. Expansion of the interlayer distance (due to the presence of methanol) has been shown as a function of time but was not recognised as such.

Powder XRD patterns show a strong (001) reflection associated with the interlayer distance between the sheets usually at about d = 1.34 nm. 2nd-order (002) and 3rd-order (003) peaks associated with the 001 reflection are centred at 0.67 nm and 0.45 nm, respectively. However, there is as much as ±0.15 nm variation in the values of d between various authors, which seems to be somehow related to the synthetic method. This is more than would be anticipated by inter-laboratory scatter and is evidently caused by variable composition and/or stoichiometry that in turn affect the structure [323, 324]. The crystal structure is similar to that of brucite [348, 413], a layered $Mg(OH)_2$, and as such would be expected to exhibit turbostratic disorder, that is, the brucite-like sheets can be twisted and translated relative to one another, inducing broadening and asymmetry in high angle reflections [323].

Another important observation based on XRD in several cases including results from the current work is the presence of peak(s) associated with d-spacing(s) larger than the usual interlayer distance. These peaks however are much less intense as opposed to the major low angle 001 reflection. Also position of these peaks varies as much as ±0.35 nm. In synthetic routes other than the ones using pure water, the difference may be due to the formation of non-pure zinc hydroxy acetate because of co-intercalation. Also changes in the interlayer distance and also lower angle X-ray peaks' positions can be observed. Most of the disparities between the d-spacing values can be observed in the methods that used organic solvents such as methanol, ethanol, ethylene glycol (EG) and 1,2-propandiol and also methods that used ammonia solutions. The authors in most cases simply did not consider the effect of species originating from the solvents on the end-product. Hosono *et al.,* showed the expansion of the interlayer distance after aging the material claimed to be $Zn_5(OH)_8(\mathbf{Ac})_2 \cdot 2H_2O$ in methanol. This expansion was assigned to intercalation of more than stoichiometric acetate groups in the gallery space. Here the possible reactivity of methanol has not been considered [324]. Kasai and Fujihara showed the possibility of intercalation of ethylene glycol into the structure of a precursor claimed to be $Zn_5(OH)_8(\mathbf{Ac})_2 \cdot 2H_2O$ to form a hybrid material with a reported composition of $Zn_5(OH)_8(\mathbf{Ac})_2(HOC_2H_4OH)_2 \cdot 2H_2O$. Nevertheless in this work also the precursor used for intercalation of EG was produced in anhydrous methanol [415]. Another group with reference to [415] successfully intercalated ethylene glycolate anions ($O_2C_2H_5^-$) into layered yttrium hydroxy species [423]. In the work by Poul *et al.,* [323], where zinc acetate was dissolved in a mixture of diethylene glycol/1,2-

propandiol/ethanol with concentrations of 0.5/0.5/0.1 molar, respectively, it was noticed that other compositions for the as-synthesised material (claimed to be $Zn(OH)_{1.58}\mathbf{Ac}_{0.42}\cdot 0.31H_2O$ by chemical analysis on Zn, C and H) might be possible. Interestingly carbon content was ~13% higher than expected based on the reported formula if only acetate is involved. In 2006 this issue in a new publication has been mentioned, but surprisingly the authors referred to this as a physical adsorption of polyols on the particles and excluded the effect of alcohols on the product's chemical composition [424]. In the current work it was shown that this assumption does not apply to such materials due to the possible side-reactions or co-intercalation of unwanted materials in the product. Similarly ammonia may be intercalated into the layered materials and forms ammine intercalation compounds. This may also result in expansion of the interlayer distance [425, 426].

These observations raise the question of whether it is possible to synthesise pure zinc hydroxy acetate in alcohol or ammonia environments. Do alcohols only act as solvents or are there chemical reactions between these materials? Could it be that some of the observed shifts in the XRD patterns obtained on the as-synthesised layered materials correspond to intercalation of some impurities or changes in the coordination modes? And as a result of these changes, could it be still presumed that the materials formed in the non-aqueous systems are the same as the ones made in only water?

Uncertainty regarding the presence and role of various intermediates and products such as acetone, acetic acid, acetic anhydride, zinc oxy-acetate, anhydrous zinc acetate, anhydrous $Zn_5(OH)_8(\mathbf{Ac})_2$ and $Zn_3(OH)_4(\mathbf{Ac})_2$ during thermal decomposition of the BZA also raised some debates [323, 348, 413].

Here production of *zinc hydroxy acetate dihydrate* is reported. Evidence for assigning *two* waters of hydration as opposed to other reported numbers is provided. Also evidence for the effect of alcohols on BZA is provided. Chemical bonding type of acetate in the interlayer distance is also resolved. It was previously presumed that alcohols that are used for solvation do not affect the chemical composition of the product. Here it is shown that BZA is sensitive to the medium in which it is produced.

Precipitation of BZA dihydrate (M.W=616.9) proceeds according to Reaction **5.27**.

$$8NaOH_{(aq)} + 5Zn(\mathbf{Ac})_2\cdot 2H_2O_{(aq)} \rightarrow Zn_5(OH)_8(\mathbf{Ac})_2\cdot 2H_2O_{(s)} + 8Na(\mathbf{Ac})_{(aq)} \qquad 5.27$$

Characterisation, BET surface area measurement and microscopy

Comparison of the X-ray diffraction pattern, **Figure 5.45**, with reported patterns [314, 416] indicated that the compound produced in the current work is similar to the compound with the nominal stoichiometry of $Zn_5(OH)_8(\mathbf{Ac})_2 \cdot nH_2O$. The most intense 001 peak in our X-ray result corresponds to 1.34 nm of *d*-spacing. Also other lower angle peaks (but less intense) corresponding to 1.42 nm, 1.49 nm and 1.75 nm of *d*-spacing were observed. Two peaks located at around 1.42 nm and 1.49 nm are almost buried under the asymmetric 1.34 nm peak. These peaks become more visible when the material is heated and the layered structure starts to be destroyed (see Appendix, **Figure A. 5** for the resolved *d*-spacing of low-angle peaks). 2nd-order (002) and 3rd-order (003) peaks associated with the 001 reflection were detected at 0.67 nm and 0.44 nm, respectively.

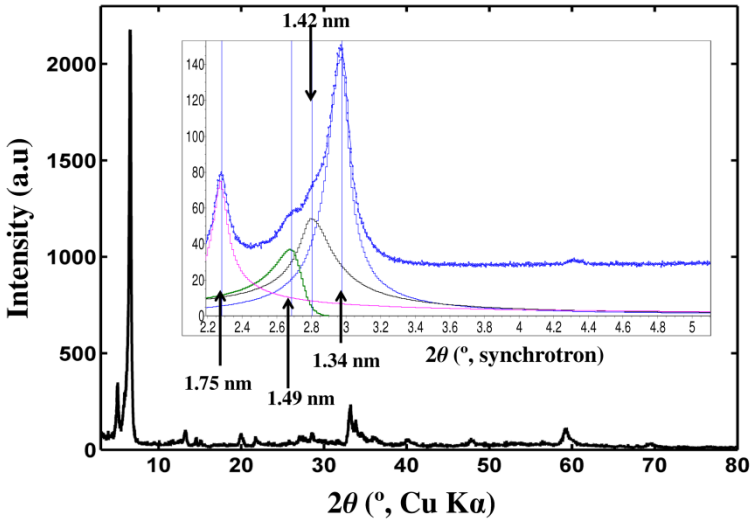

Figure 5.45. X-ray diffraction pattern of as-synthesised BZA. The positions of *d*-spacings at 1.42 and 1.49 nm are resolved from synchrotron data using Split-Pearson VII distribution function.

Evidence for the presence of lower-angle peak(s) below the major interlayer distance peak for this class of materials is available in the published literature [373, 411, 420, 421, 427]. In some cases where only one peak is reported [324, 348, 419], the range of 2θ angles used in the X-ray diffraction patterns was insufficient to include any peaks for *d*-spacings greater than 1.7 nm anyway. From these observations and the data in

Table 5.4 it was concluded that (1) multiple low-angle peaks are the norm not the exception for this compound, and (2) different reported interlayer spacings are due to

the actual chemical composition of the compound, which depends on the synthetic route. Possibly, pure BZA dihydrate can only be synthesised in pure water.

A bulk sample of BZA that was calcined at 400 °C for two hours was found by XRD (Cu Kα) to be ZnO (01-089-0510), **Figure 5.46** with a BET specific surface area of 15.4 m^2/g. The whiteness of the ZnO produced from BZA was lower than the products produced from other basic zinc salts mentioned before but the specific surface area is relatively high.

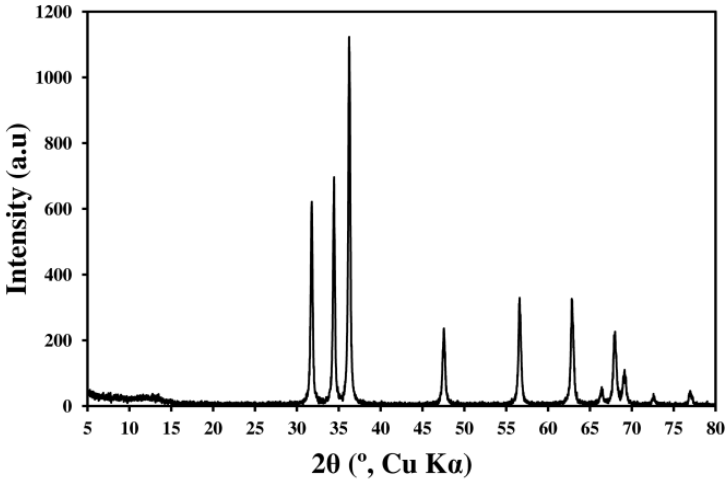

Figure 5.46. XRD (Cu Kα) on the product shows peaks associated with ZnO.

SEM images of the BZA powder and the resultant ZnO particles are shown in **Figure 5.47** while TEM images, **Figure 5.48**, shows that the diameters of the individual ZnO crystals in **Figure 5.48** are in the range of 20 to 100 nm (average = 41.1 nm, *s* = 21.1 nm, *n* = 111 crystals, each measured in two directions).

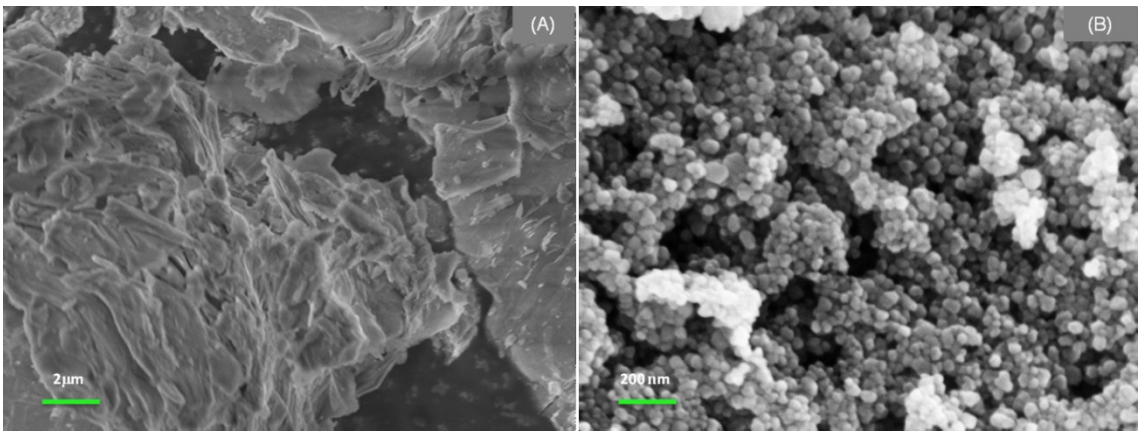

Figure 5.47. SEM images of (A) BZA and (B) the calcination product, ZnO.

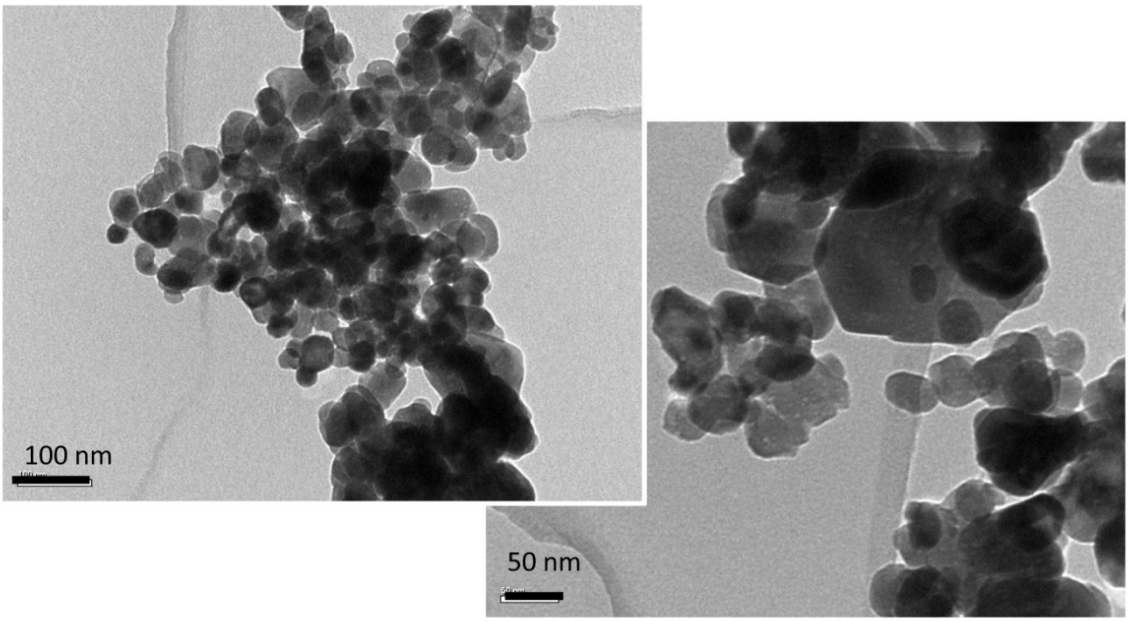

Figure 5.48. Transmission electron images of the ZnO nanocrystals formed by calcination at 400 °C. The characteristic hexagonal crystal habit of ZnO is clearly visible in some of the larger particles (courtesy of Dr A. Dowd).

FTIR spectroscopy

FTIR spectra are useful means for differentiating between coordination types of carboxylate to metal. Various forms of coordination of the carboxylate to metal can exist: (1) unidentate, (2) chelating, (3) bridging bidentate in a syn-syn, syn-anti or anti-anti configurations, and (4) monatomic bridging alone, with additional bridging, or in configurations involving chelation and bridging [428]. In addition to coordination configurations, ionic bonds are also possible [428]. There is an empirical correlation between the carboxylate stretching frequencies and the types of its coordination to divalent metal cation. Frequency separation between the COO^- antisymmetric and symmetric stretches ($\Delta\nu_{a-s} = \nu_a$ (COO^-) - ν_s (COO^-)) and the types of carboxylate bonding to divalent metal cations can be expressed as $\Delta\nu_{a-s}$ (unidentate) > $\Delta\nu_{a-s}$ (ionic) ≥ $\Delta\nu_{a-s}$ (bridging bidentate) > $\Delta\nu_{a-s}$ (chelating) [428]. The corresponding value for sodium acetate is reported to be $\Delta\nu_{a-s}$ = 164 cm^{-1} [429, 430], which is attributed to free (ionic) carboxylate ion. It is reported that the bridging bidentate mode results in COO^- frequency separation smaller than or almost equal to ionic value [428]. Nevertheless distinguishing between these coordination modes only by an IR technique is not conclusive [412] and there are reports that this sort of coordination assignment might be

wrong in some cases [428]. Therefore combination of FTIR and other techniques such as solid-state NMR can provide better understanding of the bonding modes. In this work for the first time, solid NMR on BZA has been performed, which is explained shortly.

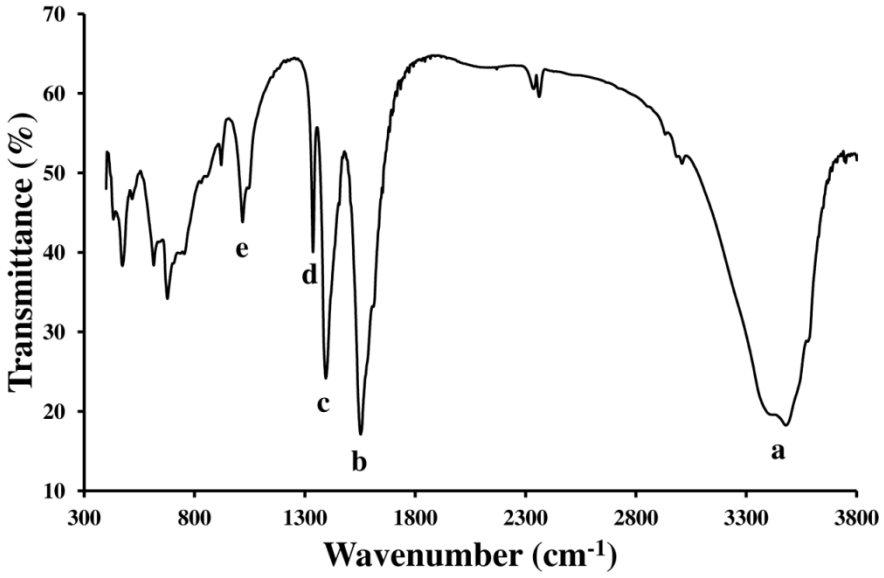

Figure 5.49. FTIR spectrum of BZA dihydrate.

FTIR spectrum of BZA and associated spectral assignments are shown in **Figure 5.49** and **Table 5.5**, respectively. A broad band centred at around 3403 cm^{-1} indicates the resonation of coordinated water molecules in the crystal lattice [429, 431]. There is a major COO^- frequency separation ($\Delta\nu_{a-s}$) of 1552-1394 = 158 cm^{-1}. This value is less than 164 cm^{-1} for sodium acetate with the ionic bonding and thus might suggest a bridging bidentate or chelating coordination types. This is not, however, conclusive when only based on IR data.

Table 5.5. FTIR spectral assignments for BZA.

Peak label	Wavenumbers (cm^{-1})	Assignments	Ref
a	3577, 3479, 3403	OH stretching vibrations	[429, 432]
b	1612w, 1583w, 1552	COO^- antisymmetric stretch	[348, 432]
c	1456w, 1419w, 1394	COO^- symmetric stretch	[410]
d	1336	CH_3 symmetric bending	[410, 433]
e	1039w, 1016	CH_3 rocking	[410, 433]

Note: "w" denotes weak signal.

CP-MAS ^{13}C NMR

The CP-MAS ^{13}C NMR spectrum of BZA is shown in **Figure 5.50**. Two signals assigned to resonances of the carbon atoms associated with the CH_3 and C=O groups were observed at 25 and 180 ppm, respectively. Chemical shift associated with carbonyl carbon depends on the coordination mode and also on the coordination number of metal ion [412]. This technique has proven useful to distinguish acetate/metal coordination modes [412]. Although it was claimed only based on FTIR that the bonding of acetates to zinc cations in BZA are purely ionic [348] or unidentate/chelating [410, 411], it is known that the coordination mode of carboxylates cannot be resolved using only FTIR data [412].

Comparison of the current signals with the CP-MAS ^{13}C NMR chemical shifts of carbonyl groups in related zinc compounds that bear carboxylate groups [412] suggests that the acetate group is coordinated in a bidentate bridging fashion. Importantly relative to chelating coordination of the carbonyl group (which appears at around 184 ppm) the chemical shifts of unidentate and bidentate types undergo about 8 and 4 ppm upfield shift, respectively [412]. This is consistent with the observed signal at 180 ppm.

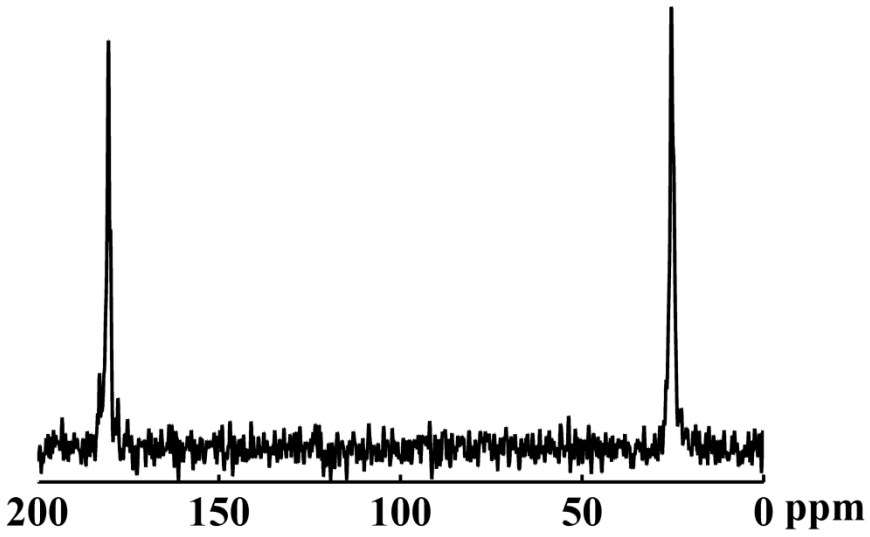

Figure 5.50. CP-MAS ^{13}C NMR spectra of BZA.

TGA-DTA

TGA-DTA, **Figure 5.51**, showed a mass loss of 37.4% upon heating up to 1000 °C (Note that zones are only used for simplicity; some reactions can overlap between zones). This would ostensibly suggest that $n = 4$ if all the mass loss were due to the decomposition of the precursor into only ZnO. This conclusion has been drawn by some previous workers in the field [348, 413]. The sample contains ~0.9% of unbound water up to the temperature of ~60 °C. As shown in the section on sublimation below, the thermal decomposition involves the formation of some volatile zinc species calculated to be responsible for an excess mass of ~1.8-2.9%. Therefore, a lower value of $n = 2$ is concluded, in agreement with the work of Morioka *et al.,* and Cui *et al.,* [373, 408], see Sublimation test section and Appendix.

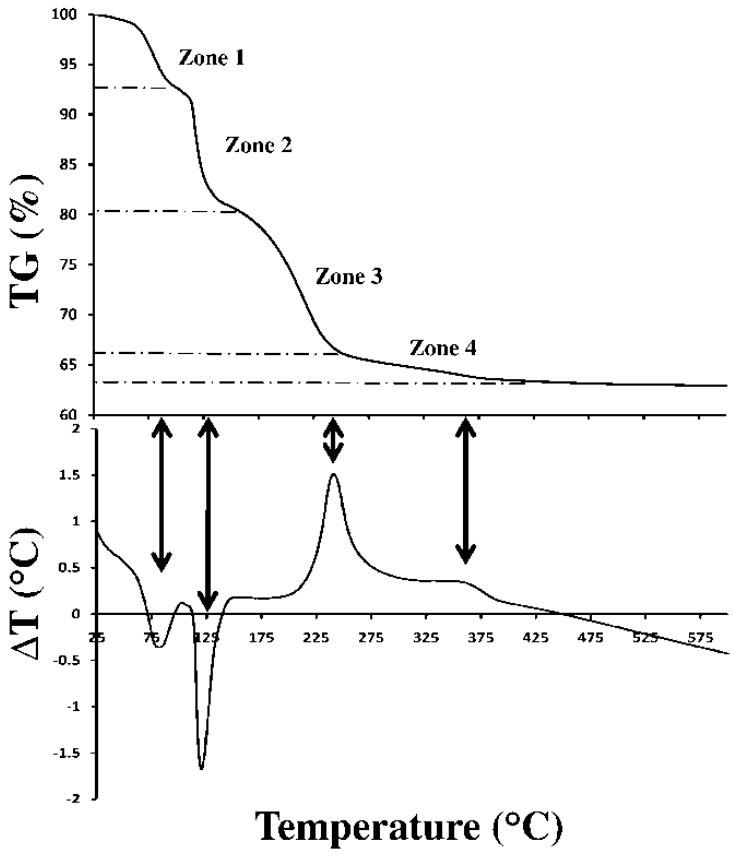

Figure 5.51. TGA-DTA in air on BZA with heating rate of 5 °C min^{-1}.

An endothermic process at 82 °C (zone 1) is associated with a 5.8% mass loss up to from 60-93 °C. This has been assigned to dehydration. A second endothermic process at 93-147 °C (zone 2) corresponds to a 12.3% mass loss. Note that mass loss in 60-147 °C (zone 1 and 2) is 18.1% that is quite close to theoretical mass loss (17.5%) associated

with release of six moles of water. The Zn**Ac**$_2$ steadily decomposes in zone 3 at 147 to 250 °C with an exothermic peak centred at 242.3 °C with an associated mass loss of 14.7%. At 362.3 °C a broad exothermic peak can be detected, which is associated with 2.7% mass loss at 250 to 400 °C.

Synchrotron radiation study

Figure 5.52 and **Figure 5.53** show X-ray diffraction patterns data collected from *in-situ* real-time calcination experiments using synchrotron radiation.

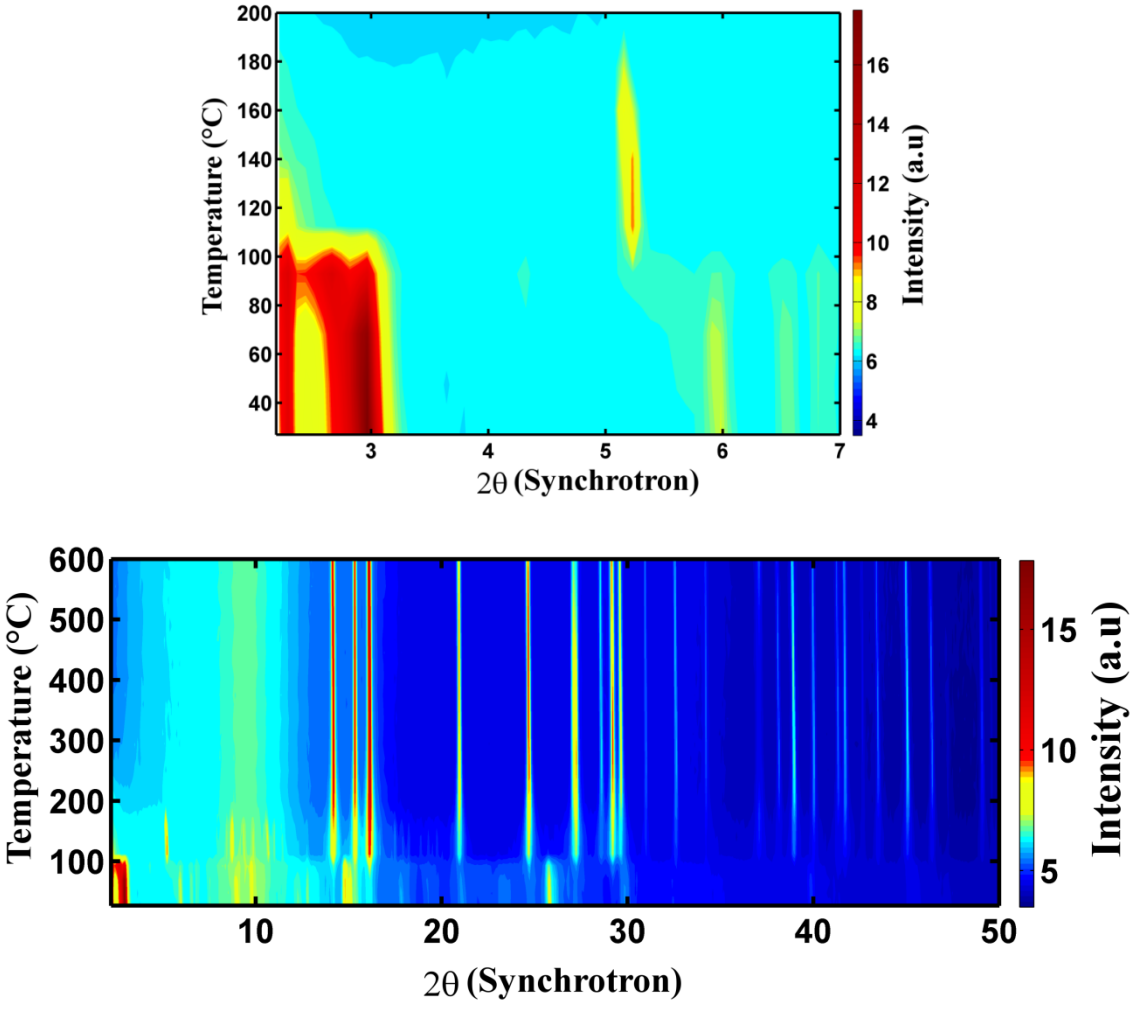

Figure 5.52. Colour-coded contour graphs generated from XRD (synchrotron) data show the real-time transformation of BZA to ZnO. The intensity is colour-coded. Top and bottom contour graphs show different ranges of 2θ *vs.* temperature.

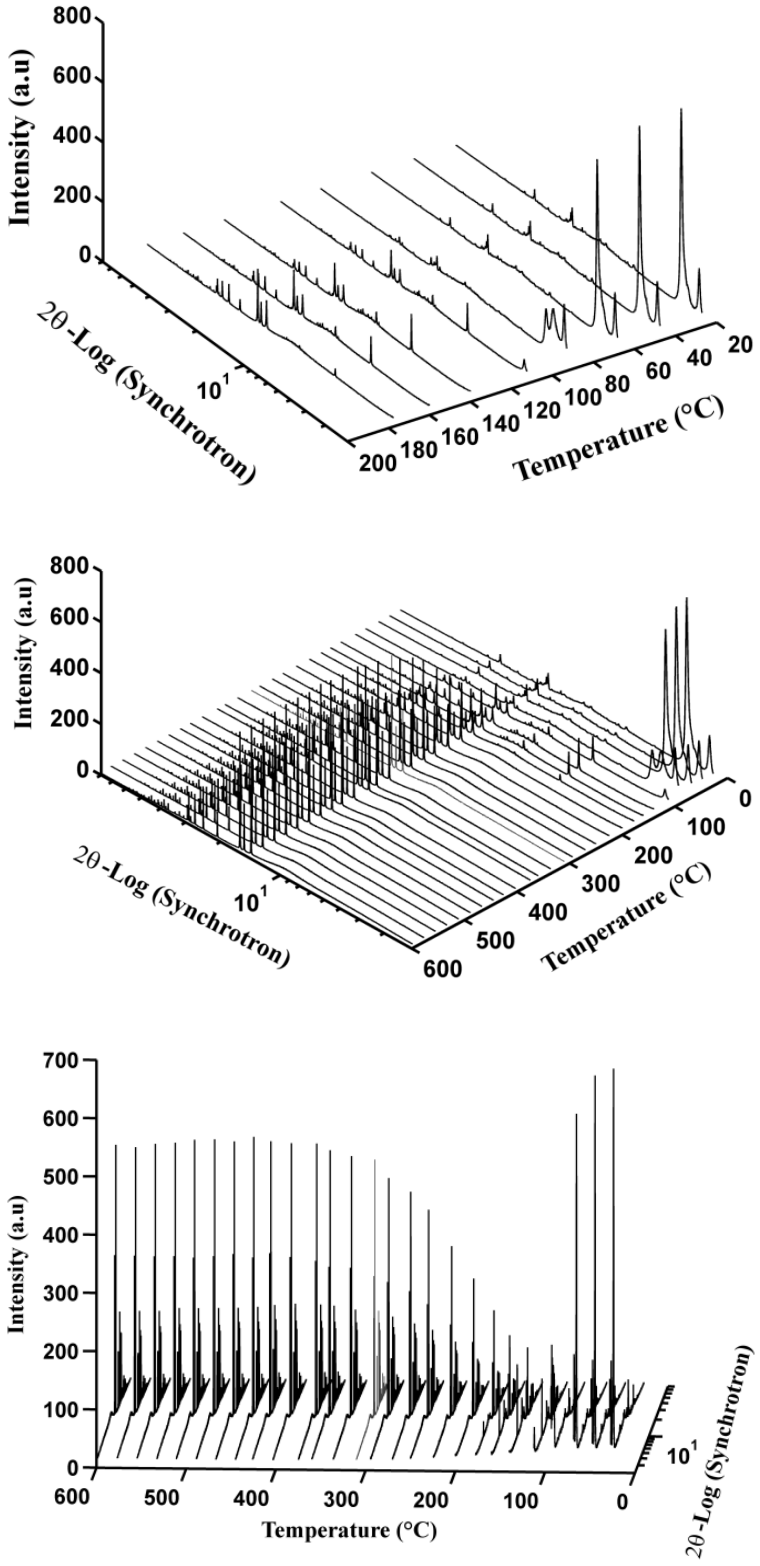

Figure 5.53. 3D-stacked XRD (synchrotron) graphs from different views and in different ranges of temperatures for clarity.

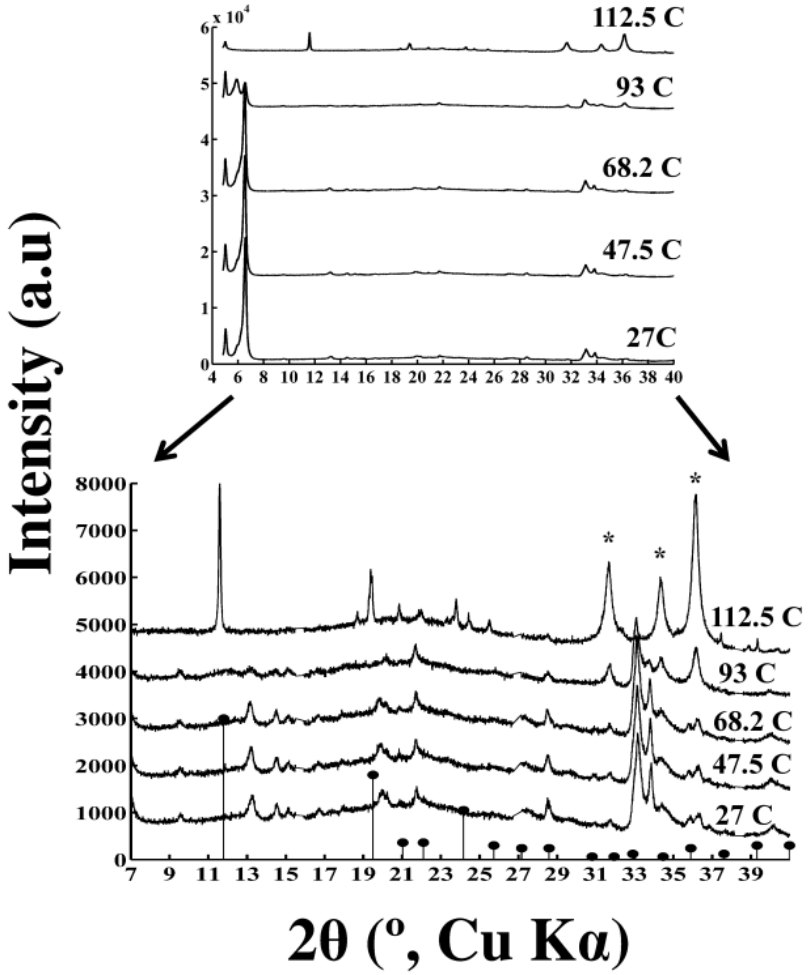

Figure 5.54. XRD data collected from 27 to 113 °C in a synchrotron. 2θ values are converted to corresponding Cu Kα values for comparison reasons. Peaks marked with * correspond to ZnO and stick lines correspond to anhydrous zinc acetate (JC-PDF 00-001-0089).

As shown in **Figure 5.54**, up to 68 °C, XRD shows peaks associated with *d*-spacings of 1.34 nm and 1.75 nm and two other peaks, which were deconvoluted to be located at 1.42 nm and 1.49 nm (see also Appendix for resolved peaks in low angle region). As the temperature approaches 93 °C, the peak associated with d = 1.34 nm shrinks in intensity. Also, the first signs of the formation of ZnO can already be detected at this low temperature. The XRD peaks obtained at 93 °C, which were found by deconvolution to be approximately 1.47 nm and 1.50 nm, grow in intensity relative to the 1.34 nm peak. These peaks might be associated with lower-hydrated phase. Based on the TGA, up to 93 °C around 6.9% mass loss occurs that includes ~0.9% due to

release of free moisture. Therefore 5.8% mass loss between 60 to 93 °C matches perfectly with the loss of two waters. This suggests the probable formation of intermediate anhydrous BZA phase in this narrow temperature range.

Nevertheless there is another possible explanation that the intermediate peaks are actually the same as the ones observed for the precursor at RT, which are buried under the major interlayer peak. The shift in the position of these intermediate peaks is not as much to be conclusive. Available published data is not sufficient to be conclusive on the nature of the intermediate peaks and more crystallographic work is needed. At ~113 °C, the small peak centred at ~1.75 nm can still be detected (see Appendix) and the rate of formation of ZnO slowed markedly and a new crystalline phase appeared. From its XRD pattern this phase was identified as anhydrous zinc acetate (JC-PDF 00-001-0089), **Figure 5.54**. The presence of this phase during the thermal decomposition of BZA was also deduced by Biswick *et al.,* [348]. These authors also commented on the fact that there were two overlapping thermal processes occurring between 50 and 160 °C, which they attributed to the formation of a $Zn_5(OH)_8(\mathbf{Ac})_2$ and a material tentatively identified as $Zn_3(OH)_4(\mathbf{Ac})_2$, which in turn decomposed to $Zn\mathbf{Ac}_2$. Evidence for the presence of these intermediate phases was sought in this work.

In the *in-situ* XRD experiments, no diffraction pattern for $Zn_3(OH)_4(\mathbf{Ac})_2$ was evident although peaks corresponding to those reported for this material in *ex-situ* XRD experiments on material obtained by isothermal heating $Zn_5(OH)_8(\mathbf{Ac})_2 \cdot 2H_2O$ at 90 °C for 1 hour could be identified, **Figure 5.55**. Here peaks associated with ZnO together with peaks associated with anhydrous zinc acetate (JC-PDF 00-001-0089) with the major reflection at d = 0.74 nm were observed. A lower angle peak centred at 0.94 nm was also detected. This is in accordance with the peak reported by Biswick *et al.,* [348], which was assigned to $Zn_3(OH)_4(\mathbf{Ac})_2$ phase. In fact, a 2nd-order peak at 0.47 nm and a 3rd-order peak at 0.315 nm have been also detected. This finding indicates that the heating rate may significantly affect the formation of intermediate phases. Also, decomposition of BZA might undergo processes that overlap in this range of temperatures.

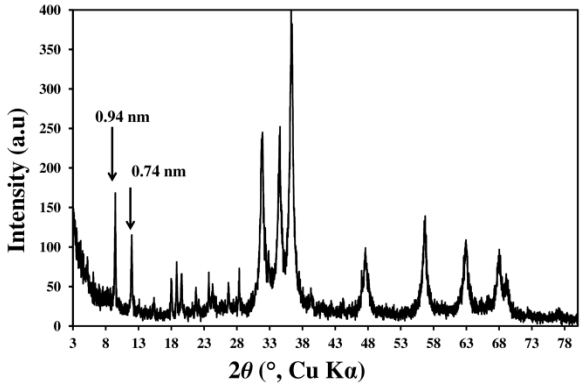

Figure 5.55. XRD (Cu Kα) on the product collected after heating at 90 °C shows the presence of ZnO mixed with anhydrous zinc acetate and a phase reported to be $Zn_3(OH)_4(\mathbf{Ac})_2$.

The amount of Zn$\mathbf{Ac}_2$ peaks at about 140 °C, after which it declines, while the amount of ZnO continues to increase. There are no peaks attributable to Zn($\mathbf{Ac}$)$_2$ in the XRD patterns obtained at temperatures >200 °C. Beyond this temperature the integrated area of the selected ZnO peak does not change much although the height of this ZnO peak continues to increase slightly to about 500 °C indicating that the ZnO crystallites are growing and/or annealing, which decreases the width of the XRD peak. Above that temperature there is a slight decrease in height due to thermal effects that reduce the intensity of the diffraction pattern.

TGA-MS

TGA-MS was used to examine the gases evolved during heating, **Figure 5.56**. Note, however, that an inert environment was used. Release of water was detected at temperatures below 100 °C and the rate of water evolution peaked in the region 100-150 °C, where CO_2 was also detected. Clearly, the reactions associated with the formation of the intermediate phase and initial formation of ZnO mainly produced H_2O as a gaseous product. The small CO_2 peak is likely due to the expulsion of adsorbed atmospheric CO_2.

The TGA-MS indicates that the main pulses of CO_2, acetic acid and traces of acetic anhydride, which indicate decomposition of the acetate moity, only appear at temperatures in excess of 200 °C. In particular at about 280 °C there is a peak in CO_2 evolution and some consumption of residual O_2, indicating that some combustion is

occurring. Acetone was also evolved simultaneously at this stage. This is puzzling as the XRD signal for anhydrous zinc acetate disappears from the powder diffraction pattern at 200 °C, and only ZnO is evident in it at higher temperatures. This apparent mismatch between XRD and TGA-MS will be explained shortly.

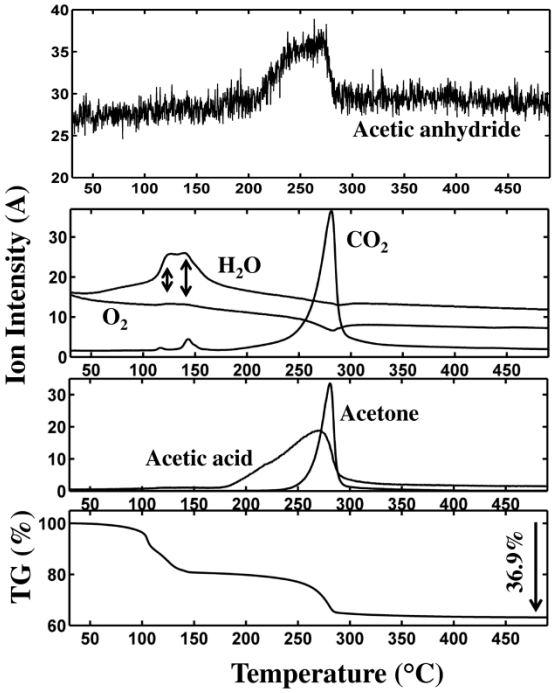

Figure 5.56. TGA-MS data produced by the decomposition of aged zinc hydroxy acetate under argon atmosphere at a heating rate of 3 °C min^{-1}. Channels I_{44} (CO_2), I_{18} (H_2O), I_{32} (O_2), I_{60} (acetic acid) and I_{58} (acetone) are scaled $\times10^{10}$, $\times10^{9}$, $\times10^{10}$ and $\times10^{12}$ and $\times10^{11}$, respectively. (Channel I_{102} (acetic anhydride) data comes from a separate but similar sample of BZA to the other data (scaled $\times10^{14}$)).

It appears that the sequence of reactions up to the temperature of 147 °C is as follows. First, the BZA undergoes dehydration according to Reaction **5**.**28** in the temperature range of 68-93 °C with a mass loss of ~5.8% (from TGA, exact temperature depends on sample and heating rate). A mass loss of 5.8% is predicted for the formation of anhydrous $Zn_5(OH)_8(\mathbf{Ac})_2$, in good agreement with the measured value. In a narrow range of temperature between 93-113 °C, evidence for the formation of $Zn_3(OH)_4(\mathbf{Ac})_2$ was obtained by an independent technique. This process follows Reaction **5**.**29**, which depends on the heating rate. The reason that this phase could not be detected in the synchrotron radiation study is probably because the temperature and time steps were too

coarse. $Zn_3(OH)_4(\mathbf{Ac})_2$ phase seems to be very unstable even at such a low temperature and quickly changes to $Zn(\mathbf{Ac})_2$ and ZnO by releasing water according to Reaction **5.30**.

$$Zn_5(OH)_8(\mathbf{Ac})_2{\cdot}2H_2O \xrightarrow{68-93\,℃} Zn_5(OH)_8(\mathbf{Ac})_2 + 2H_2O \quad 5.28$$

$$Zn_5(OH)_8(\mathbf{Ac})_2 \xrightarrow{93-113\,℃} 2ZnO + Zn_3(OH)_4(\mathbf{Ac})_2 + 2H_2O \quad 5.29$$

$$Zn_3(OH)_4(\mathbf{Ac})_2 \xrightarrow{93-147\,℃} 2ZnO + Zn(\mathbf{Ac})_{2\,(s)} + 2H_2O \quad 5.30$$

$Zn(\mathbf{Ac})_2$ behaves quite differently under different heating conditions and atmospheres. Its decomposition or volatilisation behaviour over heating is sensitive to humidity of the atmosphere. In dry atmospheres, it can be volatilised completely without forming any ZnO residue. In highly humid atmospheres, however, it can be decomposed completely to ZnO and acetic acid according to Reaction **5.31** without volatilisation. Therefore the amount of volatilised material, if any, depends on the vapour pressure of water in the system [427, 434]. In the MS experiment, acetic acid was detected that can be related to the following reaction:

$$Zn\mathbf{Ac}_2 + H_2O \xrightarrow{147-200\,℃} ZnO + 2CH_3CO_2H \quad 5.31$$

In dry atmospheres, $Zn(\mathbf{Ac})_2$ is reported [435] to form zinc oxy-acetate, $Zn_4O(CH_3CO_2)_6$, according to Reaction **5.32** by releasing acetone, which was detected by MS. $Zn_4O(CH_3CO_2)_6$ may also melt and be decomposed to ZnO, acetone and CO_2 according to Reaction **5.33** [435]. This tetramer of zinc is a two-shell compound and is composed of oxocentred tetrahedra $[OZn_4]^{4+}$ surrounded by six acetate groups and is also called μ_4-oxo-hexakis(μ-acetato)tetrazinc [354, 407, 436-439].

$$4Zn(CH_3CO_2)_{2\,(s)} \xrightarrow{180-250\,℃} Zn_4O(CH_3CO_2)_{6\,(s)} + (CH_3CO)_2O_{(g)} \quad 5.32$$

$$Zn_4O(CH_3CO_2)_{6(s)} \xrightarrow{T>250\,℃} Zn_4O(CH_3CO_2)_{6(l)} \xrightarrow{T>250\,℃} 4ZnO_{(s)} + 3CH_3COCH_{3(g)} + 3CO_{2(g)} \quad 5.33$$

$Zn_4O(CH_3CO_2)_6$ can also be sublimed [435] and this might be responsible for the excess of mass loss during the TGA studies. This will be examined further shortly.

Presence of traces of acetic anhydride in the MS may also be assigned to Reaction **5.34** [348].

$$Zn\mathbf{Ac}_{2\,(s)} \xrightarrow{147-250\,^{\circ}C} ZnO_{(s)} + (CH_3CO)_2O_{(g)} \qquad 5.34$$

Anhydrous zinc acetate can also melt with a reported melting point of at around 240-250 °C [434, 435]. However DTA in this region shows an exothermic peak, which can be originated from Reactions **5.31** and **5.32**, and might cover the endothermic peak associated with melting of Zn**Ac**$_2$. Molten Zn**Ac**$_2$ decomposes to ZnO and acetone and CO_2 according to Reaction **5.35**. Oxidation of acetic anhydride to CO_2 and water is also possible according to Reaction **5.36** [419]. This is consistent with MS data that shows consumption of O_2 and a sudden drop in the acetic anhydride signal at the same time with release of CO_2.

$$Zn\mathbf{Ac}_{2\,(l)} \xrightarrow{T > 240\,^{\circ}C} ZnO_{(s)} + CH_3COCH_{3\,(g)} + CO_{2\,(g)} \qquad 5.35$$

$$(CH_3CO)_2O + 4O_2 \rightarrow 4CO_2 + 3H_2O \qquad 5.36$$

As explained before, over 200 °C, XRD shows only ZnO peaks. However TGA-DTA and MS show other higher temperature events especially at ~280 °C. It is presumed that molten materials such as Zn**Ac**$_2$ and $Zn_4O(CH_3CO_2)_6$ (m.p. ~250 °C [406, 435]) can cause this issue.

Although there are multiple reactions involved in this temperature region, the mass loss observed by TGA in Zone 3 between 147 to 250 °C (14.7%) can be mainly assigned to the formation of ZnO, which is in excellent agreement with the calculated mass loss for the decomposition of anhydrous zinc acetate to ZnO from any possible route.

However, there is a further 2.7% mass loss between 250 and 400 °C with a broad exothermic peak in the DTA at 362 °C. This is assigned to release of volatile zinc-bearing material, which results in an excess of mass loss in the TGA studies. Importantly release of volatile zinc-containing material from BZA in the course of heating has never been reported. This issue may explain the range of reported waters of hydration in the literature. Note that in Zones 3 and 4 in TGA multiple reactions can happen simultaneously and therefore the separation of steps is not possible in the current experimental conditions.

No evolved species were detected in MS at temperatures >300 °C. Note that detecting the volatile $Zn_4O(CH_3CO_2)_6$ by MS was not possible due to limitations on the molecular mass.

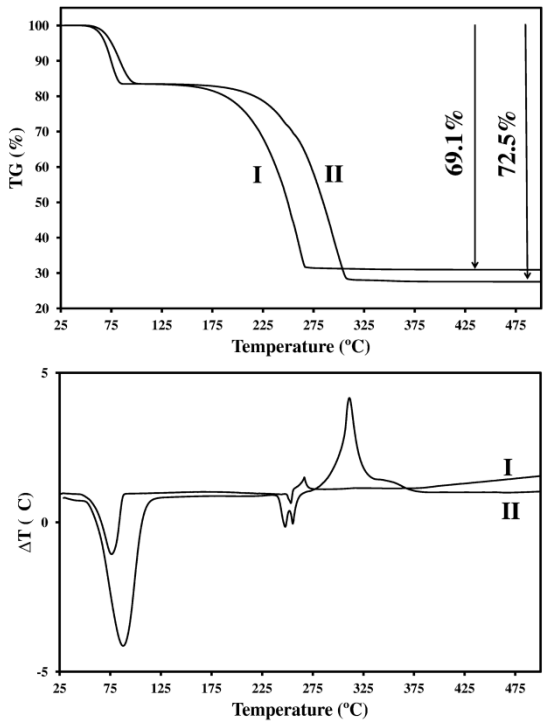

Figure 5.57. TGA-DTA on zinc acetate dihydrate in air. (I) heating rate: 1 °C min^{-1} and (II) heating rate 5 °C min^{-1}.

TGA-DTA experiments, **Figure 5.57**, showed that pure zinc acetate dihydrate undergoes dehydration to form anhydrous Zn(**Ac**)$_2$ with an associated 16.6% mass loss (*c.f.* a theoretical value of 16.4%) at ~50-100 °C. Endothermic peaks at ~250 °C are assigned to the melting of Zn(**Ac**)$_2$, which then undergoes decomposition and/or volatilisation with an exothermic peak located at ~310 °C. The overall theoretical mass loss for the decomposition of zinc acetate dihydrate to ZnO is 62.9% but in a similar fashion to the zinc hydroxy acetate experiments, more than expected mass loss values were observed, which are attributed to the volatilisation of zinc-bearing materials. TGA experiments with zinc acetate dihydrate with heating rates of 1 and 5 °C min^{-1} reveal extra mass loss values of 6.2% and 9.6%, respectively. Although the decomposition of pure zinc acetate may proceed differently to that generated during the decomposition of zinc hydroxy acetate, there is sufficient evidence to conclude that volatile species are evolved during the calcination of zinc hydroxy acetate as well. Including this extra mass

loss component of 6.2 - 9.6% of the ~20% of the ZnO formed *via* Zn(**Ac**)$_2$ into TGA calculations to determine *n,* the waters of hydration, it is concluded that *n* = 2. In addition, this finding may have industrial significance.

Evidence for the formation of sublimate

To prove that the evolution of zinc-containing sublimate upon heating was responsible for the excess mass loss, a separate experiment was conducted in a sublimation apparatus according to **Figure 5.58**. BZA was dehydrated/dehydroxylated at 150 °C for 1 hour and then the sample was transferred to the sublimation apparatus under vacuum and was isothermally heated at ~350 °C for 4 hours. During this time, gas was evolved while the colour of the precursor also changed from white to brown/grey. Droplets were observed on the cold surface cooled by water. These droplets disappeared over time under vacuum. At the same time of the formation of droplets, a whitish sublimate was deposited in the apparatus.

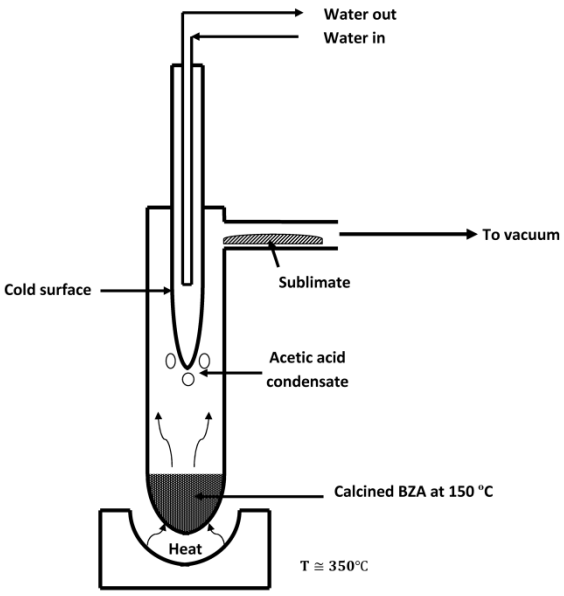

Figure 5.58. Sublimation apparatus to trap the volatile zinc-bearing material.

The sublimate and decomposed end-product were collected and analysed by XRD and SEM. The non-volatile product was ZnO as expected (see Appendix, **Figure A. 7**). TGA was also done on the remaining ZnO and showed mass loss of around 0.6% up to 1000 °C (see Appendix, **Figure A. 8**). The sublimate was crystalline and its XRD pattern matched that of a mixture of Zn**Ac**$_2$ (JC-PDF 00-001-0089) and Zn**Ac**$_2$·2H$_2$O

(JC-PDF 00-033-1464), **Figure 5.59**. SEM images of the sublimate are shown in **Figure 5.60**.

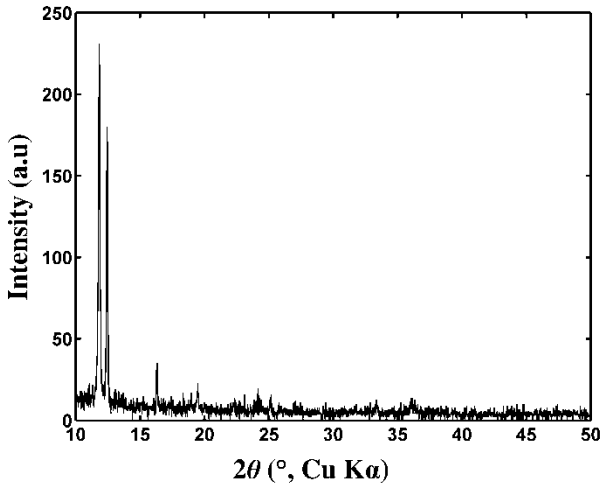

Figure 5.59. XRD of the sublimate collected during thermal decomposition of dehydrated BZA.

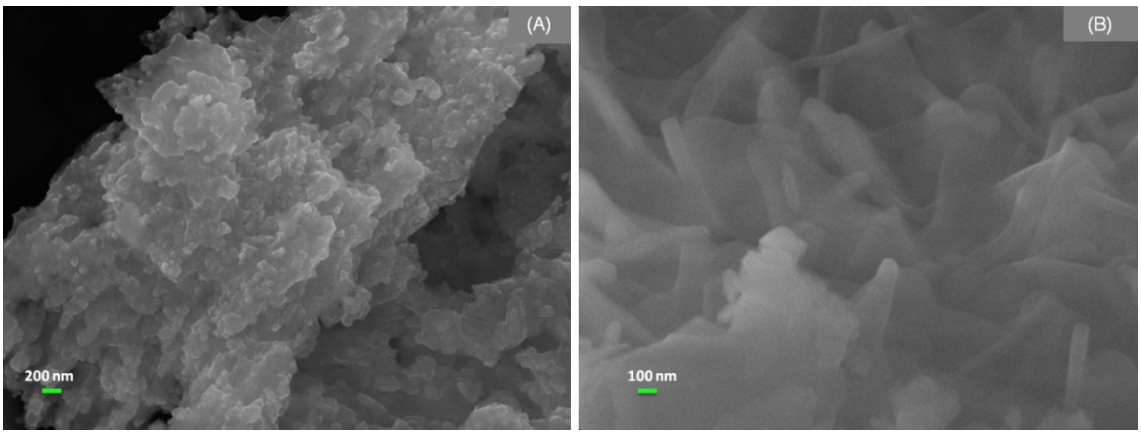

Figure 5.60. SEM images of the sublimate.

It is reported that zinc oxy-carboxylates can react with carboxylic acids to produce neutral salts of zinc [439] according to the Reaction **5.37**.

$$Zn_4O(CH_3CO_2)_6 + 2CH_3CO_2H \rightarrow 4Zn(\mathbf{Ac})_2 + H_2O \qquad 5.37$$

In this work, presence of volatile compound $Zn_4O(CH_3CO_2)_6$ could not be shown; rather zinc acetate was collected. Nevertheless it is assumed that the sublimate deposited was originally $Zn_4O(CH_3CO_2)_6$, and that this was converted to zinc acetate

during exposure to acetic acid vapour formed in the system afterwards according to Reaction **5.37**.

Mechanism

Based on experiments in this work, the thermal decomposition of zinc hydroxy acetate dihydrate to ZnO is suggested to follow the **Scheme 5.4**.

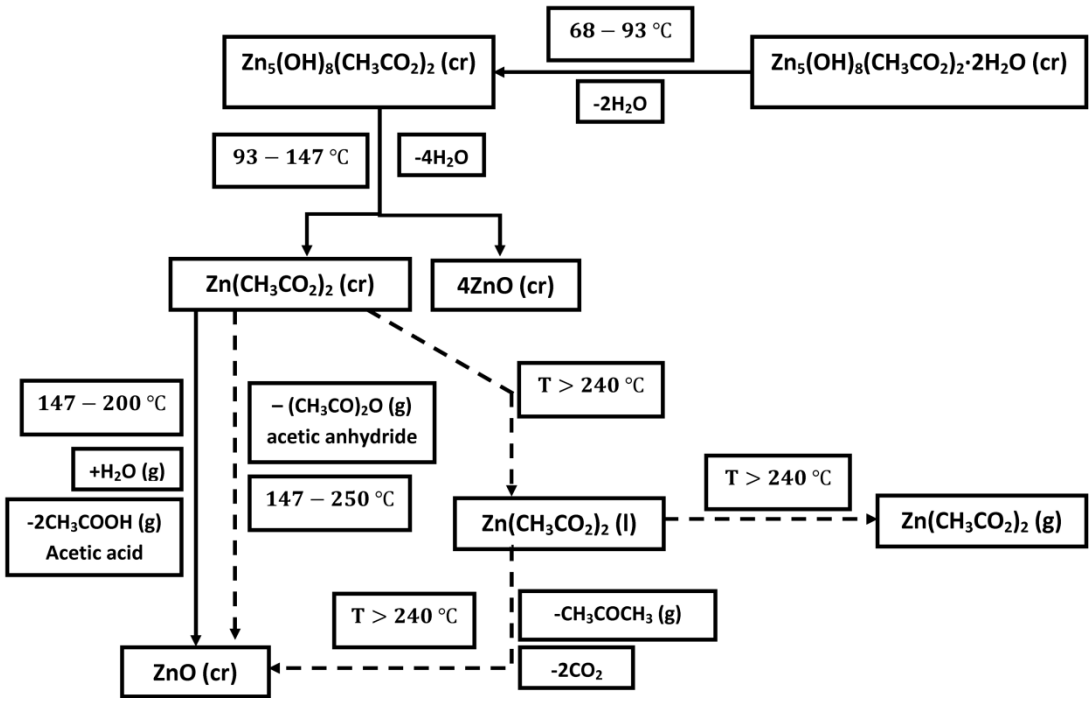

Scheme 5.4. Schematic of suggested mechanism for thermal transformation of BZA·$2H_2O$ to ZnO. Dotted arrows show side reactions.

Reactivity of zinc hydroxy acetate dihydrate with ethanol

As described before, various synthesis methods for zinc hydroxy acetate are reported in the literature, some of which make use of alcohols. It was noticed in the course of this work that non-aqueous reaction media might have a significant effect on the product of the reaction. This issue was investigated further by a reaction between BZA and ethanol according to the experimental section. The identity of the product was investigated by the following methods.

- ***X-ray Diffraction***

XRD, **Figure 5.61** (see also Appendix, **Figure A. 9**), showed that after the reaction between BZA and ethanol, the peak associated with the interlayer distance at about 1.34 nm is diminished and new peaks associated with ZnO are formed. Nevertheless the minor peak associated with *d*-spacing at around 1.75 nm can still be observed. Effect of drying the products by two independent techniques i.e. (1) at 50 °C under the reduced pressure and (2) freeze-drying for 24 hours was also investigated to ensure the product is free of surface-adsorbed ethanol (see Appendix, **Figure A. 9**). Here, it is shown that in contrast to previous report [424] on the presence of surface-adsorbed alcohols in the materials made via the so-called *"Chimie douce"* methods, alcohol is not just physically adsorbed on the particles; rather new materials with different chemical compositions may be formed.

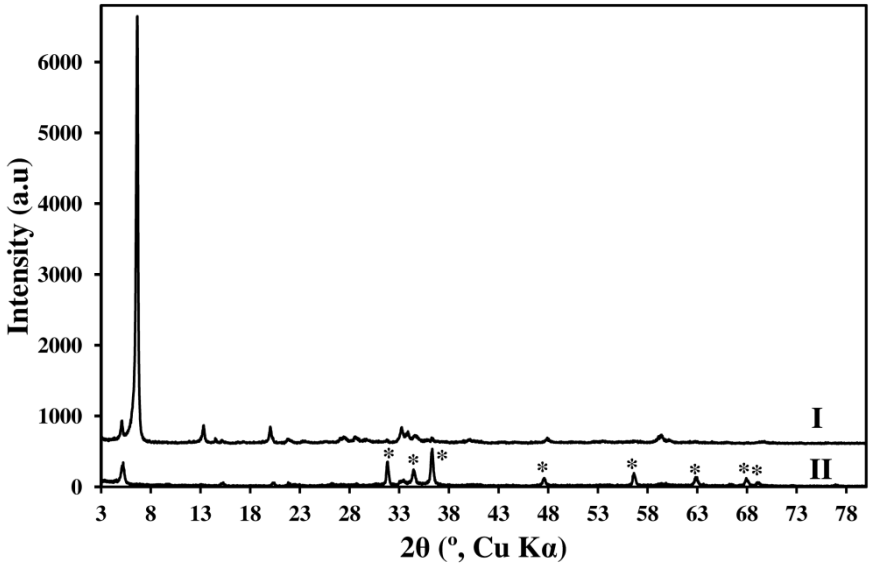

Figure 5.61. XRD on (I) BZA and (II) the freeze-dried product of the reaction between BZA and ethanol. Peaks marked with '*' correspond to ZnO (JC-PDF 01-089-0510).

- ***TGA-DTA***

TGA, **Figure 5.62**, showed that the total mass loss value for the product is 20.3%, which is decreased significantly compared to that of BZA (37.4%). There is around 0.9% mass loss up to the temperature of 110 °C. A dehydration stage cannot be detected for this material. Between 110-150 °C, a sharp mass loss of around 7.5% is observed.

This is associated with an endothermic peak at 133 °C, **Figure 5.63**. Further heating up to around 190 °C results in ~6.6% mass loss, which is associated with a small and broad endothermic peak centred at 183 °C. Between 190-400 °C a further mass loss of around 4.5% is observed. There is a broad exotherm centred at 197 °C. From TGA-DTA data, it can be concluded that the product is dehydrated.

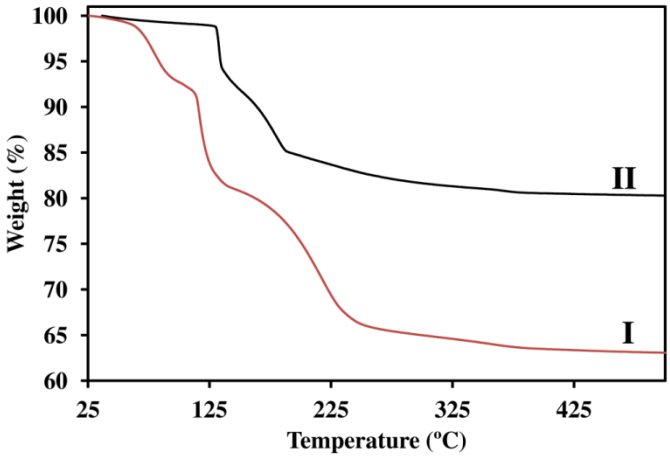

Figure 5.62. TGA on (I) BZA and (II) the freeze-dried product of the reaction between BZA and ethanol.

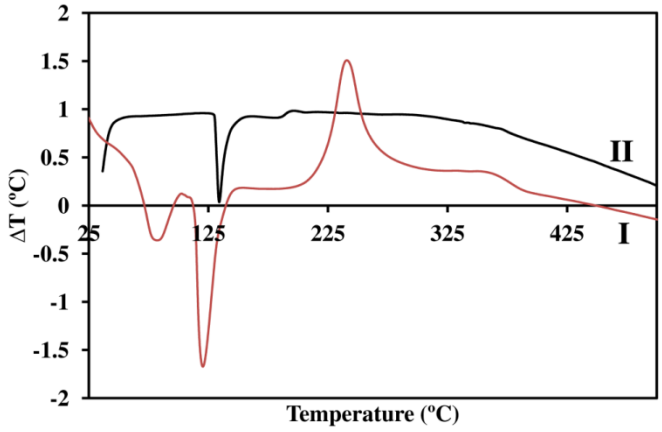

Figure 5.63. DTA on (I) BZA and (II) the freeze-dried product of the reaction between BZA and ethanol.

From XRD data, it was shown that the product of the reaction between BZA and ethanol contains an amount of ZnO. This is consistent with the TGA data that shows a lower mass loss value as opposed to that of $Zn_5(OH)_8(\mathbf{Ac})_2$. Total theoretical mass loss value of $Zn_5(OH)_8(\mathbf{Ac})_2$ is 30%, if there is no sublimation process involved. However, because of the probable involvement of sublimation process for the product, it is

difficult to calculate the exact ZnO : $Zn_5(OH)_8(\mathbf{Ac})_2$ ratio from the total mass loss values. Nevertheless by the knowledge gained on the decomposition mechanism of BZA, here a slightly different method was applied to obtain the mass ratio of ZnO : $Zn_5(OH)_8(\mathbf{Ac})_2$. Mass loss of the first decomposition stage of $Zn_5(OH)_8(\mathbf{Ac})_2$ that releases four moles of water can be used to calculate the ZnO : $Zn_5(OH)_8(\mathbf{Ac})_2$ ratio. This stage is independent from the possible sublimation processes that may occur at higher temperatures. The formula below is applied in the temperature range of 110-150 °C where X% is the mass fraction of $Zn_5(OH)_8(\mathbf{Ac})_2$ in the sample.

$$X\% = \frac{Observed\ mass\ loss\ (\%)\ at\ 110-150\ °C}{Theoretical\ mass\ loss\ (\%)\ of\ pure\ material\ at\ 110-150\ °C} \times 100$$

Theoretical mass loss of pure $Zn_5(OH)_8(\mathbf{Ac})_2$ for this stage of reaction is around 12.4%. Here, only 7.5% mass loss was observed in this temperature range. The difference is because of the presence of ZnO in the product. The ratio of observed mass loss value for the product to the theoretical value is calculated to be 60.5%. From these data, the mass ratio of ZnO : $Zn_5(OH)_8(\mathbf{Ac})_2$ is calculated to be 39.5 : 60.5.

- ***Raman Spectroscopy***

Raman spectra on BZA and the product of the reaction between BZA and ethanol that is freeze-dried for 24 hours were recorded, **Figure 5.64**. Peaks located at around 2935 cm^{-1} are associated with symmetric CH_3 stretch [432]. Peaks centred at around 940 cm^{-1} are associated with C–C stretching [440]. A sharp peak located at 438 cm^{-1} in the spectra of the product of the reaction between BZA and ethanol corresponds to a nonpolar optical phonon E_2 (high) of ZnO [441]. Raman data is consistent with XRD data, which shows the presence of ZnO.

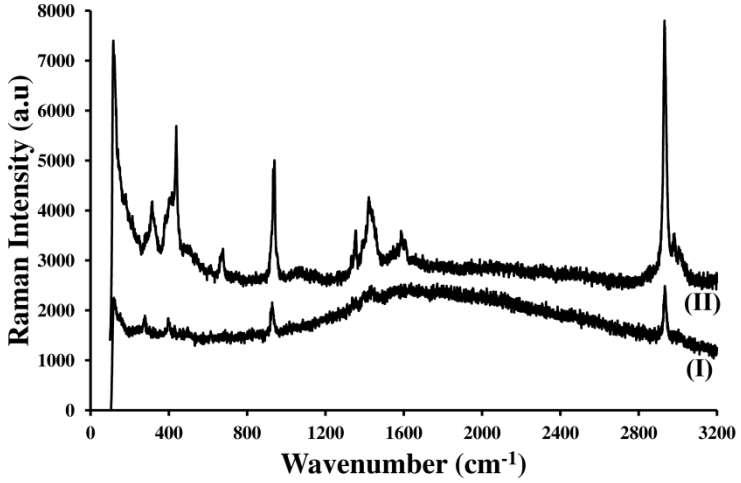

Figure 5.64. Raman spectra corresponding to (I) BZA and (II) product of the reaction between BZA and ethanol, freeze-dried for 24 hours.

- ***FTIR Spectroscopy***

FTIR spectra on the product of the reaction between BZA and ethanol that is freeze-dried for 24 hours was recorded, **Figure 5.65**. Comparison between the spectra of BZA and that of the product of the reaction with ethanol shows changes in the FTIR pattern especially in the regions of 430-470 cm^{-1} and 1300-1700 cm^{-1}. Peak centred at 437 cm^{-1} is assigned Zn–O stretching vibration [441]. Peaks located at 1614, 1583 and 1550 cm^{-1} are assigned to COO^- antisymmetric stretch and peaks located at 1456, 1419 and 1400 are assigned to COO^- symmetric stretch. Corresponding frequency separation between the COO^- antisymmetric and symmetric stretches ($\Delta\nu_{a-s} = \nu_a (COO^-) - \nu_s (COO^-)$) are 158, 164 and 150 cm^{-1}, respectively. As can be noticed, other than 158 cm^{-1}, there are two new frequency separation values for this material, one of which is greater and the other is smaller than 158 cm^{-1}. The 164 cm^{-1} frequency separation is equal to the value reported for sodium acetate. This suggests that ionic carboxylate bonding might be involved in this material. Also the value of 150 cm^{-1} suggests a chelating mode in the structure. Therefore the material might have at least three types of carboxylate bonding. However, as explained before for the BZA, resolution of this issue cannot be achieved based only on FTIR. As a result a solid-state NMR was also combined with FTIR.

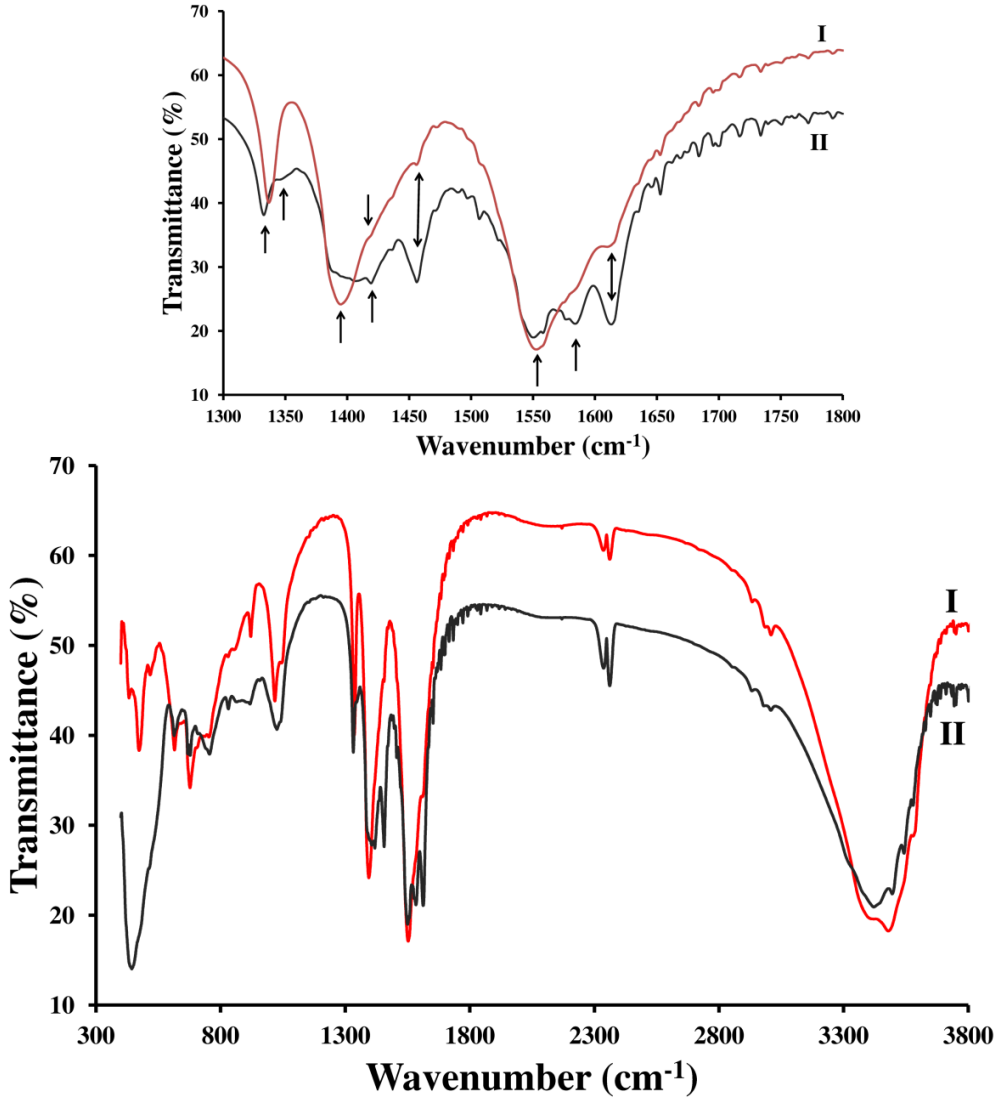

Figure 5.65. FT-IR spectra corresponding to (I) BZA and (II) product of the reaction between BZA and ethanol, freeze-dried for 24 hours.

- ***CP-MAS ^{13}C NMR***

NMR spectrum of the product of the reaction between BZA and ethanol is shown in **Figure 5.66** (see also Appendix). In contrast to the spectrum of BZA, **Figure 5.50**, that shows only two major peaks located at around 180 ppm and 25 ppm, the spectrum of the product of the reaction between BZA and ethanol, shows extra peaks in each region. Nevertheless the locations of the signals are in the same region associated with methyl (0-45 ppm) and carbonyl (160-190 ppm) groups [442]. No signal corresponding to ethoxy group in the range of 60-110 ppm [442] was detected.

Five signals assigned to resonances of the carbonyl carbon were detected: 177.6, 178.3, 181, 181.5 and 182.7 ppm. Also four signals assigned to resonances of the carbon atom associated with CH_3 were detected: 24.5, 25.4, 26.3 and 26.8 ppm. The signal at 182.7 ppm suggests the presence of chelating coordination mode for the carbonyl group whereas a resonance at 177.6 ppm suggests a unidentate mode [412]. The intermediate signals show bidentate bridging state or a combination of modes. This finding confirms the presence of acetate in the material but with different types of coordination modes compared to BZA.

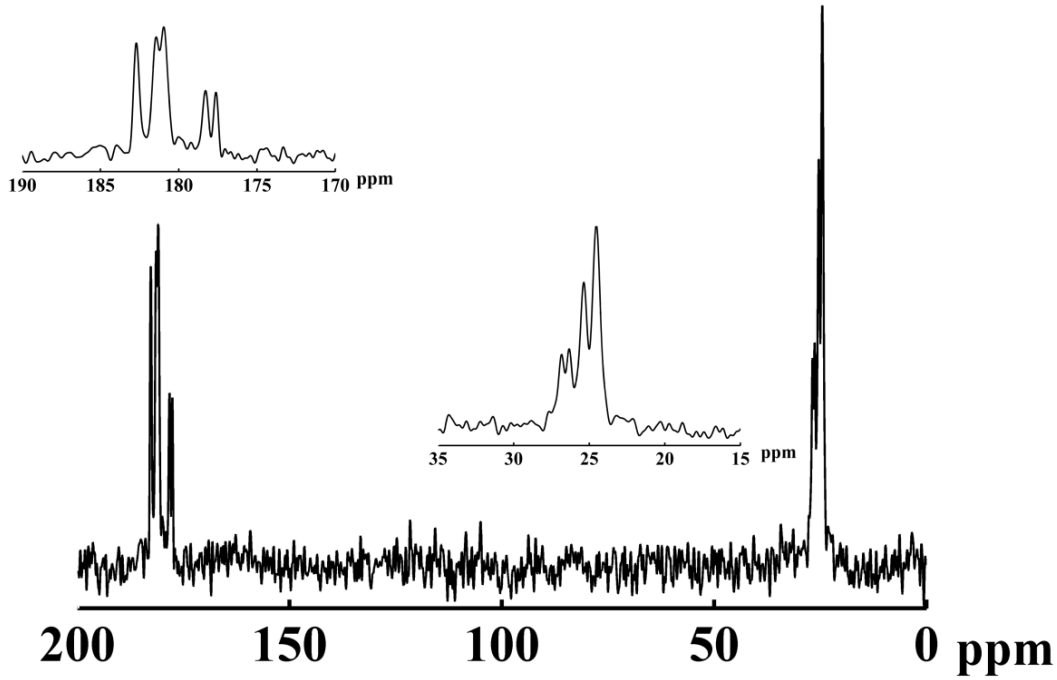

Figure 5.66. CP-MAS ^{13}C NMR spectrum of the product of the reaction between BZA and ethanol, freeze-dried for 24 hours.

Further work is required to clarify the mechanisms of such reactions. As can be seen, reactions of such organo-zinc clay complexes are quite complicated. Nevertheless, in the course of such reaction, ZnO is formed. This suggests novel materials and methods for engineering zinc oxide properties. But also methods that used alcohols to form zinc hydroxy acetate may be problematic.

5.3.6. Comparison

Thus far, in this chapter, synthesis of five zinc hydroxy salts i.e. carbonate, sulphate, chloride, nitrate and acetate have been explained. Thermal treatment of each salt has been also studied as a means for the production of zinc oxide crystallites. In the course of this work, it was noticed that the properties of the as-synthesised ZnO, is significantly affected by the nature of the precursor salt.

Here a comparison study using TGA and XRD is provided. Also RT fluorescence emission spectra of the ZnO samples produced from the same precursors are compared.

TGA

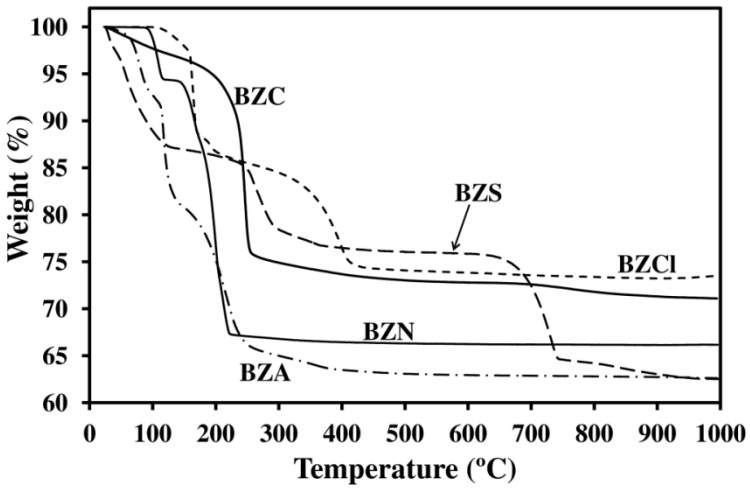

Figure 5.67. TGA in air on basic zinc salts with heating rate of 5 °C min^{-1}.

TGA-DTA on zinc hydroxy carbonate, sulphate, chloride, nitrate and acetate were previously studied in details under the relevant sections. However comparison of TG behaviour of these salts, **Figure 5.67**, provides a complete outlook on the decomposition patterns to form ZnO product. Although ZnO can be produced from any of these precursors, the temperature of decomposition plays a significant role in the formation of ZnO particles. Pure ZnO can only be formed from BZS at temperatures as high as ~900 °C. On the contrary, conversion of BZN into ZnO undergoes completion at temperatures as low as ~200 °C. ZnO from other basic salts can be formed in the intermediate range of temperatures. This is technologically quite important because

thermal decomposition behaviour directly influences the energy consumption for the production of ZnO. It must also be noted that the products made from each individual route are quite different from each other in terms of morphology, specific surface area, etc. This provides a benchmark against which ZnO with specific properties can be tailored.

XRD

X-ray diffraction patterns on the precursor basic zinc salts have been compared, **Figure 5.68** and Appendix (**Figure A. 11**).

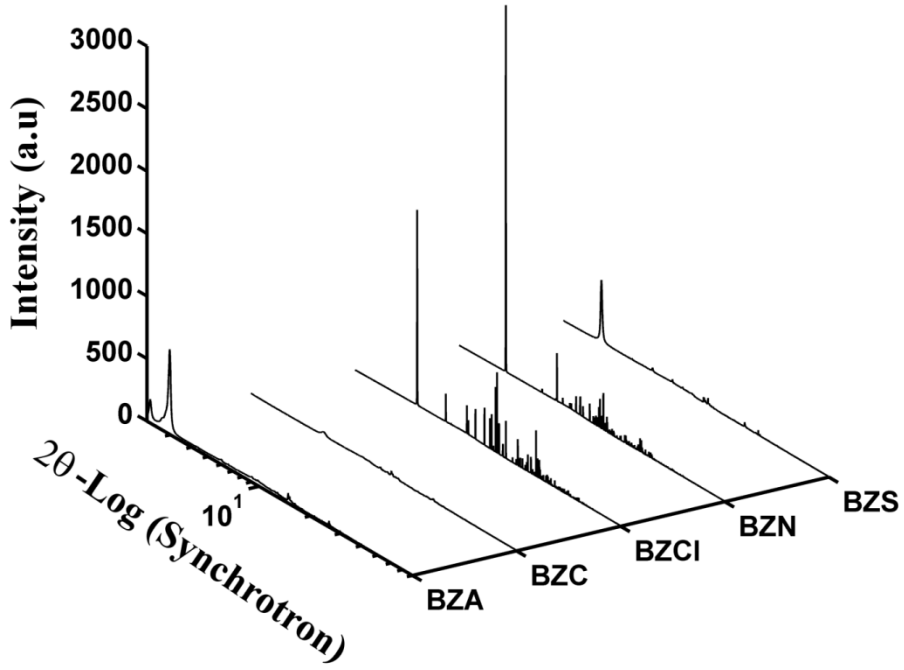

Figure 5.68. XRD (synchrotron) on the precursor basic zinc salts.

Full width at half maximum (FWHM) value was measured from the XRD data using Topas software. FWHM associated with BZC was shown to be the highest among the FWHM values associated with basic zinc salts studied here. Synchrotron XRD patterns of the ZnO materials at the maximum experimental temperatures have been also compared, **Figure 5.69**. FWHM values associated with the zinc oxide samples were also compared. It was shown that FWHM value for the zinc oxide made from BZC is

the highest among FWHM values for the ZnO samples studied here. This suggests that the particle size of the zinc oxide produced from BZC is the lowest compared to the zinc oxide products made from other basic zinc salts. This also indicates that to form a relatively high surface area ZnO, selection of BZC is the most appropriate option. On the contrary, to form lower surface area ZnO, other basic zinc salts can be selected.

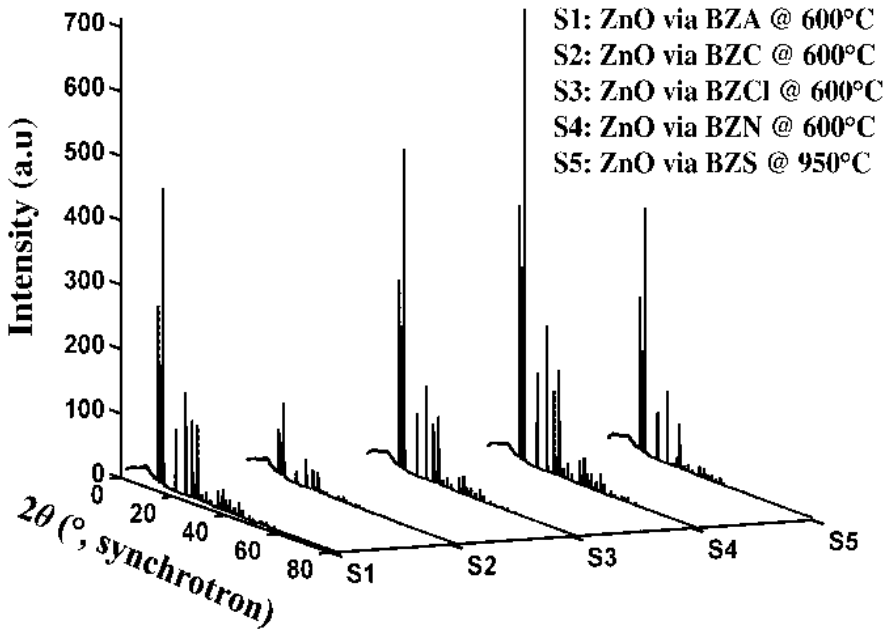

Figure 5.69. XRD (synchrotron) on the end-products of the corresponding basic zinc salts at the maximum temperature during synchrotron radiation study. (Data have been normalised to beam intensity here and everywhere else in this thesis).

Fluorescence spectroscopy

Room temperature fluorescence emission spectra on the ZnO samples produced from abovementioned precursor salts and a Zn:ZnO phosphor sample as a control were recorded after being excited at 280 nm and 310 nm, see **Figure 5.70** and **Figure 5.71**, respectively.

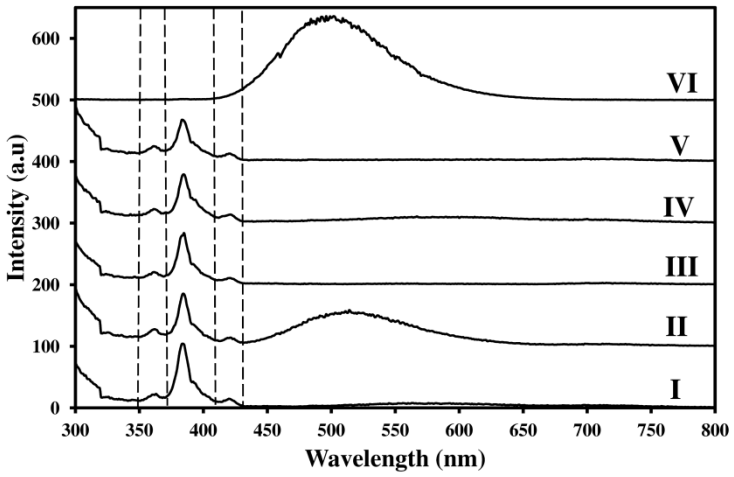

Figure 5.70. Fluorescence emission spectra of ZnO powder samples made from: (I) basic zinc carbonate at 300 °C; (II) basic zinc sulphate at 900 °C; (III) basic zinc acetate at 400 °C; (IV) basic zinc nitrate at 400 °C; (V) basic zinc chloride at 600 °C. (VI) is emission spectrum of commercial Zn:ZnO phosphor as a control. Excitation wavelength = 280 nm, excitation slit width = 5 nm (little steps at 460 and 570 nm are artefacts due to filter changes).

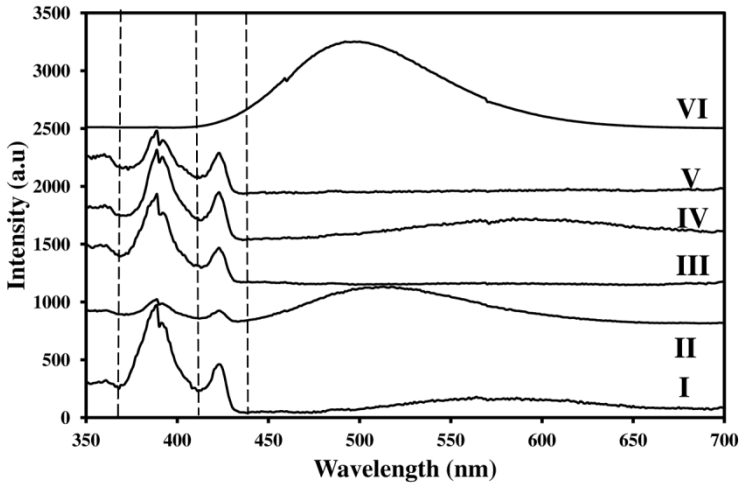

Figure 5.71. RT fluorescence emission spectra of ZnO powder samples made from: (I) basic zinc carbonate at 300 °C; (II) basic zinc sulphate at 900 °C; (III) basic zinc acetate at 400 °C; (IV) basic zinc nitrate at 400 °C; (V) basic zinc chloride at 600 °C. (VI) is the emission spectrum of commercial Zn:ZnO phosphor as a control. Excitation wavelength = 310 nm, excitation slit width = 5 nm (little steps at 460 and 570 nm are artefacts due to filter changes).

Significant changes occur when the method of production of ZnO is changed. ZnO made from BZS shows relatively higher ratio of green-band emission to the band-gap

emission when excited at 310 nm compared to the other ZnO samples. All the samples made from basic zinc salts show more than a single peak in the near-UV band and violet band. No emission peak lower than 450 nm has been observed for the Zn:ZnO phosphor, which is used as a control. Changing the excitation wavelength from 280 nm to 310 nm was shown to have effect on the emission patterns of the samples. Importantly it was indicated that higher production temperatures do not necessarily decrease the ratio of green band emission to the band-gap emission. This is shown for the oxide made from BZS at 900 °C. Relative intensity of the green band emission to the band-gap emission for the oxides made from BZCl and BZA is negligible.

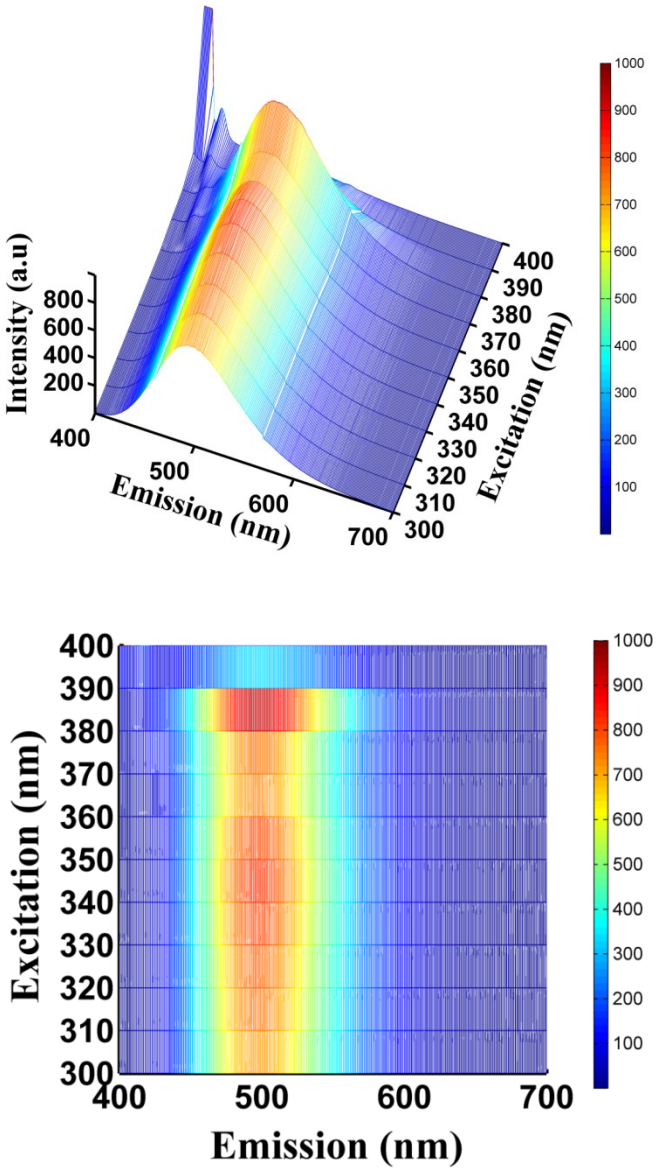

Figure 5.72. Colour-coded (top) 3D contour and (bottom) 2D top RT fluorescence emission spectra of Zn:ZnO phosphor *vs.* excitation wavelength from 300 to 400 nm.

In addition, a range of excitation wavelengths from 300 nm to 400 nm has been applied to the Zn:ZnO phosphor sample and the emission spectra were recorded at RT, **Figure 5.72**. This shows the relation between the excitation wavelength and emission spectra for this sample. This experiment was performed to show that at excitation wavelengths between 300 to 360 nm, emission peak at around 420 nm, which is seen for zinc oxide samples, does not exist.

As can be seen, broad emission band centred at around 500 nm is essentially present while the powder is excited from 300 nm to 380 nm. The emission at 500 nm peaks at excitation wavelength of 380 nm after which this emission disappears.

BET specific surface area

Specific surface area of the ZnO samples has been found to be correlated to the precursor salt. This is shown in **Table 5.6**. The highest BET surface area is associated with the ZnO made from BZC whereas the lowest surface area ZnO is made via BZS.

Table 5.6. BET specific surface area of the ZnO powder samples *vs.* precursor salt and calcination temperature.

Precursor zinc hydroxy salt	Calcination temperature (°C)	BET specific surface area (m^2/g) of as-made ZnO
BZC	250-350	47-65
BZS	900	0.7
BZCl	600	1.3
BZN	300	1.6
BZA	400	15.4

5.4. Conclusions

Zinc hydroxy carbonate, sulphate, chloride, nitrate and acetate have been synthesised in aqueous systems and were used as precursors for the production of ZnO particles by clacination. Combination of TGA-DTA, XRD, MS and BET surface area measurement, SEM, TEM, Raman and FTIR spectroscopy, CP-MAS ^{13}C NMR and RT fluorescence spectroscopy have been applied to characterise the precursors, intermediate materials

and end-products, to investigate the thermal decomposition mechanism of the basic zinc salts into ZnO and also to study some of the properties of the materials. It was observed that nature of the precursors has a major role in the nature of the end-product zinc oxides. Interestingly, for each individual precursor, a unique thermal decomposition mechanism has been detected. XRD comparative study revealed that the highest FWHM value for zinc oxide products studied here is related to the sample produced from BZC. This suggests the relatively lower crystallite size for this material. This ZnO sample has a high porosity and specific surface area as high as 65 m^2/g in the current work. On the other hand ZnO samples made from BZS, BZCl and BZN show bigger crystallite size and have low specific surface area (less than 2 m^2/g). ZnO nano-particles made from BZA are 20-100 nm in size. This grade shows intermediate surface area of 15 m^2/g (higher than that of the French process ZnO but lower than that of the active ZnO). Different fluorescence emission patterns have been also observed for each individual ZnO sample. Influence of ethanol on BZA was also studied, which provided important knowledge about the coordination types of acetate group in the interlayer distance and also possible changes in the structure of BZA precursor when non-aqueous media are applied during formation of this precursor. This finding is promising and suggests novel zinc-bearing precursors for production of zinc oxide particles.

In this chapter production of ZnO by the calcination of appropriate precursors was explored. I showed that the properties of the ZnO could be controlled by various means. This information might be helpful for the industrial manufacture of ZnO by this route.

Chapter 6

Mechanistic and Kinetic Aspects of the Solid/liquid Pathway for the Formation of Zinc Hydroxy Nitrate

Chapter 6: Mechanistic and Kinetic Aspects of the Solid/liquid Pathway for the Formation of Zinc Hydroxy Nitrate

6.1. Introduction

In the previous chapter, synthesis and some properties of zinc hydroxy carbonate, sulphate, chloride, nitrate and acetate were explained. These salts are important industrial materials in their own right as explained before, however they can also be used as precursors for the production of zinc oxide.

In the comparative study of the decomposition of the basic zinc salts presented in the previous chapter, important details have been revealed. It was shown that, amongst the five basic zinc salts that were studied, zinc hydroxy nitrate has the lowest temperature of decomposition for the complete formation of zinc oxide. This provided new insight into this material as a possible precursor for zinc oxide production. Therefore complementary work was done on this specific material to determine in greater detail the mechanism by which it was synthesised by the solid/liquid reaction used.

Layered double hydroxides (LDH) are important complexes with general formula of $[M^{II}_{1-x}M^{III}_{x}(OH)_2]^{x+}[A^{n-}]_{x/n}\cdot mH_2O$, where M^{II} and M^{III} are di- and trivalent metal respectively, and A^{n-} is an anion such as nitrate [370]. These complexes are categorised as anionic clays and consist of stacks of positively charged layers balanced in charge by intercalation of exchangeable anions located in the interlayer distance together with water of hydration [345].

A very similar structure also exists, which is called hydroxy double salt (HDS) with a general formula of $[M^{II}_{1-x}M'^{II}_{1+x}(OH)_{3(1-y)}]^{+}[A^{n-}]_{(1+3y)/n}\cdot mH_2O$ where two divalent cations are involved. HDS can be explained as a modified form of LDH where trivalent cations are replaced by divalent ones [373]. It is also possible to have a structure where M and M′ cations in HDS are the same. In this case a layered compound is formed with a general formula $[M(OH)_{2-x}][A^{n-}]_{x/n}$ that is also known as *basic* salt [345].

In the case of zinc and nitrate four forms of zinc hydroxy nitrate have been reported: (1) $Zn_5(NO_3)_2(OH)_8\cdot 2H_2O$; (2) $Zn_5(NO_3)_2(OH)_8$; (3) $Zn_3(NO_3)_2(OH)_4$ and (4) $Zn(NO_3)(OH)\cdot H_2O$ with the latter not holding a layered structure [398] that correspond

to x = 0.4 for (1) and (2), x = 0.66 for (3) and x = 1 for (4) considering the general formula above.

Here the first basic zinc nitrate, $Zn_5(NO_3)_2(OH)_8 \cdot 2H_2O$ was considered. In the crystal of this complex, two of the zinc atoms are octahedrally coordinated by six hydroxyl anions and the rest are tetrahedrally coordinated by three hydroxyls and one water molecule. The resulting sheets so formed are positive in charge and are balanced in charge by nitrate anions intercalated in the interlayer distance. Therefore the formula of this complex can also be written as $[Zn^{octa}{}_3[Zn^{tetra}(OH)_3(NO_3)]_2(OH)_2] \cdot 2H_2O$ [345, 443]. This salt can be synthesised by slow evaporation of a zinc nitrate solution [395, 397, 444, 445], by pyrolysis of zinc nitrate hexahydrate [394], by a reaction between zinc oxide and aqueous solution of zinc nitrate [334, 396] or by an equimolar reaction between urea and zinc nitrate solutions [396, 397].

A solid/liquid reaction between a transition metal oxide and its corresponding metal salt is an interesting route to form layered metal hydroxide salts. In this work solid/liquid reactions between zinc oxide and aqueous solution of zinc nitrate were conducted. Although this reaction was first reported by Feitknecht in 1933 [334] and was used thereafter with reference to Feitknecht's method [396, 400], it is surprising that no reports describing the stoichiometry, thermodynamics, kinetics or the mechanism of this reaction seem to have been published. Data concerning the solubility product, K_{sp}, is also absent. In this chapter the solubility of $Zn_5(NO_3)_2(OH)_8 \cdot 2H_2O$ is examined and it is shown that it is reasonably insoluble. This has a significant role in the precipitation mechanism. For comparison, a liquid-liquid reaction between a zinc nitrate solution and sodium hydroxide was also conducted to synthesise zinc hydroxy nitrate.

In this work, an interplay between the kinetics and thermodynamics of the reaction was shown that controls the mechanism of dissolution of zinc oxide and precipitation of the more stable zinc hydroxy nitrate in the slightly acidic condition. It was also revealed that concentration of zinc in solution has an influence on the pH of the system. Polynuclear cationic zinc species are believed to have effect on the hydrolysis reactions, which result in lower than expected pH in zinc nitrate solutions. Concentration of the materials in the system controls the thermodynamics of the system and feasibility of the reaction.

6.2. Experimental

6.2.1. General

Zinc nitrate hexahydrate, zinc oxide powder and sodium hydroxide pellets were purchased from Ajax Chemicals and used as-received. All chemicals were AR grade. Milli-Q (18.2 Ω cm^{-1}) was used as the solvent. Reactions were conducted under atmospheric conditions using a two-neck round bottom flask with a digitally-controlled magnetic heater/stirrer. A magnetic stirrer bar was used at a stirring rate of 820 rpm and isolation of the precipitates was performed by vacuum filtration followed by overnight drying at 60 °C in an oven.

X-ray diffraction, thermogravimetric analysis (TGA) and scanning electron microscopy experiments have been done according to the methods explained in Chapter 2.

Determination of the pH was conducted using a Hanna Instruments, pH211 microprocessor pH Meter and calibration was done using standard buffer solutions supplied from Sigma-Aldrich. Curve fitting was performed using MATLAB version 7.10.0.499 (R2010a).

6.2.2. Synthesis

Aqueous solutions of $Zn(NO_3)_2$ were prepared by dissolving $Zn(NO_3)_2 \cdot 6H_2O$ (with the molar amounts shown in Table 1) in 30 ml of water. The solution was added in a single step to a suspension of ZnO (molar amounts shown in **Table 6.1**) in 70 ml of water in a two-neck round bottom flask. The mixture was stirred for 4 hours at room temperature under atmospheric conditions using a digitally-controlled magnetic heater/stirrer with a magnetic stirrer bar at a rate of 820 rpm. The solid material was isolated from the supernatant solution by vacuum filtration, washed with water and dried at 60 °C in an oven. The solids were characterised by XRD and TGA-DTA. The solids isolated from Reactions A, B and C yielded zinc hydroxy nitrate $[Zn_5(NO_3)_2(OH)_8 \cdot 2H_2O]$ together with amounts of ZnO. No $[Zn_5(NO_3)_2(OH)_8 \cdot 2H_2O]$ was detected in the solids from Reaction D.

Table 6.1. Mole ratios of the reactants and pH data.

Reaction	ZnO (mol)	$Zn(NO_3)_2$ (mol)	pH of $Zn(NO_3)_2$ solution	ZnO/$Zn(NO_3)_2$ (mol/mol)	pH of ZnO suspension
A	0.09	0.09	2.85	1 : 1	7.16
B	0.045	0.09	2.85	1 : 2	6.6
C	0.09	0.045	3.2	2 : 1	7.16
D	0.09	0.0225	3.65	4 : 1	7.16

The filtrate from Reaction A from the above procedure was examined separately. Aqueous sodium hydroxide was added dropwise to the filtrate until a pH of 6.5 was obtained. A white precipitate formed, which was collected immediately by filtration, washed with water and dried at 60 °C. The solid was characterised by XRD and TGA-DTA and found to be pure $Zn_5(NO_3)_2(OH)_8 \cdot 2H_2O$. This material was then used for the determination of the solubility.

6.2.3. Kinetics

Separately, a reaction with the same conditions explained in Section 2.2 was repeated. In the course of this reaction, at times 2, 5, 10, 15, 20, 30, 40, 50, 60, 90, 120, 180 and 240 minutes between 1 to 2 ml of samples were pipetted, filtered and washed immediately with Milli-Q water to separate the precipitate from the unreacted species.

Using the reaction conditions described for Reaction A above, aliquots of ~2 mL were collected at intervals of 2, 5, 10, 15, 20, 30, 40, 50, 60, 90, 120, 180 and 240 minutes. The samples were filtered and the collected solids washed immediately with water. A sample was also obtained from a reaction where stirring was stopped after 4 hours and the mixture was allowed to stand for 72 hours. The solids were characterised using XRD and TGA-DTA.

6.2.4. Determination of solubility of zinc hydroxy nitrate

Pure [$Zn_5(NO_3)_2(OH)_8 \cdot 2H_2O$] (0.0208 g, 3.34×10^{-5} mol) was added to 100 ml of water in a volumetric flask. The suspension was shaken vigorously and sonicated. It was

allowed to stand overnight. The mixture was filtered twice (Whatman grade 42). A blank Milli-Q water sample was also prepared using the same procedures.

Nitrogen concentrations (nitrate) were measured using a Lachat Instruments-QuikChem 8500 Flow Injection Analysis System. Standard potassium nitrate solutions (with N concentrations 0, 175, 350, 700, 1050 and 1750 μg/L) were used for calibration.

Zinc concentrations were measured using an Agilent Technologies 7500ce series ICP-MS with sample introduction via a micromist concentric nebuliser (Glass expansion) and a Scott type double pass spray chamber cooled to 2 °C. The sample solution and the spray chamber were pumped. The ICP operating parameters and the lens conditions were selected to maximise the sensitivity of a 1% HNO_3:HCl solution containing 1ng/ml of Li, Co, Y, Ce and Tl. Helium was added into the octopole reaction cell to reduce interferences. Calibration curves were constructed and the results analyzed using Agilent Technologies Masshunter software. Zinc stock solution was obtained from Choice Analytical, Thornleigh, Australia. Baseline nitric acid (HNO_3) was purchased from Seastar chemicals, Sidney, Canada. Calibration standards were prepared in 1% nitric acid. Samples were spiked with nitric acid to a level of 1% to matrix match the calibration standards.

6.3. Results and Discussion

6.3.1. Characterisation and stoichiometry of the reaction

Investigation of the stoichiometry of the reaction between ZnO and zinc nitrate is an essential part of this work. It is possible to balance the equation in different ways with various numbers of reactants, products and stoichiometric coefficients. Some hypothetical reactions between zinc oxide and nitrate are shown below. Note that these combinations are only based on a mass balance and some of these reactions and products may not exist at all.

$$ZnO_{(s)} + Zn(NO_3)_2 + H_2O \rightarrow Zn_2(NO_3)_2(OH)_2$$

$$2ZnO_{(s)} + Zn(NO_3)_2 + 2H_2O \rightarrow Zn_3(NO_3)_2(OH)_4$$

$$4ZnO_{(s)} + Zn(NO_3)_2 + 6H_2O \rightarrow Zn_5(NO_3)_2(OH)_8 \cdot 2H_2O$$

$$5ZnO_{(s)} + 5Zn(NO_3)_2 + 15H_2O \rightarrow 2Zn_5(NO_3)_2(OH)_8 \cdot 2H_2O + 6HNO_3$$

$$9ZnO_{(s)} + Zn(NO_3)_2 \cdot 6H_2O \rightarrow 2Zn_5(NO_3)_2(OH)_8 \cdot 2H_2O$$

To investigate the stoichiometry of solid/liquid reaction between zinc oxide and zinc nitrate, aqueous solutions of zinc nitrate were added to suspensions of ZnO in water in the amounts shown in **Table 6.1** (Reactions A-D). The resultant solids were characterised by XRD and TGA-DTA. The filtrate from Reaction A was further reacted with aqueous sodium hydroxide and the resultant precipitate was also characterised by XRD and TGA.

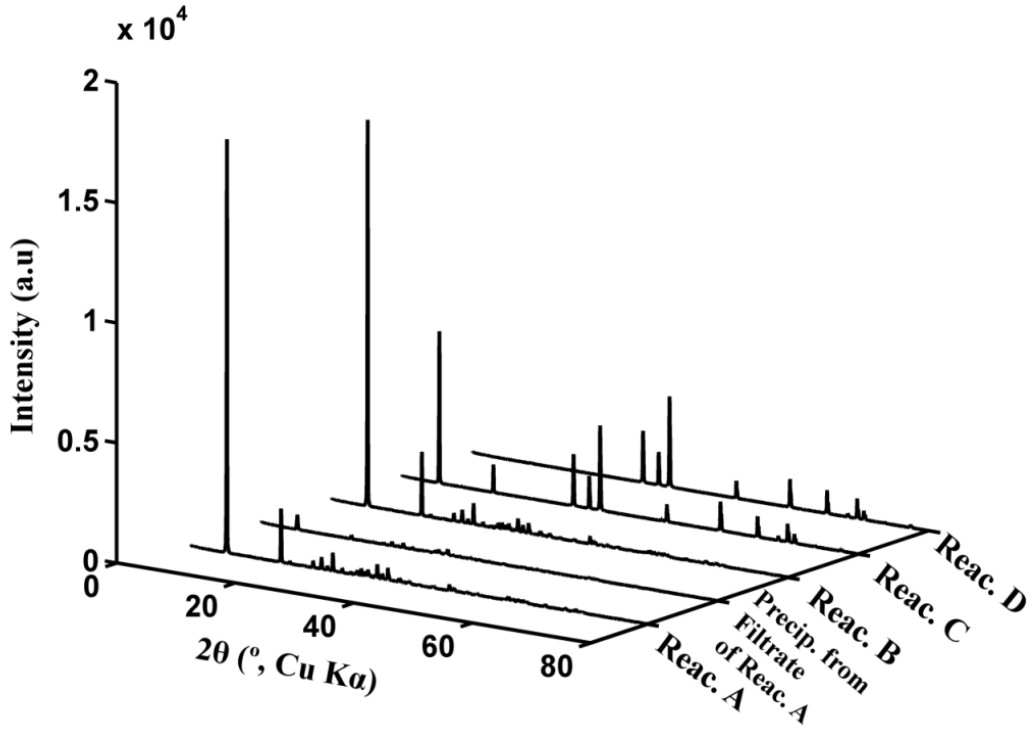

Figure 6.1. XRD on the products of Reactions A - D and the precipitate from the filtrate of Reaction A.

Powder XRD patterns for the solids obtained from Reactions A-D together with the solid obtained from basification of the filtrate of Reaction A are shown in **Figure 6.1**. The diffraction pattern obtained for the solid collected from Reaction D is consistent with pure zinc oxide. The patterns recorded for the products of Reactions A-C are consistent with $Zn_5(NO_3)_2(OH)_8 \cdot 2H_2O$ (JC-PDF 01-072-0627) together with some zinc oxide. The pattern obtained for the material collected upon adding base to the filtrate of Reaction A corresponds to that of pure $Zn_5(NO_3)_2(OH)_8 \cdot 2H_2O$ (JC-PDF 01-072-0627)

although the diffraction peaks are somewhat broader than those of the products collected from the other reactions. This implies a relatively lower crystallinity of this product compared to the others. From this data, it can be concluded that the filtrate of Reaction A still contains unreacted zinc and nitrate. Adding base to the filtrate in a pH-controlled manner leads to the fast formation of pure zinc hydroxy nitrate. This confirms that liquid-liquid route to the formation of zinc hydroxy nitrate is kinetically faster than solid/liquid methods. XRD results limited the possible chemical formula of the hypothetical zinc hydroxy nitrates to $Zn_5(NO_3)_2(OH)_8 \cdot 2H_2O$.

The remaining parameters for determination of the stoichiometry are the other possible by-products and also the stoichiometric coefficients. This will be examined shortly.

Mass losses during thermal treatment of the reaction products were used to determine the conversion of the starting materials to $Zn_5(NO_3)_2(OH)_8 \cdot 2H_2O$. Thermal decomposition of $Zn_5(NO_3)_2(OH)_8 \cdot 2H_2O$ to ZnO results in a mass loss of 34.7%. A mass loss less than this indicates incomplete reaction and the ratio of this value to the theoretical value indicates the conversion of ZnO into $Zn_5(NO_3)_2(OH)_8 \cdot 2H_2O$, which is shown in the formula below where conversion (X%) is a function of time (t):

$$X(t)\% = \frac{Observed\ mass\ loss\ (\%)}{Theoretical\ mass\ loss\ (\%)\ of\ pure\ material} \times 100$$

Note: The ratio of the observed mass loss to the theoretical mass loss during TGA can only be used to calculate the conversion ratio for the reactions where the $ZnO/Zn(NO_3)_2$ molar ratio is less than or equal to 1. For the molar ratios greater than 1, the unreacted ZnO (which is not involved in the reaction) is mixed with the product, which results in the observed mass loss values much less than expected.

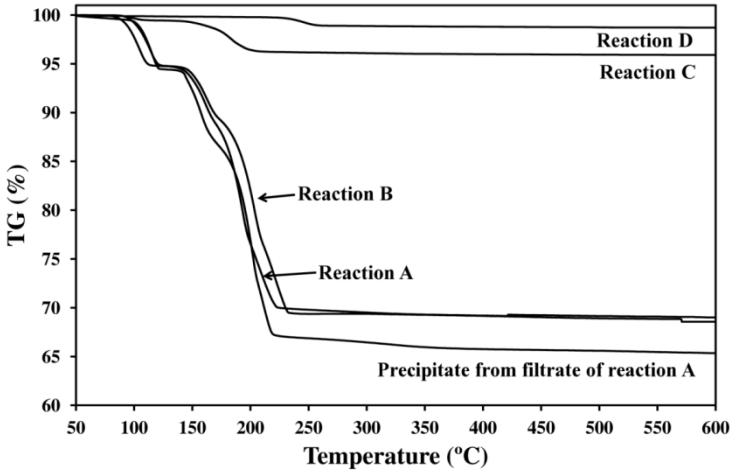

Figure 6.2. TGA of the products of Reaction A-D and the precipitate from the filtrate of Reaction A.

Table 6.2. Reaction data from solid/liquid reactions between ZnO and $Zn(NO_3)_2$.

Reaction	A	B	C	D
$ZnO/Zn(NO_3)_2$ (mol/mol)	1 : 1	1 : 2	2 : 1	4 : 1
pH at t = 0 hr	6.5	6.35	6.45	6.22
pH at t = 4 hr	6.4	5.93	6.29	6.14
Weight recovered (g) after reaction	12.28	6.08	6.93	6.81
Conversion (%)-based on TGA	89.7	91.1	11.2	3.9
Weight of $Zn_5(NO_3)_2(OH)_8 \cdot 2H_2O$ (g)	11.05	5.54	0.78	0.27
Moles of $Zn_5(NO_3)_2(OH)_8 \cdot 2H_2O$	0.0177	0.0089	0.0012	0.0004
Moles of $Zn_5(NO_3)_2(OH)_8 \cdot 2H_2O$ on the basis of 100% conversion	0.0197	0.0098	-	-

TGA data for the solids obtained from Reactions A-D together with the solid obtained from adding base to the filtrate of Reaction A are shown in **Figure 6.2**. In Reaction A, ~90% conversion is achieved after 4 hours reaction time, which is similar to the conversion in Reaction B where the initial amount of ZnO is halved. However, the mass of solid recovered decreased significantly from Reaction A to B (**Table 6.2**). The number of moles of $Zn_5(NO_3)_2(OH)_8 \cdot 2H_2O$ produced by Reaction A is almost twice of that produced by Reaction B (0.0197 moles *vs.* 0.0098 moles) on the basis of 100% conversion of ZnO to $Zn_5(NO_3)_2(OH)_8 \cdot 2H_2O$ (note: number of moles of $Zn_5(NO_3)_2(OH)_8 \cdot 2H_2O$ on the basis of 100% conversion is calculated by dividing the actual number of moles of $Zn_5(NO_3)_2(OH)_8 \cdot 2H_2O$ by the conversion ratio). Data for

Reactions C and D show that increasing the amount of ZnO relative to $Zn(NO_3)_2$ decreases the conversion dramatically.

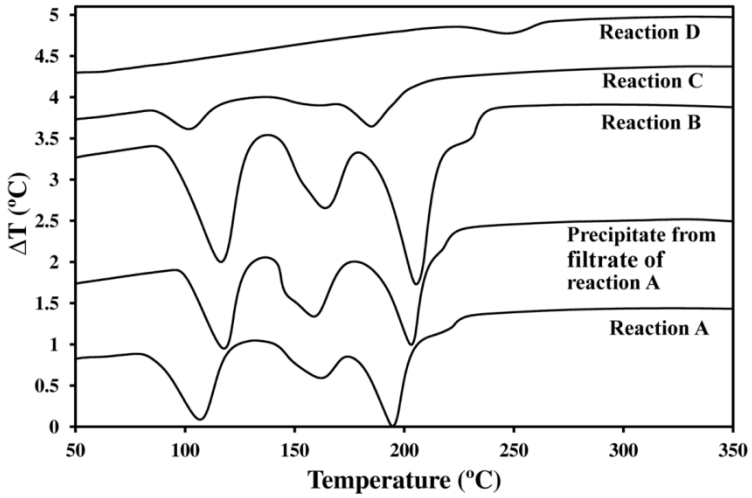

Figure 6.3. DTA of the products of Reaction A to D and the precipitate from the filtrate of Reaction A (graphs are offset for clarity).

TGA experiments on the products of Reactions C and D reveal very little mass loss compared to those of the products of Reactions A and B and the precipitate from the filtrate of Reaction A. This is consistent with the XRD data that indicates that ZnO is the only crystalline material in Reaction D and that the product from Reaction C contains mostly ZnO. DTA data, **Figure 6.3**, reveal that each of the processes associated with the mass losses are endothermic. A single, very small endothermic peak for the product of Reaction D is observed and occurs at a somewhat higher temperature than those of the other products, suggesting a thermally more stable compound than the other reaction products with higher conversion ratios. The XRD data shows only signals associated with ZnO for this product and so the small mass loss is assigned to an amorphous compound, possibly a zinc hydroxy nitrate species product. This is consistent with the products obtained with reaction times less than 30 minutes (see kinetics data below).

In the solid/liquid Reactions A and B, only a fraction of the initial zinc is recovered in the solid product suggesting that a significant amount of zinc remained in the solution. For example in Reaction (A), where 0.09 moles of ZnO and zinc nitrate are used, only ~0.02 moles of $Zn_5(NO_3)_2(OH)_8 \cdot 2H_2O$ was recovered (on the basis of 100% conversion), see **Table 6.1** and **Table 6.2**. This shows that ~0.08 mol of zinc is remained in solution. In Reaction B it was also shown that only ~0.01 moles of

$Zn_5(NO_3)_2(OH)_8 \cdot 2H_2O$ was recovered (on the basis of 100% conversion). This was due to decreasing the number of moles of ZnO to half.

To confirm that zinc remained in solution, the filtrate from Reaction A was reacted with NaOH and a precipitate of $Zn_5(NO_3)_2(OH)_8 \cdot 2H_2O$ was obtained (characterised by XRD and TGA, as discussed above). SEM images of the $Zn_5(NO_3)_2(OH)_8 \cdot 2H_2O$ precipitated from this reaction are shown in **Figure 6.4**. Comparison of this product with those formed from the solid/liquid reactions (see below) indicates that the latter are somewhat more crystalline in nature.

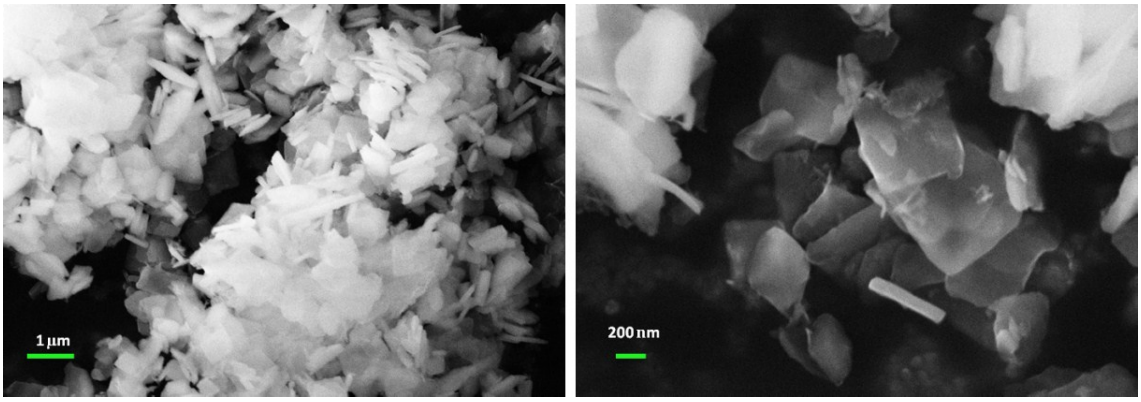

Figure 6.4. SEM images on the zinc hydroxy nitrate precipitated from the filtrate of Reaction A.

Based on the conversion ratio data and the associated reactant ratios, the following overall reaction, Equation **6.1**, for the solid/liquid reaction between ZnO and aqueous zinc nitrate is proposed.

$$9ZnO_{(s)} + 9Zn(NO_3)_{2(aq)} + 19H_2O \rightarrow 2Zn_5(NO_3)_2(OH)_8 \cdot 2H_2O_{(s)} + 8Zn(OH)NO_{3(aq)} + 6HNO_{3\,(aq)} \quad 6.1$$

6.3.2. Thermodynamics

The following equations are involved in this system:

$$Zn(NO_3)_2 \rightarrow Zn^{2+}_{(aq)} + 2(NO_3)^-_{(aq)} \quad 6.2$$

$$aZn^{2+}_{(aq)} + bH_2O \rightleftharpoons Zn_a(OH)_b^{(2a-b)+}{}_{(aq)} + bH^+_{(aq)} \quad 6.3$$

$$Zn^{2+}_{(aq)} + H_2O \rightleftharpoons ZnOH^+_{(aq)} + H^+_{(aq)} \quad 6.4$$

$$2Zn^{2+}_{(aq)} + H_2O \rightleftharpoons Zn_2(OH)^{3+}_{(aq)} + H^+_{(aq)} \quad 6.5$$

$$4Zn^{2+}_{(aq)} + 4H_2O \rightleftharpoons Zn_4(OH)_4^{4+}{}_{(aq)} + 4H^+_{(aq)} \quad 6.6$$

$$ZnO_{(s)} + 2H^+_{(aq)} \rightleftharpoons Zn^{2+}_{(aq)} + H_2O \quad 6.7$$

$$ZnO_{(s)} + H^+_{(aq)} \rightleftharpoons ZnOH^+_{(aq)} \quad 6.8$$

$$5ZnOH^+_{(aq)} + 2(NO_3)^-_{(aq)} + 5H_2O \rightleftharpoons Zn_5(NO_3)_2(OH)_8 \cdot 2H_2O_{(s)} + 3H^+_{(aq)} \quad 6.9$$

Upon dissolving zinc nitrate hexahydrate in water, Equation **6.2**, the zinc species undergo hydrolysis reactions. Zinc hydrolysis reactions are quite complex; a general form of the hydrolysis reactions of Zn^{2+} is shown in Equation **6.3**. Mononuclear $ZnOH^+$ and polynuclear $Zn_2(OH)^{3+}$ and $Zn_4(OH)_4^{4+}$ species have been identified in acidic conditions [289, 446]. The concentration of polynuclear zinc hydroxo-complexes is a function of Zn^{2+} concentration and temperature with the concentration of polynuclear species increasing as zinc concentration increases [79, 289, 446]. Here it is proposed that for zinc concentrations of ~3M, these polynuclear species contribute to the decrease in the pH of the solution due to the hydrolysis Reactions **6.5** and **6.6**.

The system is not in the equilibrium condition immediately after dissolution starts and this state is only reached when hydrolysis Equations **6.4**, **6.5** and **6.6** are complete. The standard Gibbs free energy of hydrolysis Equation **6.4** is positive ($\Delta_r G^\circ$= 42.34 kJ mol^{-1}, calculated from thermodynamic data from [289]). Gibbs free energy of a reaction in non-standard conditions is defined as $\Delta_r G = \Delta_r G^\circ + RT \ln Q_r$ where R is the gas constant (8.314 J mol^{-1} ºK), T is the temperature (ºK) and Q_r is the reaction quotient (for Equation **6.4**: $\frac{[H^+][ZnOH^+]}{[Zn^{2+}]}$). Under non-standard conditions (pH = 2.85 ≡ $[H^+]$ = 1.41×10^{-3} M and $[Zn^{2+}]$ = 3M), $\Delta_r G$ was calculated to be +7.1 kJ·mol^{-1}. Surprisingly the positive value is in contradiction to the experiment data (i.e. the reaction is observed to proceed). Based on Equation **6.4**, the equilibrium concentration of H^+ is calculated to be 3.16×10^{-4} M or pH ≈ 3.5, which is lower than the measured concentration at pH 2.85. The difference in the pH is assigned to contributions from other hydrolysis reactions such as **6.5** and **6.6**, which generate more protons in the system. Calculations for the equilibrium concentration of H^+ (based on Equation **6.4**) for zinc concentrations of 1.5 M and 0.75 M also result in lower concentrations than those measured but as the

concentration of zinc decreases, the difference between the measured and calculated equilibrium concentration values becomes smaller, see **Table 6.3**. This supports the proposition that decreasing the zinc concentration results in lower contributions from polynuclear species to the hydrolysis reactions.

Table 6.3. Difference between the measured and calculated equilibrium pH of zinc nitrate solution. The pH is calculated based on the hydrolysis reaction $Zn^{2+}_{(aq)} + H_2O \rightleftharpoons ZnOH^{+}_{(aq)} + H^{+}_{(aq)}$.

$Zn(NO_3)_2$ molarity (M)	Measured pH of $Zn(NO_3)_2$ sol	Calculated equilibrium pH of $Zn(NO_3)_2$ sol	Difference between the measured and calculated equilibrium pH of $Zn(NO_3)_2$ sol
3	2.85	3.48	0.63
1.5	3.2	3.63	0.43
0.75	3.65	3.78	0.13

On the other hand, zinc oxide in water is in equilibrium with numerous zinc species including $Zn^{2+}_{(aq)}$, $ZnOH^{+}_{(aq)}$, $Zn(OH)_{2\ (aq)}$, $Zn(OH)_3^-{}_{(aq)}$ and $Zn(OH)_4^{2-}{}_{(aq)}$ [447] and also $ZnO_{(aq)}$ depending on the pH [79].

Upon addition of zinc nitrate solution to ZnO suspension in water, the equilibrium in both systems is disturbed and they become dynamic again. The available protons in the zinc nitrate solution react with $ZnO_{(cr)}$ whereupon it dissolves according to Equations **6**.**7** and **6**.**8**. Amphoteric ZnO acts as a base providing cationic zinc species that may undergo further reactions. In acidic conditions, Zn^{2+}, $ZnOH^{+}$, and polynuclear $Zn_2(OH)^{3+}$ and $Zn_4(OH)_4^{4+}$ are the major soluble zinc species in water with Zn^{2+} dominating at pH < 6 [79, 290, 447]. Since protons are consumed upon dissolving ZnO, the pH increases and so does the availability of $ZnOH^{+}$ in solution. Nevertheless, in acidic conditions the Zn^{2+} concentration is generally much greater than that of $ZnOH^{+}$ [447]. In the current experiments, the pH was measured to be 6.5 immediately after mixing the starting materials. After 4 hr the pH was 6.4.

While Reaction **6**.**7** depletes the system of protons and adds Zn^{2+} and water, the hydrolysis Reactions **6**.**4**, **6**.**5** and **6**.**6** shift to favour product formation according the Le Chatelier's Principle. Under the conditions studied here, the pH range is optimal for the formation of cationic zinc hydroxo-complexes. In these conditions, Reaction **6**.**9** is

favourable when the availability of zinc hydroxo-complexes in solution increases. Calculation of $\Delta_r G$ for this reaction shows that in the standard state $\Delta_r G^\circ$ = +76.8 kJ mol^{-1}. Although only the $ZnOH^+$ species was considered here, interactions between polynuclear zinc hydroxo-complexes and water and nitrates are also possible. Thermodynamic figures in standard conditions for $Zn_5(NO_3)_2(OH)_8 \cdot 2H_2O$ have been obtained from [448]. $\Delta_r G = \Delta_r G^\circ + RT \ln Q_r$ for this reaction in non-standard conditions was then applied. Having considered the reaction quotient for this reaction as $\frac{[H^+]^3}{[NO_3^-]^2[ZnOH^+]^5}$ and knowing the pH of the system that is ~6.5 at t = 0 minutes and relatively higher concentration of nitrate in solution that originates from the zinc nitrate solution mixed with the suspension of ZnO in water ($[NO_3^-] = 1.8\ M \equiv \frac{0.18}{0.03+0.07} mol/lit$), $\Delta_r G$ for Reaction **6.9** is calculated to be still positive (≈ +44 kJ mol^{-1}), see the calculations below:

- At t = 0 minute:

  $\Delta_r G^\circ = +76.8\ kJ \cdot mol^{-1}$

  $pH = 6.5 \equiv [H^+] = 3.16 \times 10^{-7}\ M$

  $[NO_3^-] = 1.8\ M \equiv \frac{0.18}{0.03 + 0.07} mol/lit$

  $[ZnOH^+] = 1.41 \times 10^{-3}\ M$ (equilibrium concentration based on Reaction 6.4)

Since $\Delta_r G = \Delta_r G^\circ + RT \ln Q_r$ and $Q_r = \frac{[H^+]^3}{[NO_3^-]^2[ZnOH^+]^5}$, therefore by substitution $\Delta_r G = +43.96\ kJ \cdot mol^{-1}$ is obtained.

Over time and due to the availability of ZnO in the system, some protons are consumed and result in production of more $ZnOH^+$ in solution. When the concentration of $ZnOH^+$ re-equilibrates at t_{eq}, the Gibbs free energy of Reaction **6.9** reaches zero and over this concentration this reaction becomes spontaneous, see calculations below. In these conditions, positively charged layers of the hydrated zinc hydroxide with the form of $[Zn_5(OH)_8(H_2O)_2]^{2+}$ nucleate and intercalate available nitrates in solution in the interlayer space to balance the charge. This results in formation of $Zn_5(NO_3)_2(OH)_8 \cdot 2H_2O$. This species was confirmed by XRD to be the end-product of the overall reactions. Based on the kinetics study, t_{eq} is suggested to be around 20 minutes where the first signs of the formation of crystals of zinc hydroxy nitrate can be observed (see Kinetics Section).

- At $t = t_{eq}$ minutes (~20 minutes):

  $\Delta_r G = 0\ \text{kJ} \cdot \text{mol}^{-1}$

Solving the equation of the Gibbs free energy of reaction ($\Delta_r G = \Delta_r G^{\circ} + RT \ln Q_r$) to calculate the equilibrium concentration of $ZnOH^+$ results in:

$[ZnOH^+] = 4.95 \times 10^{-2}$ M (equilibrium concentration based on Reactions 6.4 and 6.8)

While Reaction **6.9** continues, the concentrations of $ZnOH^+$ and nitrate in solution decrease due to the precipitation of the $Zn_5(NO_3)_2(OH)_8 \cdot 2H_2O$. Depletion of $ZnOH^+$ from the system contributes to shift the hydrolysis reactions towards right, which provides more protons to the solution phase available for dissolution of remaining ZnO and also shifting Reaction **6.8** towards right according the Le Chatelier's Principle.

Along with the precipitation of $Zn_5(NO_3)_2(OH)_8 \cdot 2H_2O$ according to Reaction **6.9**, some protons are regenerated into the solution, which can react with the unreacted ZnO. Consequently, in this system protons have a catalytic role.

Calculation of the Gibbs free energy of Reaction **6.9** at $t = 4$ hours shows that for this reaction to be at equilibrium relative to the previous times, higher concentration of $ZnOH^+$ is needed. Since the concentration of $ZnOH^+$ after around 75 minutes starts to decrease due to the acceleration of the precipitation Reaction **6.9**, the Gibbs free energy for this reaction becomes zero as a result of not having enough $ZnOH^+$ in solution at around 180 minutes. This controls the equilibrium of this reaction, see calculations below:

- At $t = 240$ minutes:

  $pH = 6.4 \equiv [H^+] = 3.98 \times 10^{-7}$ M

  $[NO_3^-] = 1.446\ \text{M} \equiv \frac{0.18 - 2 \times 0.0177}{0.1}\ \text{mol/lit}$ (some nitrates and $ZnOH^+$ have already been precipitated as $Zn_5(NO_3)_2(OH)_8 \cdot 2H_2O$)

Hence: For $\Delta_r G = 0\ \text{kJ mol}^{-1}$, a higher concentration of $ZnOH^+$ is needed:

Needed concentration: $[ZnOH^+] = 6.15 \times 10^{-2}$ M

An important issue is the low solubility of $Zn_5(NO_3)_2(OH)_8 \cdot 2H_2O$ in water. Here for the first time, the solubility product (K_{sp}) of this compound is reported to be in the range of 7.4×10^{-11} to 8.5×10^{-11}, with these values corresponding respectively to ICP-MS analyses of zinc and nitrogen-measurement in the aqueous phase (see later for more detail).

As can be seen, the interactions between species in this system are quite complex and the concentration of the cationic zinc species is very important. Competition of various reactions in equilibrium conditions is the controlling factor for the overall reaction. Initially, only the dissolution reactions happen as $\Delta_r G$ for Reaction **6.9** is positive. As more $ZnOH^+$ is produced, $\Delta_r G$ becomes zero and then negative at times over 20 minutes. The dissolution and precipitation reactions then take place in parallel until the rate of dissolution becomes less and as a result this forces the precipitation reaction to decelerate as well. Reactants in solution are depleted due to the precipitation until $\Delta_r G$ of Reaction **6.9** approaches zero again at around 180 minutes. The system then is at equilibrium (see **Figure 6.5**).

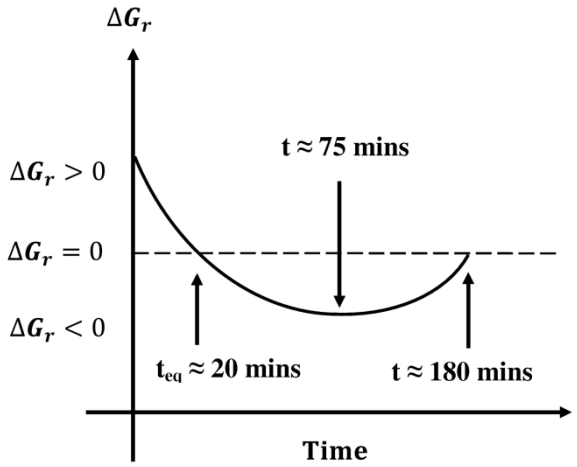

Figure 6.5. Gibbs free energy of Reaction **6.9** is positive at t = 0. As time passes, it becomes negative (over $t_{eq} \approx 20$ minutes) and reaches its minimum at around 75 minutes. Then it approaches zero again at around 180 minutes due to the change in Q_r (as a result of changes in concentrations of the species in solution).

6.3.3. Kinetics

During the course of the solid/liquid reaction, samples were removed from the system and immediately washed with Milli-Q water to quench the reaction. After drying, the samples were characterised by XRD and TGA-DTA.

XRD (**Figure 6.6**) revealed the first indication of the formation of crystalline $Zn_5(NO_3)_2(OH)_8 \cdot 2H_2O$ (01-072-0627) at ~30 minutes. Before this time, only peaks associated with zinc oxide were detected. As the reaction proceeds, the intensity of the

peaks associated with $Zn_5(NO_3)_2(OH)_8 \cdot 2H_2O$ increased along with a decrease in the intensity of peaks associated with zinc oxide.

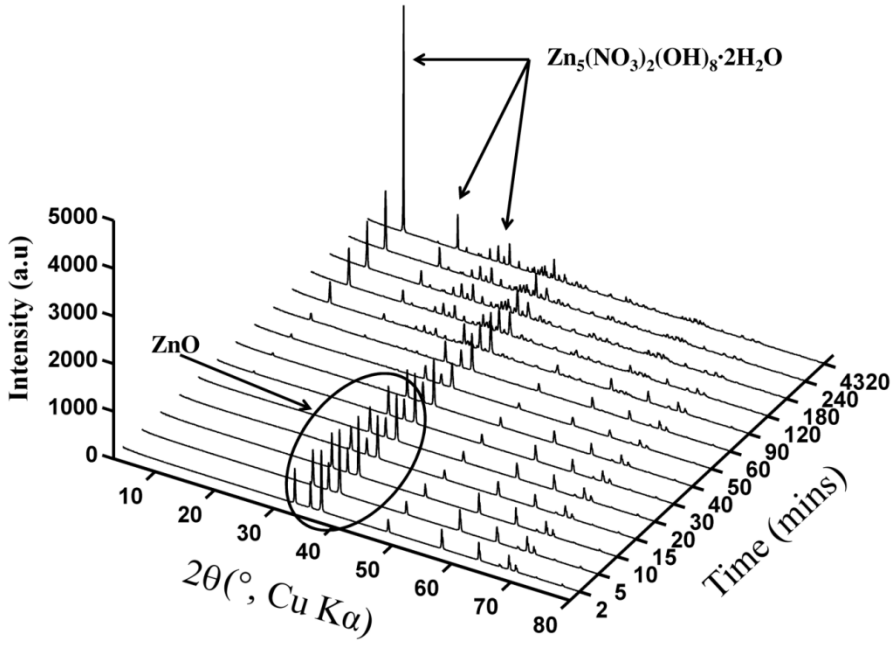

Figure 6.6. XRD patterns of the samples collected in the course of reaction.

After 240 minutes reaction time, the product was mostly $Zn_5(NO_3)_2(OH)_8 \cdot 2H_2O$ with minor peaks associated with zinc oxide. This is consistent with the TGA data, which show that conversion is ~90% after 240 mins. Unreacted zinc oxide was detected in the sample reacted for 3 days; for which the conversion was ~98% (by TGA).

Figure 6.6 shows that peaks associated with $Zn_5(NO_3)_2(OH)_8 \cdot 2H_2O$ are significantly more intense for the 3 day sample that those of the 4 hour specimen. This change was assigned to coarsening and crystal growth of the basic zinc salt over time as well as a small contribution from the increase in conversion of zinc oxide to zinc hydroxy nitrate.

TGA data (**Figure 6.7**) for samples reacted for times 2, 5, 10, 15, 20, 30, 40, 50, 60, 90, 120, 180, 240 minutes and 3 days show that samples with reaction times up to ~30 minutes exhibit one major mass loss at temperatures above 250 °C. For samples with reaction times >30 minutes, this major decomposition shifts towards lower temperatures. XRD data obtained for reaction times up to 30 minutes show only peaks associated with ZnO and therefore the decomposition patterns for the samples reacted for up to 30 minutes are assigned to amorphous zinc hydroxy nitrate species, which is

proposed to be formed as intermediate species. As the reaction proceeds, the amount of ZnO remaining decreases. DTA (**Figure 6.8**) for samples with reaction times below 20 minutes show very small peaks at temperatures around 250 °C. From this time onwards, endothermic peaks associated with zinc hydroxy nitrate occur at lower temperatures.

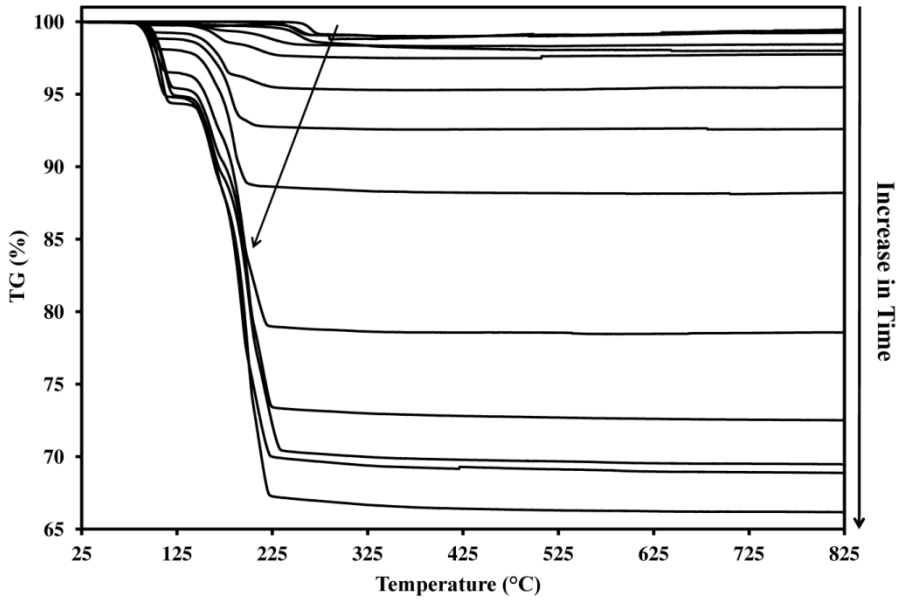

Figure 6.7. TGA on the samples collected in the course of reaction.

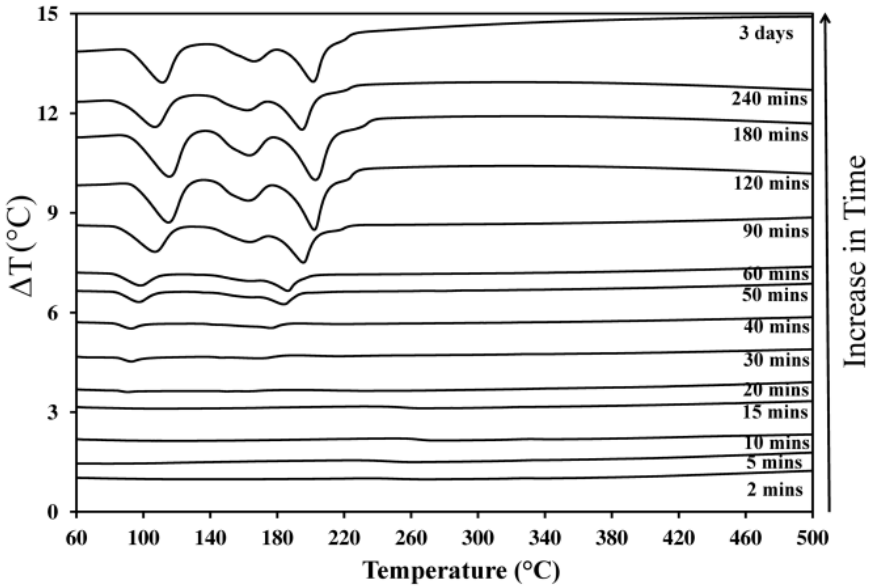

Figure 6.8. DTA on the samples collected in the course of reaction (graphs are offset for clarity).

Using TGA data, it was observed that the conversion curve versus time of the solid/liquid reaction between ZnO and zinc nitrate to form zinc hydroxy nitrate is *S*-

shaped. Two possible equations were considered to fit a curve to the pattern: (1) the Avrami equation, $X\% = 100 - e^{(-Kt^n)}$ and (2) the Sigmoid function, $X\% = \frac{100}{a+b\times e^{(-ct)}}$ where X% is the conversion in % and K, n, a, b and c are constants. Using the Avrami equation, $\ln(\ln(conversion\%))$ *vs.* $\ln(time)$ was not linear. This can be seen in **Figure 6.9**. However sigmoid function was a reasonable fit to the data, **Figure 6.10**.

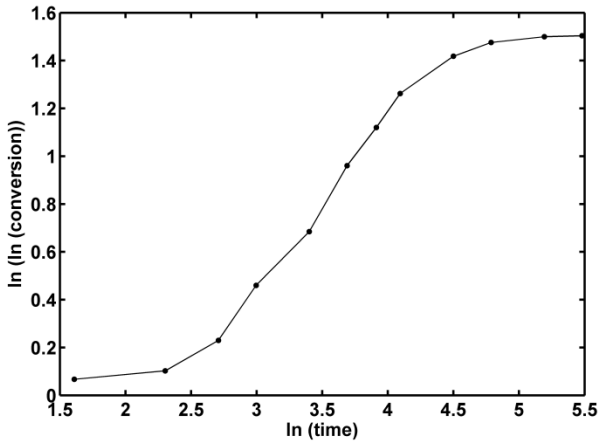

Figure 6.9. Graph of ln(ln(conversion)) *vs.* ln(time) is not linear.

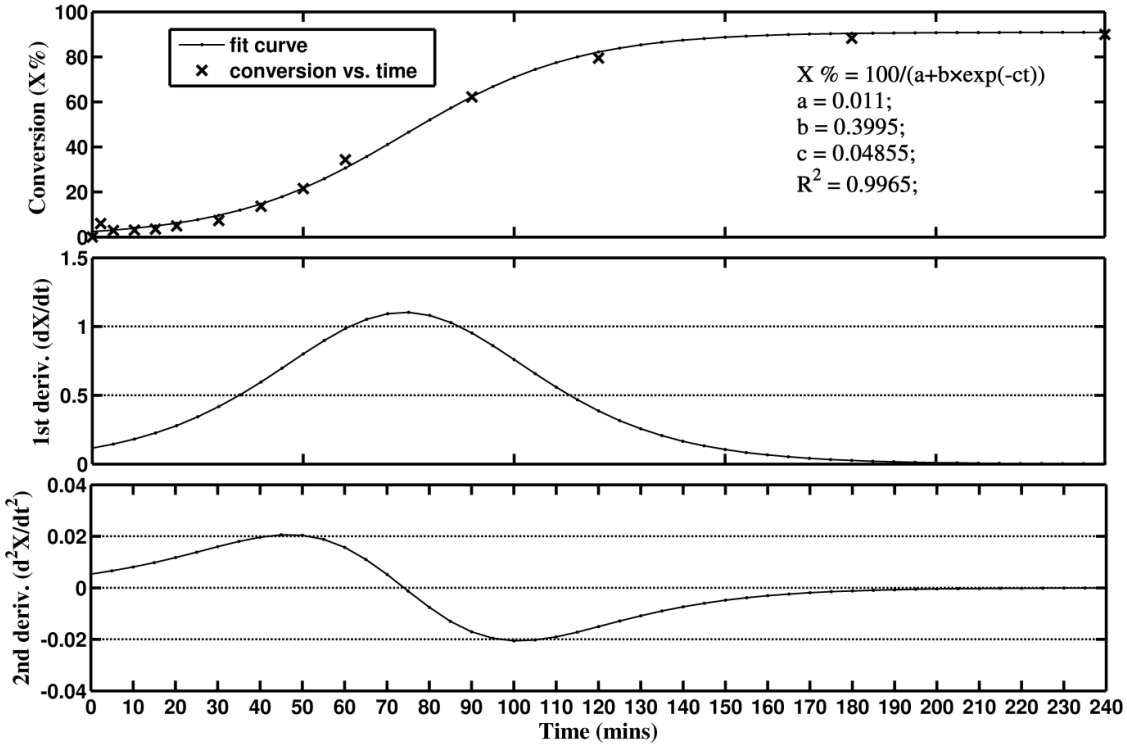

Figure 6.10. Sigmoid function curve fitting for conversion *vs.* time and the 1st and 2nd derivatives of the fitted curve *vs*. time. Maximum rate of conversion was shown to be at around 75 minutes.

The first and the second derivatives of the curve were used to calculate the conversion rate and its maximum rate. The maximum rate of conversion occurs at ~75 minutes. This corresponds to a point of inflection on the curve, which is also represented in its 2nd derivative curve.

In the beginning of the reaction, the concentration of the cationic zinc species is insufficient for the Reaction **6.9** to proceed (see above). As oxide dissolves, Reaction **6.8**, and the concentration of $ZnOH^+$ increases, Reaction **6.9** accelerates and reaches a maximum rate at ~75 minutes. After this time, Reaction **6.9** decelerates due to the consumption of the available precursors in solution until $\Delta_r G$ becomes zero again. From t = 120 minutes to 180 minutes less than 10% conversion is observed and from t = 180 minutes to 240 minutes only ~1.5% conversion takes place.

SEM images of samples collected at various times are shown in **Figure 6.11** and **Figure 6.12**. Five minutes after starting the reaction an amorphous phase is formed among the ZnO crystals. This is apparently the result of dissolution and fusing of the oxide particles into each other and combining with nitrate to form an amorphous material, which is shown by TGA-DTA to have a mass loss at around 260 °C. Before 20 minutes of reaction, small crystals of zinc oxide are the major observed materials. From 30 minutes onwards (**Figure 6.12**), sheet-like 2D structures with a relatively large size as compared to the ZnO crystals can be observed. This is consistent with XRD and TGA-DTA data that show the onset of the formation of crystalline $Zn_5(NO_3)_2(OH)_8 \cdot 2H_2O$ at ~30 minutes. As the time passes, the amount ZnO crystals decreases and the crystallinity of the end-product is improved. Again this is in accordance with the XRD and TGA-DTA data described above.

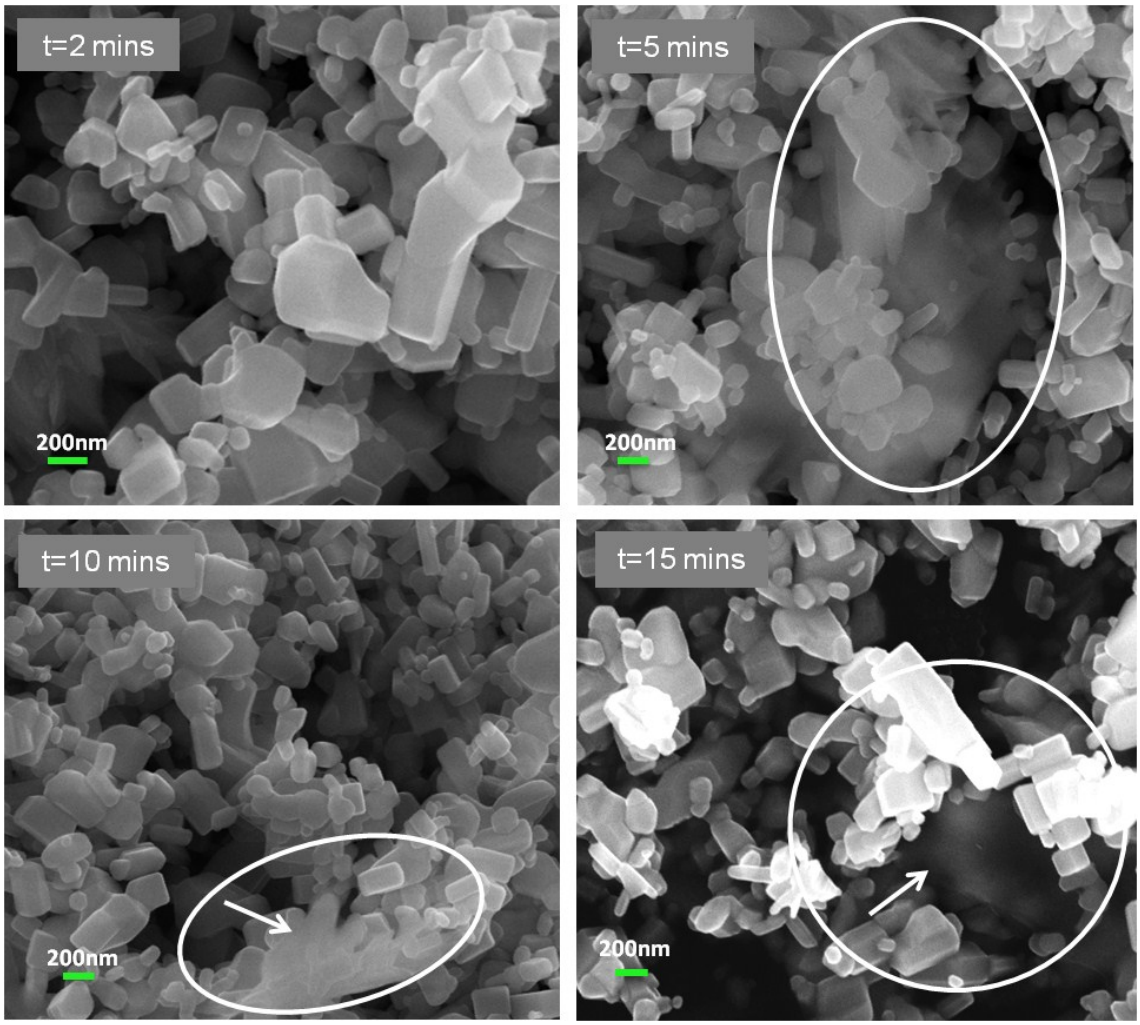

Figure 6.11. SEM images on the samples collected at times 2, 5, 10 and 15 minutes in the course of reaction.

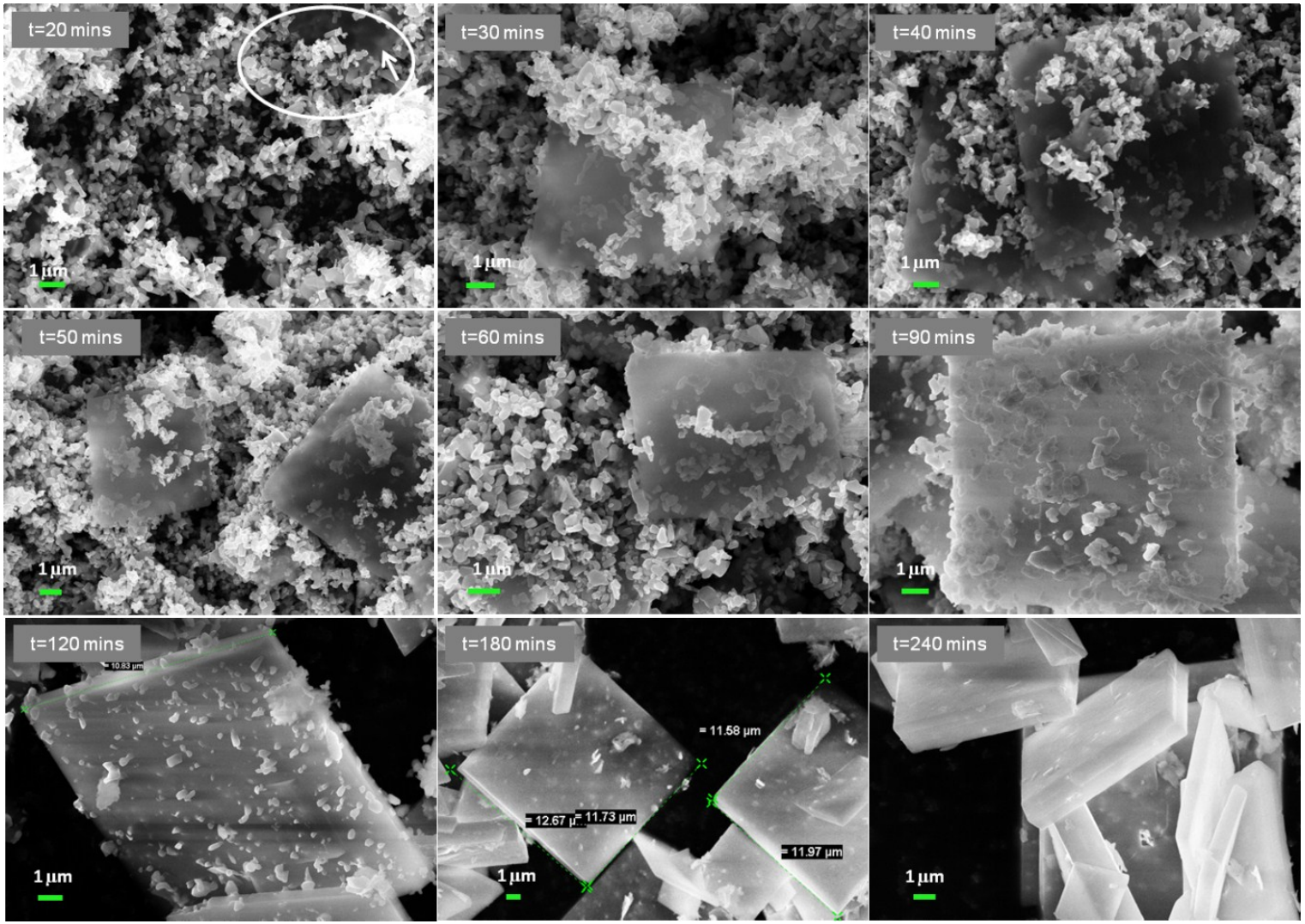

Figure 6.12. SEM images on the samples collected at times 20 to 240 minutes in the course of reaction.

6.3.4. Solubility

The solubility of $Zn_5(NO_3)_2(OH)_8 \cdot 2H_2O$ was measured for the first time using two independent techniques; i.e. Zn measurement using ICP-MS and nitrogen-measurement. ICP-MS measurements revealed a concentration of 17.3 ppm of zinc ions in solution, which yields a molar solubility of 2.64×10^{-4} mol/L. Nitrogen concentration was measured to be 7.8 ppm, which provides a molar solubility for nitrate of 5.53×10^{-4} mol/L. It was noticed that the molar solubility of nitrate is almost twice of that of Zn.

It may be expected that the solubility of zinc hydroxy nitrate is governed by Equation 6.10, where S_1 is the solubility in mol/L.

$$Zn_5(NO_3)_2(OH)_8 \cdot 2H_2O_{(s)} \rightleftharpoons 5Zn^{2+}_{(aq)} + 2(NO_3)^-_{(aq)} + 8(OH)^-_{(aq)} + 2H_2O \qquad \textbf{6.10}$$

$$-S_1 \qquad +5S_1 \qquad +2S_1 \qquad +8S_1$$

Based on Equation 6.10, a molar solubility ratio of 2 : 5 for nitrate to zinc is expected. However, this does not consider the relatively low solubility of zinc hydroxide, Equation **6.11** (where S_2 is the solubility of $Zn(OH)_2$ in mol/L), which was discussed in Chapter 2. Upon initial dissociation of zinc hydroxy nitrate, 4 of the 5 moles of zinc may interact with 8 moles of hydroxide (see Equation **6.10**). Using K_{sp} data for zinc hydroxide, **Table 6.4**, the solubility of zinc, S_2 in Equation **6.11**, is 2.0×10^{-6} mol/L, which is less than 1% of the solubility of zinc measured by ICP-MS. It is evident that the solubility of $Zn_5(NO_3)_2(OH)_8 \cdot 2H_2O$ is largely governed by the solubility of the remaining Zn and nitrate in a ratio of 1 : 2, which corresponds to the measured data.

$$Zn(OH)_{2\,(s)} \rightleftharpoons Zn^{2+}_{(aq)} + 2(OH)^-_{(aq)} \qquad \textbf{6.11}$$

$$-S_2 \qquad +S_2 \qquad +2S_2$$

Self-ionisation reaction of water was also considered in this system, Equation **6.12**.

$$H_2O_{(l)} + H_2O_{(l)} \rightleftharpoons H_3O^+_{(aq)} + OH^-_{(aq)} \qquad \textbf{6.12}$$

$$-S_3 \quad -S_3 \qquad +S_3 \qquad +S_3$$

Ionic product of water (K_w) at 25 °C is 10^{-14} ($K_w = [H_3O^+]\times[OH^-] = [S_3]\times[S_3] = [S_3]^2$) [449]. Concentration of hydroxide (S_3) produced by Reaction **6.12** is therefore calculated to be 10^{-7} mol/L. This value is negligible in this system when compared with the concentration of hydroxide produced by Reaction **6.10**.

Consequently, the solubility product, K_{sp}, of zinc hydroxy nitrate is calculated based on Equation **6.13** using the measured values of S_1 from the two independent techniques: $K_{sp} = [Zn^{2+}]\times[(NO_3)^-]^2 = [S_1]\times[2S_1]^2$. The measured solubility of 2.64×10^{-4} mol/L for zinc yields a K_{sp} of 7.4×10^{-11}. Alternatively, the solubility value of 5.53×10^{-4} mol/L for nitrate provides a K_{sp} of 8.5×10^{-11}.

$$Zn_5(NO_3)_2(OH)_8\cdot2H_2O_{(s)} \rightleftharpoons 4Zn(OH)_{2\,(s)} + Zn^{2+}_{(aq)} + 2(NO_3)^-_{(aq)} + 2H_2O \qquad \textbf{6.13}$$

$$-S_1 \qquad\qquad +S_1 \qquad +2S_1$$

Table 6.4. Solubility products of some zinc compounds compared to the reported values for zinc hydroxy nitrate in the current work.

Chemical	Solubility product (K_{sp}), 298 ºK	Ref.
Zinc hydroxy chloride, $Zn_5(OH)_8Cl_2\cdot H_2O$	8.2×10^{-76}	[450]
Zinc hydroxy carbonate, $Zn_5(OH)_6(CO_3)_2$	$10^{-14.9\pm0.1}$ 2.0×10^{-15}	[451] [452]
Zinc carbonate (Smithsonite), $ZnCO_3$	$10^{-7.25\pm0.1}$	[453]
Zinc hydroxy sulphate, $Zn_4(OH)_6(SO_4)$	2.51×10^{-56}	[452]
ZnO	2.2×10^{-17}	[291]
$Zn(OH)_2$	3.5×10^{-17}	[290]
Zinc hydroxy nitrate, $Zn_5(NO_3)_2(OH)_8\cdot2H_2O$	7.4×10^{-11} (Zn measurement) 8.5×10^{-11} (nitrogen measurement)	This work

6.3.5. Mechanism and catalytic role of H^+

Based on the stoichiometry, thermodynamics and kinetics studies, the formation of zinc hydroxy nitrate from zinc oxide is suggested to follow the overall Reaction **6.1**. Reactions **6.2** to **6.9** are involved in the system for the dissolution of zinc oxide and precipitation of zinc hydroxy nitrate.

Initially, dissolution reactions are dominant. The rate of the overall reaction and its progress was shown to be a function of reaction quotient of Reaction **6.9**, which controls the thermodynamics of the overall reaction as well. Mechanism of the overall reaction follows the route shown in **Figure 6.13**. It was shown that H^+ has catalytic role in the progress of the overall reaction. From 9 moles of protons, which are generated

due to the hydrolysis reactions and are consumed for the dissolution of ZnO, 6 moles are regenerated that can dissolve more ZnO into the solution until the system reaches thermodynamic equilibrium. As can be seen in all reactions, pH after 4 hours drops slightly as opposed to the beginning of the reaction. The system remains in the slightly acidic conditions at equilibrium. While the system approaches equilibrium, the Gibbs free energy of the Reaction **6.9** controls the progress of the reaction and some ZnO remain unreacted in the solid-phase. Liquid phase also contains cationic zinc species balanced in charge with the excess of nitrate. In this pH range, Zn^{2+} : $ZnOH^{+}$ ratio in solution is around 90%-10% [447]. In such conditions Reactions **6.7** and **6.8** are in equilibrium. These control the amount of cationic zinc species in solution in equilibrium with unreacted ZnO.

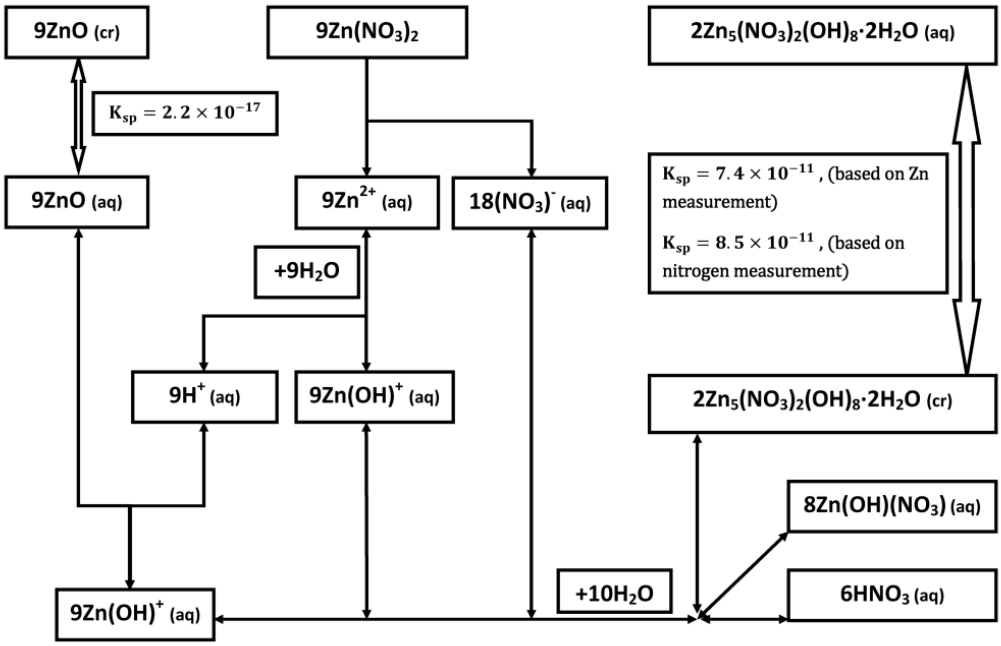

Figure 6.13. Schematic of the suggested mechanism for the solid/liquid reaction between ZnO and zinc nitrate solution. H^{+} shows a catalytic role in this system.

6.4. Conclusions

The solid/liquid reaction between ZnO and zinc nitrate, which results in layered crystals of zinc hydroxy nitrate, $Zn_5(NO_3)_2(OH)_8 \cdot 2H_2O$, follows a H^{+}-catalysed dissolution-precipitation mechanism with a 1 : 1 reactant mol ratio. The reaction is

thermodynamically controlled by the concentration of cationic zinc species, such as $ZnOH^+$. This is formed due to the dissolution of ZnO in acidic solution of zinc nitrate. Concentration of zinc species originating from zinc nitrate and oxide has been shown to control the pH of the system and consequently reaction quotient for the precipitation reaction of zinc hydroxy nitrate. Kinetic behaviour of the reaction was shown to be *S*-shaped with a sigmoid function fit to it. Maximum conversion rate of zinc oxide to zinc hydroxy nitrate happens at around 75 minutes. The reaction was shown to be quite slow before 30 minutes and after 120 minutes due to thermodynamic limitations. Solubility product of $Zn_5(NO_3)_2(OH)_8 \cdot 2H_2O$ has been measured for the first time by two independent techniques of zinc and nitrogen measurements to be 7.4×10^{-11} and 8.5×10^{-11}, respectively.

Chapter 7

General Conclusions and Future Directions

Chapter 7: General Conclusions and Future Directions

7.1. General Conclusions

Zinc oxide is an important material industrially and scientifically. It has been used for thousands of years and its applications have evolved significantly. Although zinc oxide may look like a simple material that is made only of one zinc atom and one oxygen atom in its formula, it is actually quite a complicated material. It shows various forms and morphologies and properties. The properties of this material such as porosity, specific surface area and optical properties can change significantly by changing the synthetic method and process conditions.

There are numerous production methods, some of which are currently limited only to academic works. There has been a dramatic increase of publications on this material recently. Nevertheless, most are due to a scientific interest for development of potential *p*-type zinc oxide, which has been unsuccessful so far.

In terms of mass production, it seems that pyrometallurgical techniques, in particular the French process, will continue to serve the major role in the global manufacture of ZnO. Although many hydrometallurgical processes are chemically feasible, the economics of the processes dictate the process feasibility. Consequently, it seems that processes with minimal ongoing process cost, and that use cheaper raw materials and simpler and more integrated techniques with lower energy consumption may compete with conventional processes.

Knowledge of the synthetic methods is important in order to engineer and manufacture zinc oxide with tailored properties. This work focused on the production of ZnO using various techniques amenable to large-scale production. A variety of precursors and synthetic routes have been explored including single-stage and multi-stage methods. Mechanisms of the reactions to form ZnO have been studied.

In the single-stage methods, production of ZnO was achieved by reactions between a zinc salt aqueous solution and a base. The resultant oxide was shown to have specific surface area larger than the French process ZnO. This route provides simple means for the formation of ZnO nano-particles at moderate temperatures with high controllability. Effects of reaction temperature, concentration of the reactants and feeding techniques on

the products have been studied. It was also shown that using different alkaline reagents (such as NaOH and ammonia solution) change the end-product zinc oxide.

In the multi-stage methods, zinc-bearing precursors such as zinc peroxide and zinc hydroxy salts were first produced. ZnO was then produced by thermal treatment of these precursors. The zinc-bearing precursors are important materials per se. This work aimed to produce materials that can be either used directly or can be converted to ZnO, if need be. This provides flexibility for the production of multiple zinc-bearing products via integrated processes.

In the course of this work, interesting and important properties of the zinc hydroxy salts have been recognised. Identification of the properties of these salts provided an insight into a variety of potential precursors for the production of zinc oxide.

It was shown that properties of ZnO end-products are acutely affected by the method of production. The nature of the starting materials and processing technique, therefore dictates the nature of the end-product ZnO. Thermal decomposition of each individual precursor material to ZnO was shown to follow a unique mechanism. For example single stage decomposition patterns were determined for zinc hydroxy carbonate and zinc peroxide. On the other hand, multi-stage decomposition patterns have been detected for zinc hydroxy sulphate, chloride, nitrate and acetate.

Some starting materials such as zinc peroxide and zinc hydroxy nitrate show relatively low temperatures of decomposition. Some others such as zinc hydroxy sulphate and chloride were indicated to have relatively higher temperatures of decomposition.

Gaseous materials evolved in the course of thermal decomposition of zinc-bearing precursors are important as well. Various gaseous species such as O_2, CO_2, NO_2, NO, SO_2, SO_3 have been detected depending on the precursors used. It was shown that zinc hydroxy chloride and acetate can form zinc-bearing sublimates in the course of heating. Formation of the sublimates in these systems is responsible for a mass loss more than the theoretical mass loss when ZnO is the only zinc-bearing product. This has been a major oversight in various publications, which has been clarified in this work.

Initially it was thought that the ZnO products made by thermal decomposition of zinc-containing precursors are more crystalline when the temperature of decomposition is higher. In the course of this work, it was revealed that this is not necessarily the

situation. Thermal decomposition of some precursors to ZnO at low temperatures results in highly crystalline zinc oxides. ZnO produced from zinc hydroxy nitrate was shown to have the highest crystallinity among the products formed from other zinc hydroxy salts in this work. It was observed that the crystallinity of the end-product ZnO is correlated to the crystallinity of the precursor; i.e. the more crystalline ZnO products are produced from the more crystalline starting material.

It was shown that active ZnO having specific surface area more than 50 m^2/g can be produced from zinc hydroxy carbonate. This is due to the low crystallinity of the precursor. Nevertheless obtaining such a high surface area ZnO from the other precursors studied here was shown to be difficult due to the high crystallinity of the precursors. Therefore it was shown that although there are various possible zinc-containing materials to form ZnO, the number of options available to produce active zinc oxide is limited, at least by using the precursors studied in this work. CO_2 and water vapour are the only gaseous products, which are evolved during thermal decomposition of basic zinc carbonate.

Another important finding was the low solubility of zinc hydroxy nitrate in water. The solubility product of zinc hydroxy nitrate was measured by two independent techniques for the first time in the current work.

7.2. Future Directions

In the course of this work, the importance of counterions of zinc (anions) in zinc salts and counterions of hydroxide (cations) in alkaline reagents in the formation of zinc oxide in solution was recognised. This suggests new future research areas by changing the zinc-bearing reactants containing various inorganic or organic anions such as nitrate, chloride, fluoride, iodide, various carboxylates or by changing the alkaline reagents containing various cations such as sodium, potassium and lithium and ammonium. The reagents influence the chemical interactions in solution (thermodynamically and kinetically) or contamination (doping), which should result in changes in properties of the end-product ZnO.

There has been little research in the area of zinc hydroxy salts. The importance of these materials per se and also the diversity of the materials that can be formed within

this class of compounds enabled an insight into the novel zinc-containing precursors for the production of ZnO. It was recognised that by changing the anions in zinc hydroxy salts, novel materials can be formed that in turn lead to the formation of tailored zinc oxide particles with unique properties.

There are many other possible routes for the formation of zinc oxide. Melt-melt reactions between molten zinc salts and molten alkaline reagents seem to be very attractive due to the high viscosity of the reaction media and an absence of water and a perfect environment for the growth of zinc oxide crystals in the melt. In the current work, some reactions have been performed using NaOH and zinc chloride in the molten form, which resulted in quite attractive zinc oxide particles. These methods could be further explored to examine these alternative methods for the synthesis of single crystals.

Appendix

Appendix

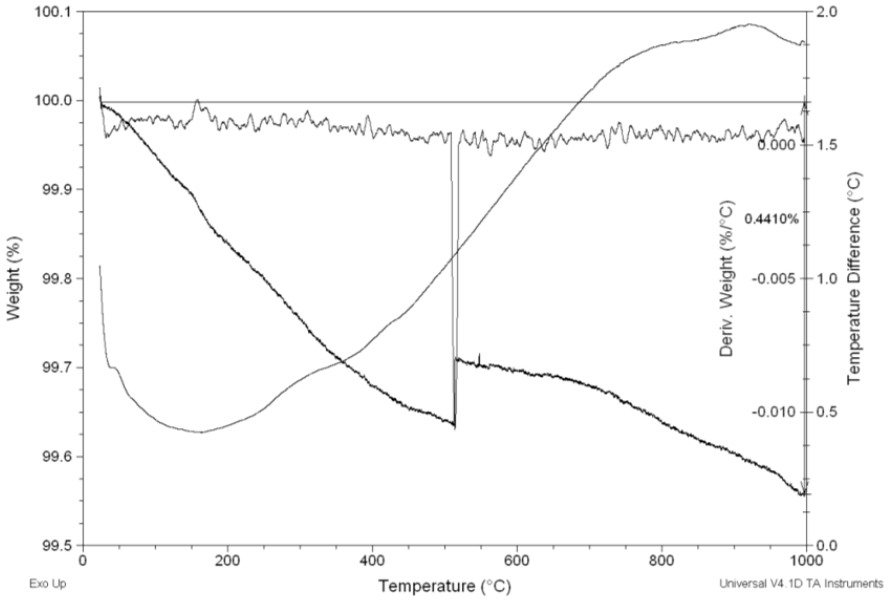

Figure A. 1. TGA-DTA on ZnO made at 600 °C from BZCl aged for 14 months shows small mass loss of ~0.4% up to 1000 °C.

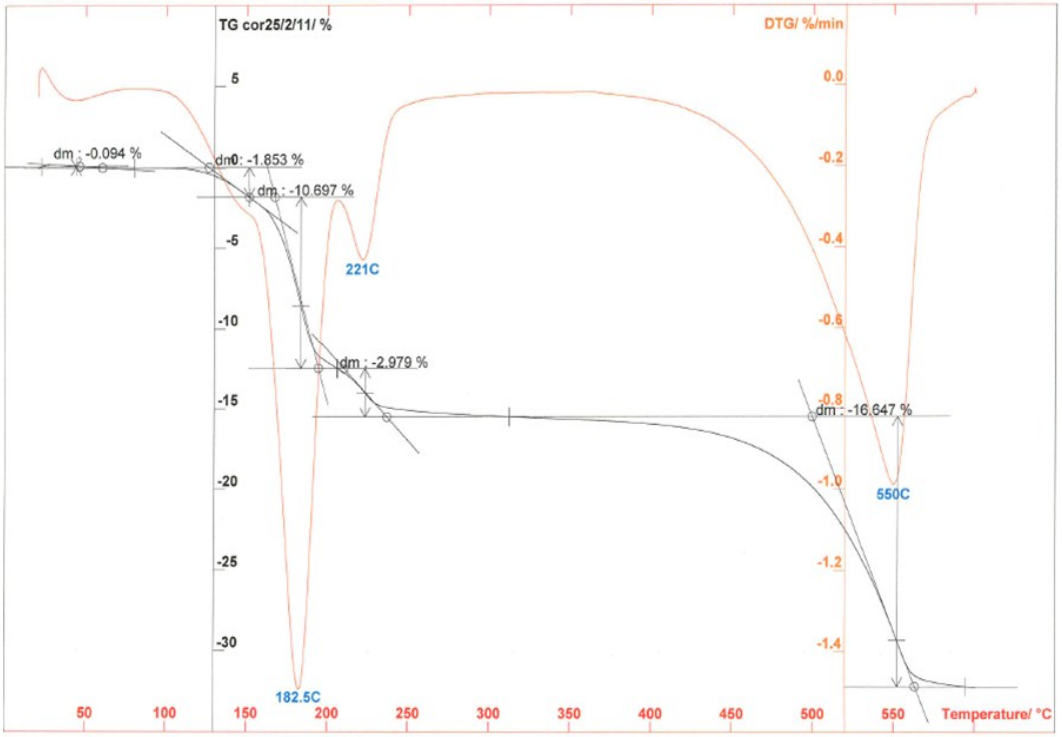

Figure A. 2. In-situ TGA during MS on BZCl under Ar atmosphere with a heating rate of 4 °C min^{-1} and up to 600 °C.

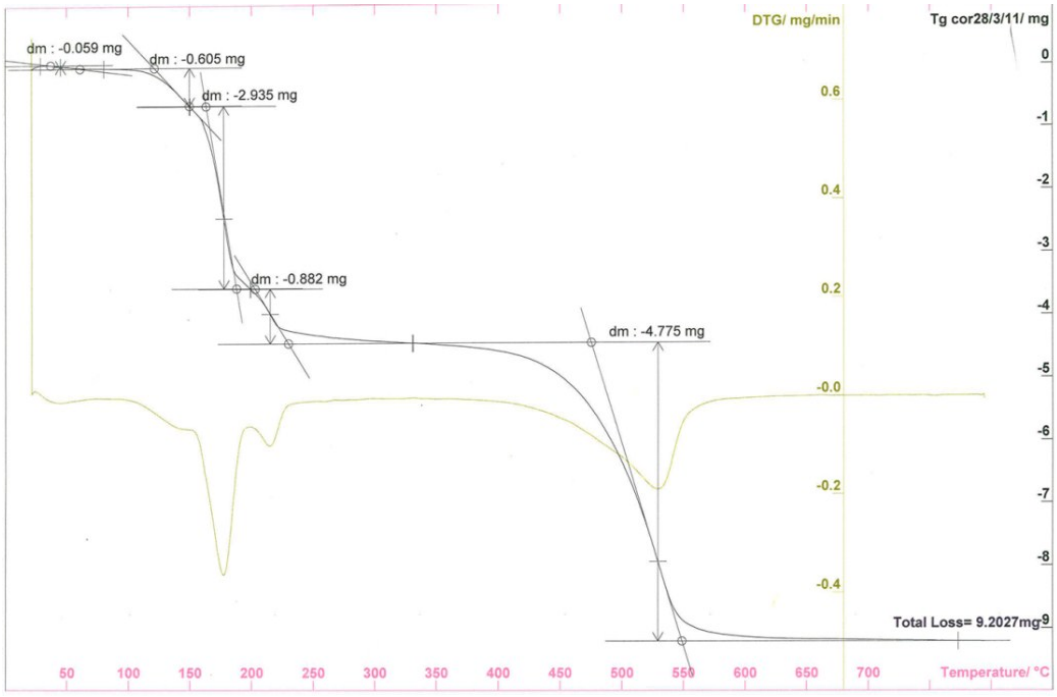

Figure A. 3. In-situ TGA during MS on BZCl under Ar atmosphere with a heating rate of 3 °C min^{-1} and up to 800 °C (original mass=28.2 mg).

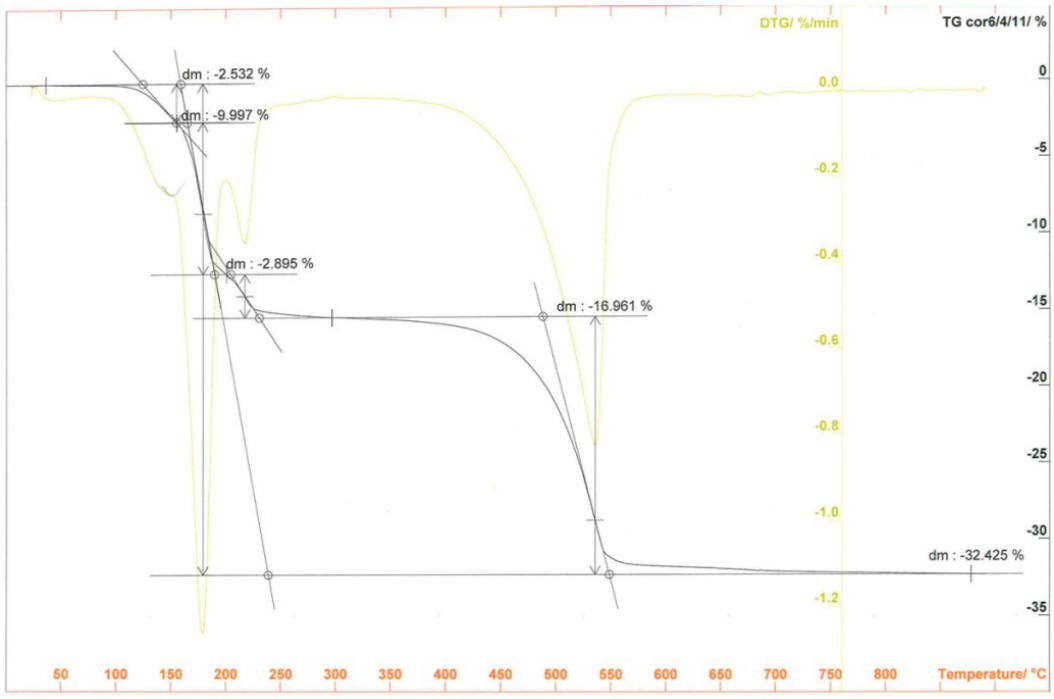

Figure A. 4. In-situ TGA during MS on BZCl under Air atmosphere with a heating rate of 3 °C min^{-1} and up to 900 °C.

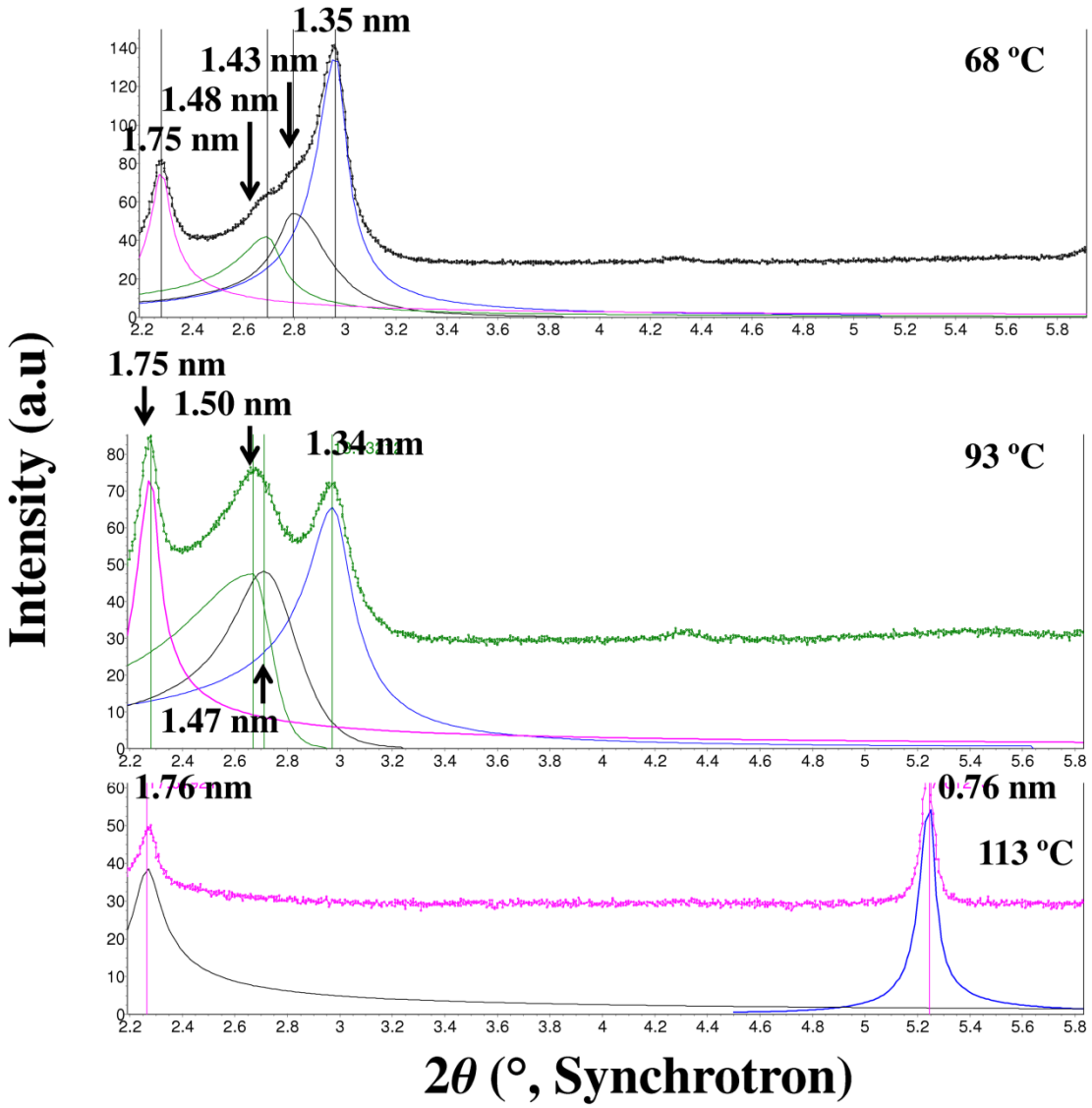

Figure A. 5. Synchrotron X-ray data collected at 68 °C, 93 °C and 113 °C on BZA and the resolved *d*-spacing of low-angle peaks using Split-Pearson VII distribution function.

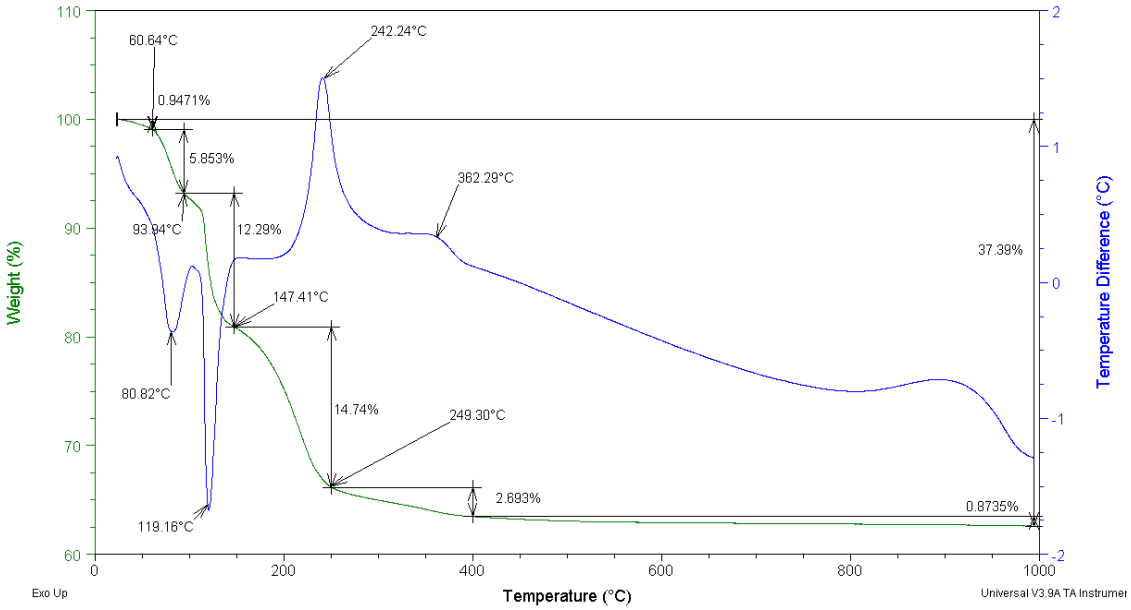

Figure A. 6. TGA-DTA on BZA, 5 °C min^{-1} in air.

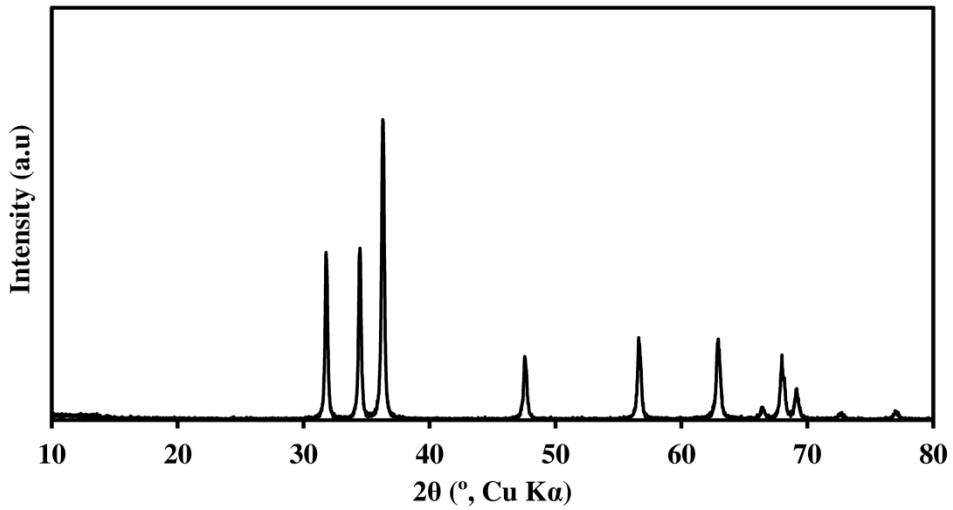

Figure A. 7. XRD on the product of calcination of BZA at 350 °C in the sublimation set-up shows only ZnO.

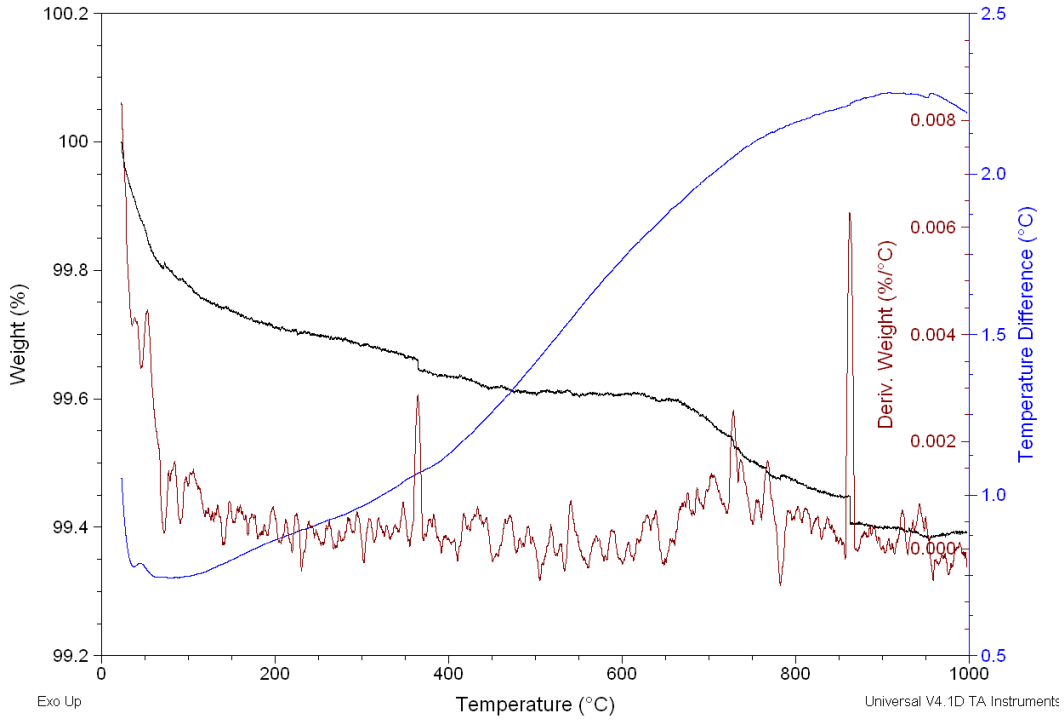

Figure A. 8. TGA-DTA on the product of calcination of BZA at 350 °C in the sublimation set-up.

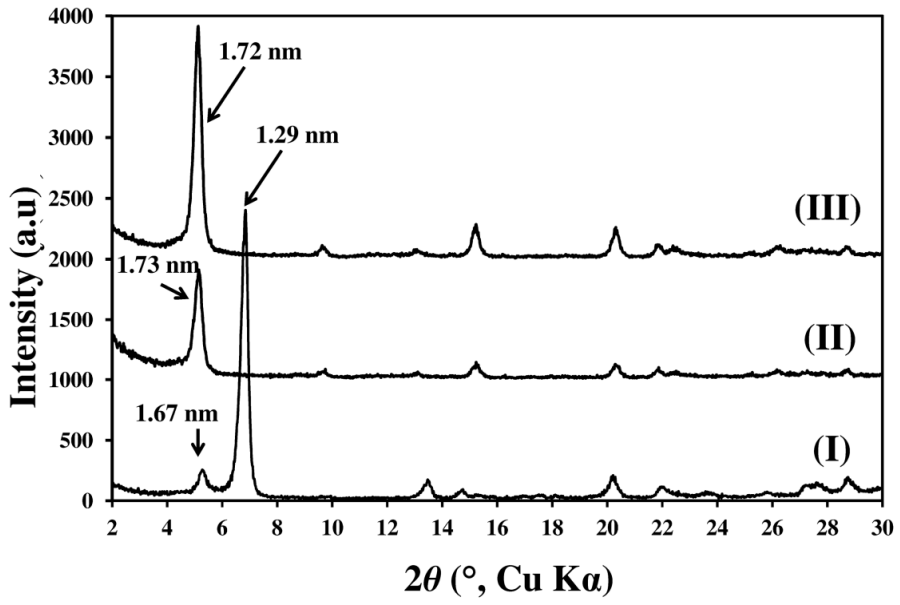

Figure A. 9. XRD on (I) BZA dihydrate, (II) product of the reaction between BZA and ethanol dried at 50 °C under reduced pressure and (III) the same product but freeze-dried for 24 hours. Step size = 0.02 °, time per step = 3 s, divergent slit = 1 °, receiving slit = 0.1 mm, scan angle range = 1.62-30 °.

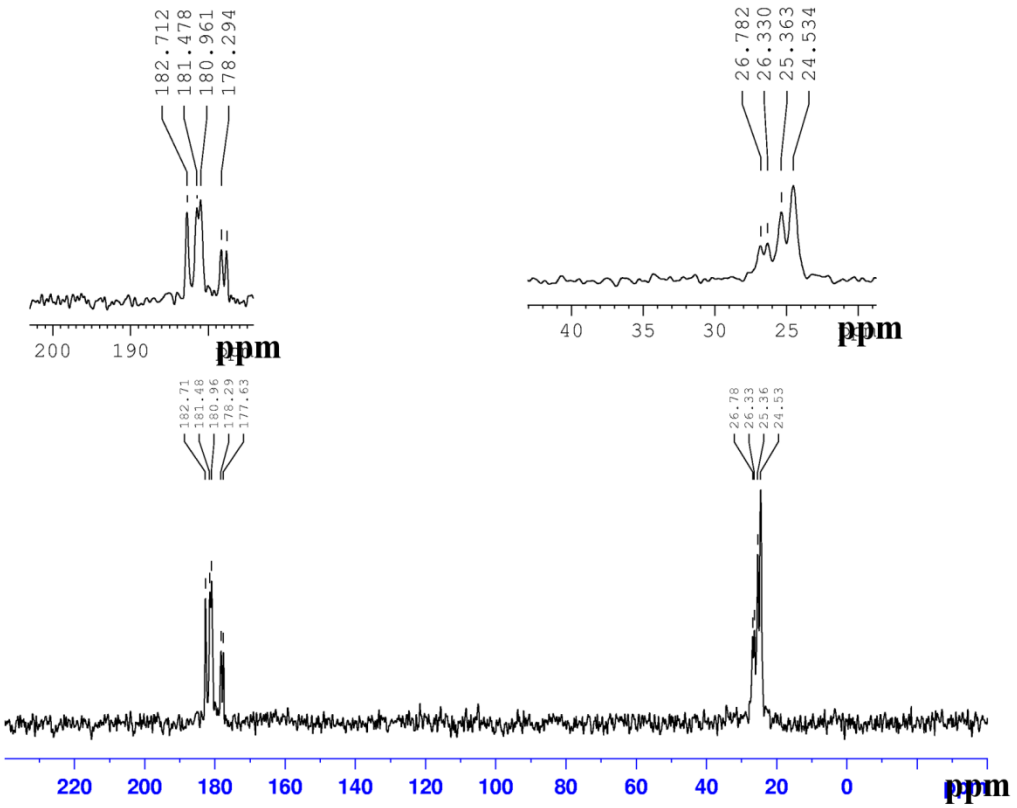

Figure A. 10. CP-MAS ^{13}C NMR spectrum of the product of the reaction between BZA and ethanol, freeze-dried for 24 hours.

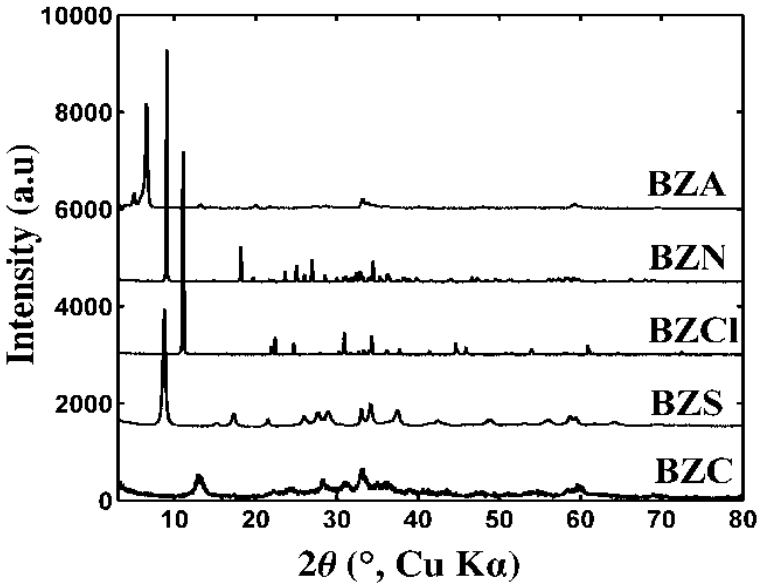

Figure A. 11. XRD (Cu Kα) on basic zinc salts for comparison.

References

[1] C.J. Frederickson, J.-Y. Koh, A.I. Bush, The neurobiology of zinc in health and disease, Nat. Rev. Neurosci., 6 (2005) 449 -462.
[2] U. Ozgur, I.A. Ya, C. Liu, A. Teke, M.A. Reshchikov, S. Dogan, V. Avrutin, S.J. Cho, H. Morkoc, A comprehensive review of ZnO materials and devices, J. Appl. Phys., 98 (2005) 041301.
[3] C. Klingshirn, ZnO: from basics towards applications, Phys. Status Solidi B, 244 (2007) 3027-3073.
[4] C. Klingshirn, ZnO: Material, Physics and Applications, ChemPhysChem, 8 (2007) 782-803.
[5] A.B. Djurisic, Y.H. Leung, Optical properties of ZnO nanostructures, Small, 2 (2006) 944-961.
[6] A. Janotti, C.G. Van de Walle, Fundamentals of zinc oxide as a semiconductor, Rep. Prog. Phys., 72 (2009) 126501/126501-126501/126529.
[7] S. Baruah, J. Dutta, Hydrothermal growth of ZnO nanostructures, Sci. Technol. Adv. Mater., 10 (2009) 013001.
[8] C. Wöll, The chemistry and physics of zinc oxide surfaces, Prog. Surf. Sci., 82 (2007) 55-120.
[9] M.D. McCluskey, S.J. Jokela, Defects in ZnO, J. Appl. Phys., 106 (2009) 071101-071113.
[10] Transparent Conductive Zinc Oxide, Springer Berlin Heidelberg, 2008.
[11] A. Moezzi, A.M. McDonagh, M.B. Cortie, Zinc oxide particles: Synthesis, properties and applications, Chem. Eng. J., 185-186 (2012) 1-22.
[12] B. Halioua, B. Ziskind, Medicine in the Days of the Pharaohs, Belknap Press of Harvard University Press, 2005.
[13] F. Habashi, Zinc- the metal from the East, CIM Bull., 94 (2001) 71-76.
[14] A.K. Biswas, Rasa-Ratna-Samuccaya and Mineral Processing State-of-Art in the 13th Century A.D. India, IJHS, 22 (1987) 22-46.
[15] H.C. Hoover, Georgius Agricola, de Re Metallica, Dover Publications, Inc., New York, 1950.
[16] M.i.A.S.a.-D. Al-Muqaddasi, Ahsan at-Taqasim fi Ma`rifat il-Aqhalim.
[17] J.S. Kharakwal, L.K. Gurjar, Zinc and brass in archaeological perspective, Ancient Asia, 1 (2006) 139-159.
[18] P.T. Craddock, S.C. La Niece, D.R. Hook, Brass in the medieval Islamic world, 2000 Years of Zinc and Brass, British Museum occasional paper No. , 50 (1990) 73-113.
[19] P.T. Craddock, The copper alloys of the medieval Islamic world - Inheritors of the classical tradition, World Archaeology, 11 (1979) 68-79.
[20] F. Habashi, Discovering the 8th Metal- A History of Zinc, International Zinc Association.
[21] Marco Polo, The Travels of Marco Polo, [cited 22/03/2011], Available from: http://en.wikisource.org/wiki/The_Travels_of_Marco_Polo/Book_1/Chapter_21#cite_note-note_2-1.
[22] M.E. Weeks, The discovery of the elements. III. Some eighteenth-century metals, J. Chem. Educ., 9 (1932) 22-30.
[23] M.E. Weeks, The discovery of the elements. Chronology, J. Chem. Educ., 10 (1933) 223-227.

[24] G. Auer, W.D. Griebler, B. Jahn, Industrial Inorganic Pigments, Third ed., Wiley-VCH Verlag GmbH & Co. KGaA, Weinheim, 2005.
[25] Winsor & Newton, The History of Pigments, [cited 11/08/2010], Available from: http://www.winsornewton.com/about-us/our-history/history-of-pigments/.
[26] A.C. Downs, Zinc for Paint and Architectural Use in the 19th Century, Bull. APT, 8 (1976) 80-99.
[27] W.W. Zeno, Jr., N.J. Frank, S.P. Pappas, A.W. Douglas, Pigments, in: Organic Coatings (Third Edition), John Wiley & Sons, Inc., 2007, pp. 417-434.
[28] S. Wetherill, Improvement in processes for making zinc-white, U.S. Patent 0013806 (1855).
[29] S. Wetherill, Apparatus for collection of white oxide of zinc, U.S. Patent 0012418 (1855).
[30] P.J. Nieuwenhuizen, Zinc accelerator complexes.: Versatile homogeneous catalysts in sulfur vulcanization, Appl. Catal., A, 207 (2001) 55-68.
[31] E.H.M. Moors, G.P.J. Dijkema, Embedded industrial production systems: Lessons from waste management in zinc production, Technol. Forecast. Soc. Change, 73 (2006) 250-265.
[32] Zinc Guide. (2004), International Zinc Association
[33] R.-q. Li, J.G. Peacey, Direct smelting or zinc concentrates and residues, U.S. Patent 5443614 (1995).
[34] A.C. Tolcin, 2009 Minerals Yearbook- ZINC. (2011), U.S. Geological Survey.
[35] International Zinc Association- Zinc oxide information center, [cited 18/05/2010], Available from: http://www.znoxide.org/index.html.
[36] A.S. Perl, Minerals review. Zinc oxide, Am. Ceram. Soc. Bull., 76 (1997) 140, 143.
[37] F. Porter, Zinc Handbook: Properties, Processing, And Use In Design, Marcel Dekker, 1991.
[38] P. Stephens, A. Chanse, Tyre tread compound, European Patent EP0461857 (1996).
[39] International Rubber Study Group, Statistical summary of world rubber situation, Rubber Stat. Bull., April-June 2011 (2011).
[40] F.C. Sahin, B. Derin, O. Yucel, Chloride removal from zinc ash, Scand. J. Metall., 29 (2000) 224-230.
[41] M. Barakat, The pyrometallurgical processing of galvanizing zinc ash and flue dust, JOM, 55 (2003) 26-29.
[42] P. Oustadakis, P.E. Tsakiridis, A. Katsiapi, S. Agatzini-Leonardou, Hydrometallurgical process for zinc recovery from electric arc furnace dust (EAFD): Part I: Characterization and leaching by diluted sulphuric acid, J. Hazard. Mater., 179 (2010) 1-7.
[43] J.B. Cashman, Converting zinc chloride to zinc oxide during the hydrometallurgical processing of flue dust, U.S. Patent 6361753 (2002).
[44] ASTM Standards, Standard Classification for Rubber Compounding Materials—Zinc Oxide (D 4295 - 89). (2005).
[45] Leclaire, Barruel, Making white zinc, U.S. Patent 0007351 (1850).
[46] S. Mahmud, M.J. Abdullah, Tapered head facets of zinc oxide nanorods, Solid State Sci. Technol., 15 (2007) 108-115.
[47] S. Mahmud, M. Johar Abdullah, G. Putrus, J. Chong, A. Karim Mohamad, Nanostructure of ZnO fabricated via French process and its correlation to electrical properties of semiconducting varistors, Synth. React. Inorg., Met.-Org., Nano-Met. Chem., 36 (2006) 155-159.

[48] B.K. Jung, Dust collector with assembly of cylindrical and hexahedral bag filter, U.S. Patent 6786946 (2004).
[49] R.D. Laundon, Zinc oxide and a process of making it, U.S. Patent 5876688 (1999).
[50] ASTM Standards, Standard Specification for Zinc Oxide Pigments (D 79 – 86). (2009).
[51] M.A. Bright, N.J. Deem, J. Fryatt, The advantages of recycling metallic zinc from the processing wastes of industrial molten zinc applications, [cited 09/01/2012], Available from: http://www.pyrotek.info/documents/techpapers/2007--adv_recycling_zinc_from_waste-tp-bright_deem_fryatt.pdf.
[52] J. Fryatt, Sustainability in galvanizing from in-house applied waste management of general hot dip galvanizing ashes and skimmings and continuous galvanizing line top drosses, [cited 09/01/2012], Available from: http://www.pyrotek.info/documents/techpapers/2010-09--Latingalva--Sustainability_InHouse_Zinc_Recovery--TP--Fryatt.pdf.
[53] ISO Standard, Rubber compounding ingredients - Zinc oxide - Test methods (9298:1995(E)). (1995).
[54] S. Mahmud, M.J. Abdullah, J. Chong, A.K. Mohamad, M.Z. Zakaria, Growth model for nanomallets of zinc oxide from a catalyst-free combust-oxidized process, J. Cryst. Growth, 287 (2006) 118-123.
[55] G.B. Lundevall, Zinc refining, U.S. Patent 2939783 (1960).
[56] Umicore Group, [cited 09/08/2010], Available from: http://www.umicore.com/en/.
[57] A. Richardson, Scrap zinc recycling at Challenge Metals and Technologies Limited, West Footscray, Vic, Aust. Min. Metall., Monograph 19-The Sir Maurice Mawby Memorial-2nd Edition (1993) 586-588.
[58] Henan Bailing Machinery Co., Zinc-oxide Rotary Kiln, [cited 28/03/2011], Available from: http://www.rotarykilns.org/Zinc-oxide_kiln.html.
[59] H. Serbent, G. Reuter, W. Schnabel, G. Kossek, Waelz process of volatilizing zinc and lead from iron oxide-containing materials, U.S. Patent 4238222 (1980).
[60] D. Temple, Zinc-lead blast furnace—the key developments, Metall. Trans. B, 11 (1980) 343-352.
[61] A.F.S. Schoukens, F. Shaw, E.C. Ghemaly, The enviroplas process for the treatment of steel-plant dusts, J. S. Afr. Inst. Min. Metall., 93 (1993) 1-7.
[62] W.P.C. Duyvesteyn, T. Bakker, M.R. Lastra, Hydrometallurgical process for producing zinc oxide, U.S. Patent 5441712 (1995).
[63] H. Kogoi, J. Tanaka, H. Yamaya, Ultrafine particulate zinc oxide and production process thereof, U.S. Patent 6416862 (2002).
[64] H.A. Depew, Zinc Oxide in Rubber, Ind. Eng. Chem., 25 (1933) 370-374.
[65] J.G. Speight, Chemical and Process Design Handbook, McGraw Hill, Inc., New York, 2002.
[66] ValoRes GmbH, The Waelz Kiln, [cited 10/06/2010], Available from: http://www.valo-res.com/pdf/WaelzKilnDescription-EN.pdf.
[67] S. Turner, S. Tavernier, G. Huyberechts, E. Biermans, S. Bals, K. Batenburg, G. Van Tendeloo, Assisted spray pyrolysis production and characterisation of ZnO nanoparticles with narrow size distribution, J. Nanopart. Res., 12 (2009) 615-622.
[68] X. Zhao, B. Zheng, C. Li, H. Gu, Acetate-derived ZnO ultrafine particles synthesized by spray pyrolysis, Powder Technol., 100 (1998) 20-23.
[69] J. Zhang, Y. Liu, J. Zeng, F. Xu, L. Sun, W. You, Y. Sawada, Thermodynamic properties and thermal stability of the synthetic zinc formate dihydrate, J. Therm. Anal. Calorim., 91 (2008) 861-866.

[70] H.K. Kammler, L. Mädler, S.E. Pratsinis, Flame Synthesis of Nanoparticles, Chem. Eng. Technol., 24 (2001) 583-596.
[71] G. Richards, J. Brimacombe, G. Toop, Kinetics of the zinc slag-Fuming process: Part i. industrial measurements, Metall. Trans. B, 16 (1985) 513-527.
[72] M.A. Abdel-latif, Fundamentals of zinc recovery from metallurgical wastes in the Enviroplas process, Miner. Eng., 15 (2002) 945-952.
[73] G.A. Yurko, Slag Fuming Process At The Cominco Smelter, Trail, British Columbia, in: World Symposium on Mining & Metallurgy of Lead & Zinc, 1970, pp. 330-347.
[74] G.G. Richards, S.L. Cockcroft, J.K. Brimacombe, G.W. Toop, Method for slag fuming and reduction, U.S. Patent 4820340 (1989).
[75] Zinc Clinker, [cited 04/01/2012], Available from: http://www.boliden.com/Products/Zinc-Clinker/
[76] Arc Fume, [cited 04/01/2012], Available from: http://www.scanarc.se/pages.asp?PageID=4145.
[77] K. Verscheure, M. Van Camp, B. Blanpain, P. Wollants, P. Hayes, E. Jak, Continuous fuming of zinc-bearing residues: Part II. The submerged-plasma zinc-fuming process, Metall. Mater. Trans. B, 38 (2007) 21-33.
[78] Environment Australia, Hazard Status of Zinc and Copper Ash, Dross and Residues under the Hazardous Waste Act, [cited 17/10/2011], Available from: http://www.environment.gov.au/settlements/chemicals/hazardous-waste/publications/pubs/gdzinc01.pdf
[79] A. Moezzi, M. Cortie, A. McDonagh, Aqueous pathways for the formation of zinc oxide nanoparticles, Dalton Trans., 40 (2011) 4871-4878.
[80] L.C. Ellis, Process for manufacture of stable sodium dithionite slurries, U.S. Patent 4283303 (1981).
[81] Silox, [cited 07/04/2011], Available from: http://www.silox.com/EN/SILOX-ENGIS/index.php.
[82] Zinc oxide, [cited 07/04/2011], Available from: http://www.brueggemann.com/english/zinkoxid.html.
[83] L.A. Pratt, The manufacture of sodium hyposulfite, Ind. Eng. Chem., 16 (1924) 676-677.
[84] F. Zhang, J. Yang, Preparation of nano-ZnO and its application to the textile on antistatic finishing, Int. J. Chem., 1 (2009) 18-22.
[85] M. Miksits, C. Tiburtius, J. Kischkewitz, K. Butje, A. Warth, F. Herzig, R. Langner, Finely divided, highly pure neutral zinc oxide powder, a process for its preparation and its use, U.S. Patent 5527519 (1996).
[86] R.L. Nip, Method of preparing zinc carbonate, U.S. Patent 6555075 (2003).
[87] Z. Zhang, Z. Zhang, J. Peng, L. Zhang, W. Qu, W. Li, Pyrolysis kinetic of basic zinc carbonate from spent catalyst and preparation of active ZnO by microwave heating, Adv. Mater. Res. (Zuerich, Switz.), 79-82 (2009) 2051-2054.
[88] W. Preis, H. Gamsjäger, (Solid + solute) phase equilibria in aqueous solution. XIII. Thermodynamic properties of hydrozincite and predominance diagrams for (Zn^{2+} + H_2O + CO_2), J. Chem. Thermodyn., 33 (2001) 803-819.
[89] J.A. Dean, Lange's Handbook of Chemistry, 15th ed., McGraw Hill, Inc., New York, 1999.
[90] N. Kanari, D. Mishra, I. Gaballah, B. Dupré, Thermal decomposition of zinc carbonate hydroxide, Thermochim. Acta, 410 (2004) 93-100.

[91] H.G. Wiedemann, A. Van Tets, R. Giovanoli, Determination of activation energy in moist and dry conditions for the pyrolysis of zinc hydroxide carbonate ($Zn_5(OH)_6(CO_3)_2$), Thermochim. Acta, 203 (1992) 241-250.
[92] Y. Sawada, M. Murakami, T. Nishide, Thermal analysis of basic zinc carbonate. Part 1. Carbonation process of zinc oxide powders at 8 and 13°C, Thermochim. Acta, 273 (1996) 95-102.
[93] N. Ohkuma, Y. Funayama, H. Ito, N. Mizutani, M. Kato, Adsorption and reaction of carbon dioxide gas on the surface of zinc oxide fine particles in the atmosphere, Hyomen Kagaku, 9 (1988) 452-458 (Japanese, English abstract).
[94] S. Homma, S. Ogata, J. Koga, S. Matsumoto, Gas-solid reaction model for a shrinking spherical particle with unreacted shrinking core, Chem. Eng. Sci., 60 (2005) 4971-4980.
[95] J.H. Calbeck, Production of zinc oxide, U.S. Patent 2603554 (1952).
[96] V.S. Robinson, Method for preparing particulate zinc oxide shapes of high surface area and improved strength, U.S. Patent 4071609 (1978).
[97] V.S. Robinson, Process for desulfurization using particulate zinc oxide shapes of high surface area and improved strength, U.S. Patent 4128619 (1978).
[98] C. Yan, D. Xue, Morphosynthesis of Hierarchical Hydrozincite with Tunable Surface Architectures and Hollow Zinc Oxide, J. Phys. Chem. B, 110 (2006) 11076-11080.
[99] K. Yu, Z. Jin, X. Liu, J. Zhao, J. Feng, Shape alterations of ZnO nanocrystal arrays fabricated from $NH_3 \cdot H_2O$ solutions, Appl. Surf. Sci., 253 (2007) 4072-4078.
[100] Z. Fang, Y. Wang, X. Peng, X. Liu, C. Zhen, Structural and optical properties of ZnO films grown on the AAO templates, Mater. Lett., 57 (2003) 4187-4190.
[101] R.A. Asmar, G. Ferblantier, F. Mailly, A. Foucaran, Structural and optical properties of ZnO fabricated by reactive e-beam and rf magnetron sputtering techniques, Phys. Status Solidi C, 2 (2005) 1331-1335.
[102] Y. Sun, G.M. Fuge, M.N.R. Ashfold, Growth of aligned ZnO nanorod arrays by catalyst-free pulsed laser deposition methods, Chem. Phys. Lett., 396 (2004) 21-26.
[103] D.C. Look, Recent advances in ZnO materials and devices, Mater. Sci. Eng., B, 80 (2001) 383-387.
[104] M.J. Coutts, H.M. Zareie, M.B. Cortie, M.R. Phillips, R. Wuhrer, A.M. McDonagh, Exploiting zinc oxide re-emission to fabricate periodic arrays, ACS Appl. Mater. Interfaces, 2 (2010) 1774-1779.
[105] A.A. Ashkarran, A. Iraji zad, S.M. Mahdavi, M.M. Ahadian, ZnO nanoparticles prepared by electrical arc discharge method in water, Mater. Chem. Phys., 118 (2009) 6-8.
[106] G.P. Zhu, C.X. Xu, X.F. Wu, Y. Yang, X.W. Sun, Y.P. Cui, Zinc oxide nanorods grown by arc discharge, J. Electron. Mater., 36 (2007) 494-497.
[107] Alfa Aesar, Nanoparticles and Dispersions, [cited 09/09/2010], Available from: http://www.alfa.com/en/docs/NanoparticlesandDispersionsBrochure.pdf.
[108] T.X. Wang, T.J. Lou, Solvothermal synthesis and photoluminescence properties of ZnO nanorods and nanorod assemblies from ZnO_2 nanoparticles, Mater. Lett., 62 (2008) 2329-2331.
[109] J.S. Jang, C.-J. Yu, S.H. Choi, S.M. Ji, E.S. Kim, J.S. Lee, Topotactic synthesis of mesoporous ZnS and ZnO nanoplates and their photocatalytic activity, J. Catal., 254 (2008) 144-155.
[110] L. Shen, N. Bao, K. Yanagisawa, A. Gupta, K. Domen, C.A. Grimes, Controlled synthesis and assembly of nanostructured ZnO architectures by a solvothermal soft chemistry process, Cryst. Growth Des., 7 (2007) 2742-2748.

[111] M. Palumbo, S.J. Henley, T. Lutz, V. Stolojan, S.R.P. Silva, A fast sonochemical approach for the synthesis of solution processable ZnO rods, J. Appl. Phys., 104 (2008) 074906/074901-074906/074906.
[112] A. Moballegh, H.R. Shahverdi, R. Aghababazadeh, A.R. Mirhabibi, ZnO nanoparticles obtained by mechanochemical technique and the optical properties, Surf. Sci., 601 (2007) 2850-2854.
[113] R. Aghababazadeh, B. Mazinani, A. Mirhabibi, M. Tamizifar, ZnO nanoparticles synthesised by mechanochemical processing, J. Phys.: Conf. Ser., 26 (2006) 312-314.
[114] J. Lu, K.M. Ng, S. Yang, J. Feng, One-step, paste-state mechanochemical process for the synthesis of zinc oxide nanoparticles, U.S. Patent 20100034730 (2010).
[115] J. Lu, K.M. Ng, S. Yang, Efficient, one-step mechanochemical process for the synthesis of ZnO nanoparticles, Ind. Eng. Chem. Res., 47 (2008) 1095-1101.
[116] F. Stenger, S. Mende, J. Schwedes, W. Peukert, The influence of suspension properties on the grinding behavior of alumina particles in the submicron size range in stirred media mills, Powder Technol., 156 (2005) 103-110.
[117] F. Stenger, S. Mende, J. Schwedes, W. Peukert, Nanomilling in stirred media mills, Chem. Eng. Sci., 60 (2005) 4557-4565.
[118] H. Liu, C. Hu, L. Wang Zhong, Composite-hydroxide-mediated approach for the synthesis of nanostructures of complex functional-oxides, Nano Lett., 6 (2006) 1535-1540.
[119] P. Patnaik, Handbook of Inorganic Chemicals, McGraw Hill, New York, 2003.
[120] Umicore, EU Classification - Directive 67/548/EEC, [cited 22/10/2010], Available from: http://www.zincchemicals.umicore.com/zcProducts/fineZincPowders/EHS/classification.htm.
[121] Regulation (EC) No 1272/2008 of the European Parliament and of the Council of 16 December 2008 on classification, labelling and packaging of substances and mixtures, amending and repealing Directives 67/548/EEC and 1999/45/EC, and amending Regulation (EC) No 1907/2006, OJEU, 51 (2008).
[122] G. Heideman, J. Noordermeer, W. M. , R. Datta, N. , B.v. Baarle, Various Ways to Reduce Zinc Oxide Levels in S-SBR Rubber Compounds, Macromolecular Symposia, 245-246 (2006) 657-667.
[123] M. Mortimer, K. Kasemets, A. Kahru, Toxicity of ZnO and CuO nanoparticles to ciliated protozoa Tetrahymena thermophila, Toxicology, 269 (2010) 182-189.
[124] World Health Organization (WHO), Environmental Health Criteria 221 - Zinc. (2001): Geneva.
[125] G.J. Nohynek, J. Lademann, C. Ribaud, M.S. Roberts, Grey goo on the skin? Nanotechnology, cosmetic and sunscreen safety, Crit. Rev. Toxicol., 37 (2007) 251-277.
[126] Australian Government, A review of the scientific literature on the safety of nanoparticulate titanium dioxide or zinc oxide in sunscreens, Department of Health and Aging-Therapeutic Goods Administration, Editor. (2009).
[127] N.C. Mueller, B. Nowack, Exposure modeling of engineered nanoparticles in the environment, Environ. Sci. Technol., 42 (2008) 4447-4453.
[128] A. Kahru, H.-C. Dubourguier, From ecotoxicology to nanoecotoxicology, Toxicology, 269 (2010) 105-119.
[129] M.E. Burnett, S.Q. Wang, Current sunscreen controversies: a critical review, Photodermatol. Photoimmunol. Photomed., 27 (2011) 58-67.
[130] Z.L. Wang, Zinc oxide nanostructures: Growth, properties and applications, J. Phys.: Condens. Matter, 16 (2004) R829-R858.

[131] S. Mahmud, M. Johar Abdullah, M.Z. Zakaria, Nanoscopic inhomogeneity in French process for large scale manufacturing of zinc oxide, Proceedings Of The International Meeting On Frontiers Of Physics (IMFP 2005), (2005).
[132] K. Kakiuchi, E. Hosono, T. Kimura, H. Imai, S. Fujihara, Fabrication of mesoporous ZnO nanosheets from precursor templates grown in aqueous solutions, J. Sol-Gel Sci. Technol., 39 (2006) 63-72.
[133] S. Mahmud, M.J. Abdullah, Nanotripods of zinc oxide, IEEE Conf. Emerging Technol.--Nanoelectron., (2006) 442-446.
[134] L. Shen, H. Zhang, S. Guo, Control on the morphologies of tetrapod ZnO nanocrystals, Mater. Chem. Phys., 114 (2009) 580-583.
[135] Y. Ding, Z.L. Wang, Structures of planar defects in ZnO nanobelts and nanowires, Micron, 40 (2009) 335-342.
[136] Z.L. Wang, Nanostructures of zinc oxide, Mater. Today, 7 (2004) 26-33.
[137] W. Yu, C. Pan, Low temperature thermal oxidation synthesis of ZnO nanoneedles and the growth mechanism, Mater. Chem. Phys., 115 (2009) 74-79.
[138] M.N.R. Ashfold, R.P. Doherty, N.G. Ndifor-Angwafor, D.J. Riley, Y. Sun, The kinetics of the hydrothermal growth of ZnO nanostructures, Thin Solid Films, 515 (2007) 8679-8683.
[139] J. Xie, P. Li, Y. Li, Y. Wang, Y. Wei, Morphology control of ZnO particles via aqueous solution route at low temperature, Mater. Chem. Phys., 114 (2009) 943-947.
[140] M.C. Newton, P.A. Warburton, ZnO tetrapod nanocrystals, Mater. Today, 10 (2007) 50-54.
[141] G. Walde, A. Rudy, Oxyde de zinc, carbonate de zinc et carbonate de zinc basique, leur procédé de fabrication et leur utilisation, French Patent FR2641268 (1990).
[142] D.C. Look, B. Claflin, P-type doping and devices based on ZnO, physica status solidi (b), 241 (2004) 624-630.
[143] F. Mao, H. Deng, L. Dai, J. Chen, Z. Yuan, Y. Li, High quality p-type ZnO film growth by a simple method and its properties, Chin. Sci. Bull., 53 (2008) 2582-2585.
[144] L.P. Dai, H. Deng, F.Y. Mao, J.D. Zang, The recent advances of research on p-type ZnO thin film, J. Mater. Sci.: Mater. Electron., 19 (2008) 727-734.
[145] M. Kawasaki, A. Ohtomo, T. Fukumura, A. Tsukazaki, M. Ohtani, Method of Manufacturing Thin Film, Method of Manufacturing P-Type Zinc Oxide Thin Film and Semiconductor Device, U.S. Patent 20080118769 (2008).
[146] K. Jacobs, D. Schulz, D. Klimm, S. Ganschow, Melt growth of ZnO bulk crystals in Ir crucibles, Solid State Sci., 12 (2010) 307-310.
[147] D. Schulz, S. Ganschow, D. Klimm, K. Struve, Inductively heated Bridgman method for the growth of zinc oxide single crystals, J. Cryst. Growth, 310 (2008) 1832-1835.
[148] D. Schulz, S. Ganschow, D. Klimm, M. Neubert, M. Roßberg, M. Schmidbauer, R. Fornari, Bridgman-grown zinc oxide single crystals, J. Cryst. Growth, 296 (2006) 27-30.
[149] Springer Handbook of Electronic and Photonic Materials, Springer, 2006.
[150] D.C. Look, B. Claflin, P-type doping and devices based on ZnO, Phys. Status Solidi B, 241 (2004) 624-630.
[151] D.C. Look, D.C. Reynolds, J.R. Sizelove, R.L. Jones, C.W. Litton, G. Cantwell, W.C. Harsch, Electrical properties of bulk ZnO, Solid State Commun., 105 (1998) 399-401.

[152] H.-C. Hsu, C.-Y. Wu, H.-M. Cheng, W.-F. Hsieh, Band gap engineering and stimulated emission of ZnMgO nanowires, Appl. Phys. Lett., 89 (2006) 013101/013101-013101/013103.
[153] V.A. Karpina, V.I. Lazorenko, C.V. Lashkarev, V.D. Dobrowolski, L.I. Kopylova, V.A. Baturin, S.A. Pustovoytov, A.J. Karpenko, S.A. Eremin, P.M. Lytvyn, V.P. Ovsyannikov, E.A. Mazurenko, Zinc oxide - analogue of GaN with new perspective possibilities, Cryst. Res. Technol., 39 (2004) 980-992.
[154] C. Klingshirn, R. Hauschild, J. Fallert, H. Kalt, Room-temperature stimulated emission of ZnO: Alternatives to excitonic lasing, Phys. Rev. B: Condens. Matter Mater. Phys., 75 (2007) 115203/115201-115203/115209.
[155] Y.Y. Li, Y.X. Li, Y.L. Wu, W.L. Sun, Preparation and photoluminescent properties of zinc oxide phosphor, J. Lumin., 126 (2007) 177-181.
[156] C.H. Lin, B.-S. Chiou, C.H. Chang, J.D. Lin, Preparation and cathodoluminescence of ZnO phosphor, Mater. Chem. Phys., 77 (2003) 647-654.
[157] W.H. Hirschwald, Zinc oxide: an outstanding example of a binary compound semiconductor, Acc. Chem. Res., 18 (1985) 228-234.
[158] K. Kyoung Hun, S. Seung Hwan, S. Kwang Bo, N. Koichi, H. Junichi, Microstructural and Thermoelectric Characteristics of Zinc Oxide-Based Thermoelectric Materials Fabricated Using a Spark Plasma Sintering Process, J. Am. Ceram. Soc., 88 (2005) 628-632.
[159] E. Guilmeau, A. Maignan, C. Martin, Thermoelectric Oxides: Effect of Doping in Delafossites and Zinc Oxide, J. Electron. Mater., 38 (2009) 1104-1108.
[160] Y. Inoue, Y. Okamoto, J. Morimoto, Thermoelectric properties of porous zinc oxide ceramics doped with praseodymium, J. Mater. Sci., 43 (2008) 368-377.
[161] H. Cheng, X.J. Xu, H.H. Hng, J. Ma, Characterization of Al-doped ZnO thermoelectric materials prepared by RF plasma powder processing and hot press sintering, Ceram. Int., 35 (2009) 3067-3072.
[162] T. Dietl, A ten-year perspective on dilute magnetic semiconductors and oxides, Nature Mater., 9 (2010) 965-974.
[163] H. Yoshida, K. Sato, Ferromagnetic p-type single-crystal zinc oxide material and manufacturing method thereof, U.S. Patent 7022182 (2006).
[164] K.R. Kittilstved, N.S. Norberg, D.R. Gamelin, Chemical manipulation of high-T_C ferromagnetism in ZnO diluted magnetic semiconductors, Phys. Rev. Lett., 94 (2005) 147209.
[165] M.A. Garcia, J.M. Merino, E. Fernandez Pinel, A. Quesada, J. de la Venta, M.L. Ruiz Gonzalez, G.R. Castro, P. Crespo, J. Llopis, J.M. Gonzalez-Calbet, A. Hernando, Magnetic Properties of ZnO Nanoparticles, Nano Lett., 7 (2007) 1489-1494.
[166] B.-Y. Oh, M.-C. Jeong, T.-H. Moon, W. Lee, J.-M. Myoung, J.-Y. Hwang, D.-S. Seo, Transparent conductive Al-doped ZnO films for liquid crystal displays, J. Appl. Phys., 99 (2006) 124505/124501-124505/124504.
[167] C.H. Park, S.B. Zhang, S.-H. Wei, Origin of p-type doping difficulty in ZnO: The impurity perspective, Phys. Rev. B, 66 (2002) 073202.
[168] D.C. Look, D.C. Reynolds, C.W. Litton, R.L. Jones, D.B. Eason, G. Cantwell, Characterization of homoepitaxial p-type ZnO grown by molecular beam epitaxy, Appl. Phys. Lett., 81 (2002) 1830-1832.
[169] A. Tsukazaki, A. Ohtomo, T. Onuma, M. Ohtani, T. Makino, M. Sumiya, K. Ohtani, S.F. Chichibu, S. Fuke, Y. Segawa, H. Ohno, H. Koinuma, M. Kawasaki, Repeated temperature modulation epitaxy for p-type doping and light-emitting diode based on ZnO, Nat. Mater., 4 (2005) 42-46.

[170] T. Yamamoto, H. Yoshida, T. Yao, P-type single crystal zinc-oxide having low resistivity and method for preparation thereof, U.S. Patent 6896731 (2005).
[171] D. Look, Progress in ZnO materials and devices, J. Electron. Mater., 35 (2006) 1299-1305.
[172] G.G. Gadzhiev, The thermal and elastic properties of zinc oxide-based ceramics at high temperatures, High Temp., 41 (2003) 778-782.
[173] N. Combe, P.-M. Chassaing, F. Demangeot, Surface effects in zinc oxide nanoparticles, Phys. Rev. B: Condens. Matter Mater. Phys., 79 (2009) 045408/045401-045408/045409.
[174] K.C. Waugh, Methanol synthesis, Catal. Today, 15 (1992) 51-75.
[175] B. Xin, J. Hao, Reversibly switchable wettability, Chem. Soc. Rev., 39 (2010) 769-782.
[176] X. Zhou, X. Guo, W. Ding, Y. Chen, Superhydrophobic or superhydrophilic surfaces regulated by micro-nano structured ZnO powders, Appl. Surf. Sci., 255 (2008) 3371-3374.
[177] G. Kwak, M. Seol, Y. Tak, K. Yong, Superhydrophobic ZnO Nanowire Surface: Chemical Modification and Effects of UV Irradiation, J. Phys. Chem. C, 113 (2009) 12085-12089.
[178] S. Liufu, H. Xiao, Y. Li, Investigation of PEG adsorption on the surface of zinc oxide nanoparticles, Powder Technol., 145 (2004) 20-24.
[179] K. Victor, K. Markus, K. Mathias, M. Klaus, Surface Functionalized ZnO Particles Designed for the Use in Transparent Nanocomposites, Macromol. Chem. Phys., 206 (2005) 95-101.
[180] E. Tang, G. Cheng, X. Pang, X. Ma, F. Xing, Synthesis of nano-ZnO/poly(methyl methacrylate) composite microsphere through emulsion polymerization and its UV-shielding property, Colloid & Polymer Science, 284 (2006) 422-428.
[181] E.J. Tait, B.C. Richard, B.A. Eugene, Photoconductive zinc oxide pigment, U.S. Patent 3060134 (1962).
[182] M.A. Sayyadnejad, H.R. Ghaffarian, M. Saeidi, Removal of hydrogen sulfide by zinc oxide nanoparticles in drilling fluid, Int. J. Environ. Sci. Technol., 5 (2008) 565-569.
[183] H.C. Lau, A.H. Hale, L.A. Bernardi Jr., Drilling fluid, U.S. Patent H001685 (1997).
[184] J.S. Gentry, G.R. Shelar, M.D. Shannon, R.L. Lehman, J.L. Resce, R.F. Hayden, O.D. Furin, A.B. Norman, T.A. Perfetti, Cigarette, U.S. Patent 5074321 (1991).
[185] G. Heideman, 2004, 'Reduced zinc oxide levels in sulphur vulcanisation of rubber compounds; mechanistic aspects of the role of activators and multifunctional additives', PhD. Thesis, University of Twente, Enschede, the Netherlands.
[186] S. Sahoo, S. Kar, A. Ganguly, M. Maiti, A. Bhowmick, Synthetic zinc oxide nanoparticles as curing agent for polychloroprene, Polym. Polym. Compos., 16 (2008) 193.
[187] P.M. Sabura Begum, K.K. Mohammed Yusuff, R. Joseph, Preparation and use of nano zinc oxide in neoprene rubber, Int. J. Polym. Mater., 57 (2008) 1083-1094.
[188] R.S. Hattori, J.F. Goncalves, The effects of metal oxides on thermal stabilization of EPDM insulation compounds, Conf. Rec. IEEE Int. Symp. Electr. Insul., (1992) 173-176.
[189] B.T. Poh, S.K. Chow, Effect of zinc oxide on the viscosity, tack, and peel strength of ENR 25-based pressure-sensitive adhesives, J. Appl. Polym. Sci., 106 (2007) 333-337.

[190] S. Moshref, Topical zinc oxide adhesive tape for keloid management, EJS, 25 (2006).
[191] R.L. Nip, Zinc oxide coated particles, compositions containing the same, and methods for making the same, U.S. Patent 20070072959 (2007).
[192] ASTM Standards, Standard Test Method for Evaluating the Effective Surface Area of Zinc Oxide in Rubber (D 4620 – 02). (2007).
[193] G. Heideman, J.W.M. Noordermeer, R.N. Datta, B. van Baarle, Zinc loaded clay as activator in sulfur vulcanization: A new route for zinc oxide reduction in rubber compounds, Rubber Chem. Technol., 77 (2004) 336-355.
[194] D.M. Eshelman, Treatment for reducing the dusting of treated zinc oxide, U.S. Patent 4270955 (1981).
[195] Digitalfire, Digitalfire Ceramic Oxides Directory-Zinc oxide, [cited 28/04/2011], Available from: http://digitalfire.com/4sight/oxide/zno.html.
[196] Nav Bharat Metallic Oxide Industries Pvt. Limited, Applications of zinc oxide, [cited 15/09/2009], Available from: http://www.navbharat.co.in/clients.htm.
[197] Umicore, Zinc Oxide Applications, [cited 17/05/2011], Available from: http://www.zincchemicals.umicore.com/ZincOxide/ZNOmarketApplications/.
[198] V.S. Ramachandran, Handbook of thermal analysis of construction materials, Noyes Publications, New York, USA, 2002.
[199] R.Y. Hong, L.L. Chen, J.H. Li, H.Z. Li, Y. Zheng, J. Ding, Preparation and application of polystyrene-grafted ZnO nanoparticles, Polym. Adv. Technol., 18 (2007) 901-909.
[200] K.H. Ding, G.L. Wang, M. Zhang, Characterization of mechanical properties of epoxy resin reinforced with submicron-sized ZnO prepared via in situ synthesis method, Mater. Des., 32 (2011) 3986-3991.
[201] Kirk-Othmer Encyclopedia of Chemical Technology, 4th ed., John Wiley and Sons, 1998.
[202] G. Peng, Q. Li, Y. Yang, H. Wang, Degradation of nano ZnO-glass fiber-unsaturated polyester composites, J. Appl. Polym. Sci., 114 (2009) 2128-2133.
[203] F.J. Honn, Stabilization of perfluorochlorocarbon plastics, U.S. Patent 2985620 (1961).
[204] A. Ammala, A.J. Hill, P. Meakin, S.J. Pas, T.W. Turney, Degradation studies of polyolefins incorporating transparent nanoparticulate zinc oxide UV stabilizers, J. Nanopart. Res., 4 (2002) 167-174.
[205] J.R. Brand, T.I. Brownbridge, J.W. Kauffman, Chemically inert pigmentary zinc oxides, U.S. Patent 4923518 (1990).
[206] U. Szerreiks, M. Baum, Linoleum floor covering, U.S. Patent 6831023 (2004).
[207] D. Reichwein, M. Ess, G. Burmeister, K.-h. Schwonke, Use of flame retardants in linoleum or cork-based floor coverings, U.S. Patent 20050048278 (2005).
[208] R. Putnam, M. Martin, Surprising Zinc, International Zinc Association.
[209] FDA, Sun Protection, [cited 19/05/2011], Available from: http://www.fda.gov/Radiation-EmittingProducts/RadiationEmittingProductsandProcedures/Tanning/ucm116445.htm.
[210] M.A. Mitchnick, D. Fairhurst, S.R. Pinnell, Microfine zinc oxide (Z-Cote) as a photostable UVA/UVB sunblock agent, J. Am. Acad. Dermatol., 40 (1999) 85-90.
[211] G. Hallmans, Wound healing with adhesive zinc tape. An animal experimental study, Scand. J. Plast. Reconstr. Surg., 10 (1976) 177-184.
[212] T.P. De Graaf, E. Galley, K.E. Butcher, Use of an antimicrobial agent, European Patent EP1079799 (1999).

[213] J. Brahms, J. Mattai, R. Jacoby, S. Chopra, E. Guenin, Dry deodorant containing a sesquiterpene alcohol and zinc oxide, U.S. Patent 20050191257 (2005).
[214] M. Regner, M.J. Prendergast, O. Thurlby, Oral zinc compositions, U.S. Patent 20070224134 (2007).
[215] A.E. Winston, T.W. Domke, A.L. Joseph, Dentifrices containing zinc oxide particles, U.S. Patent 5330748 (1994).
[216] D.J. Dhabhar, N.B. Shah, Zinc derivatives and their use in mouthwash compositions, U.S. Patent 4289754 (1981).
[217] Charles Flora Consumer Products, LLC [cited 26/05/2010], Available from: http://www.charlesflora.com/.
[218] Lavoris® History, [cited 26/05/2010], Available from: http://www.lavoris.com/history.html.
[219] P.J.A. Tijm, F.J. Waller, D.M. Brown, Methanol technology developments for the new millennium, Appl. Catal., A, 221 (2001) 275-282.
[220] H. Dreyfus, Manufacture of methyl alcohol, U.S. Patent 1868096 (1932).
[221] P. Davies, F.F. Snowdon, G.W. Bridger, D.O. Hughes, P.W. Young, Water-gas conversion and catalysts therefor, UK Patent GB1010871 (1965).
[222] C. Baltes, S. Vukojevic, F. Schueth, Correlations between synthesis, precursor, and catalyst structure and activity of a large set of $CuO/ZnO/Al_2O_3$ catalysts for methanol synthesis, J. Catal., 258 (2008) 334-344.
[223] A.B. Stiles, Methanol synthesis catalyst, U.S. Patent 4111847 (1978).
[224] R.W. Missen, Introduction to chemical reaction engineering and kinetics, John Wiley & Sons, Inc., 1999.
[225] J.E. Baker, R. Burch, S.J. Hibble, P.K. Loader, Properties of silica-supported Cu/Co bimetallic catalysts in the synthesis of higher alcohols, Applied Catalysis, 65 (1990) 281-292.
[226] A.H. Weiss, S. Trigerman, Zinc oxide as a formose catalyst, React. Kinet. Catal. Lett., 14 (1980) 259-263.
[227] H.S. Rosenberg, Process for simultaneous removal of SO_2 and NO_x from gas streams, U.S. Patent 4640825 (1987).
[228] H.F. Johnstone, A.D. Singh, Recovery of Sulfur Dioxide from Waste Gases, Industrial & Engineering Chemistry, 32 (1940) 1037-1049.
[229] V.L. Hartmann, Gas-solid reaction modeling as applied to the fine desulfurization of gaseous feedstocks, Chem. Eng. J., 134 (2007) 190-194.
[230] P.J. Denny, P.J.H. Carnell, Desulphurisation, European Patent EP0230146 (1991).
[231] C.J. Van Lookeren-campagne, S.P. Moore, E.D.A. Obeng, Gas treatment process, U.S. Patent 4758417 (1988).
[232] S. Shirakawa, Y. Kitano, Y. Kawai, S. Owada, Zinc-oxide surge arrester, U.S. Patent 4262318 (1981).
[233] O. Imai, R. Sato, Process for manufacturing a voltage non-linear resistor and a zinc oxide material to be used therefor, U.S. Patent 5250281 (1993).
[234] P. Stengard, Surge arrester, U.S. Patent 4853670 (1989).
[235] K.H. Brown, K.R. Wessells, S.Y. Hess, Zinc bioavailability from zinc-fortified foods, Int. J. Vitam. Nutr. Res., 77 (2007) 174-181.
[236] D.J. Eide, Zinc transporters and the cellular trafficking of zinc, Biochim. Biophys. Acta, 1763 (2006) 711-722.
[237] C.A. Swanson, J.C. King, Zinc and pregnancy outcome, Am. J. Clin. Nutr., 46 (1987) 763-771.
[238] R.J. Cousins, J.P. Liuzzi, L.A. Lichten, Mammalian zinc transport, trafficking, and signals, J. Biol. Chem., 281 (2006) 24085-24089.

[239] K.H. Brown, S.Y. Hess, International Zinc Nutrition Consultative Group technical document No. 2, Systematic reviews of zinc intervention strategies, Food Nutr. Bull., 30 (2009).
[240] G.L. Tucker, E.L. Blanton, Urea-zinc oxide composition and process, U.S. Patent 3981713 (1976).
[241] R.W. Fraley, P. Rogers, Pesticidal micronutrient compositions containing zinc oxide, U.S. Patent 5667795 (1997).
[242] H.M. Edwards, III, D.H. Baker, Bioavailability of zinc in several sources of zinc oxide, zinc sulfate, and zinc metal, J. Anim. Sci., 77 (1999) 2730-2735.
[243] ANI Zinc Oxide and Metals, Feed grade zinc oxide, [cited 20/05/2011], Available from: http://animetal.com.tr/products.php?ID=05-03.
[244] S. Herman, I.J. Griffin, S. Suwarti, F. Ernawati, D. Permaesih, D. Pambudi, S.A. Abrams, Cofortification of iron-fortified flour with zinc sulfate, but not zinc oxide, decreases iron absorption in Indonesian children, Am. J. Clin. Nutr., 76 (2002) 813-817.
[245] K.H. Brown, D.L. de Romaña, J.E. Arsenault, J.M. Peerson, M.E. Penny, Comparison of the effects of zinc delivered in a fortified food or a liquid supplement on the growth, morbidity, and plasma zinc concentrations of young Peruvian children, Am. J. Clin. Nutr., 85 (2007) 538-547.
[246] R.D. Wullschleger, S.C. Chen, F.A. Bowman, L.V. Hawblitz, Ready-to-eat cereal containing psyllium, U.S. Patent 5227248 (1993).
[247] D. Clark, E. Gillis, H. Gobble, N. Francisco, J. Kincaid, Fortified edible compositions and process of making, U.S. Patent 6168811 (2001).
[248] Kellogg, Kellogg's FiberPlus™ Antioxidants Bar Chocolate Chip, [cited 09/11/2011], Available from: http://www2.kelloggs.com/ProductDetail.aspx?id=16011.
[249] J.M. Seddon, Multivitamin-multimineral supplements and eye disease: age-related macular degeneration and cataract, Am. J. Clin. Nutr., 85 (2007) 304S-307S.
[250] NAN Pro 1 Gold Infant Formula, [cited 23/01/2012], Available from: http://www.nestlebaby.com/NR/rdonlyres/D26FF634-E877-4307-9089-6ABBDADB24C2/0/Pro_1_Gold.pdf.
[251] Locasol, [cited 23/01/2012], Available from: http://nutrition.nutricia.com/images/uploads/Locasol.pdf.
[252] W. Kim, F. Saito, Mechanochemical synthesis of zinc ferrite from zinc oxide and α-Fe_2O_3, Powder Technol., 114 (2001) 12-16.
[253] S.K. Gangwal, J.M. Stogner, S.M. Harkins, S.J. Bossart, Testing of novel sorbents for H_2S removal from coal gas, Environ. Prog., 8 (1989) 26-34.
[254] P. Hu, D.a. Pan, S. Zhang, J. Tian, A.A. Volinsky, Mn-Zn soft magnetic ferrite nanoparticles synthesized from spent alkaline Zn-Mn batteries, J. Alloys Compd., 509 (2011) 3991-3994.
[255] T.-H. Kim, J.-G. Kang, J.-S. Sohn, K.-I. Rhee, S.-W. Lee, S.-M. Shin, Preparation of Mn−Zn ferrite from spent zinc-carbon batteries by alkali leaching, acid leaching and Co-precipitation, Met. Mater. Int., 14 (2008) 655-658.
[256] A.C.F.M. Costa, E. Tortella, M.R. Morelli, R.H.G.A. Kiminami, Synthesis, microstructure and magnetic properties of Ni-Zn ferrites, J. Magn. Magn. Mater., 256 (2003) 174-182.
[257] S.G. Bachhav, R.S. Patil, P.B. Ahirrao, A.M. Patil, D.R. Patil, Microstructure and magnetic studies of Mg-Ni-Zn-Cu ferrites, Mater. Chem. Phys., 129 (2011) 1104-1109.
[258] N.E. Danjushevskaya, O.V. Alexeeva, B.G. Pogostkina, V.M. Kovalenko, Z.A. Mironova, Process for producing zinc phosphate, U.S. Patent 4207301 (1980).
[259] D.M. Schubert, Process of making zinc borate and fire-retarding compositions thereof, U.S. Patent 5342553 (1994).

[260] D. Gürhan, G.Ö. Çakal, I. Eroglu, S. Özkar, Improved synthesis of fine zinc borate particles using seed crystals, J. Cryst. Growth, 311 (2009) 1545-1552.
[261] A.M. Barnes, K.D. Bartle, V.R.A. Thibon, A review of zinc dialkyldithiophosphates (ZDDPS): characterisation and role in the lubricating oil, Tribol. Int., 34 (2001) 389-395.
[262] L.R. Rudnick, Lubricant Additives: Chemistry and Applications, Marcel Dekker, Inc., New York, 2003.
[263] C.-p. Tsou, R.-t. Chen, C.-m. Su, Process for producing modified zinc acrylate fine powder, U.S. Patent 6278010 (2001).
[264] Comprehensive Coordination Chemistry II 2nd ed., Elsevier, 2005.
[265] W. Scheunemann, IR Optical Properties of a Pyrotechnic Screening Smoke, Propell. Explos. Pyrotech., 4 (1979) 95-97.
[266] R.F.R. Brown, T.C. Marrs, P. Rice, L.C. Masek, The histopathology of rat lung following exposure to zinc oxide/hexachloroethane smoke or instillation with zinc chloride followed by treatment with 70% oxygen, Environ. Health Perspect., 85 (1990) 81-87.
[267] ASTM Standards, Standard Test Methods for Zinc and Cadmium in Paper (D 1224 - 92). (2006).
[268] X.Y. Wang, J.M. Wang, Q.L. Wang, H.B. Shao, J.Q. Zhang, The effects of polyethylene glycol (PEG) as an electrolyte additive on the corrosion behavior and electrochemical performances of pure aluminum in an alkaline zincate solution, Mater. Corros., 61 (2010).
[269] J.R. Butler, B. Lee, P.J. Buras, Crosslinking with metal oxides other than zinc oxide, U.S. Patent 20060241217 (2006).
[270] S.B. Salvin, Influence of zinc oxide on paint molds, Ind. Eng. Chem., 36 (1944) 336-340.
[271] K. Utsumi, H. Iigusa, T. Mitsuru, Y. Suzuki, Zinc oxide-based transparent conductor films, liquid crystal displays, and zinc oxide-based sputtering targets, Japanese Patent 2007329051 (2007).
[272] L. Gong, J. Lu, Z. Ye, Transparent and conductive Ga-doped ZnO films grown by RF magnetron sputtering on polycarbonate substrates, Sol. Energy Mater. Sol. Cells, 94 (2010) 937-941.
[273] Y.-S. Choi, J.-W. Kang, D.-K. Hwang, S.-J. Park, Recent advances in ZnO-based light-emitting diodes, IEEE Trans. Electron Devices, 57 (2010) 26-41.
[274] C. Czekalla, J. Lenzner, A. Rahm, T. Nobis, M. Grundmann, A zinc oxide microwire laser, Superlattices Microstruct., 41 (2007) 347-351.
[275] N. Rao, C.M. van den Bleek, J. Schoonman, Taguchi-type NOx gas sensors based on semiconducting mixed oxides, Solid State Ionics, 59 (1993) 263-270.
[276] L. Schmidt-Mende, J.L. MacManus-Driscoll, ZnO - nanostructures, defects, and devices, Mater. Today, 10 (2007) 40-48.
[277] M.J. Vellekoop, C.C.O. Visser, P.M. Sarro, A. Venema, Compatibility of zinc oxide with silicon IC processing, Sens. Actuators, A: Phys, 23 (1990) 1027-1030.
[278] J. Lozano, M.J. Fernandez, J.L. Fontecha, M. Aleixandre, J.P. Santos, I. Sayago, T. Arroyo, J.M. Cabellos, F.J. Gutierrez, M.C. Horrillo, Wine classification with a zinc oxide SAW sensor array, Sens. Actuators, B, 120 (2006) 166-171.
[279] N. Vigneshwaran, S. Kumar, A.A. Kathe, P.V. Varadarajan, V. Prasad, Functional finishing of cotton fabrics using zinc oxide-soluble starch nanocomposites, Nanotechnology, 17 (2006) 5087-5095.

[280] A. Becheri, M. Dürr, P. Lo Nostro, P. Baglioni, Synthesis and characterization of zinc oxide nanoparticles: application to textiles as UV-absorbers, J. Nanopart. Res., 10 (2008) 679-689.
[281] R.A. McBride, J.M. Kelly, D.E. McCormack, Growth of well-defined ZnO microparticles by hydroxide ion hydrolysis of zinc salts, J. Mater. Chem., 13 (2003) 1196-1201.
[282] K. Govender, D.S. Boyle, P.B. Kenway, P. O'Brien, Understanding the factors that govern the deposition and morphology of thin films of ZnO from aqueous solution, J. Mater. Chem., 14 (2004) 2575-2591.
[283] A.P.A. Oliveira, J.-F. Hochepied, F. Grillon, M.-H. Berger, Controlled precipitation of zinc oxide particles at room temperature, Chem. Mater., 15 (2003) 3202-3207.
[284] K. Jacobs, D. Balitsky, P. Armand, P. Papet, Low-temperature chemical bath deposition of crystalline ZnO, Solid State Sci., 12 (2010) 333-338.
[285] J.J. Richardson, F.F. Lange, Controlling low temperature aqueous synthesis of ZnO. 1. Thermodynamic analysis, Cryst. Growth Des., 9 (2009) 2570-2575.
[286] S. Sepulveda-Guzman, B. Reeja-Jayan, E. de la Rosa, A. Torres-Castro, V. Gonzalez-Gonzalez, M. Jose-Yacaman, Synthesis of assembled ZnO structures by precipitation method in aqueous media, Mater. Chem. Phys., 115 (2009) 172-178.
[287] A. Goux, T. Pauporté, J. Chivot, D. Lincot, Temperature effects on ZnO electrodeposition, Electrochim. Acta, 50 (2005) 2239-2248.
[288] C. Debiemme-Chouvy, J. Vedel, Supersaturated zincate solutions: A study of the decomposition kinetics, J. Electrochem. Soc., 138 (1991) 2538-2542.
[289] Y. Zhang, M. Muhammed, Critical evaluation of thermodynamics of complex formation of metal ions in aqueous solutions VI. Hydrolysis and hydroxo-complexes of Zn^{2+} at 298.15 K, Hydrometallurgy, 60 (2001) 215-236.
[290] R.A. Reichle, K.G. McCurdy, L.G. Hepler, Zinc hydroxide: solubility product and hydroxy-complex stability constants from 12.5-75 ºC, Can. J. Chem., 53 (1975) 3841-3845.
[291] T.P. Dirkse, The solubility product constant of zinc oxide, J. Electrochem. Soc., 133 (1986) 1656-1657.
[292] A.D. James, C.S. Noel, K.D. Steven, A practical guide for determining the solubility of metal hydroxides and oxides in water, Environ. Prog., 17 (1998) 1-8.
[293] Zhang, K. Yanagisawa, Hydrothermal Synthesis of Zinc Hydroxide Chloride Sheets and Their Conversion to ZnO, Chem. Mater., 19 (2007) 2329-2334.
[294] C. Chambers, A.K. Holliday, Modern Inorganic Chemistry, The Butterworth Group, London, 1975.
[295] G. Brauer, Handbook of Preparative Inorganic Chemistry, 2nd ed., Academic Press Inc., London, 1963.
[296] H.G. Dietrich, J. Johnston, Equilibrium between crystalline zinc hydroxide and aqueous solutions of ammonium hydroxide and of sodium hydroxide, J. Am. Chem. Soc., 49 (1927) 1419-1431.
[297] J. Zhang, Sun, Yin, Su, Liao, Yan, Control of ZnO Morphology via a Simple Solution Route, Chem. Mater., 14 (2002) 4172-4177.
[298] A.N. Maslii, M.S. Shapnik, A.M. Kuznetsov, Electroreduction of Zn(II) hydroxy-complexes in aqueous electrolytes: a quantum-chemical study, Russ. J. Electrochem., 37 (2001) 615-622.
[299] P. Ramamurthy, E.A. Secco, Metal hydroxy compounds. V. Heats of decomposition of zinc and cadmium halide (Cl,F) derivatives, Can. J. Chem., 46 (1968) 3605-3606.

[300] A. Shaporev, V. Ivanov, A. Baranchikov, O. Polezhaeva, Y. Tret'yakov, ZnO formation under hydrothermal conditions from zinc hydroxide compounds with various chemical histories, Russ. J. Inorg. Chem., 52 (2007) 1811-1816.
[301] M. Choi, K. McBean, P. Ng, A. McDonagh, P. Maynard, C. Lennard, C. Roux, An evaluation of nanostructured zinc oxide as a fluorescent powder for fingerprint detection, J. Mater. Sci., 43 (2008) 732-737.
[302] L. Irimpan, V.P.N. Nampoori, P. Radhakrishnan, A. Deepthy, B. Krishnan, Size dependent fluorescence spectroscopy of nanocolloids of ZnO, J. Appl. Phys., 102 (2007) 063524-063526.
[303] E. Sotelo-Gonzalez, M.T. Fernandez-Argüelles, J.M. Costa-Fernandez, A. Sanz-Medel, Mn-doped ZnS quantum dots for the determination of acetone by phosphorescence attenuation, Anal. Chim. Acta, 712 (2012) 120-126.
[304] R. Bardhan, H. Wang, F. Tam, J. Halas Naomi, Facile chemical approach to ZnO submicrometer particles with controllable morphologies, Langmuir, 23 (2007) 5843-5847.
[305] L. Rosenthal-Toib, K. Zohar, M. Alagem, Y. Tsur, Synthesis of stabilized nanoparticles of zinc peroxide, Chem. Eng. J., 136 (2008) 425-429.
[306] L. Ibarra, M. Alzorriz, Vulcanization of carboxylated nitrile rubber (XNBR) by zinc peroxide, Polym. Int., 48 (1999) 580-586.
[307] W. Chen, Y.H. Lu, M. Wang, L. Kroner, H. Paul, H.J. Fecht, J. Bednarcik, K. Stahl, Z.L. Zhang, U. Wiedwald, U. Kaiser, P. Ziemann, T. Kikegawa, C.D. Wu, J.Z. Jiang, Synthesis, Thermal Stability and Properties of ZnO_2 Nanoparticles, J. Phys. Chem. C, 113 (2009) 1320-1324.
[308] R. Hagel, K. Redecker, Use of zinc peroxide as oxidant for explosives and pyrotechnical mixtures, U.S. Patent 4363679 (1982).
[309] C.J. Kim, A.A. Koski, Zinc peroxide process, U.S. Patent 4394488 (1983).
[310] J. Li, R. Kykyneshi, J. Tate, A.W. Sleight, p-Type zinc oxide powders, Solid State Sci., 9 (2007) 613-618.
[311] N. Uekawa, N. Mochizuki, H. Kajiwara, F. Mori, Y.J. Wu, K. Kakegawa, Nonstoichiometric properties of zinc oxide nanoparticles prepared by decomposition of zinc peroxide. [Erratum to document cited in CA138:403646], Phys. Chem. Chem. Phys., 5 (2003) 1489.
[312] S. Cheng, D. Yan, J.T. Chen, R.F. Zhuo, J.J. Feng, H.J. Li, H.T. Feng, P.X. Yan, Soft-template synthesis and characterization of ZnO_2 and ZnO hollow spheres, J. Phys. Chem. C, 113 (2009) 13630-13635.
[313] A. Escobedo-Morales, R. Esparza, A. García-Ruiz, A. Aguilar, E. Rubio-Rosas, R. Pérez, Structural and vibrational properties of hydrothermally grown ZnO_2 nanoparticles, J. Cryst. Growth, 316 (2011) 37-41.
[314] H. Morioka, H. Tagaya, J.I. Kadokawa, K. Chiba, Studies on layered basic zinc acetate, J. Mater. Sci. Lett., 18 (1999) 995-998.
[315] S.P. Newman, W. Jones, Comparative study of some layered hydroxide salts containing exchangeable interlayer anions, J. Solid State Chem., 148 (1999) 26-40.
[316] J.W. Boclair, P.S. Braterman, Layered double hydroxide stability. 1. Relative stabilities of layered double hydroxides and their simple counterparts, Chem. Mater., 11 (1999) 298-302.
[317] L. Xue, X. Mei, W. Zhang, L. Yuan, X. Hu, Y. Huang, K. Yanagisawa, Synthesis and assembly of zinc hydroxide sulfate large flakes: Application in gas sensor based on a novel surface mount technology, Sens. Actuators, B, 147 (2010) 495–501.

[318] C.S. Cordeiro, G.G.C. Arizaga, L.P. Ramos, F. Wypych, A new zinc hydroxide nitrate heterogeneous catalyst for the esterification of free fatty acids and the transesterification of vegetable oils, Catal. Commun., 9 (2008) 2140-2143.
[319] A. Zieba, A. Pacula, E.M. Serwicka, A. Drelinkiewicz, Transesterification of triglycerides with methanol over thermally treated $Zn_5(OH)_8(NO_3)_2 \times 2H_2O$ salt, Fuel, 89 (2010) 1961-1972.
[320] W.D. Warinner, E.H. Conroy, Production of zinc oxysulfate, U.S. Patent 2602727 (1952).
[321] US Environmental Protection Agency, Zinc Fertilizers Made From Recycled Hazardous Secondary Materials. (2002). p. 48393-48415.
[322] D.G. Westfall, M. Amrani, G.A. Peterson, Water-solubility of zinc fertilizer: Does it matter?, Better Crops, 83 (1999) 18-22.
[323] L. Poul, N. Jouini, F. Fievet, Layered hydroxide metal acetates (metal = zinc, cobalt, and nickel): Elaboration via hydrolysis in polyol medium and comparative study, Chem. Mater., 12 (2000) 3123-3132.
[324] E. Hosono, S. Fujihara, T. Kimura, H. Imai, Growth of layered basic zinc acetate in methanolic solutions and its pyrolytic transformation into porous zinc oxide films, J. Colloid Interface Sci., 272 (2004) 391-398.
[325] Z. Li, X. Shen, X. Feng, P. Wang, Z. Wu, Non-isothermal kinetics studies on the thermal decomposition of zinc hydroxide carbonate, Thermochim. Acta, 438 (2005) 102-106.
[326] Y. Liu, J. Zhao, H. Zhang, Y. Zhu, Z. Wang, Thermal decomposition of basic zinc carbonate in nitrogen atmosphere, Thermochim. Acta, 414 (2004) 121-123.
[327] L. Shang, World development of activated zinc oxide, Xiandai Huagong, 15 (1995) 12-14.
[328] R.L. Nip, Method of preparing zinc ammonia carbonate solution, U.S. Patent 20030152508 (2003).
[329] J.B. Conn, H.W. Karl, Process for preparing zinc oxide, U.S. Patent 2898191 (1959).
[330] M.J. Engberg, Process for manufacturing basic zinc carbonate, U.S. Patent 1944415 (1934).
[331] K.E. Butcher, T.P. De Graaf, E. Galley, Odour absorbing agent, European Patent EP1079798 (2003).
[332] T.P. De Graaf, E. Galley, K.E. Butcher, Use of an antimicrobial agent, European Patent EP1079799 (2004).
[333] L.P. Hoboy, N.A. Wolf, T.F. Yoder, Process to produce simonkolleite, zinc oxide and zinc hydroxide, U.S. Patent 6863873 (2005).
[334] W. Feitknecht, Die Struktur der basischen Salze zweiwertiger Metalle, Helv. Chim. Acta, 16 (1933) 427-454.
[335] A. Riccardo, Manufacture of zinc oxide, U.S. Patent 2105394 (1938).
[336] A.H. Nobari, M. Halali, An investigation on the calcination kinetics of zinc carbonate hydroxide and Calsimin zinc carbonate concentrate, Chem. Eng. J., 121 (2006) 79-84.
[337] Zinc oxide, [cited 15/09/2009], Available from: http://en.wikipedia.org/wiki/Zinc_oxide#cite_note-mende-37.
[338] Thermochromism, [cited 08/10/2009], Available from: http://en.wikipedia.org/wiki/Thermochromism.
[339] I.J. Bear, I.E. Grey, I.E. Newnham, L.J. Rogers, The $ZnSO_4.3Zn(OH)_2$-H_2O system. I. Phase formation, Aust. J. Chem., 40 (1987) 539-556.

[340] I.J. Bear, I.E. Grey, I.C. Madsen, I.E. Newnham, L.J. Rogers, Structures of the basic zinc sulfates $3Zn(OH)_2.ZnSO_4.mH_2O$, m = 3 and 5, Acta Crystallogr., Sect. B: Struct. Sci, 42 (1986) 32-39.
[341] T. Chen, J. Dutrizac, Filter press plugging in zinc plant purification circuits, JOM, 55 (2003) 28-31.
[342] I.M. Kolthoff, T. Kameda, The hydrolysis of zinc sulfate solutions, solubility product of hydrous zinc oxide and the composition of the latter precipitated from zinc sulfate solutions, J. Am. Chem. Soc., 53 (1931) 832-842.
[343] Y. Fukuda, T. Nitta, T. Matsuoka, F. Fukushima, S. Hayakawa, Basic zinc compound flake-like crystalline particle and method for preparation thereof, U.S. Patent 4261965 (1981).
[344] J. Plewa, J. Steindor, Investigation of basic zinc sulfate thermal decomposition under nitrogen and carbon monoxide atmosphere, Thermochim. Acta, 137 (1989) 281-291.
[345] M. Rajamathi, G.S. Thomas, P.V. Kamath, The many ways of making anionic clays, Proc. - Indian Acad. Sci., Chem. Sci., 113 (2001) 671-680.
[346] B.C. Yadav, R. Srivastava, C.D. Dwivedi, P. Pramanik, Synthesis of nano-sized ZnO using drop wise method and its performance as moisture sensor, Sens. Actuators, A: Phys, 153 (2009) 137-141.
[347] T. Biswick, W. Jones, A. Pacula, E. Serwicka, J. Podobinski, The role of anhydrous zinc nitrate in the thermal decomposition of the zinc hydroxy nitrates $Zn_5(OH)_8(NO_3)_2 \cdot 2H_2O$ and $ZnOHNO_3 \cdot H_2O$, J. Solid State Chem., 180 (2007) 1171-1179.
[348] T. Biswick, W. Jones, A. Pacula, E. Serwicka, J. Podobinski, Evidence for the formation of anhydrous zinc acetate and acetic anhydride during the thermal degradation of zinc hydroxy acetate, $Zn_5(OH)_8(CH_3CO_2)_2 \cdot 4H_2O$ to ZnO, Solid State Sci., 11 (2009) 330-335.
[349] R. Narayan, A. Tabatabaie-Raissi, M.J. Antal, A study of zinc sulfate decomposition at low heating rates, Ind. Eng. Chem. Res., 27 (1988) 1050-1058.
[350] A. Tabatabaie-Raissi, R. Narayan, W.S.L. Mok, M.J. Antal, Solar thermal, decomposition kinetics of zinc sulfate at high heating rates, Ind. Eng. Chem. Res., 28 (1989) 355-362.
[351] J.G. Ibanez, W.E. Wentworth, C.F. Batten, E.C.M. Chen, Kinetics of the thermal decomposition of zinc sulfate, Rev. Int. Hautes Temp. Refract., 21 (1984) 113-124.
[352] J.G. Ibanez, W.E. Wentworth, C.F. Batten, E.C.M. Chen, Study of the reaction of ammonium sulfate (NH_4HSO_4) with zinc oxide as part of an energy storage cycle, Rev. Int. Hautes Temp. Refract., 21 (1984) 125-136.
[353] T.R. Ingraham, H.H. Kellogg, Thermodynamic properties of zinc sulfate, zinc basic sulfate, and the system Zn-S-O, Trans. Am. Inst. Min., Metall. Pet. Eng., 227 (1963) 1419-1426.
[354] S. V. Krivovichev, S. K. Filatov, T.y. F. Semenova, Types of cationic complexes based on oxocentered tetrahedra $[OM_4]$ in crystal structures of inorganic compounds, Russ. Chem. Rev., 67 (1998) 137-155.
[355] G. Hoschek, Die thermische Zersetzung der Sulfide und Sulfate zweiwertiger Kationen in Luft: Cu-, Zn-, Cd-, Hg-, Sn- und Pb-Verbindungen, Monatshefte für Chemie / Chemical Monthly, 93 (1962) 826-840.
[356] H.N. Terem, S. Akalan, Sur la dissociation des sulfates de fer, de zinc et de plomb, C. R. Hebd. Seances. Acad. Sci., 232 (1951) 973-975.

[357] R.D. Brittain, K.H. Lau, D.R. Knittel, D.L. Hildenbrand, Effusion studies of the decomposition of zinc sulfate and zinc oxysulfate, J. Phys. Chem., 90 (1986) 2259-2264.
[358] J.L. Harris, J.R. Norman, Temperature-dependent kinetic equation for catalytic oxidation of sulfur dioxide, Ind. Eng. Chem. Process Des. Dev., 11 (1972) 564-573.
[359] J.H. Sinfelt, Applied reaction kinetics-catalytic reactions, Ind. Eng. Chem., 62 (1970) 22-27.
[360] Y. Shi, M. Fan, Reaction kinetics for the catalytic oxidation of sulfur dioxide with microscale and nanoscale iron oxides, Ind. Eng. Chem. Res., 46 (2007) 80-86.
[361] J.P. Dunn, H.G. Stenger, I.E. Wachs, Molecular structure-reactivity relationships for the oxidation of sulfur dioxide over supported metal oxide catalysts, Catal. Today, 53 (1999) 543-556.
[362] J.P. Dunn, P.R. Koppula, H. G. Stenger, I.E. Wachs, Oxidation of sulfur dioxide to sulfur trioxide over supported vanadia catalysts, Appl. Catal., B, 19 (1998) 103-117.
[363] K.H. Kim, J.S. Choi, Kinetics and mechanism of the oxidation of sulfur dioxide on α-Fe_2O_3, J. Phys. Chem., 85 (1981) 2447-2450.
[364] M. Sorel, Procédé pour la formation d'un ciment très-solide par l'action d'un chlorure sur l'oxyde de zinc, C. R. Hebd. Seances. Acad. Sci., 41 (1855) 784-785.
[365] C.A. Sorrell, Suggested Chemistry of Zinc Oxychloride Cements, J. Am. Ceram. Soc., 60 (1977) 217-220.
[366] H.-E. Forsberg, W. Nowacki, On the Crystal Structure of β-ZnOHCl, Acta Chem. Scand., 13 (1959) 1049-1050.
[367] H.R. Oswald, W. Feitknecht, Über die Hydroxidchloride Me(OH)Cl. (Me = Mg, Ni, Co, Cu, Zn, Fe, Mn, Cd, Ca, Sn), Helv. Chim. Acta, 44 (1961) 847-858.
[368] S.H. Son, F. Tsukihashi, Vapor pressure measurement of zinc oxychloride, J. Phys. Chem. Solids, 66 (2005) 392-395.
[369] P. Dvorák, J. Jandová, Hydrometallurgical recovery of zinc from hot dip galvanizing ash, Hydrometallurgy, 77 (2005) 29-33.
[370] J. He, M. Wei, B. Li, Y. Kang, D.G. Evans, X. Duan, Preparation of layered double hydroxides, Struct. Bonding (Berlin, Ger.), 119 (2006) 89-119.
[371] R. Prost, T. Koutit, A. Benchara, E. Huard, State and location of water adsorbed on clay minerals: consequences of the hydration and swelling-shrinkage phenomena, Clays Clay Miner., 46 (1998) 117-131.
[372] S. Yamashita, H. Watanabe, T. Shirai, M. Fuji, M. Takahashi, Liquid phase synthesis of ZnO microrods highly oriented on the hexagonal ZnO sheets, Adv. Powder Technol., In Press (2011).
[373] H. Morioka, H. Tagaya, M. Karasu, J.-i. Kadokawa, K. Chiba, Preparation of hydroxy double salts exchanged by organic compounds, J. Mater. Res., 13 (1998) 848-851.
[374] Z. Yong, V. Mata, A.E. Rodrigues, Adsorption of carbon dioxide onto hydrotalcite-like compounds (HTlcs) at high temperatures, Ind. Eng. Chem. Res., 40 (2001) 204-209.
[375] M.K. Ram Reddy, Z.P. Xu, G.Q. Lu, J.C. Diniz da Costa, Layered double hydroxides for CO_2 capture: Structure evolution and regeneration, Ind. Eng. Chem. Res., 45 (2006) 7504-7509.
[376] W.J. Likos, N. Lu, Pore-scale analysis of bulk volume change from crystalline interlayer swelling in Na^+ - and Ca^{2+} -smectite, Clays Clay Miner., 54 (2006) 515-528.
[377] W. Oueslati, H.B. Rhaiem, A.B.H. Amara, XRD investigations of hydrated homoionic montmorillonite saturated by several heavy metal cations, Desalination, 271 (2011) 139-149.

[378] M.D. Foster, The relation between composition and swelling in clays, Clays Clay Miner., 3 (1954) 205-220.
[379] J.T. Kloprogge, J. Kristof, R.L. Frost, Thermogravimetric analysis-mass spectrometry (TGA-MS) of hydrotalcites containing CO_3^{2-}, NO_3^-, Cl^-, SO_4^{2-} or ClO_4^-, 2001 Clay Odyssey, Proc. Int. Clay Conf., 12th, (2001) 451-458.
[380] O.K. Srivastava, E.A. Secco, Studies on metal hydroxy compounds. I. Thermal analyses of zinc derivatives e-$Zn(OH)_2$, $Zn_5(OH)_8Cl_2.H_2O$, β-ZnOHCl, and ZnOHF, Can. J. Chem., 45 (1967) 579-583.
[381] O. García-Martínez, R.M. Rojas, E. Vila, J.L.M. de Vidales, Microstructural characterization of nanocrystals of ZnO and CuO obtained from basic salts, Solid State Ionics, 63-65 (1993) 442-449.
[382] J.W. Hoffman, I. Lauder, Basic Zinc Chlorides, Aust. J. Chem., 21 (1968) 1439-1443.
[383] I. Rasines, J.I. Morales de Setién, Thermal analysis of β-$Co_2(OH)_3Cl$ and $Zn_5(OH)_5Cl_2 \cdot H_2O$, Thermochim. Acta, 37 (1980) 239-246.
[384] O. Garcia-Martinez, E. Vila, J.L. Martin de Vidales, R.M. Rojas, K. Petrov, On the thermal decomposition of the zinc(II) hydroxide chlorides $Zn_5(OH)_8Cl_2.H_2O$ and β-Zn(OH)Cl, J. Mater. Sci., 29 (1994) 5429-5434.
[385] H. Tanaka, A. Fujioka, Influence of thermal treatment on the structure and adsorption properties of layered zinc hydroxychloride, Mater. Res. Bull., 45 (2010) 46-51.
[386] M. Krunks, J. Madarász, T. Leskelä, A. Mere, L. Niinistö, G. Pokol, Study of zinc thiocarbamide chloride, a single-source precursor for zinc sulfide thin films by spray pyrolysis, J. Therm. Anal. Calorim., 72 (2003) 497-506.
[387] T. Kozawa, A. Onda, K. Yanagisawa, A. Kishi, Y. Masuda, Effect of water vapor on the thermal decomposition process of zinc hydroxide chloride and crystal growth of zinc oxide, J. Solid State Chem., 184 (2011) 589-596.
[388] V. Rives, Characterisation of layered double hydroxides and their decomposition products, Mater. Chem. Phys., 75 (2002) 19-25.
[389] J. Rocha, M. del Arco, V. Rives, M. A. Ulibarri, Reconstruction of layered double hydroxides from calcined precursors: a powder XRD and 27Al MAS NMR study, J. Mater. Chem., 9 (1999) 2499-2503.
[390] H.E. Eltepe, 2004, 'The Development of Zinc Borate Production Process', MSc. Thesis, Izmir Institute of Technology, Turkey.
[391] Y.-H. Gao, Z.-H. Liu, X.-L. Wang, Hydrothermal synthesis and thermodynamic properties of $2ZnO \cdot 3B_2O_3 \cdot 3H_2O$, J. Chem. Thermodyn., 41 (2009) 775-778.
[392] F.M. Labajos, V. Rives, M.A. Ulibarri, Effect of hydrothermal and thermal treatments on the physicochemical properties of Mg-Al hydrotalcite-like materials, J. Mater. Sci., 27 (1992) 1546-1552.
[393] J.E. House, K.A. House, Descriptive Inorganic Chemistry, Academic Press, London, 2010.
[394] D. Weigel, B. Imelik, M. Prettre, Comparative investigation, by thermal analysis, of the pyrolysis of hexahydrated Mg, Zn, and Ni nitrate, Compt. Rend., 259 (1964) 2215-2218.
[395] M. Louer, D. Louer, D. Weigel, Preparation and structural analysis of the basic zinc nitrate, $Zn(NO_3)_2.2Zn(OH)_2$, C. R. Acad. Sci., Ser. C, 270 (1970) 881-884.
[396] W. Stählin, H.R. Oswald, The crystal structure of zinc hydroxide nitrate, $Zn_5(OH)_8(NO_3)_2.2H_2O$, Acta Crystallogr., Sect. B: Struct. Sci, 26 (1970) 860-863.
[397] J.-P. Auffredic, D. Louër, Etude thermodynamique de la décomposition thermique des hydroxynitrates de zinc, J. Solid State Chem., 46 (1983) 245-252.

[398] L. Eriksson, D. Louër, P.E. Werner, Crystal structure determination and rietveld refinement of $Zn(OH)(NO_3)\cdot H_2O$, J. Solid State Chem., 81 (1989) 9-20.
[399] F. Wypych, G. Guadalupe Carbajal Arízaga, J.E. Ferreira da Costa Gardolinski, Intercalation and functionalization of zinc hydroxide nitrate with mono- and dicarboxylic acids, J. Colloid Interface Sci., 283 (2005) 130-138.
[400] W. Stählin, H.R. Oswald, The infrared spectrum and thermal analysis of zinc hydroxide nitrate, J. Solid State Chem., 3 (1971) 252-255.
[401] C.C. Addison, J. Lewis, R. Thompson, The liquid dinitrogen tetroxide solvent system. Part VII. Products of reaction of zinc with liquid dinitrogen tetroxide, J. Chem. Soc., (1951) 2829-2833.
[402] M. Maneva, N. Petrov, On the thermal decomposition of zinc nitrate hexahydrate and its deuterated analog, J. Therm. Anal., 35 (1989) 2297-2303.
[403] B. Malecka, R. Gajerski, A. Malecki, M. Wierzbicka, P. Olszewski, Mass spectral studies on the mechanism of thermal decomposition of $Zn(NO_3)_2\cdot nH_2O$, Thermochim. Acta, 404 (2003) 125-132.
[404] A. Malecki, B. Malecka, Formation of N_2O during thermal decomposition of *d*-metal hydrates nitrates, Thermochim. Acta, 446 (2006) 113-116.
[405] A.C. Poshkus, Improved synthesis of basic zinc acetate, hexakis(μ-acetato)-μ-oxotetrazinc, Ind. Eng. Chem. Prod. RD., 22 (1983) 380-381.
[406] V. Auger, I. Robin, Sur un acétate basique de zinc analogue à l'acétate de glucinium, C. R. Hebd. Seances. Acad. Sci., 178 (1924) 1546-1548.
[407] A.K. Gyani, O.F.Z. Khan, P. O'Brien, D.S. Urch, On the use of basic zinc acetate $Zn_4O(CH_3CO_2)_6$ as a novel precursor for the deposition of ZnO by low-pressure metallo organic chemical vapour deposition: their characterization by low energy electron induced X-ray emission spectroscopy, Thin Solid Films, 182 (1989) L1-L4.
[408] Q. Cui, K. Yu, N. Zhang, Z. Zhu, Porous ZnO nanobelts evolved from layered basic zinc acetate nanobelts, Appl. Surf. Sci., 254 (2008) 3517-3521.
[409] R. Baggio, M.T. Garland, M. Perec, A new polymeric phase of zinc(II) oxydiacetate, Acta Crystallographica Section C, 59 (2003) m30-m32.
[410] R.Q. Song, A.W. Xu, B. Deng, Q. Li, G.Y. Chen, From layered basic zinc acetate nanobelts to hierarchical zinc oxide nanostructures and porous zinc oxide nanobelts, Adv. Funct. Mater., 17 (2007) 296-306.
[411] Y. Wang, Y. Li, Z. Zhou, X. Zu, Y. Deng, Evolution of the zinc compound nanostructures in zinc acetate single-source solution, J. Nanopart. Res., 13 (2011) 5193-5202.
[412] B.-H. Ye, X.-Y. Li, I.D. Williams, X.-M. Chen, Synthesis and structural characterization of di- and tetranuclear zinc complexes with phenolate and carboxylate bridges. Correlations between ^{13}C NMR chemical shifts and carboxylate binding modes, Inorg. Chem., 41 (2002) 6426-6431.
[413] E. Kandare, J.M. Hossenlopp, Thermal degradation of acetate-intercalated hydroxy double and layered hydroxy salts, Inorg. Chem., 45 (2006) 3766-3773.
[414] A. Kawai, Y. Sugahara, I.Y. Park, K. Kuroda, C. Kato, Preparation of zinc oxide powders from 2-dimensional hydroxy-zinc complexes of basic zinc acetate, chloride and nitrate, in: S. Hirano, G.L. Messing, H. Hausner (Eds.) Ceramic Transactions, Ceramic Powder Science IV, American Ceramic Society, 1991, pp. 75-80.
[415] A. Kasai, S. Fujihara, Layered single-metal hydroxide/ethylene glycol as a new class of hybrid material, Inorg. Chem., 45 (2006) 415-418.
[416] H. Morioka, H. Tagaya, M. Karasu, J.-i. Kadokawa, K. Chiba, Effects of zinc on the new preparation method of hydroxy double salts, Inorg. Chem., 38 (1999) 4211-4216.

[417] E. Kandare, J.M. Hossenlopp, Hydroxy double salt anion exchange kinetics: effects of precursor structure and anion size, J. Phys. Chem. B, 109 (2005) 8469-8475.
[418] D.M. Reinoso, M.B. Fernandez, D.E. Damiani, G.M. Tonetto, Study of zinc hydroxy acetate as catalyst in the esterification reaction of fatty acids, Intl. J. Low-Carbon Tech., (2011).
[419] Z. Xia, Y. Wang, Y. Fang, Y. Wan, W. Xia, J. Sha, Understanding the origin of ferromagnetism in ZnO porous microspheres by systematic investigations of the thermal decomposition of $Zn_5(OH)_8Ac_2 \cdot 2H_2O$ to ZnO, J. Phys. Chem. C, 115 (2011) 14576-14582.
[420] Y. Zhang, F. Zhu, J. Zhang, L. Xia, Converting layered zinc acetate nanobelts to one-dimensional structured ZnO nanoparticle aggregates and their photocatalytic activity, Nanoscale Res. Lett., 3 (2008) 201-204.
[421] F. Ye, Y. Peng, G.-Y. Chen, B. Deng, A.-W. Xu, Facile solution synthesis and characterization of ZnO mesocrystals and ultralong nanowires from layered basic zinc salt precursor, J. Phys. Chem. C, 113 (2009) 10407-10415.
[422] X. Qu, S. Lu, J. Wang, Z. Li, H. Xue, Preparation and optical property of porous ZnO nanobelts, Mater. Sci. Semicond. Process., (2012).
[423] Y. Xi, R.J. Davis, Intercalation of ethylene glycol into yttrium hydroxide layered materials, Inorg. Chem., 49 (2010) 3888-3895.
[424] M. Taibi, S. Ammar, N. Jouini, F. Fie´vet, Layered nickel-cobalt hydroxyacetates and hydroxycarbonates: Chimie douce synthesis and structural features, J. Phys. Chem. Solids, 67 (2006) 932-937.
[425] K.J. Frink, R.C. Wang, J.L. Colon, A. Clearfield, Intercalation of ammonia into zinc and cobalt phenylphosphonates, Inorg. Chem., 30 (1991) 1438-1441.
[426] G.G. Carbajal Arizaga, F. Wypych, F. Castillón Barraza, O.E. Contreras Lopez, Reversible intercalation of ammonia molecules into a layered double hydroxide structure without exchanging nitrate counter-ions, J. Solid State Chem., 183 (2010) 2324-2328.
[427] M. Estruga, C. Domingo, J.A. Ayllón, Mild synthetic routes to high-surface zinc oxide nanopowders, Eur. J. Inorg. Chem., 2010 (2010) 1649-1654.
[428] G.B. Deacon, R.J. Phillips, Relationships between the carbon-oxygen stretching frequencies of carboxylato complexes and the type of carboxylate coordination, Coord. Chem. Rev., 33 (1980) 227-250.
[429] U. Kumar, J. Thomas, N. Thirupathi, Factors dictating the nuclearity/aggregation and acetate coordination modes of lutidine-coordinated zinc(II) acetate complexes, Inorg. Chem., 49 (2010) 62-72.
[430] H. Noma, Y. Miwa, I. Yokoyama, K. Machida, Infrared and Raman intensity parameters of sodium acetate and their intensity distributions, J. Mol. Struct., 242 (1991) 207-219.
[431] A. Botha, C. Strydom, DTA and FT-IR analysis of the rehydration of basic magnesium carbonate, J. Therm. Anal. Calorim., 71 (2003) 987-996.
[432] J. Hedberg, S. Baldelli, C. Leygraf, Molecular structural information of the atmospheric corrosion of zinc studied by vibrational spectroscopy techniques II. Two and three-dimensional growth of reaction products induced by formic and acetic acid, J. Electrochem. Soc., 157 (2010) C363-C373.
[433] T. Ishioka, Y. Shibata, M. Takahashi, I. Kanesaka, Y. Kitagawa, K. T. Nakamura, Vibrational spectra and structures of zinc carboxylates I. Zinc acetate dihydrate, Spectrochim. Acta, Pt. A: Mol. Biomol. Spectrosc., 54 (1998) 1827-1835.
[434] T. Arii, A. Kishi, The effect of humidity on thermal process of zinc acetate, Thermochim. Acta, 400 (2003) 175-185.

[435] H.G. McAdie, The pyrosynthesis of strontium zincate, J. Inorg. Nucl. Chem., 28 (1966) 2801-2809.
[436] G.B. Kauffman, M. Karbassi, G. Bergerhoff, Metallo complexes: An experiment for the undergraduate laboratory, J. Chem. Educ., 61 (1984) 729-null.
[437] L. Hiltunen, M. Leskela, M. Makela, L. Niinisto, Crystal structure of μ_4-oxo-hexakis(μ-acetato)tetrazinc and thermal studies of its precursor, zinc acetate dihydrate, Acta Chem. Scand., Ser. A, A41 (1987) 548-555.
[438] C.-C. Lin, Y.-Y. Li, Synthesis of ZnO nanowires by thermal decomposition of zinc acetate dihydrate, Mater. Chem. Phys., 113 (2009) 334-337.
[439] R.M. Gordon, H.B. Silver, Preparation and properties of tetrazinc μ_4-oxohexa-μ-carboxylates (basic zinc carboxylates), Can. J. Chem., 61 (1983) 1218-1221.
[440] J. Hedberg, S. Baldelli, C. Leygraf, E. Tyrode, Molecular structural information of the atmospheric corrosion of zinc studied by vibrational spectroscopy techniques I. Experimental approach, J. Electrochem. Soc., 157 (2010) C357-C362.
[441] A.J. Reddy, M.K. Kokila, H. Nagabhushana, J.L. Rao, C. Shivakumara, B.M. Nagabhushana, R.P.S. Chakradhar, Combustion synthesis, characterization and Raman studies of ZnO nanopowders, Spectrochim. Acta, Pt. A: Mol. Biomol. Spectrosc., 81 (2011) 53-58.
[442] A. De Marco, R. Spaccini, P. Vittozzi, F. Esposito, B. Berg, A. Virzo De Santo, Decomposition of black locust and black pine leaf litter in two coeval forest stands on Mount Vesuvius and dynamics of organic components assessed through proximate analysis and NMR spectroscopy, Soil Biol. Biochem., 51 (2012) 1-15.
[443] F.C. Hawthorne, E. Sokolova, Simonkolleite, $Zn_5(OH)_8Cl_2(H_2O)$, a decorated interrupted-sheet structure of the form $[M\Phi_2]_4$, Can. Mineral., 40 (2002) 939-946.
[444] M. Louer, D. Grandjean, D. Weigel, Structural study of nickel and zinc hydroxynitrates. II. Crystal structure of the basic zinc nitrate, zinc dihydroxide-zinc dinitrate (2Zn(OH)2.Zn(NO3)2), Acta Crystallogr., Sect. B, 29 (1973) 1703-1706.
[445] P. Bénard, J.P. Auffrédic, D. Louër, A study of the thermal decomposition of ammine zinc hydroxide nitrates, Thermochim. Acta, 232 (1994) 65-76.
[446] W. Wang, D. Breisinger, The acid-base behavior of zinc sulfate electrolytes: The temperature effect, Metall. Mater. Trans. B, 29 (1998) 1157-1166.
[447] A. Degen, M. Kosec, Effect of pH and impurities on the surface charge of zinc oxide in aqueous solution, J. Eur. Ceram. Soc., 20 (2000) 667-673.
[448] J.P. Auffredic, D. Louër, E. Bonjour, R. Lagnier, Heat capacity of three zinc hydroxynitrates in the range 5 to 300 K, J. Chem. Thermodyn., 10 (1978) 1077-1081.
[449] Vogel's Textbook of Macro and Semimicro Qualitative Inorganic Analysis, 5th ed., Longman Group Limited, 1979.
[450] L.A. Hernandez-Alvarado, L.S. Hernandez, J.M. Miranda, O. Dominguez, The protection of galvanised steel using a chromate-free organic inhibitor, Anti-Corros. Methods Mater., 56 (2009) 114-120.
[451] A.K. Alwan, P.A. Williams, Mineral formation from aqueous solution. Part I. The deposition of hydrozincite, $Zn_5(OH)_6(CO_3)_2$, from natural waters, Transition Met. Chem., 4 (1979) 128-132.
[452] H.L. Clever, M.E. Derrick, S.A. Johnson, The solubility of some sparingly soluble salts of zinc and cadmium in water and in aqueous electrolyte solutions, J. Phys. Chem. Ref. Data, 21 (1992) 941-1004.
[453] W. Preis, E. Königsberger, H. Gamsjäger, Solid-solute phase equilibria in aqueous solution. XII. Solubility and thermal decomposition of Smithsonite, J. Solution Chem., 29 (2000) 605-618.